Prepared for:

RIKZ

Development of a mud transport model for the Scheldt estuary in the framework of LTV

Phases 1 and 2

WATERBOUWKUNDIG LABORATORIUM

FLANDERS HYDRAULICS RESEARCH

Report

December, 2006

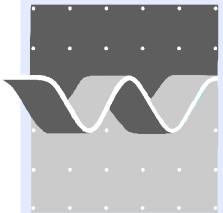

WL | delft hydraulics

Z4210.00

Prepared for:

RIKZ

Development of a mud transport model for the Scheldt estuary in the framework of LTV

Phases 1 and 2

Thijs van Kessel
Joris Vanlede
Ankie Bruens

Report

December, 2006

WL | delft hydraulics

CLIENT:	RIKZ
TITLE:	Development of a mud transport model for the Scheldt estuary in the framework of LTV

ABSTRACT:

On 7 August 2006 RIKZ commissioned WL | Delft Hydraulics to develop a process-based numerical model to support mud management issues in the Scheldt estuary (contract RKZ – 1740 MB). This project has been carried out in cooperation with Flanders Hydraulics (Waterbouwkundig Laboratorium Borgerhout) in the framework of LTV (Long Term Vision) Schelde.

This end report describes the steps taken towards the development of the mud transport model. It deals with the following topics: system description, data-analysis, set-up and calibration of the hydrodynamic model and set-up and calibration of the mud transport model. Management issues are discussed shortly; they have been elaborated in more detail in a separate note.

It is concluded that the mud transport model is technically operational. It has been set-up such that it can be used for both short-term and long-term simulations with different levels of details. Potentially, the model is suitable to simulate seasonal dynamics. However, further calibration is advised prior to the application of the model to support management issues. The estuarine turbidity maximum near Antwerp is not yet properly reproduced. Boundary conditions and wave forcing should be further refined. At the start of the project it was already anticipated that further refinements would probably be required during a subsequent phase of the project. The objectives of the present project (*i.e.* phase 1 and 2) have been realised.

REFERENCES: contract RKZ – 1740 MB

VER	AUTHOR		DATE	REMARKS	REVIEW		APPROVED BY	
1.0	dr ir T. van Kessel		5/12/2006		ir C. Kuijper		ir T. Schilperoort	

PROJECT NUMBER:	Z4210
KEYWORDS:	mud transport, three-dimensional models, estuary models, Scheldt
NUMBER OF PAGES:	79 + appendices
CONFIDENTIAL:	☐ YES ☒ NO
STATUS:	☐ PRELIMINARY ☐ DRAFT ☒ FINAL

Contents

1 Introduction

This report describes the first steps towards the development of a numerical silt transport model for the Scheldt estuary that can be used to support mud management issues herein. First, a concise system description of the Scheldt estuary is given with a focus on fine sediment (Chapter 2). Subsequently, available field data are listed, partially analysed and discussed (Chapter 3). In Chapter 4 the set-up and calibration of the hydrodynamic model is discussed. Chapter 5 discusses the set-up and first calibration of the mud transport model. This report ends with conclusions and recommendations (Chapter 6). Appendices A, B, H and S contain additional information or figures on the results from the hydrodynamic model (A, H) and mud model (B, S).

The remainder of Chapter 1 sets these activities in a wider framework.

1.1 Problem description

Mud behaviour in the Scheldt Estuary affects the navigational and ecological function. For example, the deposition of mud can lead to siltation in harbours and navigation channels, whereas the concentration level of mud particles in the water column and on the bed affects habitats.

Managers have to deal with issues concerning navigability and (European) environmental regulations. Therefore they are confronted with questions such as: *How can we reduce the frequency and amount of dredging? Does dumping of mud or other human interference influence habitats?* etc.

1.2 The role of expert knowledge and numerical models

To answer these questions knowledge on the behaviour of mud is needed, as well as prediction of this behaviour. Ideally, experts possess the required knowledge to describe the system in detail and, based on this knowledge, they can predict future development as well as predict the effect of human interference. In reality though, the behaviour of a natural system is complex (amongst others due to the many interaction between processes) and therefore not all behaviour is understood, let alone be described by mathematical relationships. In case experts are able to predict future behaviour, the prediction is usually qualitative whereas a more quantitative prediction is needed.

The available knowledge on hydrodynamics and sediment behaviour is used to develop numerical models. These models can be used for diagnostic studies (*i.e.* to investigate which physical processes affect mud behaviour, how they interact and which role they play in management issues) or as predictive tools, not only qualitatively but also quantitatively.

1.3 Objective of the present study

RWS-RIKZ manages the Dutch Western Scheldt area, the Flemish government manages the Belgian Scheldt area. Both are frequently confronted with above mentioned management issues and questions. In a joint project they asked WL | Delft Hydraulics and WL Borgerhout to set up a hydrodynamic and mud model, using state-of-the-art knowledge. The applicability of the model for management issues is to be tested, leading to insight in the strength and weaknesses of the model. This insight is of use not only to extend the usage of the model, but also for future development of the model (the weaknesses set the priority for model improvements).

1.4 Methodology

This study starts with a system description, a brief description of the physical processes playing a role in mud behaviour and subsequently in management issues. Understanding of the system is needed to validate results from numerical models.

In this study attention is not only paid to physical parameters such as sediment concentration, flow velocity, erosion rate etc., but also to management parameters such as volume and frequency of dredging, habitats. Special attention is also paid to the various temporal and spatial scales involved in the different management issues.

Besides the system description (Chapter 2), a description of available measurement data is given (Chapter 3). This data is previously used to increase the knowledge on the system behaviour, and is in the present study also used to calibrate and validate the model.

The next requirement for the construction of a mud transport model is the availability of a hydrodynamic model (Chapter 4), which forms the basis for sediment transport computations.

Finally, the set-up and first calibration of the mud transport model for the Scheldt estuary is discussed in Chapter 5.

1.5 Delineation

This study involves the Scheldt and Western Scheldt estuary and its mouth. The study focuses on the physical processes; biological and chemical processes are not yet taken into account. The model describes mud transport in suspension, and does not include bottom transport.

2 System description

2.1 Introduction

Mud behaviour in the Scheldt Estuary is induced and affected by the hydrodynamics of the system. Mud on its turn can affect the hydrodynamic characteristics. In this chapter a brief overview of the involved physical processes is given. This overview is based on available literature; for an extensive system description the reader is referred to this literature.

The first section of this chapter concerns the relevant hydrodynamic processes, the second section focuses on the mud characteristics and processes. The final section summarizes the anthropogenic activities. An overview of relevant processes and parameters for the various management issues is not included in this report, but is given in an additional note (Bruens *et al.*, 2006).

The drainage basin of the Scheldt River covers an area of nearly 22,000 km^2 and is situated in the north-east of France, the west of Belgium and the south-west of the Netherlands. The river is 350 km long and the water level difference between source and mouth is only 100m, making it a typical lowland river system with low current velocities and thus meanders. The Scheldt Estuary is open to the southern North Sea, see Figure 2.1. The Scheldt estuary extends 160 km in length and includes an approximately 60 km long fresh water tidal zone stretching from near the mouth of Rupel to Ghent, representing one of the Western Europe largest freshwater tidal areas.

The Western Scheldt consists of 6 estuarine sections, each consisting of a flood- and ebb channel, intertidal area and interconnecting channels.

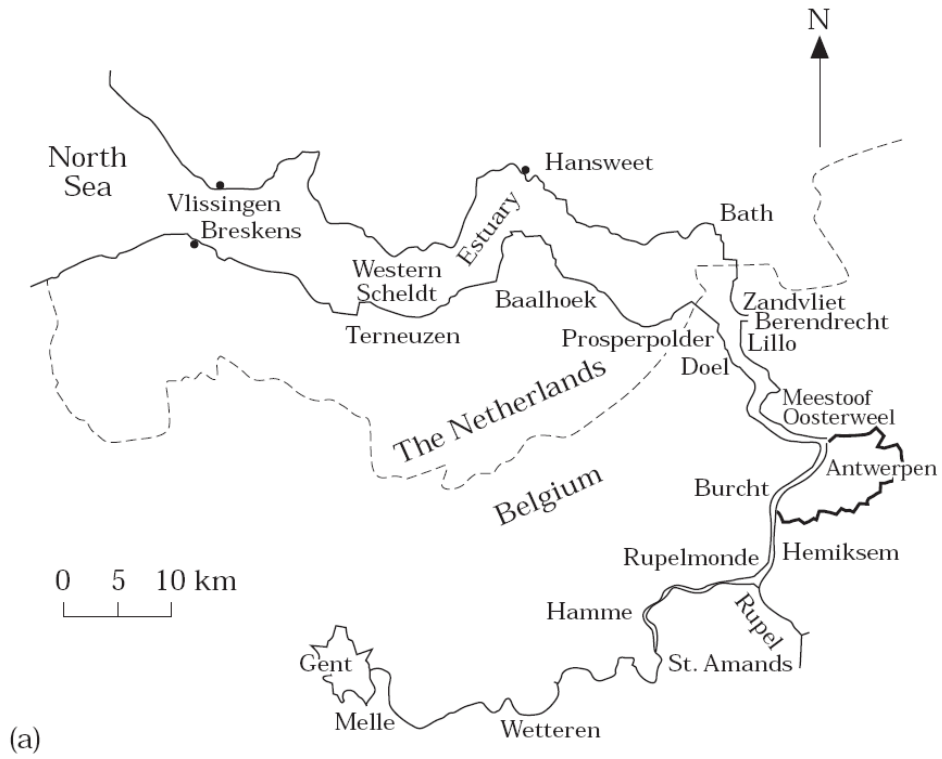

Figure 2.1: The Scheldt estuary (from Fettweis *et al.*, 1998).

2.2 Hydrodynamics

2.2.1 Tide

Tidal range

The estuary has a semidiurnal meso- to macro-tidal regime. The tidal wave penetrates the estuary up to Gentbrugge (situated just downstream of Gent, 156 km from the mouth) where it is stopped by a sluice. The mean tidal range is 3.85 m at the mouth (Vlissingen) and increases up to 5.24 m at Schelle (1 km downstream of Rupelmonde, 91 km from the mouth). Further upstream it decreases to a value of 1.89 m at Gentbrugge (156 km). During spring tide (neap tide) the tidal range is 4.46 m (2.97 m) at Vlissingen and 5.93 m (4.49 m) at Schelle. The tidal wave first increases and decreases in upstream direction as it is affected by convergence, reflection and dissipation. The mean period of the tide is 12 hours 25 minutes, the period during spring tide is 12 hours 20 minutes and during neap tide 12 hours and 41 minutes.

The time period between high water in the estuary (Terneuzen, Hansweert and Bath) and high water near Vlissingen decreases (in the 17th century it was 5 hours, in 1900 2,5 hours, nowadays it is 2 hours). Since 1950 it decreased with approximately 10 minutes (10 to 30 %). This decrease is due to land reclamation, decrease in tidal area and deepening of the navigation channels (Verlaan, 1998).

The high water levels increase (with 15 cm near Vlissingen and 25 cm near Bath and Antwerp) as well as the low water levels (5 cm increase near Vlissingen, 10 cm and 25 cm decrease near Bath and Antwerp, respectively). Possibly the first deepening had a large impact on the water levels. The tidal range increased between 1900 and 1980 with 15 cm near Vlissingen and 35 cm near Bath. The largest increase took place during 1971 and 1980 (half of the mentioned values) (Verlaan, 1998).

Tidal discharge
Near the estuary mouth the tidal discharge has an annual average of 50,000 m^3/s for both ebb and flood tides. More than 10^9 m^3 enters and leaves the estuary twice a day with the tide.

Tidal asymmetry
Due to bottom friction the crest travels faster than the trough, leading to a faster rise and therefore a shorter flood (with higher flow velocities) and a longer ebb (with lower flow velocities). Due to covering and uncovering of tidal flats, the cross-sectional area and thereby the current velocity is suddenly increased or decreased, resulting in an asymmetrical velocity curve (even when the tidal elevation curve is symmetrical).

The ratio between tidal rise and fall time decreases from 0.88 at Flushing to 0.75 at Rupelmonde and 0.39 at Gent. This is a result of the fact that the tidal wave propagates with a velocity proportional to the root of the water depth, so high water travels faster. Towards the head of the estuary this effect is enhanced by a faster decreasing water depth.

The local morphology (*e.g.* channel geometry) influences the local flood/ebb dominance.

The ebb to flood ratio changes from 2 in the upper estuary, to 1.1–1.2 in the middle estuary (indicating a quasi-equilibrium) to a value below unity in the lower part. The local morphology has a large effect on the amount of sediment transport, for example near 58 km the ebb to flood ratio is 3.2 near the right side and 0.8 near the left side of the river bend.

Analyses of the tidal asymmetry in terms of the phase difference between the M_2 and M_4 component of the tide has been carried out by Wang et al. 2002. In the period 1955-1982 ebb dominance decreased between Terneuzen en Hansweert, from 1982 the (minimal) ebb dominance no longer altered. In the period 1971-1987 the flood dominance between Hansweert and Bath decreased, followed by a period in which the flood dominance hardly altered. In Vlissingen and Terneuzen the tidal asymmetry hardly changed in the period 1970-1997. Overall, the tidal asymmetry has declined, suggesting also a decline in natural transport processes.

Tidal velocity
The mean tidal wave propagation between Vlissingen and Gent is 7.5 m/s for high water and 5 m/s for low water. The average cross-sectional ebb and flood currents lie around 0.7 m/s (maximum near Rupelmunde, 1.2 m/s during ebb and 1.4 during flood, diminishing both upstream and downstream, having a minimum near the Belgian/Dutch border and increasing towards the North Sea).

2.2.2 River Discharge

The river discharge varies from 50 m^3/s during dry summer to 300 m^3/s during wet winter. The annual average lies between 100 and 200 m^3/s, which is small compared to the tidal discharge. It is also small compared to the discharge of other European rivers (Rhine, 2200 m^3/s, Meuse 250 m^3/s). During a tidal cycle only 5×10^6 m^3 of freshwater is discharged into the North Sea. 90% of the fluvial sediment is discharged in less than 10% of the time during high water discharges.

2.2.3 Waves

Waves only influence the Western part near the mouth. Sediment transport is mainly determined by tidal flow, but waves have an effect on the morphology. Tides build intertidal areas, whereas waves break them down.

2.2.4 Salinity & Estuarine circulation

Peters (1975) and Nihoul et al. (1978) distinguish three zones in the estuary. A zone of practically fresh water between Gentbrugge (156 km) and Rupelmonde (92 km), a partially-mixed zone between Rupelmonde (92 km) and Hansweert (39 km) and a well-mixed zone between Hansweert (39 km) and the mouth. This classification corresponds roughly with the transition of a one channel river to a system with one main channel, flood channels and sand banks and further downstream to a complex region of multiple channels (flood and ebb channels) and sand banks. During low freshwater discharge the Scheldt estuary can be classified as a well-mixed estuary.

The salinity in the estuary varies from fresh water at Rupelmonde (92 km) to nearly the value of seawater at the mouth. During high discharge, sea water only penetrates to Antwerp, whereas during low discharge it penetrates farther than Rupelmonde. The zero salinity point can shift over a distance of about 40 km. Figure 2.2 (from Verlaan 1998, after Claessens, 1988) shows the longitudinal salt distribution.

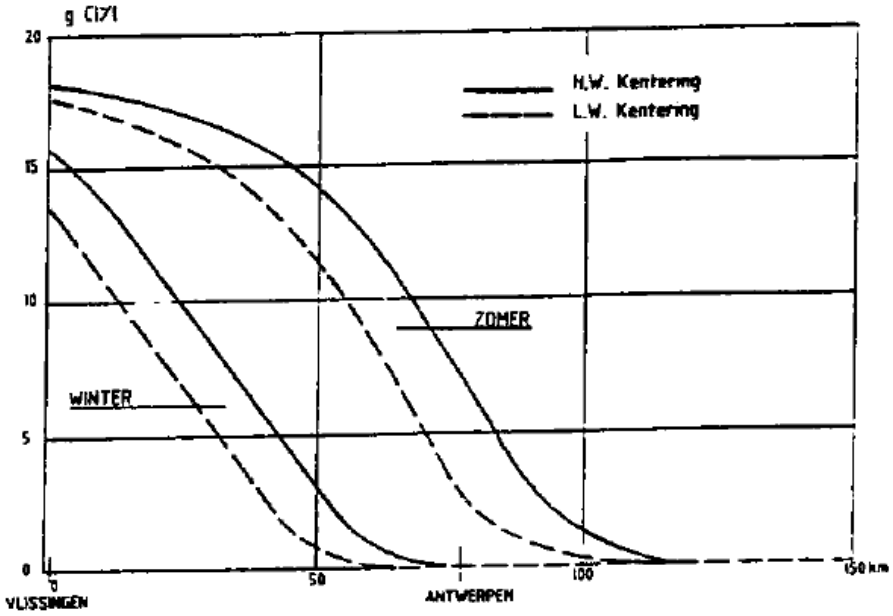

Figure 2.2: Longitudinal salinity distribution in the Scheldt estuary for a high and a low discharge situation. The dashed line indicates high water slack and the solid line low water slack (after Claessen, 1988). Figure from Verlaan (1998).

In the mixing zone (between Rupelmonde and Vlissingen) the vertical salinity difference is $1^0/_{00}$, in the partially mixed zone (between Antwerp and the Belgian/Dutch border) this difference is higher than upstream (homogeneous zone) and downstream. The difference is higher during spring ($4^0/_{00}$) than during neap tide ($2.8^0/_{00}$), averaged over a tidal cycle the difference is $1^0/_{00}$. Lateral differences are larger where a distinct separation between ebb and flood channels exist.

Usually, it is assumed that most of the fresh water in the Belgian waters comes from the Scheldt. Lacroix *et al.* (2004) used a 3D hydrodynamic model to determine the relative impact of the Scheldt and Rhine/Meuse freshwater plume. Results from their model indicate that the salinity of the Belgian waters is dominated by inflow of the Channel water mass which mixes with freshwater originating mainly from the Rhine/Meuse with a much smaller contribution from the Scheldt Estuary.

Estuarine circulation
The longitudinal pressure gradient (barotropic force) acts in downstream direction, the longitudinal density (salinity) gradient (baroclinic force) acts landwards and increases linearly with depth. The combined effect is a residual circulation, landwards (upstream) in the lower part of the water column and downstream (seaward) in the upper part. Averaged over a water column the residual movement is seaward.

In Verlaan (1998) the densimetric Froude number and the estuarine Richardson number are given. The Richardson number decreases from 0.006 at Antwerp to 0.0002 at the mouth, indicating that stratification effects on the estuarine circulation is negligible. In Figure 3.11 from Verlaan (1998) the stratification-circulation diagram of Hansen and Rattry is given and depicts the parameter regime of the Scheldt estuary from Antwerp to the mouth. The diffusion parameter decreases from 0.99 to 0.9 indicating that the upstream salt flux is mainly caused by diffusion, gravitational convection hardly contributes.

2.2.5 Energy levels and residual currents

The mud processes and patterns are mainly induced by the energy level (as the energy level determines where and when resuspension, erosion, deposition and consolidation take place). Total energy levels result from the (above mentioned) sources:

- small time- and spatial scale level turbulence
- larger scales like the tidal cycle (flood-ebb, neap-spring, lunar cycles)
- more a-periodic energy input like river discharge and waves.

Based on the average tidal and runoff conditions the energy distribution as given in Figure 2.3 (from Chen *et al.*, 2005) can be calculated. Far upstream from the river mouth (> 120 km) the river energy (fresh water discharge) is larger than tide energy. Wave energy is relatively small and only present up to 40 km upstream from the river mouth. Tidal energy first increases in upstream direction from the river mouth due to convergence, further upstream it decreases due to friction. In the Scheldt estuary a total energy maximum is situated between 58 and 100 km.

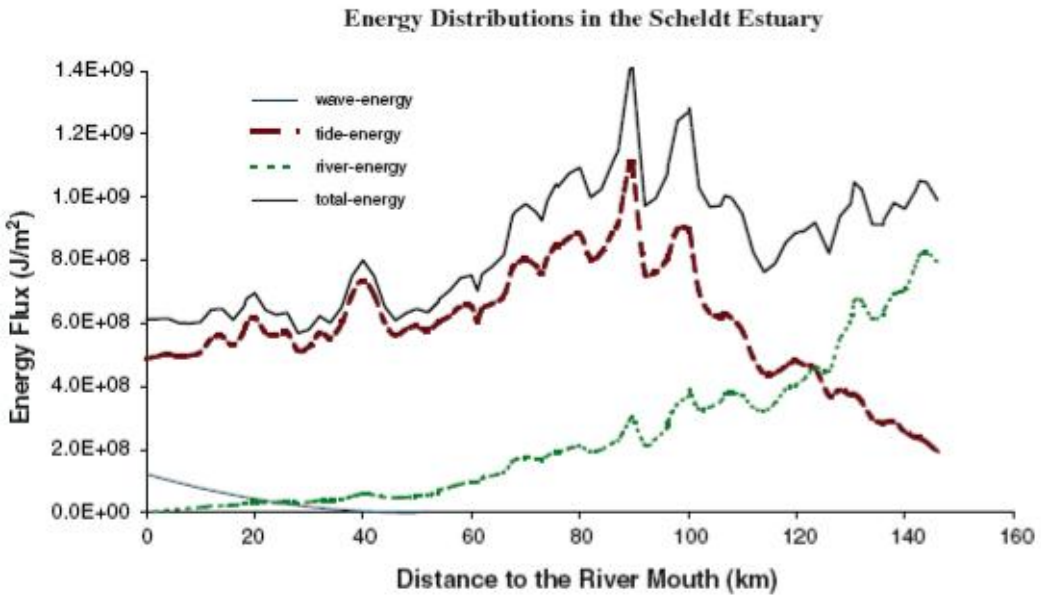

Figure 2.3: The Scheldt energy distributions. Wave energy (based on average wave height) ranges from 2.5 x 10^7 J/m^2 at the river mouth (at Vlissingen) to zero near 50 km, and is multiplied by a factor 5 to be able to show up on the given y-axis scale of this figure. Data from Wartel and Francken (1998). Tidal energy is based on average tidal range; river energy is based on average runoff. Figure from Chen *et al*., 2005.

In the uppermost 1 m water-layer the residual currents have a seaward direction. The velocity decreases in downstream direction (velocity ranging from 0.17 to 0.28 m/s at 58 km from the mouth, 0.09 m/s at 40 km upstream). In the lowermost 1 m water-layer, the residual currents vary in direction; they are orientated seaward in the upper estuary and landward in the lower estuary. The location where near bottom residual currents are in equilibrium depend on tidal and discharge conditions. For spring tide and average discharge the equilibrium is observed in the vicinity of 70 km (Chen *et al.*, 2005).

The local morphology (*e.g.* channel geometry) influences the local residual flow pattern.

2.2.6 Residence time

The residence time of freshwater in the Scheldt estuary is estimated at 2 – 3 months.

2.3 Mud dynamics

2.3.1 Mud sources

Marine mud in the Scheldt estuary originates from the English Channel and the Flemish Banks. The amount of marine mud entering at the mouth is an unknown, estimated values range from 50.000 to 350.000 ton/yr (Verlaan, 1998). The amount of marine mud that is retained in the mixing zone between Rupelmonde and Vlissingen is estimated to be around 30%.

Fluvial mud originates from domestic, industrial and agricultural effluent and material eroded from muddy beds. The amount of mud entering the estuary has been obtained from measurements of freshwater discharge and suspended sediment concentrations at six locations on the edge of the estuarine zone. Between 1992 and 1997 the amount of fluvial sediment varied between 75.000 and 250.000 ton/yr. In this period the amount has decreased with approximately 50%. This reduction is caused by the increased treatment of domestic waste water in Flanders and Wallonia and the increased deposition upstream of Rupelmonde due to construction of a number of weirs and sluices. Most of this sediment (80%) is retained; only a minor portion reaches the sea.

The mixing curve of suspended matter (marine and fluvial) differs from that of water (saline and fresh). Whereas the seawater fraction increases linearly with distance from the landward end of the mixing zone, the marine suspended matter increases more rapidly. The difference between seawater and marine suspended matter is higher near the landward than seaward side. With higher river discharges the mixing curves are shifted seaward, but the shape remains nearly the same.

2.3.2 Mud properties

The average floc size is given in Figure 2.4 (from Chen *et al.*, 2005). The average floc size increases from near 58 km in upstream direction, reaching values of 120 μm. Floc sizes are minimal between 40 and 80 km.

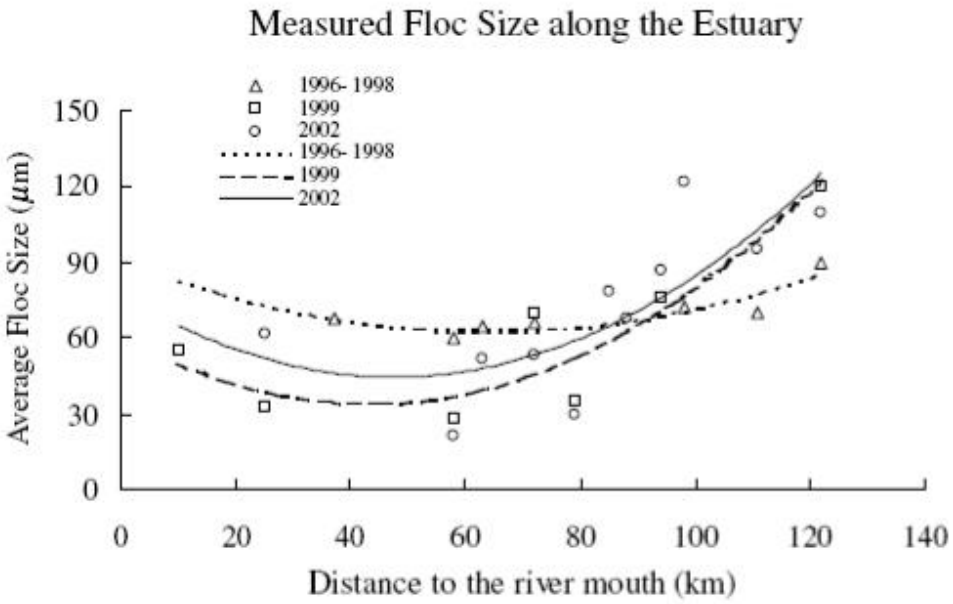

Figure 2.4: Average floc size distribution in the Scheldt Estuary. Each point in the plot represents an average of over 400 measurements. Lines are second order polynomial trendline.

2.3.3 Mud processes

Deposition, resuspension and erosion
The sediment concentration depends not only on the flow velocity, but also on turbulence level, regional distribution of sediment deposits, local morphology, consolidation etc. These parameters influence the deposition, resuspension and erosion rate and therefore the sediment concentration. Measurements from concentration profiles in the Scheldt estuary indicate that the maximum of depth-averaged suspended sediment concentration not always coincides with the maximum of depth-averaged current velocities. This indicates that other processes than simply resuspension and erosion (once the velocity in the water-layer exceeds a critical value) play a role. The sediment concentration often lags the flow velocity due to a combination of settling lag, threshold lag, scour lag and erosion lag. Also generation of turbulence due to velocity gradients (in vertical or longitudinal direction) may influence the development of the local concentration profile during a tidal cycle.

A critical erosion velocity of about 0.56 m/s is found (Chen *et al.*, 2005). Equivalent bed shear stress is 0.87 Pa for C = 60 $m^{0.5}/s$. In previous model studies on siltation in Deurganckdok a value of τ_{crit} = 0.4 Pa has been used (IMDC, 1998). Based on erosion flume studies on mud out of the Kallo access channel, a value of τ_{crit} of 0.6 Pa to 0.7 Pa has been reported in Toorman (1997)

Deposition rates are high in entrance channels to the locks. In the Kallo lock for example 1.3 cm/day. Sedimentation rates of the order 0.8 to 1.7 cm/yr on the salt marshes are derived.

Flocculation
Floc size is a function of turbulence level, sediment concentration, organic matter, salinity, residence time, differential settling. Large flocs are regularly observed around the contact of fresh and saline water, this explains the increase in floc size in upstream direction in the

Scheldt estuary. The high energy level in the middle of the estuary results in a decrease in floc size.

2.3.4 Mud distribution

Distribution of turbidity maxima
In the Scheldt estuary a multilayer structure is often encountered: a permanently suspended fraction or washload fraction and a tidally-fluctuating fraction which is alternately deposited and resuspended during a tidal cycle. The transport of the washload fraction is controlled by the estuarine circulation whereas the transport of tidally-fluctuating fraction is determined by the combined effect of the tidal asymmetry and the estuarine circulation.

The best known mechanism for an estuarine turbidity maximum (ETM) is the residual circulation that results in an seaward surface flow and a landward bottom flow. Upstream in the river there is a seaward flow in both the upper and lower layer, so there exists a convergence in the bottom flow at the so called null point near the head of the salt intrusion. Fluvial mud particles in the upper layer flow seawards and settle to the lower layer where they are carried landwards (together with already present marine mud) to the null point where an ETM exist without the need for erosion processes. The location depends on river discharge but ebb and flood also shift the turbidity maximum up and down. A higher river discharge results in higher mass of sediment due to higher fluvial sediment supply (concentrations on the other hand don't have to become larger as the cross sectional area can be larger downstream). At high river discharge, the stratification can become so high, that the upper and lower water layer are decoupled and a large amount of fluvial sediment passes through the estuary in the upper layer and reaches the sea.

A second mechanism for an ETM is tidal asymmetry (so-called tidal pumping). As the flood velocities are higher than ebb velocities more sediment is carried landwards, up to the point where the downstream river discharge becomes dominant in transporting sediment. Also the duration of slack water is longer at high water, leading to more sedimentation.

A third mechanism for the formation of an ETM is the flocculation process.

In the Scheldt, the formation of an ETM near the port of Antwerp is usually explained by a combination of estuarine circulation and tidal pumping. The fact that the ETM is located landwards of the mixing zone may imply that tidal pumping is mainly responsible for its existence. At low discharge, it is located up to 110 km from the mouth (near St. Amands), whereas at high discharge it is located down to 50 km from the mouth (near the Belgian-Dutch border). This ETM is situated in the area of maximal energy. The residence time of sediment is longer here compared with other regions of the estuary. Concentrations in the ETM vary with a factor 2 to 10 within a tidal cycle. As the concentrations correlates well with varying tidal velocities it is expected that a major part of the suspended material is subject to deposition and resuspension within a tidal cycle whereas a minor part, the so-called washload fraction, remains in suspension. The ETM is present during maximum current velocities and nearly absent during slack water.

During high river discharge a ETM is formed near the Dutch-Belgian border (at salinities around $5^0/_{00}$) suggesting that then also estuarine circulation is contributing to the formation of the ETM.

An ETM is also observed near Vlissingen. According to Chen *et al.* (2005), this ETM is marine-dominated and characterised by high wave and tide energy with SPM concentrations reaching more than a few hundred mg/l. Also convergence of residual currents and hydrodynamic trapping of SPM have been proposed to explain the high SPM concentration in front of the Scheldt mouth.

A river-dominated ETM, which only occurs in case of a discharge greater than 70 m^3/s, is present near Gent: the area of the river-dominated energy maximum is also the area of high SPM concentrations (reaching up to 300 mg/l).

Sediment concentrations show variations on different time scales:

- flood- ebb tide
- spring- neap tide (higher during spring)
- seasonal variations depending on differences in erosion in the river (high values in winter-spring and low in summer-autumn, see Figure 2.5 (from Chen *et al.*, 2005).
- decades, possibly resulting from climate change.

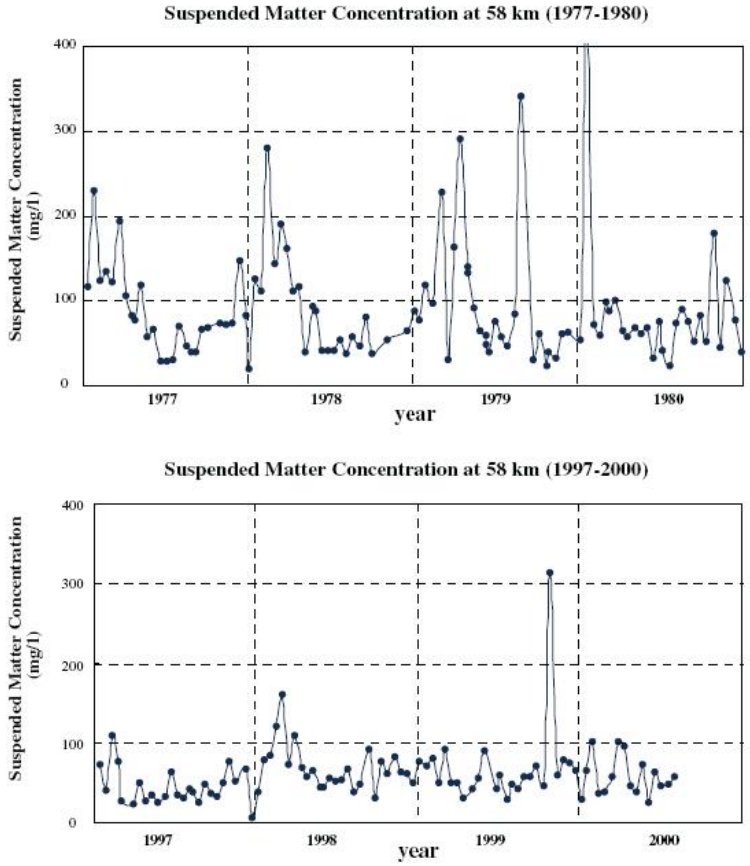

Figure 2.5: Suspended matter concentration over two decades (1977-1980 and 1997-2000). Fortnight measurements near 58 km at low water levels around spring tide. Data from Directorate-General for public works and water management, Institute for inland water management and waste water treatment (RIZA), the Netherlands (2002). Figure from Chen *et al.*, 2005.

Distribution of mud concentrations

As mentioned above a multilayer structure is often encountered consisting of a an upper washload layer and a tidally fluctuating lower layer. The uniform upper layer has more or less a constant concentration in time. In longitudinal direction the sediment concentration shows a large variety. Values in the upper 25 % of the water column reported in literature are typically in the order of 110 ± 50 mg/l in the upper estuary, 100 ± 70 mg/l in the middle estuary and below 50 mg/l in the lower estuary. In Chen et al. (2005) the following values are reported: in the lower estuary typical values lie around 50 mg/l and seldom exceed 100 mg/l. In the middle estuary the average value in the uppermost 10% of the water column lies around 82 ± 65 mg/l and in the lowermost 10% around 150 mg/l to 2.5 g/l. Further upstream values are 110 ± 65 mg/l in the uppermost 10% and a range of 100 mg/l to 1 g/l. These numbers are summarised in Table 2.1. Figure 2.6 (from Verlaan, 1998) show the longitudinal suspended sediment concentration in the Scheldt estuary (after Van Eck *et al.*, 1991). The concentration in the lower layer varies not only spatially but also in time. It increases towards the bed where it can reach values of several g/l.

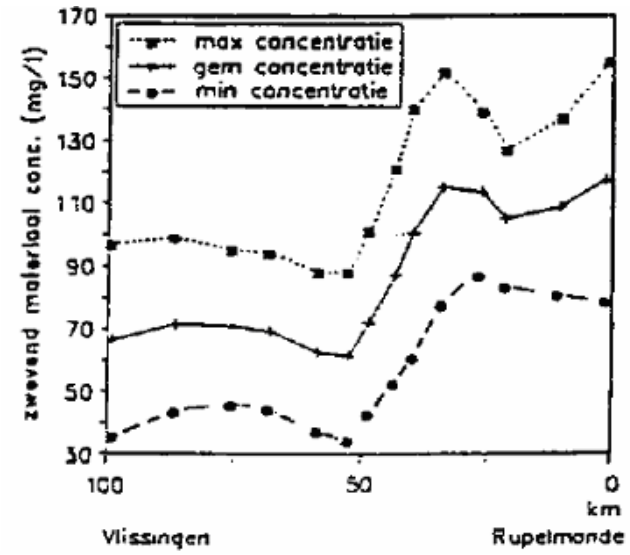

Figure 2.6: Longitudinal suspended matter concentration in the Scheldt estuary. Averaged values over 1970-1990 (after van Eck et al., 1991). The upper and lower line represent the average suspended matter concentrations during winter and summer respectively. Figure from Verlaan (1998).

	Lower	**Middle**	**Upper**
25 % upper water layer (/)	< 50 mg/l	100 ± 70 mg/l	110 ± 50 mg/l
10% upper water-layer Chen et al. (2005)	50 mg/l	82 ± 65 mg/l	110 ± 65
10 % lower water-layer Chen et al. (2005)	50 mg/l	150 mg/l to 2.5 g/l	100 mg/l to 1 g/l

Table 2.1: Typical SPM concentrations according to Verlaan (1998) and Chen *et al.* (2005).

In Chen et al. 2005 examples of changes in vertical concentration distribution in time are given. Figure 2.7 shows such an example. In this example an increase in flow velocity results in resuspension and possible erosion, increasing the sediment concentration, this effect is larger during ebb (higher concentrations and a thicker lower layer). In the middle estuary maximum concentrations correlate with maximum flow velocities, this suggests that resuspension is an important process. The critical flow velocity in the lowermost 1 m water-layer for this resuspension is found to be 0.56 m/s. Measurement in the middle estuary also shows that hysteresis takes place, during ebb and/or flood (see for example Figure 2.8 from Chen *et al.*, 2005). In the upper and lower estuary suspended concentration varies little over the tide and shows no correlation with the current velocity. These measurements indicate that, as already mentioned in paragraph 2.3.3, sediment concentrations and the concentration profile depends not only on the flow velocity, but also on settling lag, threshold lag, scour lag and erosion lag, and also on turbulence level, regional distribution of sediment deposits, local morphology, consolidation etc. Therefore sediment profiles are not uniform in longitudinal direction and when analysing measured (or modelled) concentration profiles, the large-scale patterns as ETM distribution as well as these local conditions have to be taken into account.

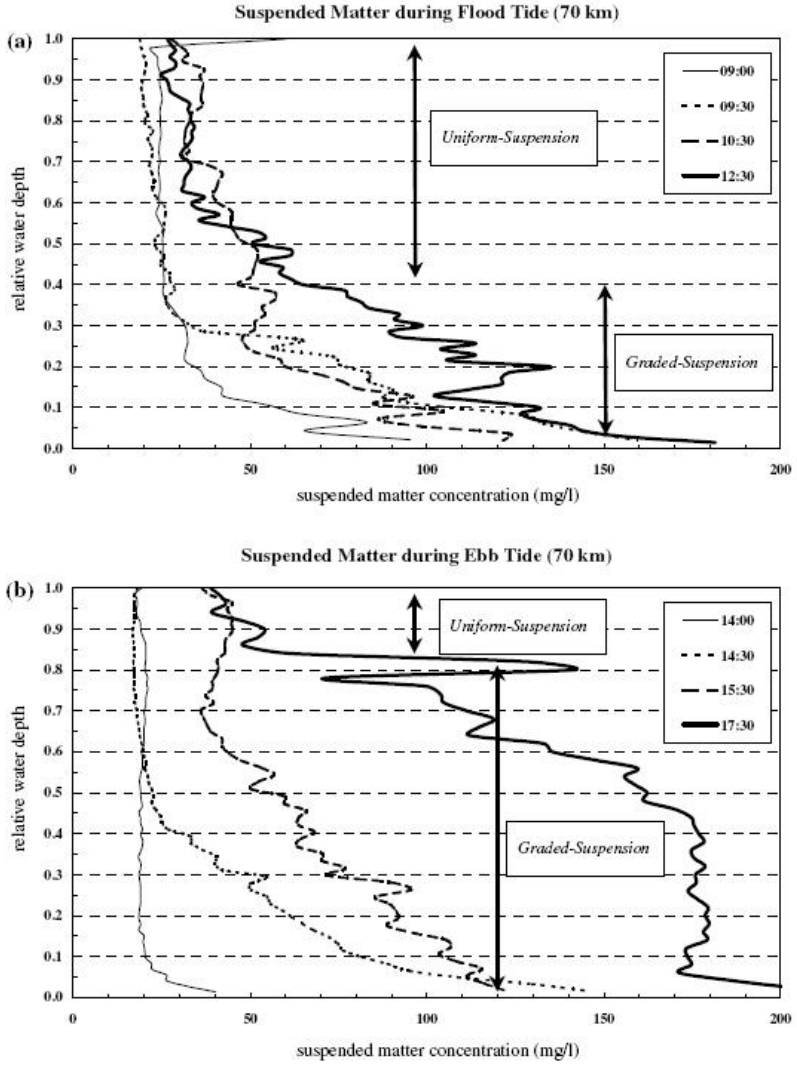

Figure 2.7: Vertical distribution of suspended matter during a tidal cycle. An example of measurements carried out at an anchored station near 70 km. Y-axis indicates relative water depth, where 1 is water-surface and 0 is bottom.

Chen *et al.* (2005) derived the amount of suspended sediment transport through various cross sections, the average results are shown in Table 2.2.

	Upper	**Middle**	**Lower**
Ebb	1.1 ton/m^2	0.7 ton/m^2	3.3 ton/m^2
Flood	0.5 ton/m^2	0.7 ton/m^2	2.4 ton/m^2

Table 2.2: Suspended sediment transport per tide in the Scheldt Estuary according to Chen *et al.* (2005).

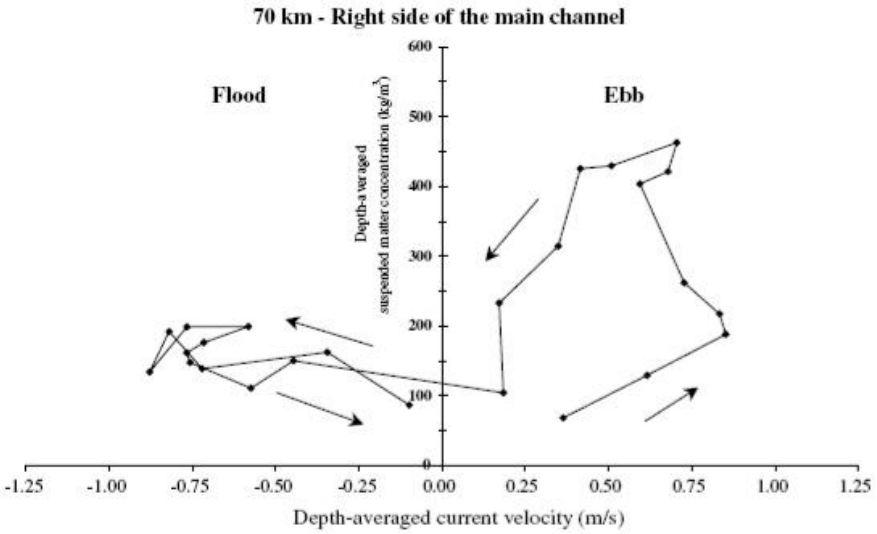

Figure 2.8: Suspended matter concentrations over a complete tidal cycle in the middle estuary. An example of measurements carried out at an anchored station within the ETM – near 70 km at the right side of the main channel. Conventionally, flood current velocity is indicated as negative. Each point on the figure stands for every 30 min measurements. Figure from Chen *et al.*, 2005.

Distribution of bottom sediments

The mean grain size of bottom sediments increases with the tidal current speed. Average velocities are highest at Rupelmonde, diminishing downstream, have a minimum near the border and increase towards the mouth. Upstream of Rupelmonde medium to coarse sand is found, between Rupelmonde and Antwerp coarse sand and locally gravel is found, between Antwerp and the Dutch-Belgian border sand, sandy mud and mud are found. The mud fraction is highest on the bars in the navigation channel (10 to 50%).

From the intertidal flats to the salt marshes the clay content increases (particles size decreases); the finest particles from the lower tidal flats are transported to the higher tidal flats and salt marshes. Sedimentation rates of the order 0.8 to 1.7 cm/yr on the salt marshes are derived. In summer the storage capacity on flats is higher due to biological stabilisation.

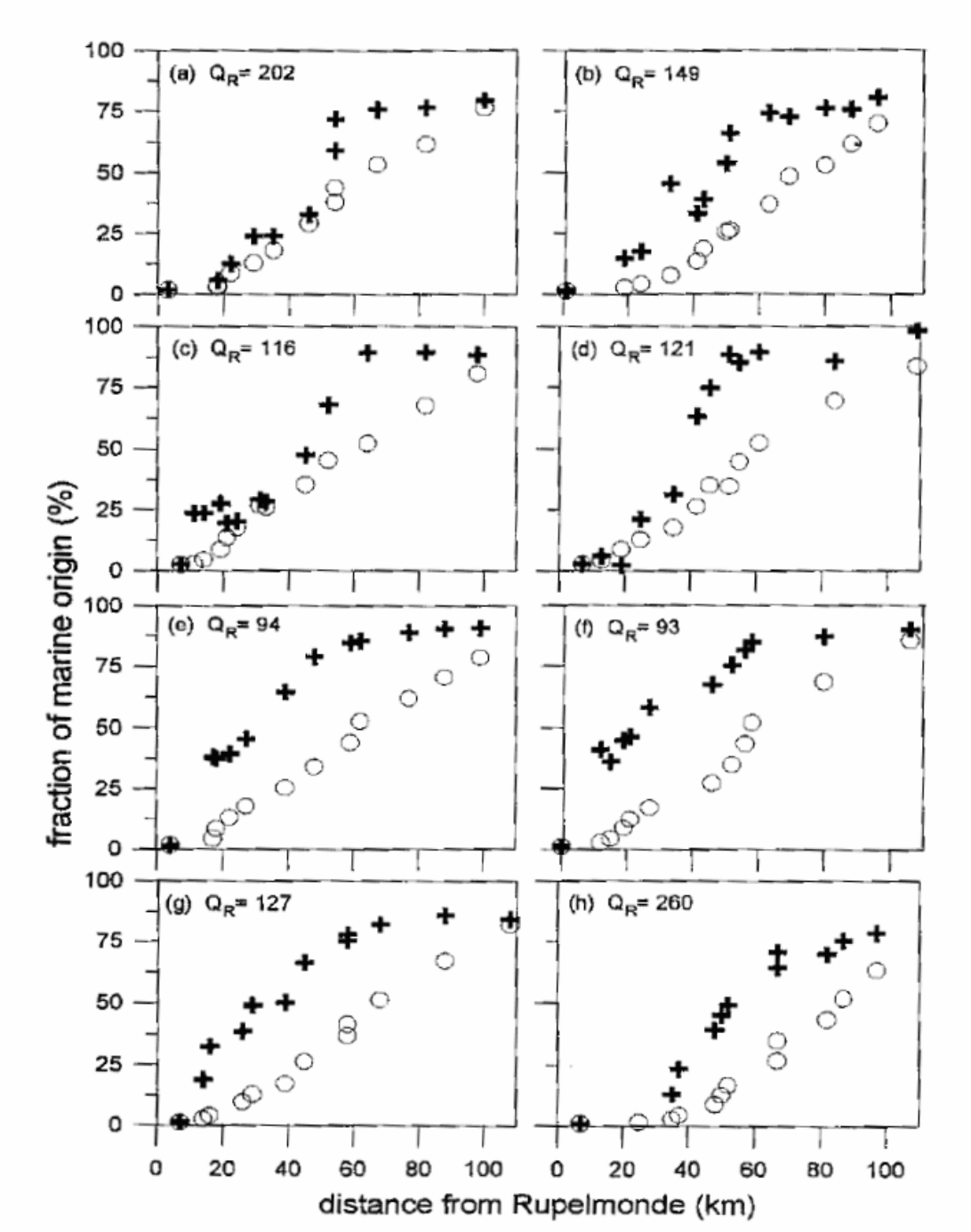

Figure 2.9: The sea water fraction and the fraction of marine suspended sediment versus the distance from Ruppelmonde. The Scheldt discharge (QR) is specified for each cruise. Cruises were carried out in 1987 and 1988. Figure from Verlaan (1998). o = sea water fraction; + = fraction marine suspended matter.

In Verlaan (1998) the ratio of marine to fluvial suspended matter in the Scheldt estuary is calculated. Figure 2.9 shows the fraction of the marine material and the sea water fraction for various river discharges (Q_R). As described in Verlaan: 'The sea water fraction depends almost linearly on the longitudinal distance. The fraction of marine suspended matter was always higher than the sea water fraction. Moreover the fraction of marine suspended matter showed the largest longitudinal gradient at low salinity values. Figures 2.9a through 2.9h

demonstrate that the fraction of marine suspended matter was close to zero landward of the salt intrusion. So marine suspended matter cannot come further landward than sea water'.

In the same study the ratio of marine to fluvial bottom mud in the Scheldt estuary is calculated. In most of the upper estuary the marine fraction is below 10%. Between Lillo and Saeftinghe the fraction increases sharply from 10% to 70%. Further seawards it gradually increases from 70% to 95%. No influence of the dumpsites of Zeebrugge and the canal Gent-Terneuzen has been detected in the data set. Figure 2.10 shows the marine fraction versus distance from Rupelmonde. As described in Verlaan: 'The data suggests that marine material from the Western Scheldt is mostly deposited in the entrance channels of Zandvliet-Berendrecht whereas relatively small amounts are deposited further upstream. Apparently, these entrance channels act as a trap of marine material that is transported upstream from the Western Scheldt. Conversely, fluvial suspended matter is mainly deposited in the upper estuary between Antwerp and the Dutch-Belgian border. Hardly any deposition of fluvial material occurs in the Western Scheldt. Again, the entrance channels of Zandvliet-Berendrecht act as a trap of fluvial suspended matter that is transported seawards'.

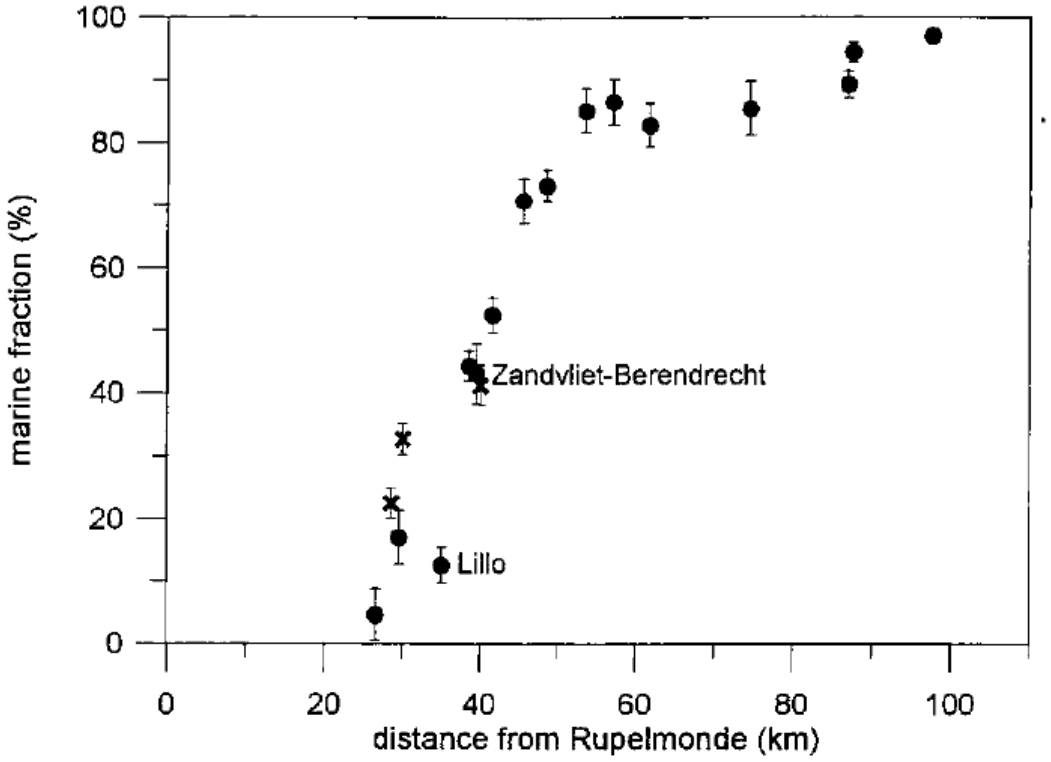

Figure 2.10: Fraction of marine bottom sediment versus the distance from Rupelmonde. Figure from Verlaan (1998).

Figure 2.9 and 2.10 show that under low and moderate discharge conditions the marine fraction of suspended matter in the upper estuary is much higher than the marine fraction of bottom mud, which suggests that under these conditions hardly any suspended matter is permanently deposited in the upper estuary. On the other hand, under high river discharge conditions mixing curves of bottom mud and suspended matter are almost identical. The higher deposition during high river discharge can be explained by the position of the ETM at these conditions: at the Dutch-Belgian border where low turbulence level spots are present.

2.3.5 Involved time- and space scales

From the system description it can be concluded that different time- and spatial scales play a role in the distribution and concentration patterns of mud in the Scheldt. On a large spatial scale the location of the ETM is determined by river discharge, which varies mainly on a seasonal timescale. On a smaller spatial scale the location is determined by neap- and springtide (time scale of weeks), and on an even smaller spatial scale flood- and ebb tide (*i.e.* time scale smaller than a day) play a role.

Vertical concentration profiles vary on even smaller time- and spatial scales (also within an ETM). The local morphology (for example channel pattern, a few 100 meters) plays a role, but also constructions like locks, weirs, dams, etc (tens of meters) influence the mud distribution. The involved timescales go from seasonal, springtide, ebb- flood tide down to turbulence level. At present, no single model is capable to simulate all the involved timescales accurately on the spatial scale of the complete Scheldt estuary. Large timescales processes like spring- and neap tide can be modelled for the whole estuary, but such a model does not include local turbulence levels and its influence on the mud concentration profiles. For such detailed modelling one dimensional vertical models can be used. When applying a model for management issues, it is therefore important to determine which processes on which time- and spatial scale play a role in the management issues.

2.4 Anthropogenic effects

2.4.1 Dredging and dumping

To ensure passages for ships, both harbours and navigation channels have to be dredged frequently. Dumping of dredged material influences temporarily the light penetration on the dumping location. It also influences the distribution pattern of mud, not only local and temporal but possibly for larger time- and spatial scales. Concise, dumping influences the turbidity and the siltation.

Most dredged material in the Western Scheldt is sand, in the Lower Sea Scheldt the sand-mud ratio is 60%–40%. As the mud is contaminated it is not always allowed to dump it.

Previously dredged material from the sandbars in the Western Scheldt were dumped in the shallows away from the main channel, but in the same stretch of the estuary. As this resulted in recirculation (towards bars) more and more material is dumped westwards.

2.4.2 Deepening and land reclamation

In the navigation channel several deepenings (to increase the maximum size of ships entering the harbour of Antwerp) have been carried out. Due to deepening the discrepancy between natural depth and ideal maintained depth increases and therefore the dredging activities.

Deepening decreases the friction for the incoming floodwater, leading to more floodwater entering the estuary and increasing the tidal range. For example in Antwerp the tidal range

increased with 18 cm between 1990 and 1998, in comparison, the anticipated sea level rise is equal to 0.1 cm/y.

The intertidal area reduced due to land reclamation. Between 1930 and 1960 the reduction of tidal area was mainly due to land reclamation, whereas in the period 1960-1990 it was mainly due to sedimentation. Land reclamation has an effect on tidal propagation and therefore tidal range and time period between high water at different locations.

Through its effect on the hydrodynamics, deepening and land reclamation influences the mud movement and distribution.

2.4.3 Management issues

As mentioned in the introduction, management issues are mainly related to navigability and ecology. Navigability involves depth of navigation channels and harbours, which depends on siltation rates. Ecology involves the presence of habitats and species, which depends on light climate and mud deposition. The relation between light climate and amount of mud in the bed and presence of habitats and species is not straightforward, i.e. that critical values are not known.

Frequently discussed management questions are related to past/present/planned human interferences: 1) Does it effect siltation/deposition and/or light climate, and 2) if an effect is expected how can we optimise/minimise the effect (can we define an optimal management strategy)? Examples of human interferences are :

- Dredging (including barriers)
- Dumping
- Harbour infrastructure works
- Construction of the Deurganck dock
- Removal of (polluted) mud from the access channel to the Kallo sluices
- Optimising fresh water supply from the drainage basin of the Scheldt
- Increasing the storage capacity by creating controlled inundation areas
- Further deepening of the navigation channel

Not only the individual effects, but also the combined (cumulative) effects of planned interferences are important.

In a separate document (Bruens *et al.*, 2006) additional to this report, the management issues are further analysed (in terms of parameters, time and spatial scales). Interviews with managers are incorporated in this document. Attention is paid to experiences with / expectations from the usage of model results in management (decision taking).

NB: Light climate is primarily steered by the finest fraction near the surface. The requirements for light modelling are therefore different than those for modelling SPM flux or harbour siltation. If sufficient fractions are modelled, the model can be optimised for both purposes. With just two fractions (marine and fluvial) optimal settings for the SPM flux and siltation may be sub-optimal regarding light climate modelling. The SPM concentration is only one of the factors determining the light climate. Other factors are: particle size, shape and composition, fraction of organic matter etc.

3 Data analysis

From the literature analysis and the system description the following key numbers are reiterated:

- Vertical tide (neap/mean/spring): 4.49/5.24/5.93 m at Schelle (location of maximum tidal range)
- Tidal volume: > 10^9 m^3. In the mouth the sum of ebb and flood volume ≈ 2×10^9 m^3.
- Freshwater discharge (summer/mean/winter): 20/120/600 m^3/s = 5.3×10^6 m^3 (mean) per tide
- Residence time freshwater: 2 – 3 months
- Average SPM concentration: 50 mg/l
- Tidal variation SPM: factor 2 to 5
- Neap-spring variation SPM: factor 1.5 to 2
- Seasonal variation SPM: factor 2
- Vertical concentration gradients: factor 2 to 10
- Siltation: slikken: increasing down-estuary from 0.2 to 1.7 cm/y (average 0.6 cm/y) towards the Belgian-Dutch border (Wartel and Van Eck, 2000), 0.8 – 1.7 cm/y at Saeftinghe salt marsh; two orders of magnitude faster at harbour basins: 1.3 cm/day at Kallo sluice (Verlaan, 1998). Tidal marshes: 1–2 cm/y according to Temmerman (2003). Harbour siltation: 1.2 MT/y (derived from dredging volume).
- Available mass of sediment (Van Maldegem, 2002):
    - 13 MT in the bed
    - 0.1 – 0.4 MT suspended
    - load from sea and upstream: 0.2 MT/y
    - load from dumping: 1.5 MT/y

From the available data of the Scheldt estuary, the following data are analysed herein in some detail:

- 13h-data NAUWESB 1970 – 1981 (Figure 3.1)
- MWTL-data (Figures 3.6 – 3.10): mean values and seasonal dynamics
- data from Western Scheldt tunnel project on point measurement at DOW (12/1998 – 2/2002) (local water depth –19 m NAP) at levels –4, –11 and –17 m and Baalhoek (12/1998 – 11/2000) (local water depth –9.5 m NAP) at levels –4.5 and –8 m.
- data from the Lower Sea Scheldt between Zandvliet (near the Belgian-Dutch border) and Schelle.

These are the main data sources to be used for the calibration of the mud transport model of the Scheldt estuary. For an overview of all data is referred to Van Maldegem (2002).

3.1 NAUWESB 13h-data 1970 – 1981

The NAUWESB dataset consists of 172 13h measurements in the Western Scheldt between Bath and Wielingen. The data have been collected in the period 1970 – 1981. Figure 3.1 shows the locations of the monitoring locations. The 172 locations can be divided into 10 sub-areas, which are shown in Table 3.1

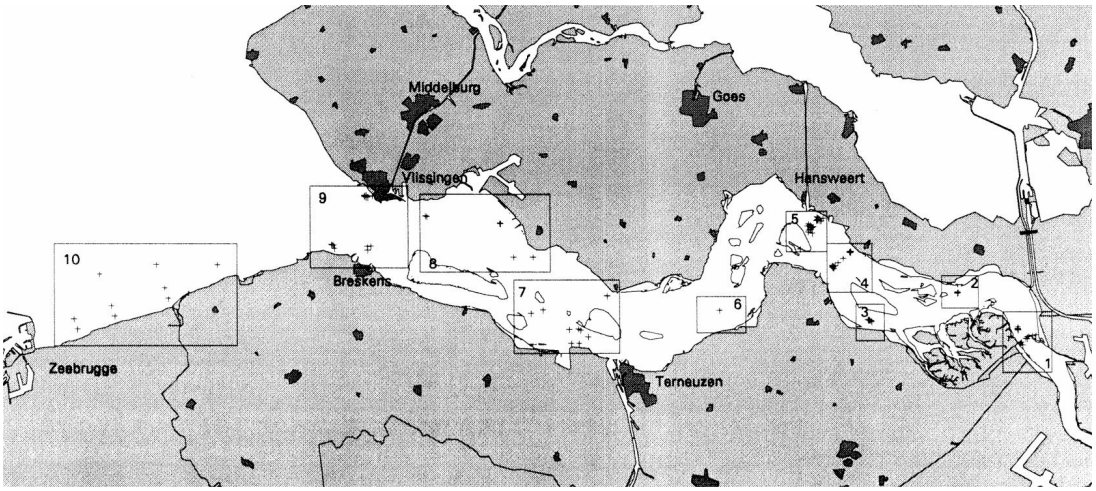

Figure 3.1: Locations and sub-areas with 13-hour measurements in the Western Scheldt according to file NAUWESB (1970 – 1981) (Mulder, 1995).

Gebied		Metingen (code)	Aantal	Geografische namen
bath	1	M49, M150-M172	24	Vaarwater boven Bath
zimmerm	2	M50-M63	14	Zimmermangeul
zgoost	3	M82-M86, M92, M101-M104	10	Zuidergat (oost)
zgatsvw	4	M64-M73 / M105-M124	30	Schaar van Waarde / Zuidergat (west)
hansweert	5	M48, M74-M81, M87-M91, M93-M100, M125-M149	47	Hansweert
ossenis	6	M47	1	Gat van Ossenisse
everter	7	M36, M37, M39-M46	10	Everingen-Terneuzen
honte	8	M29, M30 / M28, M35 / M34, M38	6	Honte (west) / Honte (oost) / Honte-Everingen
vlisbres	9	M15, M17, M18, M20-M22 / M24-M27 / M31-M33	13	Sardijngeul / Wielingen (oost) / Spijke-Hoofdplaat
wieling	10	M4-M14	11	Wielingen (west)
oostelijk deel		bath, zimmerm, zgoost, zgatsvw, hansweert, ossenis	126	
westelijk deel		everter, honte, vlisbres, wieling	40	
rest		M1-M3 / M16, M19 en M23	6	Middeldiep / Oostgat
Totaal		M1-M172	172	

Table 3.1: Subdivision in areas 1 – 10 = Bath – Wielingen.

Gebied	Aantal profielen	$c(0)/\bar{c}$		$c(h)/\bar{c}$	
		gem.	s.d.	gem.	s.d.
bath	245	1.62	1.08	0.60	0.25
zimmerm	163	1.20	0.56	0.92	0.37
zgoost	117	1.28	0.37	0.78	0.18
zgatsvw	328	1.47	0.77	0.70	0.24
hansweert	596	1.55	0.92	0.66	0.26
ossenis	18	1.30	0.80	0.74	0.22
everter	87	4.11	5.99	0.46	0.32
honte	47	3.98	4.09	0.41	0.31
vlisbres	109	2.14	2.18	0.63	0.25
wieling	124	4.03	3.94	0.41	0.25
Som deel-gebieden	1834	1.88	2.19	0.66	0.29
oostelijk deel	1467	1.48	0.86	0.70	0.28
westelijk deel	367	3.48	4.23	0.49	0.29
Totaal	1891	1.88	2.16	0.65	0.29

Table 3.2: Characteristics concentration profiles. c(0) is at the bed, c(h) is at the water surface.

The NAUWESB concentration measurements were made from survey vessels using sampling bottles. The measurement of one vertical took 5 to 20 minutes, starting near the bottom. The lowest measurement level was about 0.5 m above the bed, the highest level was about 0.5 m below the water surface. The current velocities were measured with an Ott propeller flow meter mounted on an ELMAR frame.

Table 3.2 shows the characteristics of the vertical concentration profiles. It is evident that the western part of the Western Scheldt is more stratified than the eastern part. At Everingen-Terneuzen, Honte and Wielingen the concentration at 0.5 m above the bed is approximately 10 times higher than the concentration near the surface. In the eastern part, the ratio C_{bed}/C_{surf} is typically only 2. This transition also shows up in Fig. 3.2, where the tide-averaged SPM concentration is shown for sections 1 – 11 near the surface, near the bed and depth-averaged. Near the surface the concentration is circa 50 mg/l throughout the Western Scheldt (though with some variation). Near the bed the concentration ranges between about 100 mg/l in the eastern part and 300 mg/l in the western part.

For all 172 13h measurements, the following plots are available:

1. current velocity in time at several levels in the vertical
2. SPM concentration in time at several levels in the vertical
3. SPM concentration as a function of depth at a number of times over the tide
4. SPM concentration as a function of the current velocity over the tide

For data-set M39, which was measured at 10/4/1970 at the Pas van Terneuzen, plots of type 1 and 2 are shown in Figure 3.3. This location (with Paris coordinates X, Y = 43651, 375410) lies just 720 m north of the jetty at DOW (X, Y = 43631, 374687). It is remarkable that the vertical concentration gradient is much larger for the M39 location compared with the observation point at the DOW-jetty. This can only be partly attributed to the fact that the lowest observation point is at 0.5 and 2 m above the bed, respectively. Although the depth of both locations is similar (18 m and 19 m, respectively), location M39 is situated on the northern edge of the main channel towards the Middelplaat.

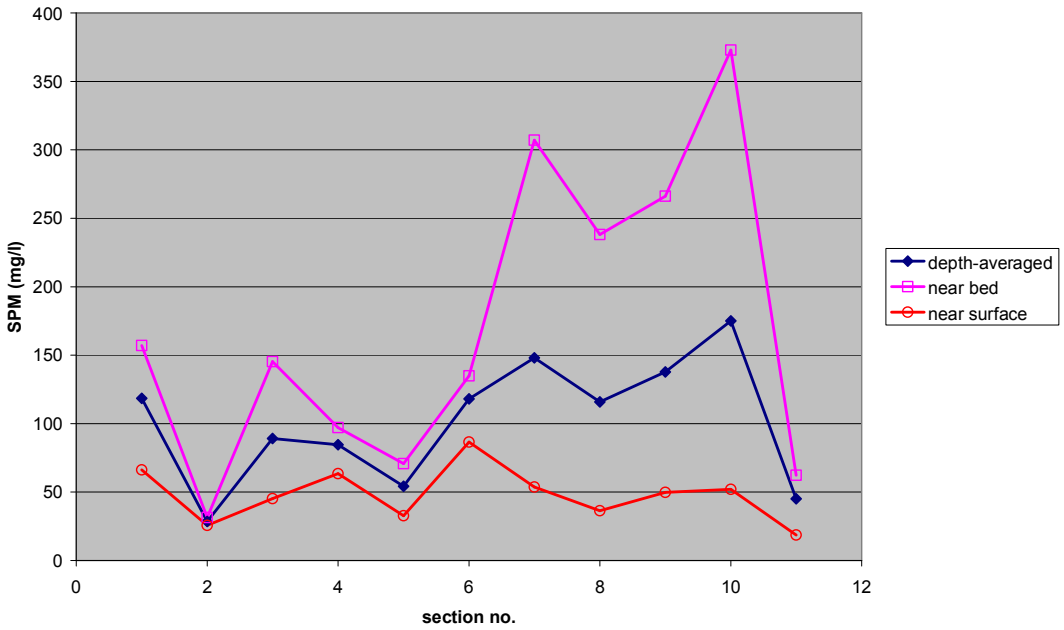

Figure 3.2: Tide-averaged SPM concentrations at the surface, near the bed and depth-averaged from sections 1 (Bath) towards 10 (Wielingen) (see Fig. 3.1, NAUWESB dataset). Section 11 is the Oostgat.

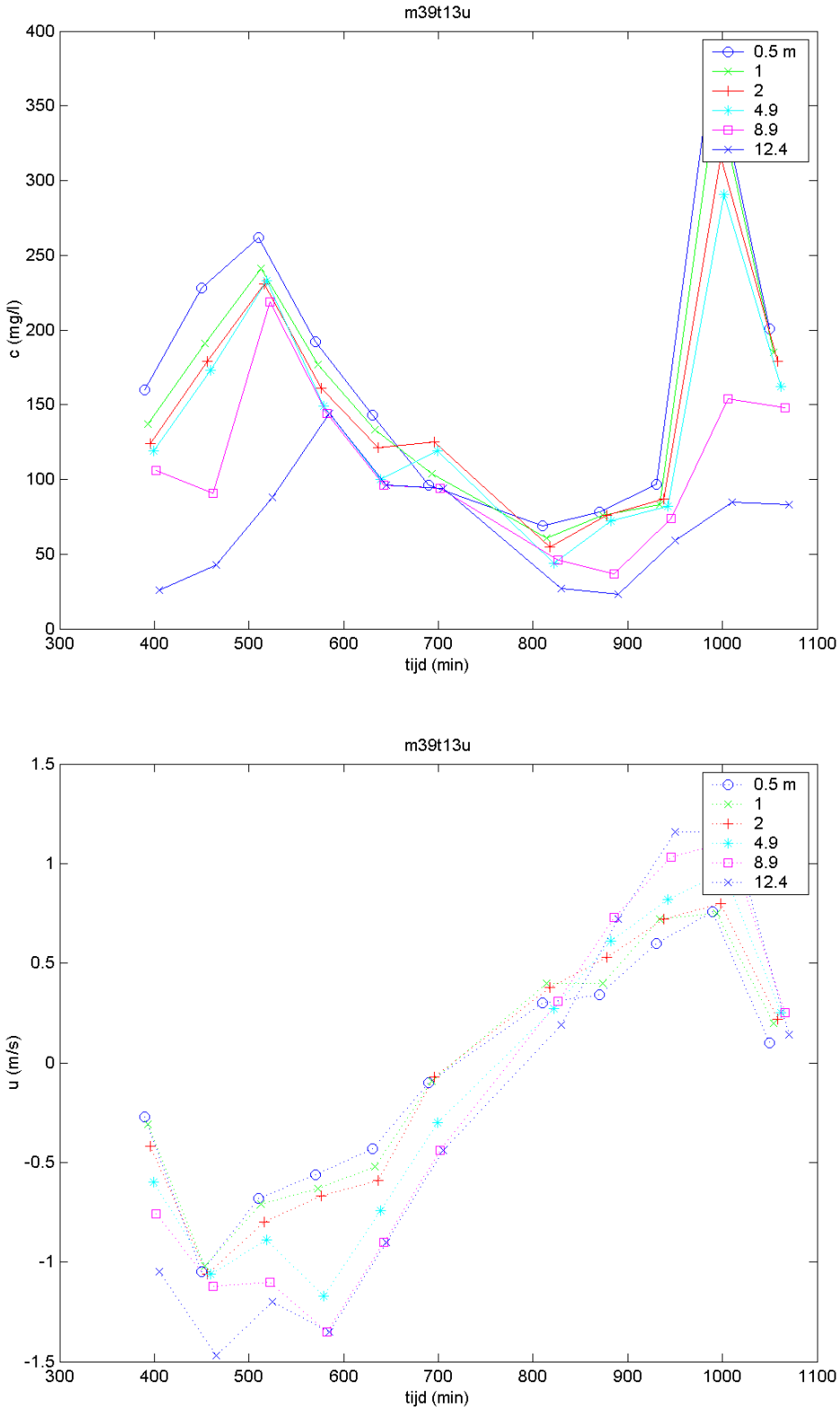

Figure 3.3: SPM concentration (top) and velocity (bottom) in Pas van Terneuzen at 10/02/1970, location (X,Y) = 43651, 375410.

3.2 MWTL-data Western Scheldt

The MWTL dataset is used to investigate the spatial and seasonal variations of the SPM levels in the Western Scheldt. Figure 3.4 shows the locations of the monitoring stations and Table 3.3 shows their names, observation period, number of samples and their statistical characteristics (mean, median, 10- and 90-percentile). All samples are taken at 1 m below the water surface at irregular intervals. Although being irregular, the sampling intervals are not random: some locations are often sampled during the same phase of the tide. The average values should therefore not be considered as representative tide-averaged concentrations.

The SPM concentrations are determined from water samples taken from the subsurface. The samples are taken at reported depths varying between 1 and 4 m below the surface before 1990 and at 1 m below the water surface after 1990. In the period 1995 – 1983 the sampling time was fixed with respect to the tidal phase, from 1994 the sampling time was arbitrary. In the data series some bias towards calm period is introduced as the survey vessel operation stops for wave heights over 2 m. The most frequently sampled stations are sampled at a fortnightly interval. Some other stations are sampled much less frequently.

Two aspects from the MWTL data are evident:

1. The SPM concentration in the Western Scheldt increases both towards the Dutch Belgium border and towards the North Sea (Fig. 3.5). The latter increase may be related to the turbidity maximum near Zeebrugge. The SPM concentration off the coast of Walcheren and in the Oostgat is much lower than in the southern part of the estuary mouth. The NAUWESB dataset shows a similar concentration distribution in the estuary mouth (Fig. 3.3) .
2. The SPM concentration shows a clear seasonal trend: in winter the concentration is much higher than in summer (see Figs. 3.6 – 3.10). The seasonal variability is at least a factor 2.

Both aspects should be reproduced by the mud transport model.

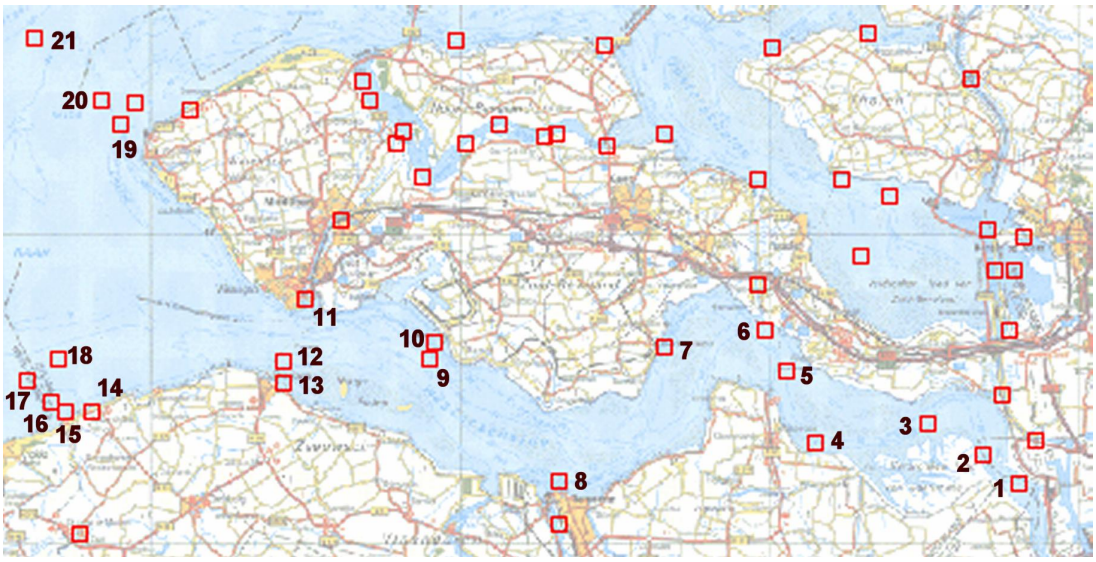

Figure 3.4: Locations of MWTL monitoring stations (see also Table 3.3).

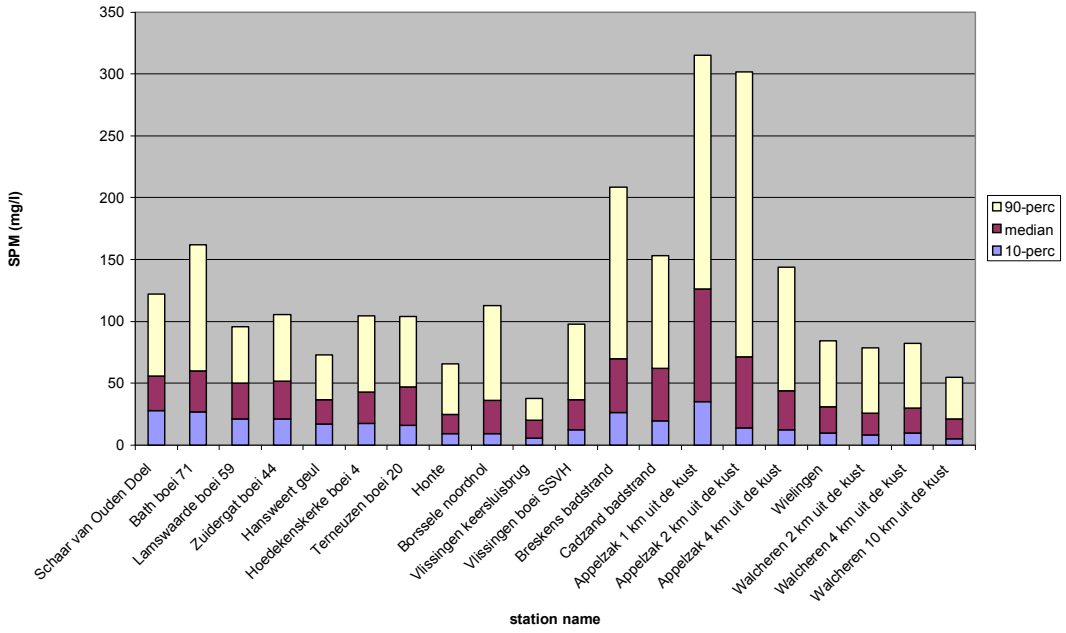

Figure 3.5: Median, 10- and 90-percentile values of observed SPM concentration at the Western Scheldt.

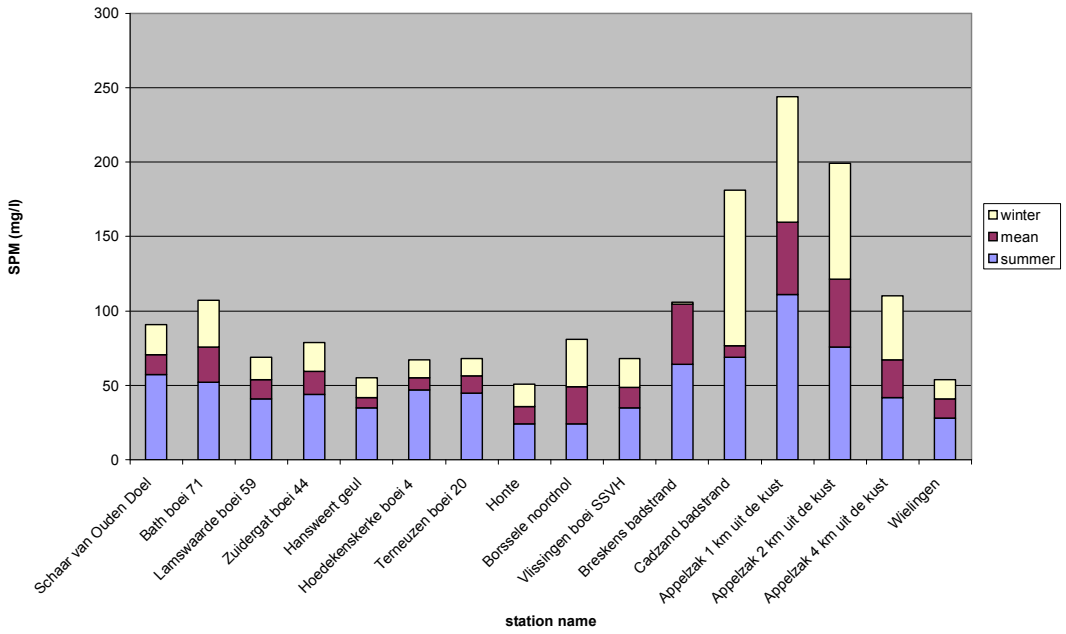

Figure 3.6: Year mean, winter mean and summer mean observed SP concentration at the Western Scheldt.

Stat. no.	Station Name	Period	No. points	mean	10-perc.	50-perc.	90-perc.	st. dev.
1	Schaar van Ouden Doel	1/78 – 12/05	608	71	28	56	122	56
2	Saeftinge boei 76	1/78	1 (!)	14				
3	Bath boei 71	1/88 – 12/95	102	76	27	60	162	54
4	Lamswaarde boei 59	1/85 – 12/96	146	54	22	50	96	30
5	Zuidergat boei 44	1/88 – 12/95	102	59	21	52	106	33
6	Hansweert geul	1/82 – 12/05	462	42	17	37	73	22
7	Hoedekenskerke boei 4	1/88 – 12/05	217	55	18	43	105	43
8	Terneuzen boei 20	1/82 – 12/05	466	56	16	47	104	41
9	Honte	1/88 – 12/95	102	36	9	25	66	34
10	Borssele noordnol	1/88 – 12/95	102	49	9	36	113	47
11	Vlissingen keersluisbrug	1/75 – 11/86	195	22	5	20	38	19
12	Vlissingen boei SSVH	1/82 – 12/05	594	49	12	37	98	41
13	Breskens badstrand	6/88 – 10/95	53	105	26	70	209	119
14	Cadzand badstrand	5/85 – 10/95	118	77	20	62	153	67
15	Appelzak 1 km	5/75 – 2/83	177	160	35	126	315	143
16	Appelzak 2 km	5/75 – 2/88	318	121	14	72	302	133
17	Appelzak 4 km	5/75 – 2/83	177	67	12	44	144	72
18	Wielingen	10/91 – 12/05	246	41	10	31	84	36
19	Walcheren 2 km	5/75 – 12/05	466	36	8	26	79	31
20	Walcheren 4 km	5/75 – 2/83	179	40	10	30	82	36
21	Walcheren 10 km	5/75 – 2/83	176	27	5	21	55	25

Table 3.3 Overview of MWTL monitoring stations in the Western Scheldt (see also Fig. 3.4) with SPM data statistics measured at 1 m below the water surface.

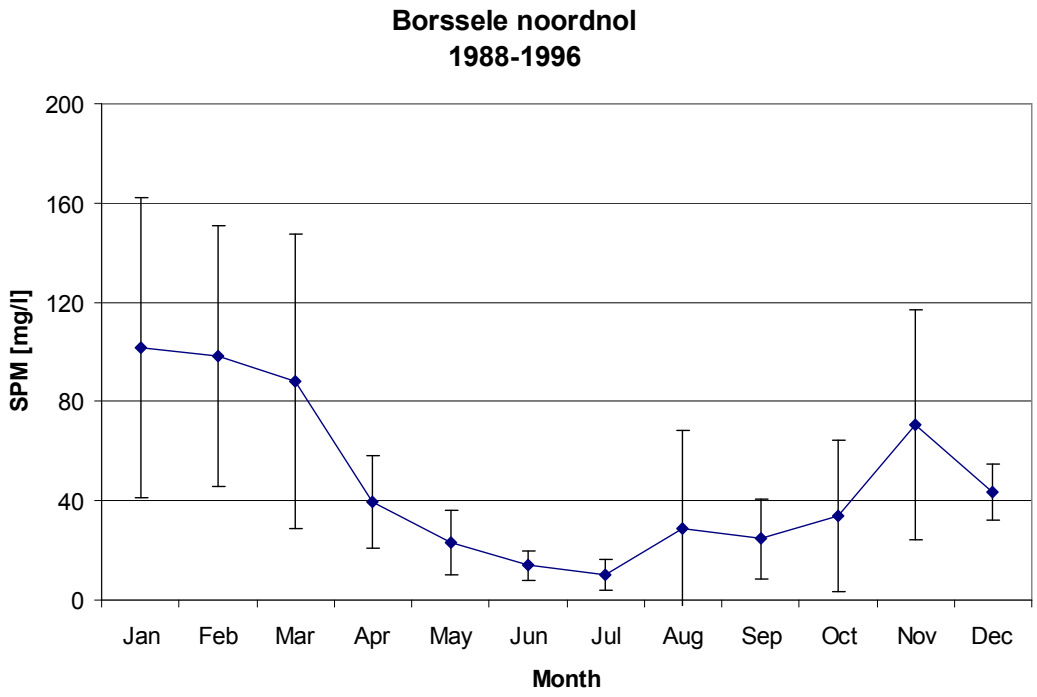

Figure 3.7: Seasonal concentration fluctuations at Borssele noordnol, period 1988 – 1996 (n_{obs} = 102)

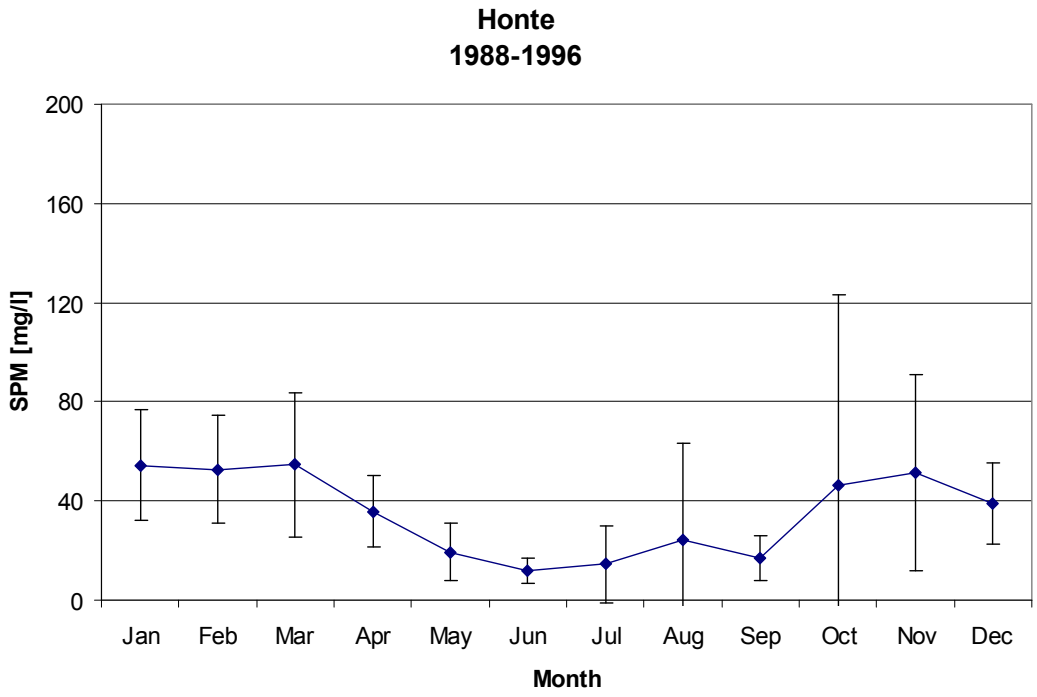

Figure 3.8: Seasonal concentration fluctuations at Honte, period 1988 – 1996 (n_{obs} = 102)

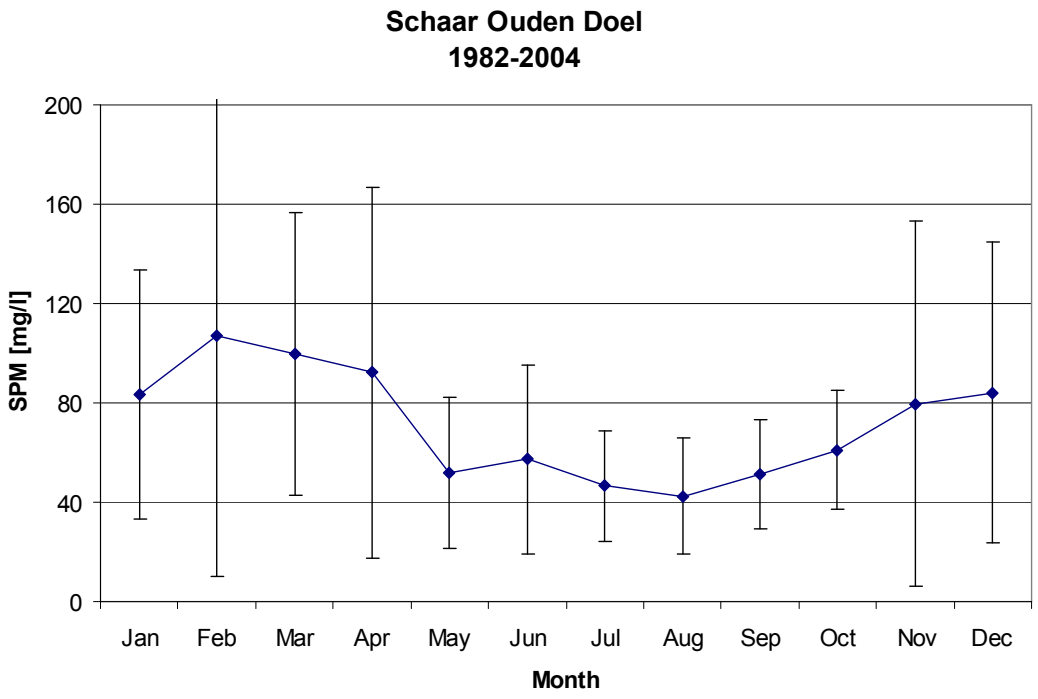

Figure 3.9: Seasonal concentration fluctuations at Schaar Ouden Doel, period 1982 – 2004 (n_{obs} = 608)

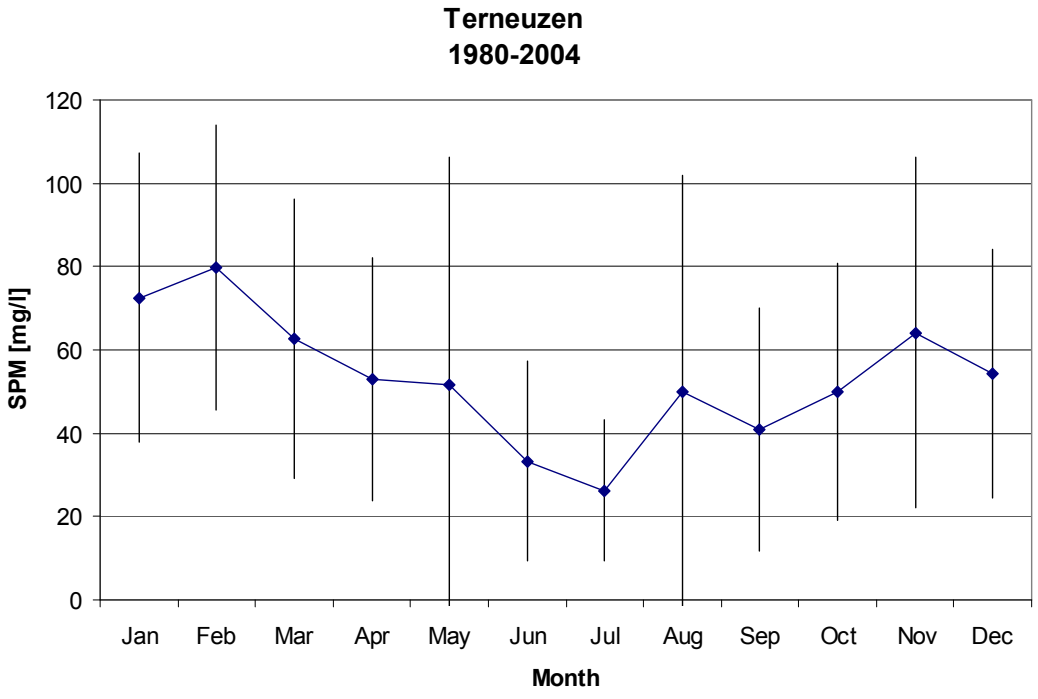

Figure 3.10: Seasonal concentration fluctuations at Terneuzen, period 1980 – 2004 (n_{obs} = 466)

3.3 Data from Western Scheldt tunnel project at Terneuzen

Figures 3.12 – 3.19 show the main characteristics regarding SPM levels of measuring campaign in the framework of the Western Scheldt tunnel project. The SPM levels were determined optically with MEX3001 turbidity sensors. The calibration curves were based on water samples taken at a 4-weekly interval. Note that slurry release took place between 1 November 1999 and 31 December 2001 near the observation point at Terneuzen. Within this time window, the observed SPM concentration may be temporarily be increased with respect to the natural background concentration because of this slurry release. Two observation points were installed: one at DOW jetty (period 12/1998 – 2/2002) (local water depth –19 m NAP) at levels –4, –11 and –17 m and another at Baalhoek (12/1998 – 11/2000) (local water depth –9.5 m NAP) at levels –4.5 and –8 m. Figure 3.11 shows an aerial photograph of the vicinity of the DOW jetty at Terneuzen.

The following conclusions may be drawn from this dataset:

- The SPM concentration is vertically quite uniform.
- The SPM fluctuations have a strong tidal component M2, M4 and S2 (12.5h tide and neap-spring cycle)
- The marked seasonal fluctuation appears to be caused by a combination of freshwater discharge and wind climate (N.B. non-physical effects forcing the seasonal cycle such as biological activity are presently excluded from the model, although they may have a significant contribution. Examples of biological activity: 1. production of SPM from algal growth; 2. stabilisation of tidal flats).

This dataset will be used first for a 1-point calibration simulations. The settings found in these simulations will be applied in the 3D sediment transport model and will then be further optimised.

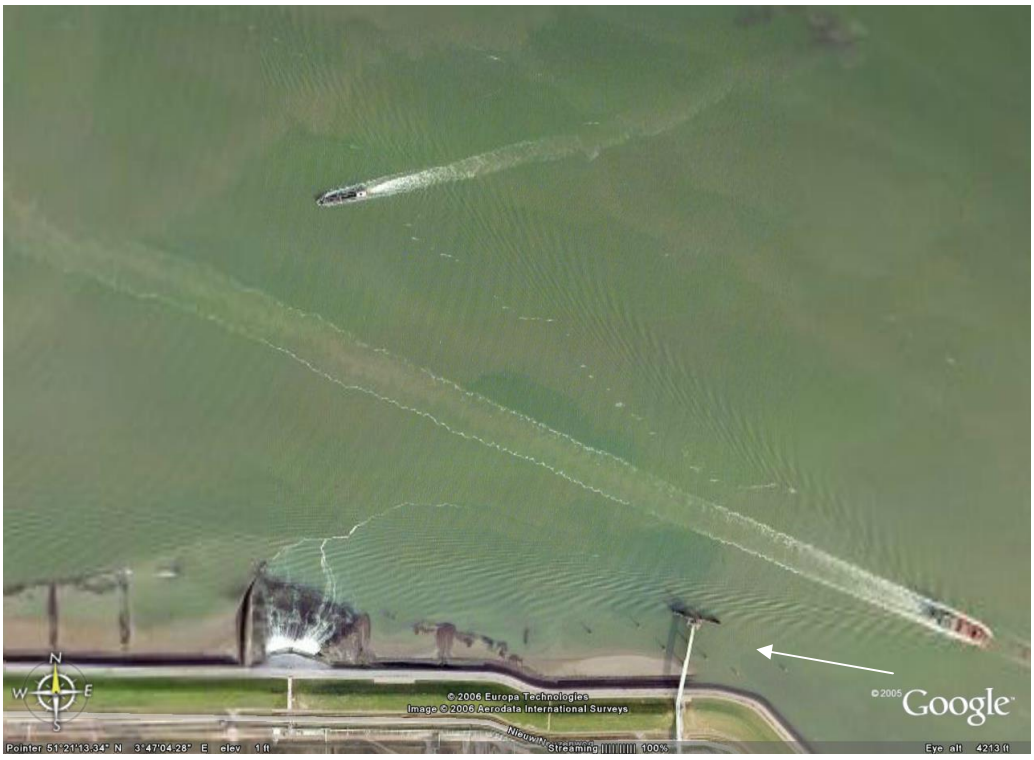

Figure 3.11: Jetty at DOW Terneuzen on which the instruments were mounted.

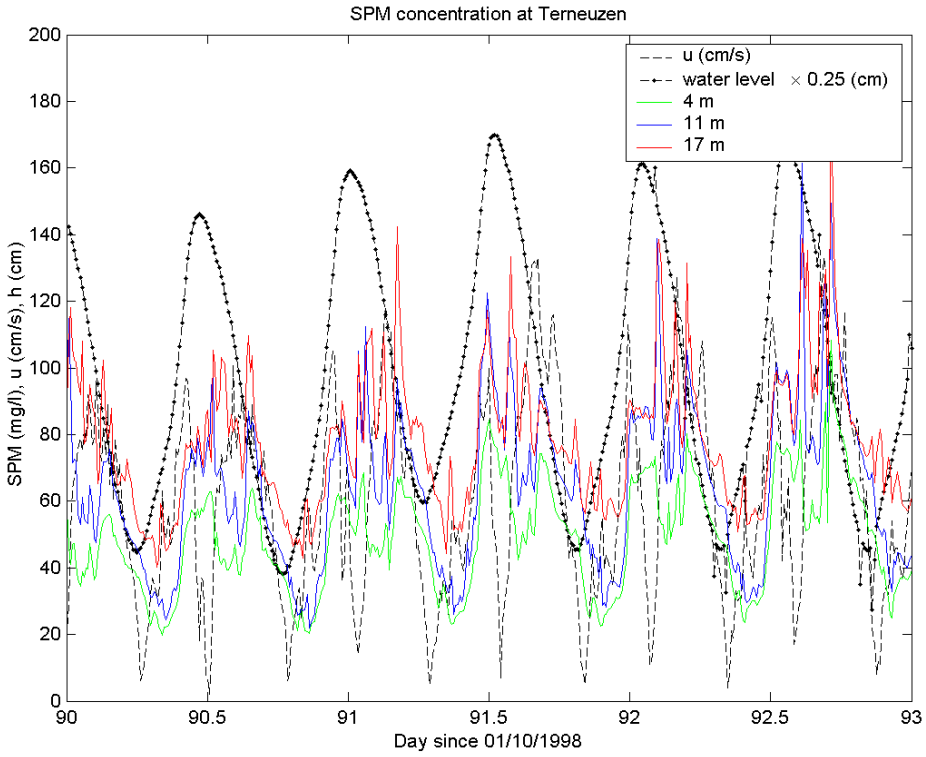

Figure 3.12: SPM concentration at Terneuzen at 3 vertical levels. The water level and velocity fluctuations are also shown. Note: reference water level = 1 m above NAP.

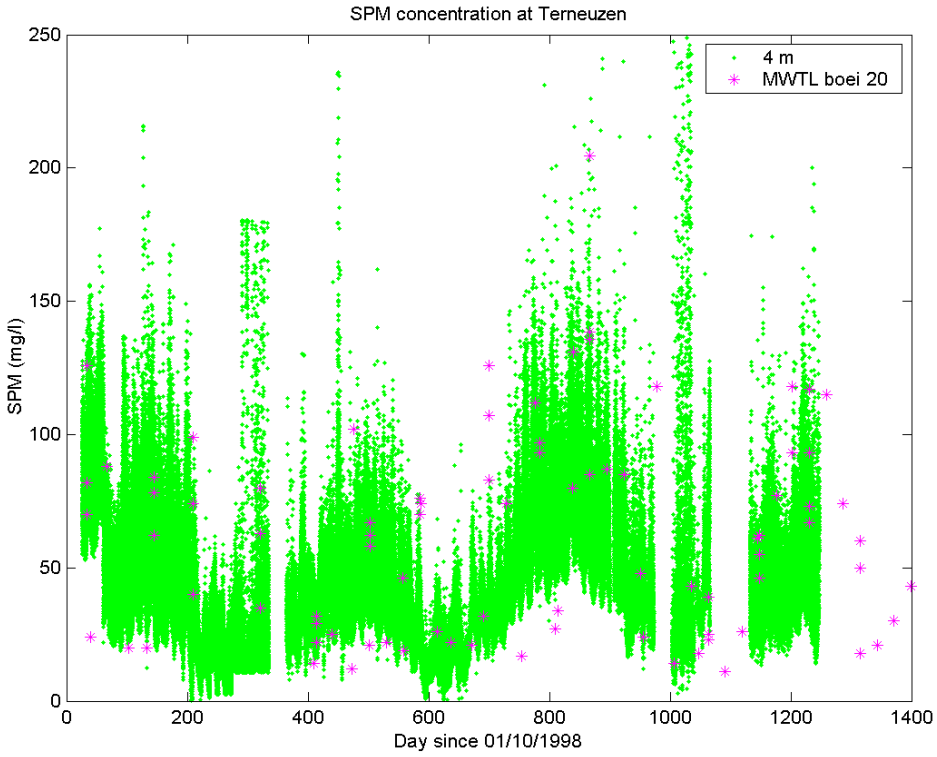

Figure 3.13: SPM concentration at Terneuzen. Green: 4 m below the water surface, 10-minute mean. Purple: 1 m below the water surface, MWTL data at nearby boei 20.

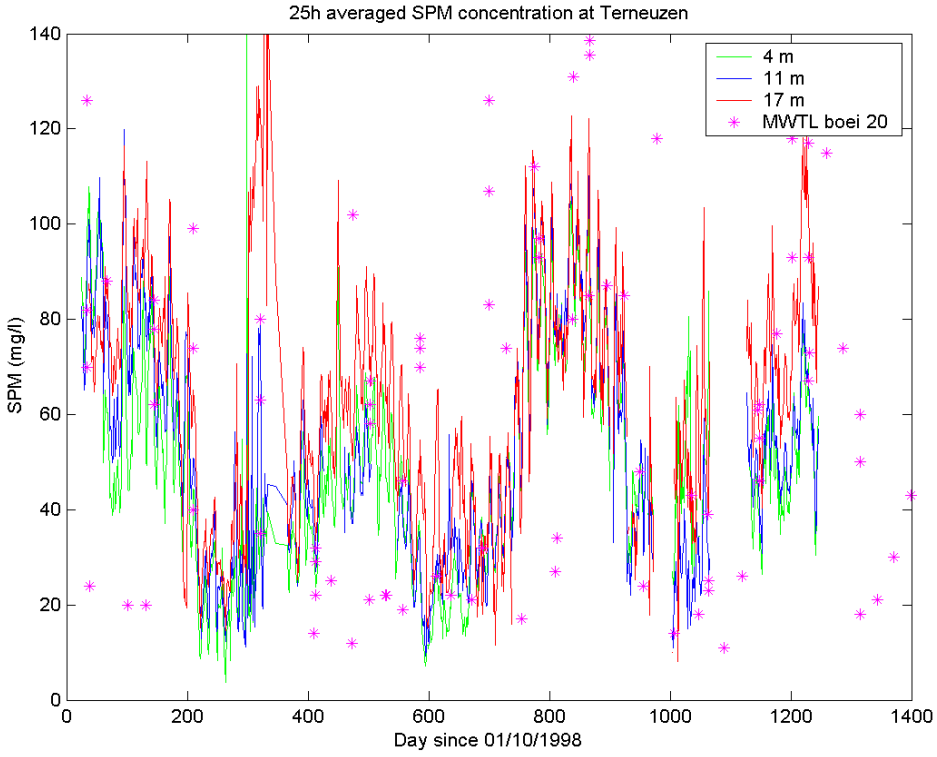

Figure 3.14: : 25h-mean SPM concentration at Terneuzen at 3 vertical levels. Purple stars: 1 m below the water surface, MWTL data at nearby boei 20

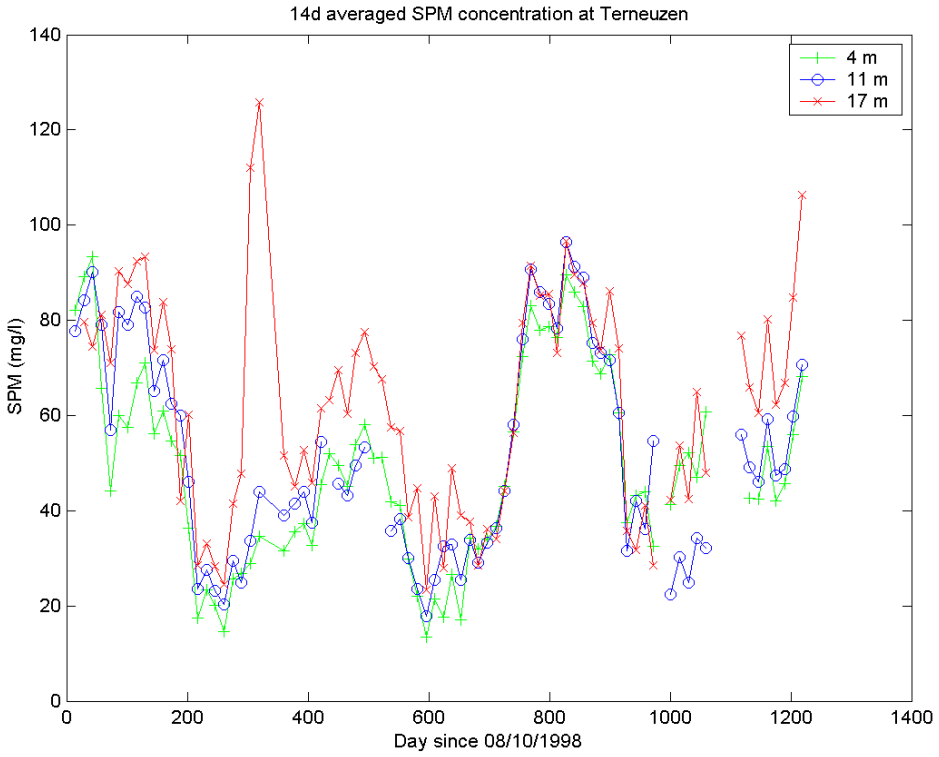

Figure 3.15: 14d-mean SPM concentration at Terneuzen at 3 vertical levels.

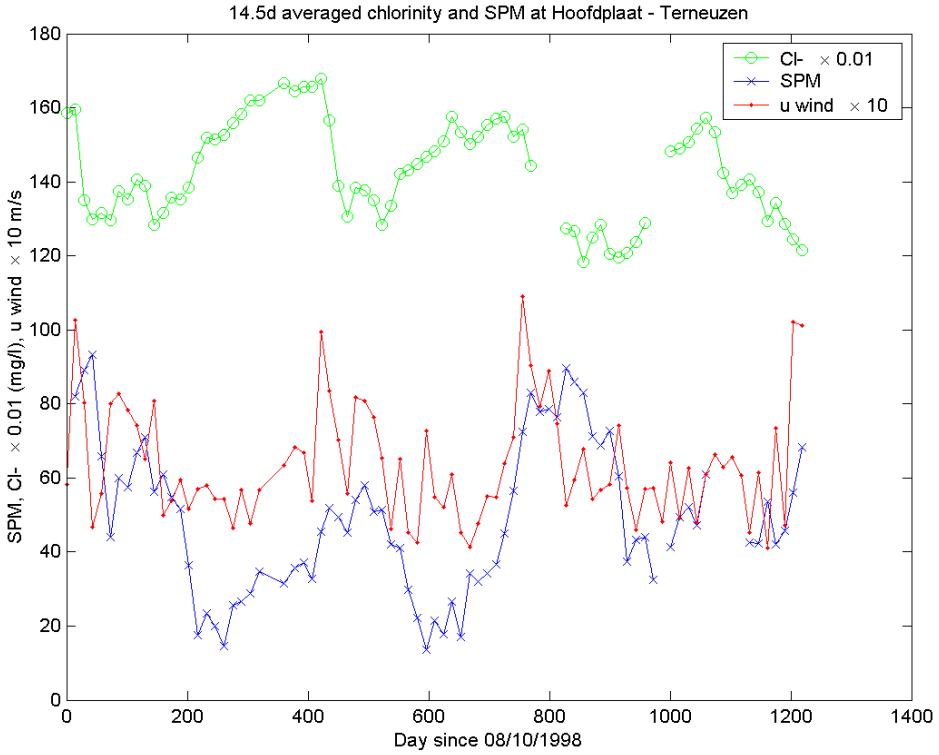

Figure 3.16: 14d-mean SPM concentration at Terneuzen at 4 m below NAP. Also shown is the 14d mean chlorinity and wind speed.

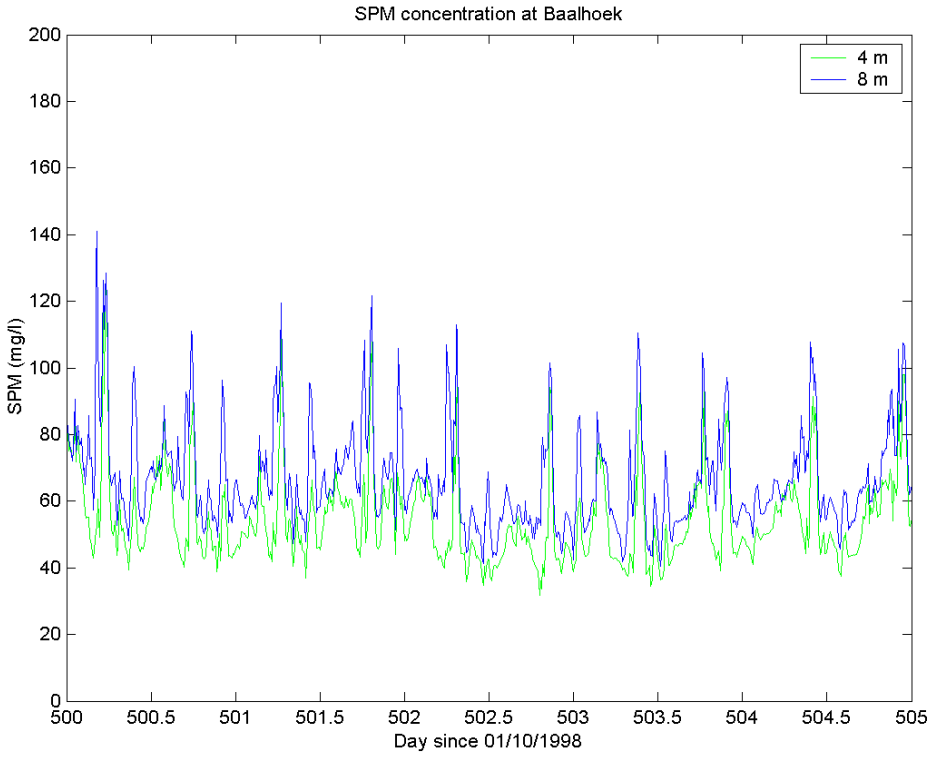

Figure 3.17: SPM concentration at Baalhoek at 4 m and 8 m below NAP (10-minute mean values).

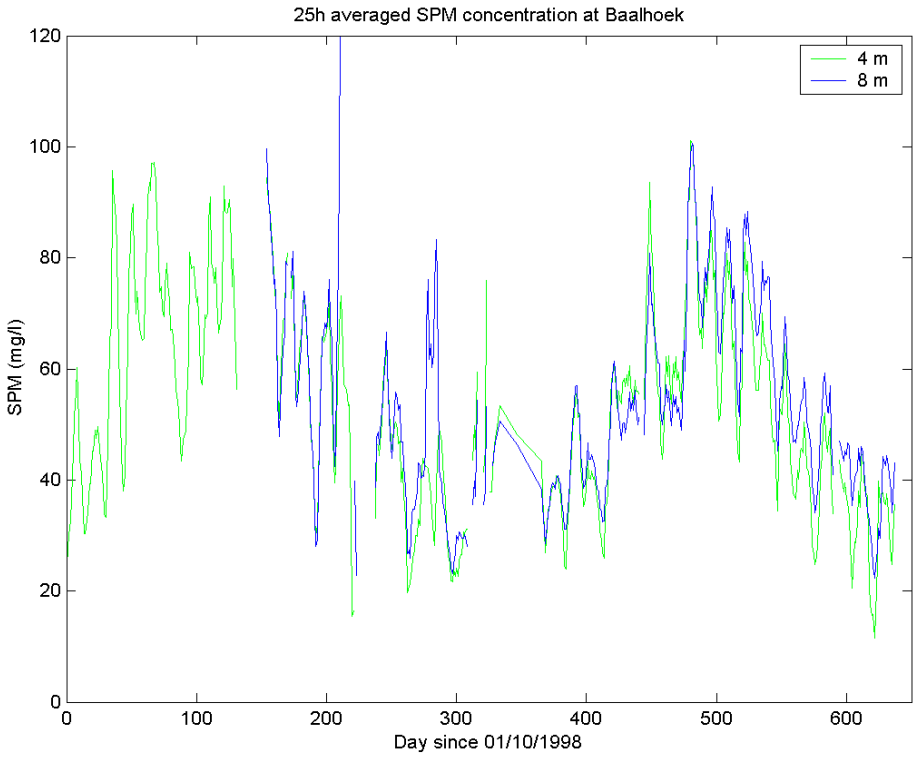

Figure 3.18: 25h mean SPM concentration at Baalhoek at 4 m and 8 m below NAP.

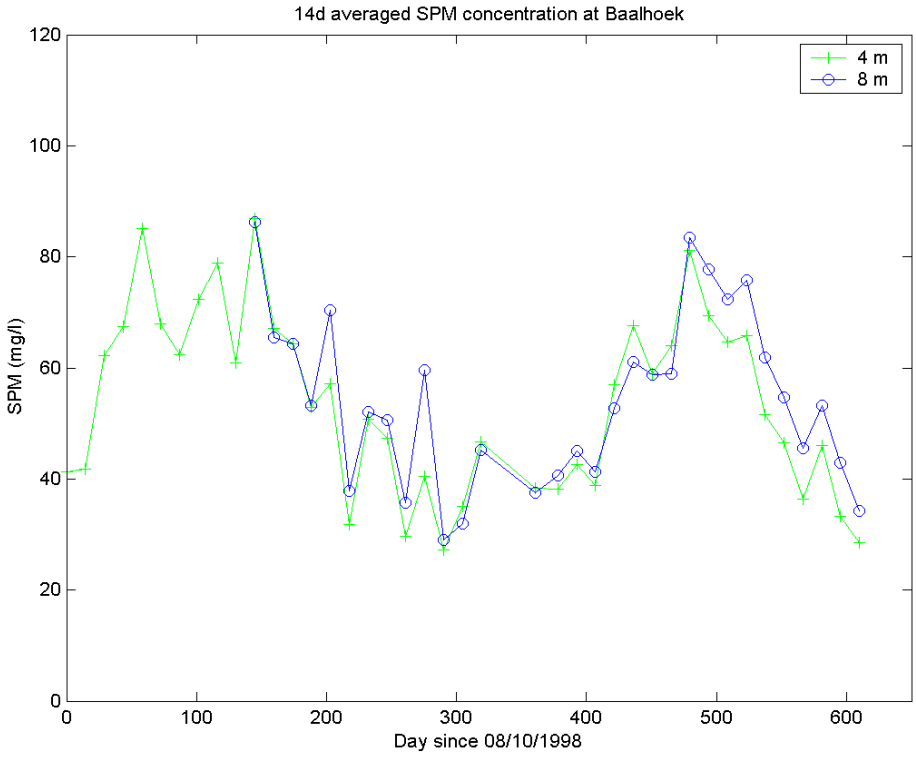

Figure 3.19: 14d mean SPM concentration at Baalhoek at 4 m and 8 m below NAP.

3.4 Mud percentage in the bed

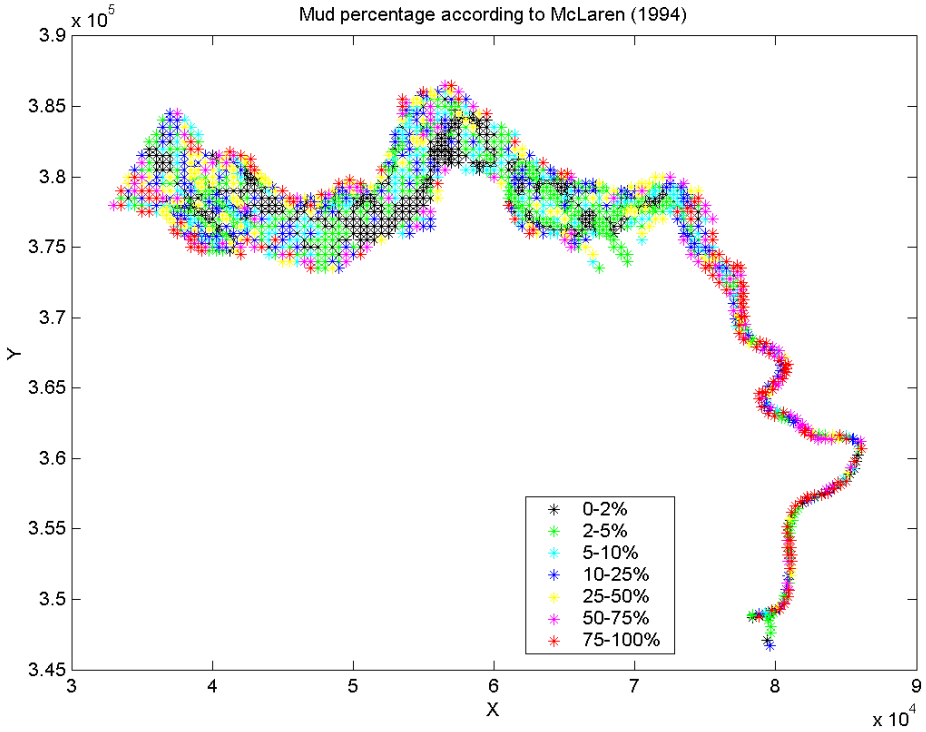

Figure 3.20: Percentage of sediment < 64 μm in the bed. After McLaren (1994).

3.5 Data on Lower Sea Scheldt

3.5.1 Relative fluvial sediment supply and freshwater discharge

Based on the operational sediment data acquisition infrastructure, a relationship has been established between the sediment flux and the average current velocity for the upper reaches of the estuary. Figure 3.21 illustrates this relationship for Dender Overboelare. The sediment flux can be estimated from SPM point measurements. This relationship is still under investigation, but it is a promising approach to estimate the fluvial sediment supply. The available dataset covers the period 1999 – 2005.

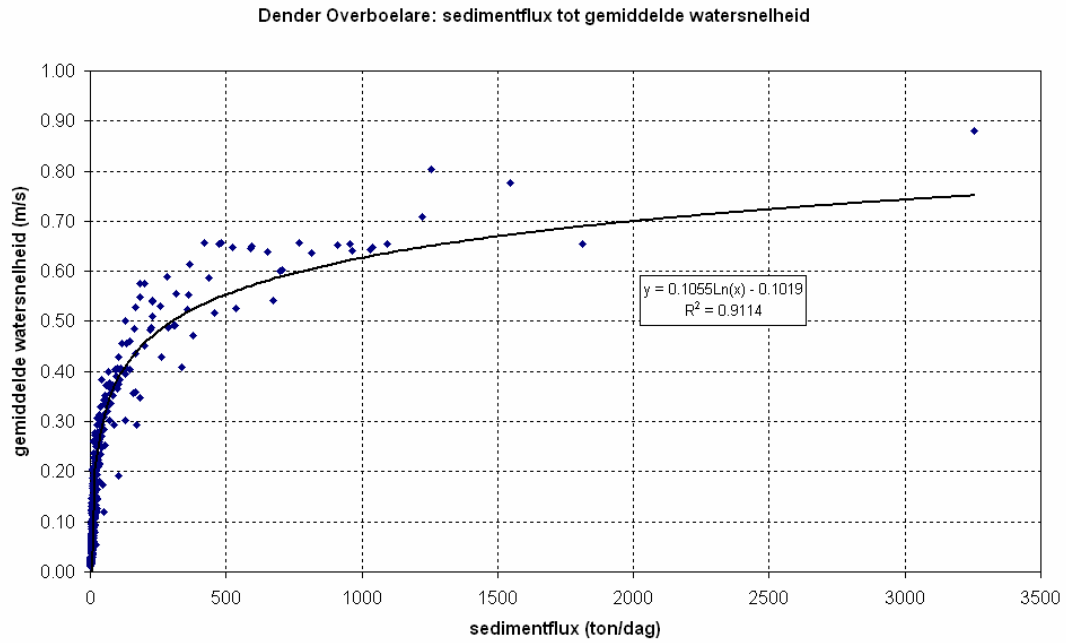

Figure 3.21: Relationship between average current velocity and sediment flux at Dender Overboelare.

3.5.2 Study Oosterweel tunnel link

In the framework of a study on the Oosterweel tunnel link SPM measurements on 3 locations have been commissioned by TVSAM (acronym for 'Tijdelijke Vereniging Studiegroep Antwerpen Mobiel'). Time series on current velocity and SPM levels are available from 5 sensors on 3 locations. Figure 3.22 displays the locations of the 3 measuring points (green dots). Information on the horizontal and vertical position of the 5 sensors is shown in Table 3.4. This dataset is similar to the dataset obtained for the Western Scheldt tunnel project at Terneuzen.

Location	Sensor Height [mTAW]	Bottom Height [mTAW]	Height above bottom	N [UTM ED50]	E [UTM ED50]	From	To
Oosterweel Right Bank Lower [TVSam]	-9	-11	2	596900	5677726	1-1-2005	31-12-2005
Oosterweel Right Bank Upper [TVSam]	-7	-11	4	596900	5677726	1-1-2005	31-12-2005
Hoboken [TVSAM]	-5	-7	2	593260	5671760	1-1-2005	31-12-2005
Boerenschans Lower [TVSAM]	-7	-9	2	592455	5679055	1-1-2005	31-12-2005
Boerenschans Upper [TVSAM]	-5	-9	4	592455	5679055	1-1-2005	31-12-2005

Table 3.4: Measuring locations TVSAM.

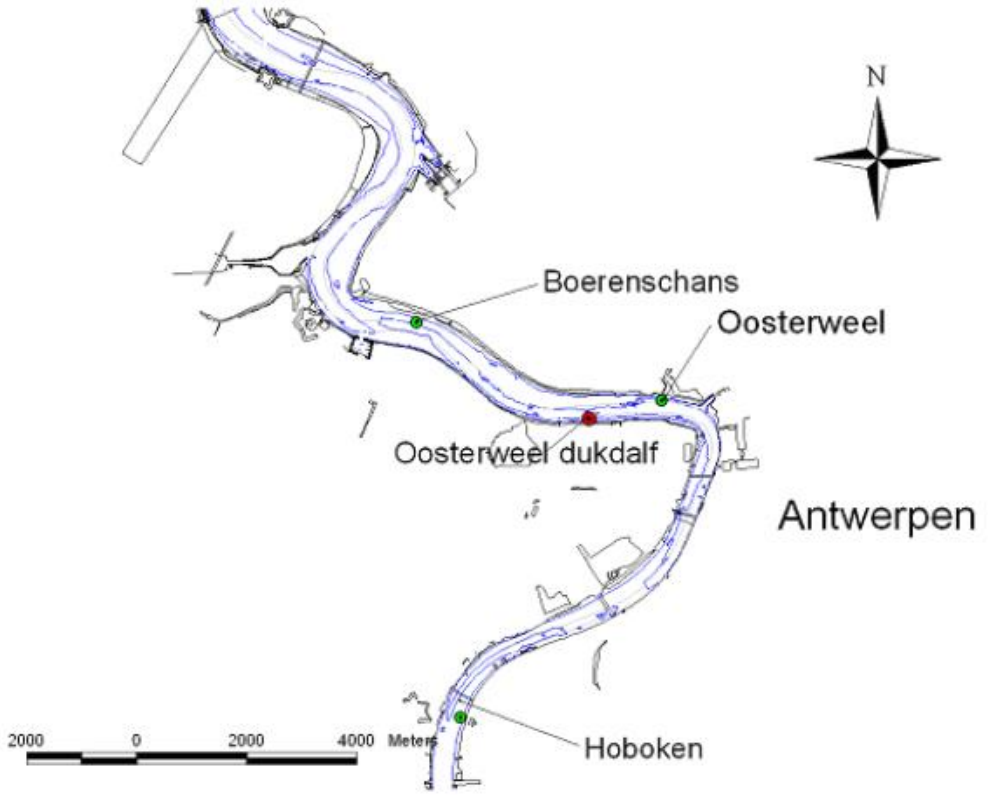

Figure 3.22: Measurement locations study Oosterweel tunnel link (green dots).

3.5.3 HCBS dataset

The HCBS measuring campaigns (High Concentration Bethic Suspensions) have been and will be carried out in separate steps between February 2005 and September 2006.
The dataset from February 2005 has been analysed for the major part and is concisely described below. This dataset has been acquired for the original layout with closed Deurganckdok (DGD). Similar measurements at similar locations are scheduled for Both March 2006 and September 2006 to:

- assess the impact of the opening of DGD on the current patterns and sediment concentrations;
- determine the summer and winter conditions for the situation with open DGD.

3.5.3.1 INSSEV measurements

The INSSEV measurements consist of an analysis of video images to determine the size and settling velocity of individual flocs. The measurements were carried out in February 2005 and were located at two positions: near the entrance of the future DGD and near Kallo sluice (see Figure 3.23). An example of the results obtained from these measurements is shown in Figure 3.24.

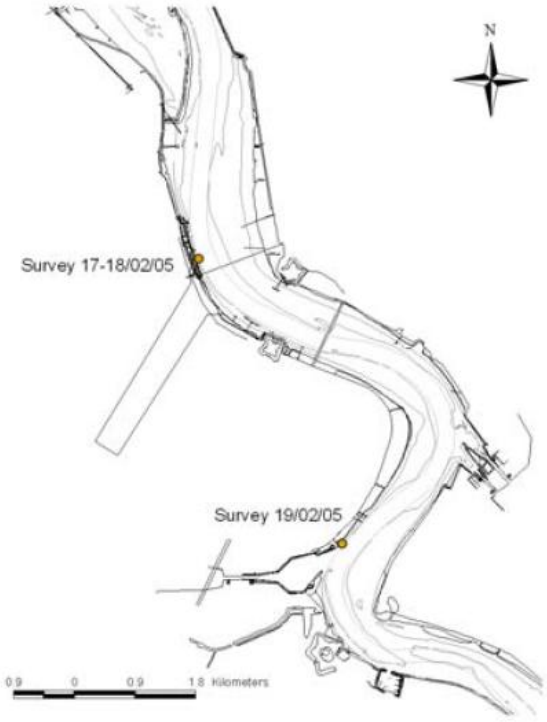

Figure 3.23: Location INSSEV measurements February, 2005.

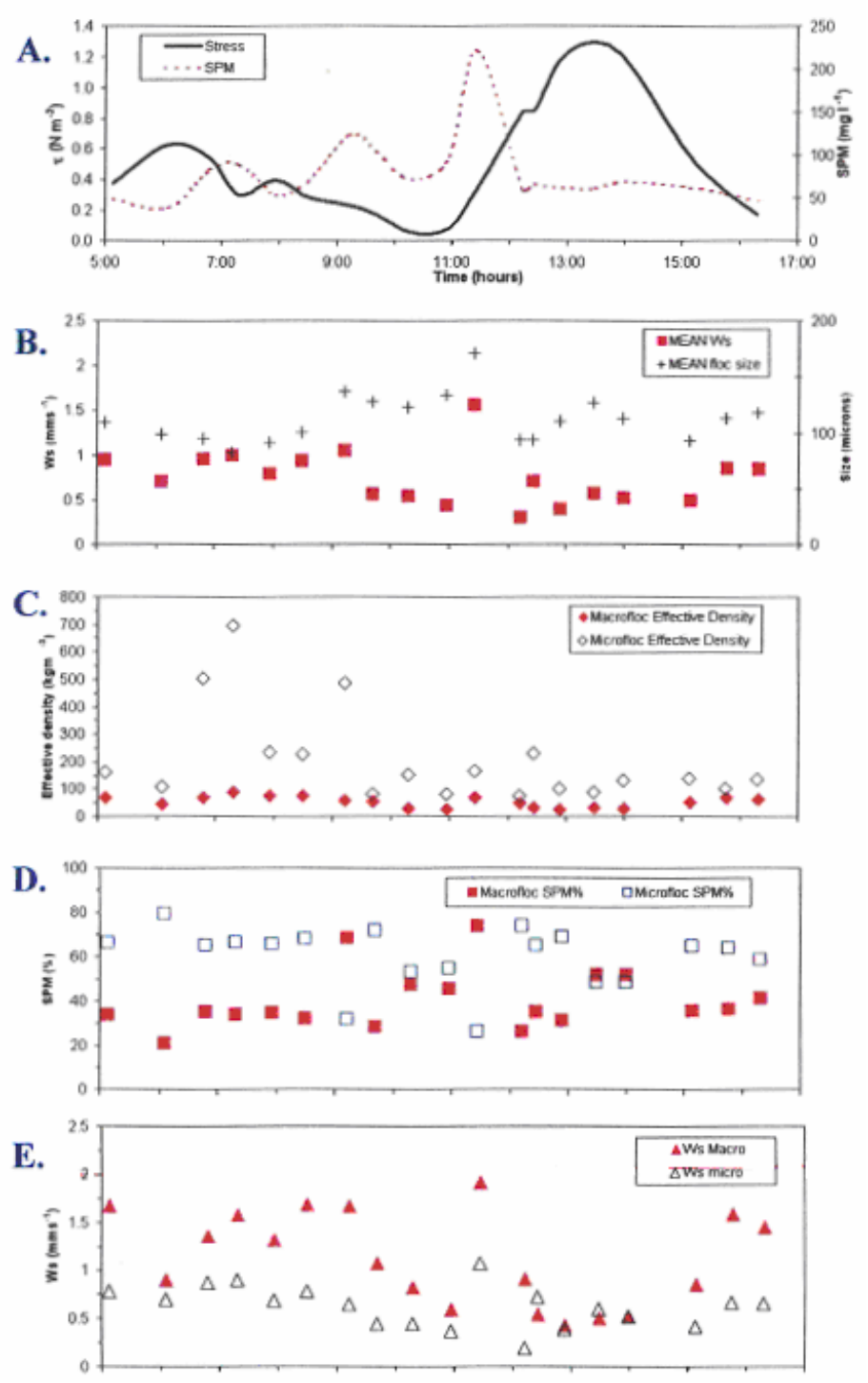

Figure 3.24: Results from INSSEV campaign February, 2005. Time series of floc properties for 18th February 2005. A) Shear stress & SPM, B) Mean floc size & settling velocity, C) Macrofloc & microfloc effective density, D) Macrofloc & microfloc SPM distribution, and E) Macrofloc & microfloc settling velocity.

3.5.3.2 ADCP and SEDIVIEW measurements

Figure 3.25 shows the transects along which current patterns, SPM concentrations and SPM fluxes were measured with an ADCP (the backscatter from the ADCP signal was correlated to the SPM concentration).

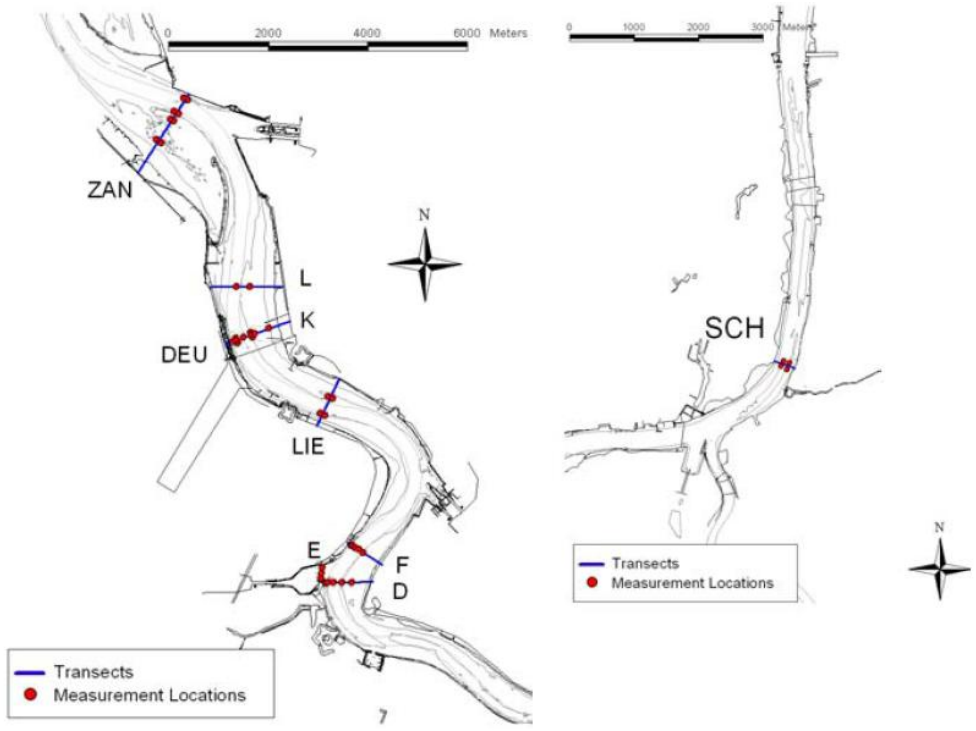

Figure 3.25: Locations of measured transects (near DGD and Schelle), February, 2005.

3.5.3.3 Siltprofiler measurements

The silt profiler has been developed to measure vertical sediment concentration profiles with a high spatial and temporal resolution. Silt profile measurements were carried out near DGD on February 16 and 17, 2005, and near Kallo sluice on February 18, 2006 (see Figure 3.26). The measurements give a very detailed insight into the vertical concentration profile at each location. A typical feature occurring in many profiles, is the strong curvature in the concentration profile close to the bed (Fig. 3.27). The measurements made at a number of times at a single location can be combined into a graph showing the time variation of the SMP concentration profile (Figure 3.28).

This dataset is unique in the sense that measurements were made very near to the bed, and that the design of the silt profiler allows for measurement with a very high vertical resolution (of about 1 cm) and up to a very high concentration (up to 50 g/l, but this value was never reached during the present data campaign).

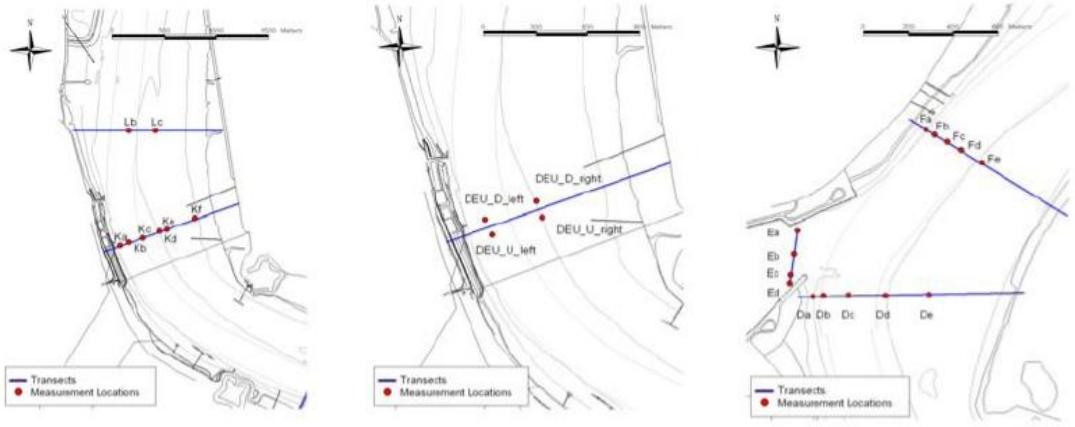

16/02/2005 17/02/2005 18/02/2005

Figure 3.26: Measuring locations silt profiler.

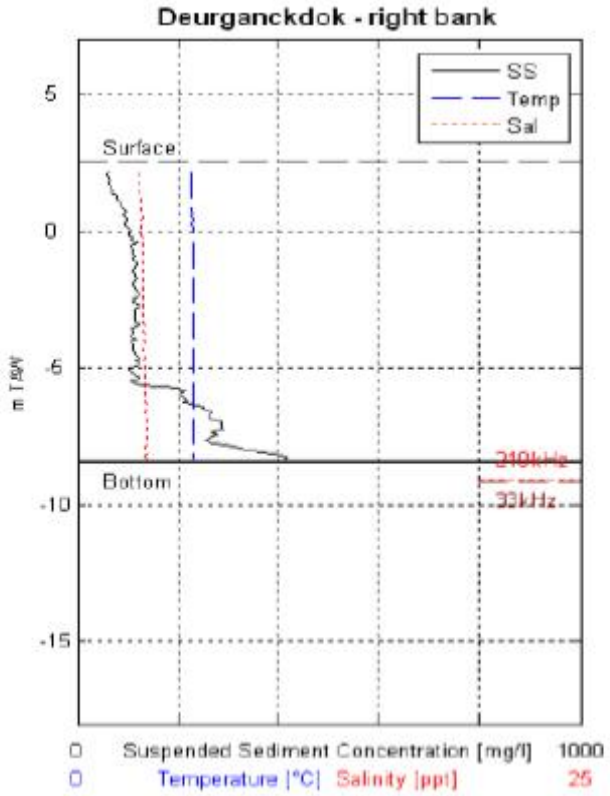

Figure 3.27: Results silt profiler measurements (black line), 17/02/2005, location DGD_right, 2u20 before HW.

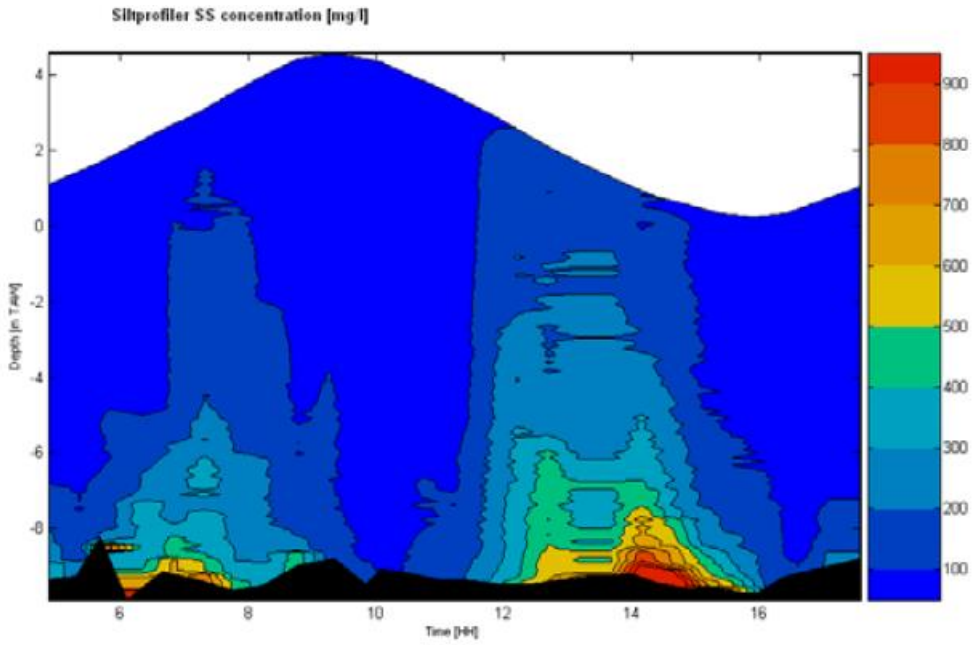

Figure 3.28: Combined results of silt profiler measurements at 17/02/2005 at location DGD_right.

3.5.3.4 HCBS: long term measurements in the Scheldt

For the benefit of the HCBS measuring campaign two additional fixed SPM monitoring points have been established in the Scheldt, one near Buoy 84, another near Buoy 97 (see Table 3.5 and Figure 3.29). The measurements will continue for one year. Only the first half of the data is presently available.

Location	Sensor Height [mTAW]	Bottom Height [mTAW]	Height above bottom	N [UTM ED50]	E [UTM ED50]	From	To
Boei 84 Upper [HCBS]	-5.6	-8.9	3.3	588971	5686097	21-9-2005	31-12-2005
Boei 84 Lower [HCBS]	-8.1	-8.9	0.8	588971	5686097	21-9-2005	31-12-2005
Boei 97 Upper [HCBS]	-5.3	-8.6	3.3	590932	5683350	20-9-2005	31-12-2005
Boei 97 Lower [HCBS]	-7.8	-8.6	0.8	590932	5683350	20-9-2005	31-12-2005

Table 3.5: Measuring locations long-term measurements in the framework of HCBS.

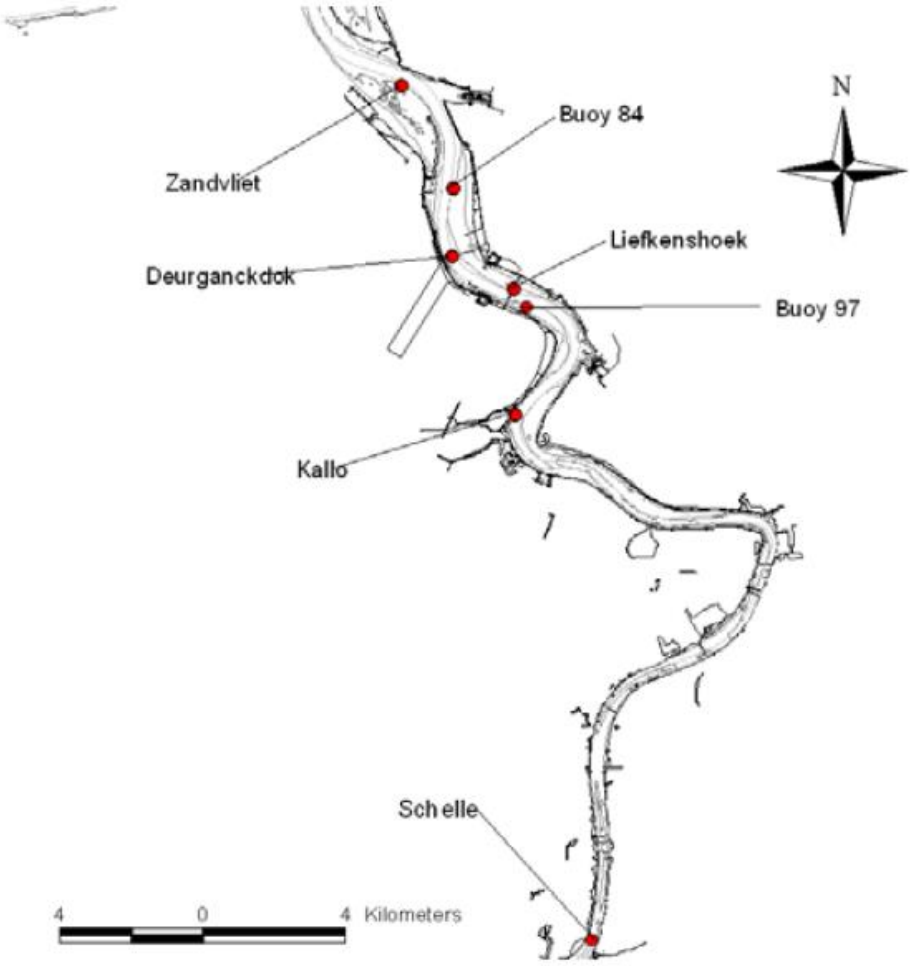

Figure 3.29: Location Boei 84 and Boei 97, temporary additional measuring points in the Scheldt.

4 Hydrodynamic model

4.1 Introduction

This chapter describes the set-up and calibration of a 3D hydrodynamic model that is the first step in the development of a numerical silt transport model. First, the set-up of the model is discussed in detail. Subsequently the results of the model are presented (water levels, flow transects and salinities). Finally the conclusions and recommendations are presented.

4.2 Set-up of the model

4.2.1 General

The 3D hydrodynamic model which is developed by WL Borgerhout for the purpose of this project relies on the experience gathered with previous 2D models. The upstream part of the model is taken out of the NEVLA model, as reported in WLB (2004). This upstream part forms also a part of the KUSTZUID model (v4) of Rijkswaterstaat, the performance of which is reported (among other models) in Alkyon (2005). The harmonic boundary conditions are calculated with a coarser version of the KUSTZUID (v4) model, called KUSTZUID (v3).
The figures that describe the set-up of the model are included in Appendix H. Grid, bathymetry, orthogonality and resolution are shown for the entire grid, but also in detail for the zone around Zeebrugge (Belgian coast), the Western Scheldt, the Sea Scheldt, the Rupel basin and the Upper Sea Scheldt.
The hydrodynamic model is set up in the SIMONA software of RIKZ. The subsequent paragraphs describe the model input (grid, gridded bathymetry, boundary conditions and parameter settings).
Two comparable hydrodynamic models are set-up: one for summer, and one for winter conditions. The seasonal difference is made in the initial conditions for salinity, in the upstream flow condition and in the uniform wind stress.

4.2.2 Grid

The grid of the model is an adaptation of the NEVLA grid. Three adaptations are performed. First, the grid is extended towards the French border. This involves adding 4914 grid cells to the grid. Secondly, Deurganckdok with a length of 2400m is added to the grid in 120 cells (width of 3 cells). Finally, the Rupel basin is schematized in 6375 cells. In the original NEVLA grid, the Rupel basin is schematized in 127.000 cells. The transition from the NEVLA grid to the LTV-slib grid in the Rupel basin is depicted in Figure H.3.
The LTV-slib grid has 170.000 active grid cells in a matrix of 379 (M-direction) to 2242 (N-direction). This gives a matrix that is filled up for 20%. The matrix filling of the grid is depicted in Figure H.2.

The grid has a resolution that varies between 400m at the northern (seaward) boundary, over 300m around Zeebrugge and the Belgian coast, to 150m in the Western Scheldt and up to 50 m in the Upper Sea Scheldt around Ghent. In comparison with KUSTZUID (v4), the LTV-slib grid has the same resolution as the KUSTZUID (v4) grid in the upstream region, and is 3 by 3 finer than KUSTZUID (v4) in the sea and in the Western Scheldt. The transition occurs gradually around the Belgian-Dutch border.
The grid and its properties are depicted in Figures H.9 through H.32.

4.2.3 Gridded bathymetry

The bathymetry is mainly taken over from the NEVLA bathymetry. The bathymetry of the extension towards the French border is interpolated out of the KUSTZUID (v4) bathymetry. The bathymetry of DGD is the "design bathymetry", which is: 19mTAW in the main channel, 17mTAW close to the quay walls and 16,5 mTAW on the sill between the river Scheldt and DGD. For the conversion between mNAP and mTAW, the value 2.35m is used.
The bathymetry for the simplified grid in the Rupel basin is interpolated linearly from a few characteristic depth values, with special attention to the conservation of the tidal storage volume.

4.2.4 Roughness

Roughness is schematised using the formulation of Manning. A uniform value of 0.022 $m^{-1/3}.s$ is used. Every 10 minutes (parameter TICVAL), a corresponding Chezy value is calculated in every grid cell from the Manning coefficient and the water depth values.

4.2.5 Thin dams and dampoints

Schematization of thin dams and dampoints is copied from the KUSTZUID (v4) grid for the harbour of Zeebrugge, the harbour of Vlissingen (east and west) and the training dams in the Sea Scheldt, see Figures H.5–7.

4.2.6 Output points and transects

Output points are included in the model at locations close to existing tidal gauges. The list of selected output points is included in Table 4.1.
Columns "Target_X" and "Target_Y" indicate the location of the tidal gauge in reality (in RD Parijs). The coordinate in the LTV-slib model is indicated in M and N coordinates. Column "distance" indicates the distance (in meters) from the selected waterlevel point in the model to the target location. The error in location remains smaller than 350m. Finally, "depth_WL" gives the depth (bathymetry in mNAP) at the selected water level point. For some locations a shift of a few M or N grid cells was performed in order to select a water level point with sufficient water depth.

	Location tidal gauge		Coordinate in the LTV-slib model			
naam	target_X	target_Y	M	N	distance	depth_WL
Antwerpen [Zege - Bonaparte]	86200.00	360360.00	117	979	129.43	4.87
Antwerpen Loodsgebouw	86039.42	360260.55	117	981	16.51	4.09
Appelzak	9134.56	376967.95	169	172	90.64	8.41
Baalhoek	65540.76	375998.47	173	635	29.11	10.43
Boei 84	77488.62	370377.12	122	829	19.96	10.27
Boei 97	79359.58	367566.83	128	861	24.18	10.22
Boerenschans	80742.22	363223.21	120	923	53.49	8.10
Bol Van Heist	2880.44	380157.06	160	130	68.87	11.10
Bol van Knokke	11029.95	383102.80	126	178	88.90	9.41
Borssele	41651.82	381517.16	55	380	85.57	4.50
Boudewijnsluis	81229.63	366280.63	112	879	49.57	10.14
Breskens	27033.00	380764.00	154	292	128.82	7.31
Cadzand	15004.07	378597.07	163	204	46.95	5.92
Dendermonde	65104.78	339199.14	130	1510	24.64	2.53
Hansweert	58390.00	384990.00	100	541	20.66	6.36
Hemiksem	81022.74	350944.55	119	1072	31.55	6.94
Hoboken	81309.38	355903.68	120	1022		7.11
Hoofdplaat	35623.90	377900.39	149	362	23.36	6.34
Kallo Sluis	79030.19	364849.60	131	899	24.17	9.43
Liefkenshoek fort	78179.64	368036.54	131	849	71.44	6.98
Lillo	78231.94	368680.50	121	847	46.21	7.10
Melle	43967.06	336169.41	128	2027	13.11	1.80
MP7 - Westhinder	-50138.13	382451.00	343	8	72.46	29.50
Oosterweel	83999.77	361345.47	127	948	24.16	7.59
Oosterweel_RB	85142.84	361749.69	118	957		12.20
Ossenisse	56041.62	380549.39	155	502	7.29	11.73
Overloop van Hansweert	56042.00	380549.00	155	502	7.78	11.73
Prosperpolder	74934.94	373871.10	128	759	31.63	6.68
Rilland-Bath	73090.35	379509.95	89	697	35.88	8.06
Schaar van de Noord	69912.78	377197.41	137	673	22.84	7.26
Schelle	79986.58	349051.91	117	1093	12.23	3.37
Terneuzen	45793.12	373070.26	171	422	338.44	11.74
Vlakte van de Raan	6083.00	392714.00	102	87	134.56	9.73
Vlissingen	30568.36	385259.06	54	310	28.22	7.46
Walsoorden	60289.62	379692.73	174	590	6.47	4.17
Wandelaar	-7754.94	380999.22	215	75	102.66	13.29
Westkapelle	19872.47	394230.44	51	176	25.42	8.86
Zandvliet	77212.90	373948.99	103	785	28.16	11.43
Zeebrugge	2655.51	375303.62	192	145	56.05	7.89

Table 4.1: Selected output points in LTV-slib model

The location of the tidal gauges in the model is depicted in Figure H.8. The transects in the model are defined from the standard “RIKZ transects“ for flow measurements. Out of the 7 standard transects, 4 were selected because they provide information on the distribution of flow between different channels. The selected output transects are tabulated in Table 4.2. Each transect consists of two parts.

Transect 5a	Zuidergat	Schaar van Waarde
Transect 7	Pas v Terneuzen	Everingen
Transect 9	Vaarwater langs Hoofdplaat	Honte / Schaar van Spijkerplaat
Transect 10	Vaarwater langs Hoofdplaat	Honte / Schaar van Spijkerplaat

Table 4.2: Selected output channels

The selected channels are depicted, together with the bathymetry, in Figure H.34.

4.2.7 Numerical settings

Name	Value	Unit
Latitude (for calculation of Coriolis)	52.5	°
Simona version	2006 – 01	n/a
Time step	0.25	min
ITERCON (max number of iterations for the continuity equation)	16	-
ITERACCURVEL (convergence criterium for flow velocities in momentum equation)	0.001	m/s
ITERACCURWL (convergence criterium for water levels in continuity equation)	0.0005	m
CHECKCONT (type of convergence criterium for continuity equation)	WL	n/a
TLSMOOTH (interpolation between initial condition and boundary conditions at the boundary)	600	elapsed minutes after midnight of starting date
Diffusion (global)	10	m^2/s
Dynamic viscosity	1	kg/m s
Eddy Viscosity	1	m^2/s
Theta (0,5 means central time integration for transport)	0.5	n/a

Table 4.3: Settings for the LTV-slib model

4.2.8 Drying and flooding

Calculations are performed with flag “DPD_GIVEN” set (default, not included in siminp file). This means that depth values are specified in the depth points (as opposed to the water level points in a staggered grid). For the drying and flooding computation however, depth values need to be computed in the water level points. For this, the flag ‘METH_DPS” is set to “MEAN_DPD”. This means that the depth in a water level point is calculated as the average depth of the four neighbouring depth points. The flag “METH_DPUV” is also set to “MEAN_DPD” (default, not included in siminp file). This means that the depth in a velocity point is calculated out of the depth of the two neighbouring depth points.

The drying and flooding criterion is parameterised in a subsequent section of the siminp file. The flag “CHECK_WL” is set to “YES”, which means that extra control for drying happens in water level points. Drying control at velocity locations always takes place. “THRES_WL_FLOODING” is set to 0.3 m. “THRES_UV_FLOODING” is left at its default value of 0.3 m. No upwind approach is used for the computation of water elevation at velocity points, which may be important in shallow areas, where the averaged approach can lead to incorrect flooding.

4.2.9 Vertical layers

The depth is discretised in 5 layers over the entire domain. A combination of z-layers and sigma layers is used. The bottom layer has a fixed thickness of 1m. The layer above has a fixed thickness of 0.5 m. The three top layers are sigma layers of equal (varying) thickness. The layers are numbered from top to bottom.

In regions of tidal flats it is possible that $H \leq h_{tot}$ (H is water depth, h_{tot} is the sum of the fixed layer depths). In such a case a so-called "shadow" sigma-coordinate approach is introduced. The sum of all constant layer thicknesses is set exactly to half the total water depth. The remaining half of the water column is partitioned over the remaining sigma layers (TRIWAQ-TECH documentation)

4.2.10 Parallelisation and speed-up

The domain is split-up in 20 subdomains in the horizontal. Every subdomain is assigned to a different processor on a LINUX cluster, and the whole domain is calculated in a parallel way.
The model calculates water movement and salinity 20 times faster than reality. The calculation of a spring-neap cycle takes less than 17 hours to calculate. It is important to note however that when the integrated velocity is written to the SDS file after every 30 minutes of calculation, the resulting file has a file size of 52 GB (for the hydrodynamics of one spring/neap cycle). The collecting of the SDS files of the different sub-domains to one SDS file for the entire domain takes 4 hours. The transfer of the SDS file from the cluster to a backup disk also takes another 17 hours. From the point of view of data storage, the calculation of a full year with this model would generate 1.3 TB of data, which cannot be processed by the current cluster at WL Borgerhout.

4.2.11 Downstream boundary: harmonic forcing

The downstream boundary is modelled as a water level opening. Harmonic constants of 94 tidal components are used to define the water level at the downstream boundary. These 94 components are generated with a run of the KUSTZUID (v3) model for one year (2004), with the harmonic analysis performed by SIMONA. The boundary points of the LTV slib model are such that they correspond to water level points in KUSTZUID (v3). This way, no interpolation is required to obtain the harmonic boundary for the LTV-slib model.

4.2.12 Upstream boundary: fresh water inflow

Table 4. provides an overview of the fresh water inflow of summer and winter model, as opposed to the "standard" fresh water inflow that is programmed into KZv4.

P	River	Discharge point	Q - KZv4	Q - summer	Q - winter
300	Kleine Nete	Grobbendonk	15	6	15
301	Grote Nete	Itegem	10	4	15
302	Dijle	Haacht	50	24	50
303	Zenne	Eppegem	0	8	20
304	Dender	Dendermonde	35	10	30
305	Bovenschelde en Leie	Melle	100	24	70
		Sum	210	76	200

Table 4.4: Fresh water inflow

Total summer and winter flows (75 m^3/s and 200 m^3/s respectively) are determined from analysis of the monthly averaged flow in Schelle, determined from a 15 year dataset (see Figure H.46).

To determine the distribution of the upstream flow over the tributaries, two periods are determined in 2005 for which the total flow correspond to the summer- respectively winter flow. For winter conditions, this is from 07-02-2005 to 16-02-2005. For summer conditions, the selected period is from 18-04-2005 till 27-04-2005. The distribution of upstream flow in the model corresponds to the distribution of upstream flows over the tributaries in the selected periods.

For comparison, the upstream flow of the KUSTZUID (v4) model are also indicated. From the data, presented in Table 4.4, it is clear that the fresh water inflow conditions in KUSTZUID (v4) corresponds to rather 'wet' conditions. The fresh water inflow is given a salinity of 0.3 ppt

4.2.13 Wind forcing

For the wind forcing a mean winter condition is determined using the months December to February. The summer condition is determined for the months June to August.

The mean components are determined such that the mean winter and summer wind-induced shear stress is applied. The Smith and Banke (1975) formulations are used to relate wind velocity to interfacial shear stress:

$$U = (u, v);\ C_D = (0.630 + 0.066\,|U|)\ 10^{-3};\ \tau = (\tau_x, \tau_y) = \rho_a\, C_D\, |U|\, (u, v), \qquad (4.1)$$

where u and v are the zonal and meridional wind components and the air density ρ_a = 1.225 kg/m^3. Degrees are clockwise from North. E.g. 90° means wind coming from the East.

	Winter	Summer
Wind speed	8.1 m/s	5.9 m/s
Wind direction	228.9°	297.0°

Table 4.5: Applied wind conditions

A constant wind drag coefficient is used of 0.0026 (default value). The height above the free surface is set to 10 m (default). Both in summer and in winter condition, wind is schematised by a set of constant values.

4.2.14 Initial conditions

Because of the availability of salinity measurements in the Sea Scheldt, the year 2005 is selected to define the initial conditions of salinity for both winter and summer conditions.
Initial conditions of salinity are based on measurements of 16th of February (winter conditions) and on 27th of April (summer conditions). Those two dates are chosen because the flow at that time approximates the fresh water inflow selected for winter or summer conditions (see §4.2.12). Salinity measurements are available for stations Vlakte van de Raan, Hoofdplaat, Baalhoek, Lillo, Boerenschans, Oosterweel and Hoboken. For the last three measurement points, the dataset of the Oosterweel tunnel project is used (TV SAM).

The salinity measurements are depicted in Figure H.50 for the entire month of April, and in Figure H.51 in detail on the 27th of April. On the 27th of April, fresh water inflow is decreasing from 100 to 60 m^3/s. The measuring point at Vlakte van de Raan is not functioning in April 2005. The measurements of salinity show no clear trend in the days before and after 27-04-2005, so the measurements give an indication of a relatively stable salinity distribution which is typical for a relatively low upstream flow condition around 75 m^3/s. In the summer model, the salinity measurements of the 27th of April are used as initial salinity conditions together with a stationary fresh water inflow of 75 m^3/s.

The salinity measurements are depicted in Figure H.48 for the entire month of February, and in Figure H.49 in detail on 16 February. On the 16th of February, fresh water inflow is decreasing from a peak of 350 m^3/s to 150 m^3/s. The high measurements of the lower sensor at Vlakte van de Raan probably correspond to erroneous results. Due to the peak in fresh water inflow from the 11th to the 15th of February, the salinity has decreased in all stations but the Vlakte van de Raan, which is situated too downstream to be affected so soon by a peak in fresh water discharge. The measurements show that the 17th of February gives a good indication of the salinity values along the estuary after a peak in fresh water inflow.

In the winter model, the salinity measurements of the 16th of February are used as initial conditions together with a steady freshwater inflow of 200 m^3/s. As starting time for the model, a HW in Westkapelle is chosen. On the first HW in Westkapelle on the selected dates, the salinity measurements along the estuary are taken to generate the initial conditions, by interpolating between the different measuring points. The interpolation is done linearly along the M-direction (flow direction). The salinity in the N-direction is uniformly initialised. Salinity is initialised uniformly over depth using a BOX commando in the SIMINP file.

		winter	summer
	time HW Westkapelle	16-02-05 6:50	27-4-2005 3:10
Name	**N (grid coordinate)**	**sal [ppt]**	**sal [ppt]**
Vlakte vd Raan	87	35	32
Hoofdplaat	362	27	27
Baalhoek	635	12	15
Lillo	847	1.1	7
Boerenschans	923	1	
Oosterweel	948	0.7	2
Hoboken	1022	0.3	0.5

Table 4.6: Initial conditions for salinity (summer and winter conditions)

The resulting initial conditions for summer and winter conditions are depicted in Figures H.53 and H.54.

The initial value of 35 ppt in winter conditions at Vlakte van de Raan is probably based on an erroneous measurement of the lower sensor. At the same timestep, the upper sensor indicates a value of 32 ppt, which would be a more appropriate initial condition of salinity. Due to time constraints, this error could not be corrected in this phase of the project. Salinity is no direct input parameter of the mud transport model. The influence is indirectly present due to the effect of salinity (density) gradients on water movement. Salinity is initialised uniformly over the water column. Water level is initialised linearly from 1.5m NAP at sea to 7m NAP in Gent. Velocities are initialised at zero velocity.

At the downstream boundary, salinity is modelled using a Thatcher Harleman condition. The background concentration (CINITIAL) is set to 32 ppt, the return time (TCRET) equals 180 min (see Figure 4.1).

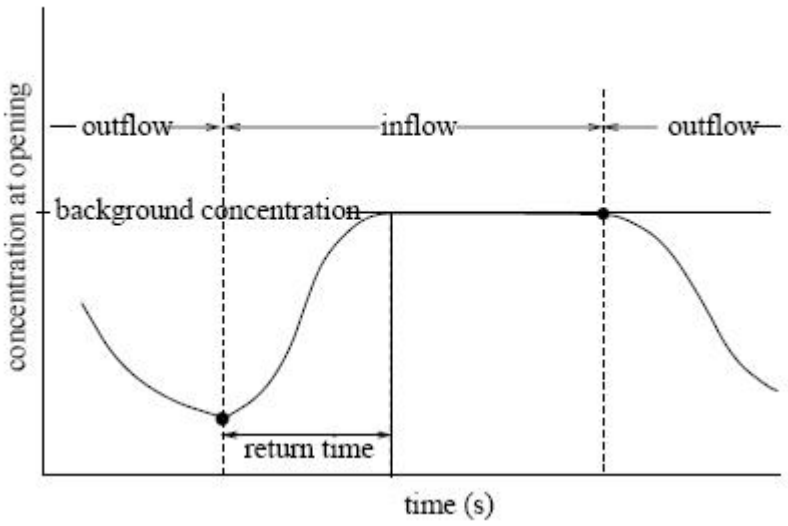

Figure 4.1 (H.1): Thatcher Harleman boundary condition (taken out of technical documentation WAQUA)

4.3 Results

The quality of the hydrodynamic model is reported with respect to three different aspects. First a comparison is made between predicted water levels with water levels calculated out of the harmonic constants for the tidal gauges. Secondly, the measured flows in the selected transects are compared to the predicted flows in comparable tidal conditions. Finally the predicted salinities are compared to measured values along the estuary.

4.3.1 Water levels

4.3.1.1 Methodology

The dataset provided by K. Doekes of RIKZ gives the 94 main tidal components for 16 stations. Because the LTV-slib model is intended for "mean" conditions, the water levels in the model are compared against this data set. As opposed to comparing model results with field measurements this methodology has the advantage that storm events have little impact on the harmonic data provided, and that they provide a true "mean" image of the water levels at 16 locations along the estuary.
It was first proposed to do a harmonic analysis in SIMONA, and to compare the phases and amplitudes of three main components (M2, M4, M6) with comparable values out of the dataset of K. Doekes. There seems to be a problem however with the calculation of harmonic components in a TRIWAQ (3D) run.
As an alternative way to compare the model results against the harmonic data provided by K. Doekes, a time series is generated out of the harmonic data for the same periods as both the summer and the winter run. Because the harmonic data consists only of phases and amplitudes, a nodal correction is performed on the amplitude and a phase correction on the phase. This correction is read out of the x_tide database of the t_tide package as a function of the year for which the time-series is generated. See Pawlowicz et al. (2002) for details on t_tide. The resulting, harmonically generated time series can easily be compared to the time series out of the model. This comparison is reported for 6 water level stations along the estuary.

4.3.1.2 Results

The comparison between calculated water levels and water levels calculated out of the harmonic components of the data of K. Doekes of RIKZ is made from Figures H.56 to H.67.

There is little difference in the accuracy of water level modelling between the summer and winter run. In both cases, the high and low waters are modelled with an accuracy of 20 to 30 cm. This is comparable with the reported results of the performance of the KUSTZUID (v4) model during the second half of 2002 (May to November). See also Alkyon (2005), report 1/3, Table 5.6c for a statistical comparison of high and low water between model and measurements.

In Westkapelle, Borssele and Antwerp, the low water is systematically 20 cm too high in the model. The high water is modelled correctly. In Liefkenshoek, Baalhoek and Overloop Hansweert there is an overprediction of both high and low water of 10 to 20 cm.

The phase of the spring-neap cycle is modelled accurately. If we look more into detail to one tidal cycle in the different stations, we can conclude that the phase of the tidal cycle is also modelled accurately.

The explanation for the deviation in water levels is to be sought in a combination of the parametrisation of wind by a constant value, deviations in the harmonic boundary conditions for water levels, the uniform roughness value and the choice of flooding/drying criterion.

4.3.2 Flow transects

4.3.2.1 Methodology

As described in §4.2.6, 4 transects (5a, 7, 9, 10) out of the 7 "standard RIKZ" transects are selected for this analysis because they provide information on the distribution of flow between two different channels.
The dataset was provided by T. van der Kaaij of WL | Delft Hydraulics, and contains for each transect a 13h flow measurement performed between 2001 and 2002. For the selected transects, data in two channels were measured simultaneously.
First, the water level measurements in Vlissingen for 2001 and 2002 are used to report the tidal conditions during the different 13h measurement campaigns. These tidal conditions are depicted in Figure H.35. The 13h measurements have all taken place around spring tide conditions. Because both the winter and summer model cover one spring-neap cycle, similar conditions can be selected. For the winter model, these conditions occur around 27th of February. For the summer model, this is around the 9th of May.
The measurement of transect 9 happened on the 13th of March 2001. From the water level at Vlissingen around that day, it follows that the conditions on that day are extra-ordinary. Measured high water in Vlissingen is more than 50cm higher than the high waters on the dates the other measurements have occurred, or than the high waters predicted by the model. Probably transect 9 was measured in storm surge conditions.

4.3.2.2 Results

The comparison between modelled and measured flows is depicted in Figures H.38 to H.45. The water level in Westkapelle is plotted together with the flow measurements. The predicted water level in Westkapelle is also plotted together with the results of the winter model. From the comparison of both we learn that the phase of peak ebb and flood current is modelled accurately for all four transects.

The form of the flow curves differs significantly between the different transects. Flow through "Schaar van Waarde" and through "Zuidergat" (transect 5a) show a distinct platform in the flow during rising tide. This platform is modelled accurately in the model. Transect 10 ("Vaarwater langs Hoofdplaat" and "Honte / Schaar van Spijkerplaat") shows no such platform, only a weak bend in the flow diagram during rising tide. This phenomenon is reproduced in both winter and summer model.

The tidal asymmetry is clearly pronounced in the flow data of transect 5a. The period from maximum flow down to minimum flow has a shorter duration than the complementary

period from minimum to maximum flow. This phenomenon is also observable in both winter and summer model.

In a more quantitative comparison between model and measurements, the peak flows of both summer and winter model are compared to the peak flows in the measurements. This comparison is tabulated in Appendix A.
For transect 5a, around 55% of the flow passes through "Zuidergat" in the measurements at peak flow (both flood and ebb). However in the model 60% of the peak flow passes through the "Zuidergat". This difference remains unaccounted for.
In transect 7, about 45% of the flow passes through "Pas van Terneuzen" during max ebb, whereas only 42% passes through "Pas van Terneuzen" during max flood. This phenomenon is reproduced accurately in both winter and summer models.
The flow through "Vaarwater langs Hoofdplaat" and through "Honte / Schaar van Spijkerplaat" is measured both in transect 9 and 10. However, as indicated above, the measurements of transect 9 probably happened during storm conditions. Therefore they will not be used in the validation of the model.
For transect 10, 10% of the flow passes through "Vaarwater langs Hoofdplaat", both during max ebb and flood. In the model this ratio is also 10%. Thus the flow pattern through "Vaarwater langs Hoofdplaat" and "Honte / Schaar van Spijkerplaat" is accurately reproduced by both winter and summer model, which are calibrated against mean conditions.

4.3.3 Salinities

4.3.3.1 Methodology

Because of the time scales involved, a stationary situation for salinity cannot be found in the measurements. That is why the first concern in the evaluation of the model is if the initial salinity distribution stays in its place during the modelled spring-neap cycle. As outlined in §4.2.14, the initial conditions for salinity is deduced from measurements for days at which the salinity is *more or less* stable. Especially for the high flows (200 m^3/s mean during winter conditions) it is hard to find a period in time where this flow of 200 m^3/s is maintained. In the selected period in February for instance, the measurements indicate that the fresh water inflow is dropping from a value around 300 m^3/s to a value lower than 200 m^3/s. The salinities in the selected period are more or less stable however.
As is expected, the initial salinity condition in summer is higher in salinity than during winter, due to a higher fresh water inflow in winter. This is clearly depicted in Figure H.52.

4.3.3.2 Results

As shown in Figure H.55, there is no significant trend in the predicted salinity of the downstream points from the start to the end of the run, both in summer and in winter conditions. There is however a clear upward trend in salinity in the upward stations. Therefore the initialised salinity field is not entirely stable in the upstream part of the model.
In the winter run, the salinity at Vlakte van de Raan converges to a constant value of 32 ppt. The initial condition however is 35 ppt. This convergence is a consequence of the Thatcher Harlemann boundary condition (which converges to an inflow of 32 ppt at the seaward

boundary). At the end of the summer run, there is still an amplitude in salinity of about 1 ppt, which is in accordance with measurements.

The salinity minima and maxima at the end of the run are compared to measured minima and maxima in Figure H.65. The modelled salinities along the estuary are systematically lower than the measured minima and maxima. The maximum difference reaches about 5 ppt around Baalhoek. Model results indicate however that this is not a consequence of an instable salinity distribution (which would lead to permanently rising or falling salinities in the model), but that this difference between measurement and model originates in the first time steps. The salinities are based on measurements, but the water levels and the initial velocities are not. It is possible that during the "warming up" of the model a part of the initial salinity disappears over the edges, which would explain the sudden drop in salinity in the first time steps; both in winter and summer models.

4.4 Conclusions and recommendations

Two comparable hydrodynamic models are set-up: one for summer, and one for winter conditions. The seasonal difference is made in the initial conditions for salinity, in the upstream flow condition and in the uniform wind stress.

Water levels are in good agreement between the model and the harmonic analysis of the measurements. The agreement has been checked by generating water level series out of the harmonic constants. The phase of the water levels is in good agreement, and the high and low water levels are predicted by the model with an acceptable accuracy of less than 30cm (depending on the station).

Important phenomena such as tidal asymmetry in ebb and flood flow are well reproduced in the model. Whereas the model is intended for "mean" conditions, the comparison between the model and a dataset of flow transects sailed between 2001 and 2002 shows a good agreement in the form of the measured and predicted flow curves, and the phase of ebb and flood flow. A comparison between the ratio of peak flows between channels shows a good agreement. For transect 5a however, a difference of 5% remains unaccounted for. In general, both winter and summer models seem capable of reproducing reasonably well the measured flow curves.

The salinity remains stable through both winter and summer model runs in the downstream region of the model. In the upstream part of the model, the salinity shows a rising trend, which indicates that the initialised salinity field is not entirely stable. Furthermore in the first timesteps, a drop is observed from the (measured) initial conditions. As a consequence, the modelled salinities remain under the measurements, both for winter and summer conditions. This is thought to be a consequence of the initial conditions for water levels and velocities, which are defined rather roughly in the current version of the model (e.g. zero velocities).

The model as it is reported gives a good approximation of the "mean" hydrodynamics in the Scheldt estuary. By initialising the hydrodynamics out of a restart file, and initialising the salinities based on measurements, it is believed that the drop in salinity can be avoided.

The hydrodynamic model is fit to be used as a basis for a mud transport model. Measurements of both water levels and flow transects give a good idea of the quality of the hydrodynamics.

Further improvement of the current hydrodynamics can easily be obtained by refining the definition of the thin dams, which are now simply copied from the (coarser) KUSTZUID (v4) model.

Water levels have been checked by comparing model results to the harmonic constants of a few important tidal stations. This methodology results in the limitation that the upstream part of the river is not validated on water levels. In order to validate the hydrodynamics in the upstream region, a comparison will have to be made between model results and measurements. The selection of the validation period is of crucial importance, because the fresh water inflow plays an important role in the water levels in the most upstream parts of the model.

The current time frame of the model (one spring neap cycle) proves to be insufficient to assess the stability of the salinity distribution. This means that the current salinity distribution still depends on the choice of initial condition. A longer warming up period for the salinity will lead to a truly stable salinity distribution. The simulation time necessary for this depends on the quality of the initial conditions, but is believed to be in the order of magnitude of 6 spring neap cycles (3 months).

5 Mud transport model

5.1 Desiderata

Based on the system description and data analysis, the following desiderata regarding the performance of the mud transport model are formulated:

1. global spatial concentration distribution (e.g. location of ETM's): mean Western Scheldt ca. 50 mg/l
2. intra-tide SPM concentration fluctuations: factor 2 to 5
3. neap/spring SPM concentration fluctuations: factor 1.5 to 2
4. vertical concentration gradients: factor 2 to 10
5. a proper overall mud balance, including a sensible mass of 'active' mud in the system
6. the spatial distribution of sandy and muddy areas (conform McLaren soil data)
7. seasonal SPM concentration fluctuations, including response time of freshwater discharge peaks and storms: factor 2
8. siltation rate of intertidal areas and salt marshes (order 1 – 2 cm/y), siltation rate in harbours (up to 1 cm/day)
9. ratio between fluvial and marine mud according to Verlaan (1998)
10. available mass of sediment (Van Maldegem, 1997):
    - 13 MT in the bed
    - 0.1 – 0.4 MT suspended
    - load from sea and upstream: 0.2 MT/y (see also Table 5.1)
    - load from dumping: 1.5 MT/y
11. long-term equilibrium between dumping from harbour maintenance and harbour siltation

5.2 Model set-up

The model grid is based on the hydrodynamic model grid (see Chapter 4). For most mud simulations, the grid is aggregated 2×2 in order to reduce the computation time. For one simulation, the original grid is used to assess the effect of the reduced spatial resolution. The number of horizontal layers is 5, which is identical to the hydrodynamic model. At the sea boundaries, mud concentrations are prescribed according to the MWTL field observations reported by Suijlen and Duin (2001). A distinction is made between summer and winter conditions. At the southern boundary the observed concentration in the Appelzak transect is applied, whereas at the northern boundary the observed concentration in the Walcheren transect is applied. Figures 5.1a and 5.1b show the observed and applied SPM concentrations for winter and summer conditions at the northern and southern boundaries. The western boundary was set at a constant value of 7 mg/l in summer and 15 mg/l in winter. At the northern boundary, a Thatcher-Harleman time lag of 2h was applied. No time lag was applied at the southern boundary, as the residual current is from south to north.

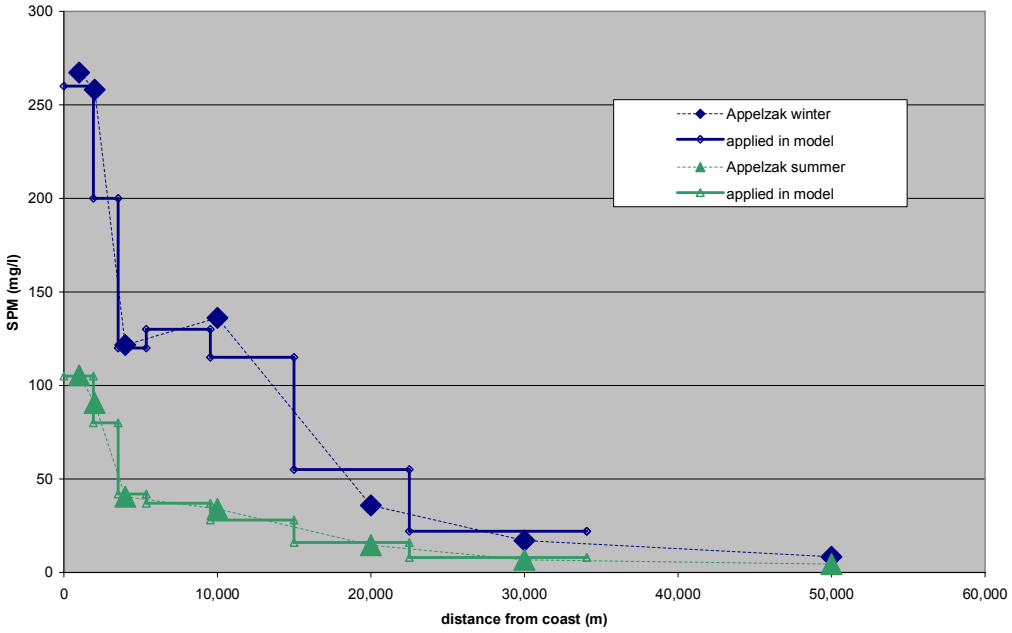

Figure 5.1a: Applied concentration at southern boundary for summer and winter conditions. Large triangles and diamonds: observed concentration in Appelzak transect for summer and winter conditions.

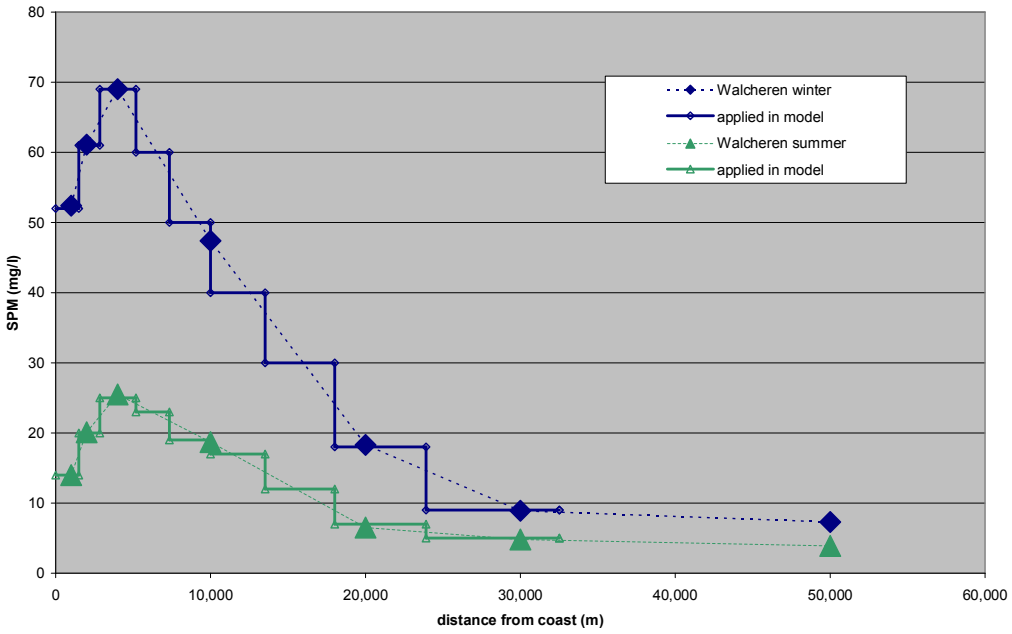

Figure 5.1b: Applied concentration at northern boundary for summer and winter conditions. Large triangles and diamonds: observed concentration in Walcheren transect for summer and winter conditions.

At the up-estuary boundary, freshwater enters the hydrodynamic model via user-defined discharge points. In the mud model, the SPM concentrations of these discharges has to be specified to arrive at the definition of the fluvial sediment load. Table 5.1 specifies these fluvial loads.

River	Discharge point	Q – summer (m^3/s)	C – summer (mg/l)	Q – winter (m^3/s)	C – winter (mg/l)
Kleine Nete	Grobbendonk	6	26	15	27
Grote Nete	Itegem	4	31	15	28
Dijle	Haacht	24	54	50	74
Zenne	Eppegem	8	0	20	0
Dender	Dendermonde	10	94	30	118
Bovenschelde en Leie	Melle	24	112	70	114
Total		76	165 kton/y	200	502 kton/y

Table 5.1: Applied fluvial sediment loads.

Figure 5.2 shows the locations of the observation points included in the model.

Table 5.2 shows the loads included in the model to take into account the dumping of dredged material from harbour maintenance. These loads, which locations are shown in Figure 5.3, are constant in time. It is noted that near Antwerp the dumping volume is increased with 1 MT/y to compensate for siltation and dredging in Deurganckdock (not yet included in historic dumping volumes).

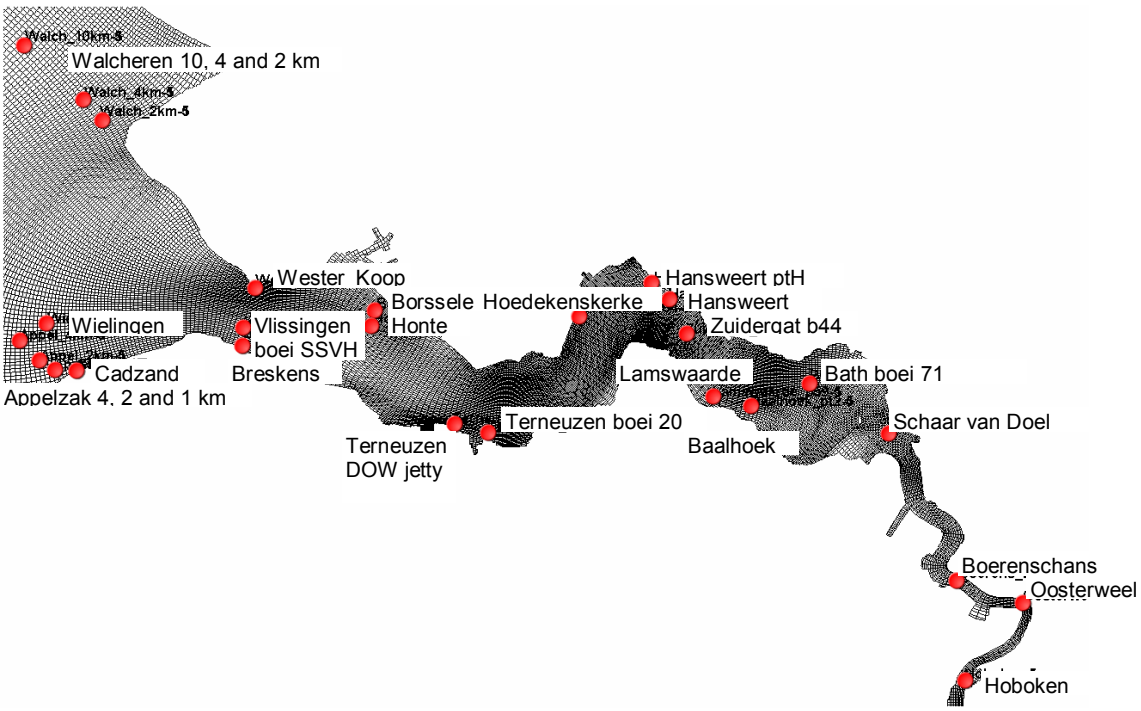

Figure 5.2: Overview of observation points in silt transport model. See also Fig. 3.4 for MWTL locations.

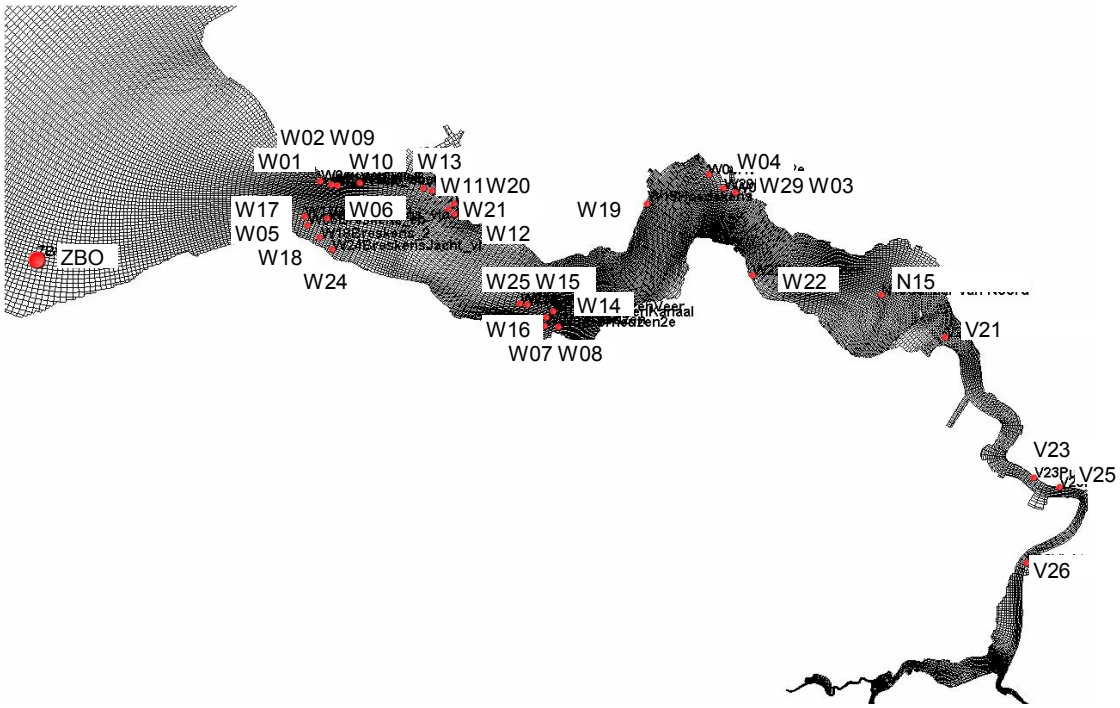

Figure 5.3: Overview of sediment discharge locations in silt transport model. See Table 5.2 for ID tags.

1. North Sea North
2. North Sea Central
3. North Sea Southern
4. Zeebrugge
5. Mouth
6. Vlissingen
7. Terneuzen West
8. Terneuzen East
9. Border NL
10. Saeftinge
11. Zandvliet sluice
12. Border B
13. Boudewijn sluice
14. Antwerp
15. Deurganckdok
16. Kallo sluice
17. Rupel
18. Dendermonde
19. Gent
20. shallow areas (not indicated)

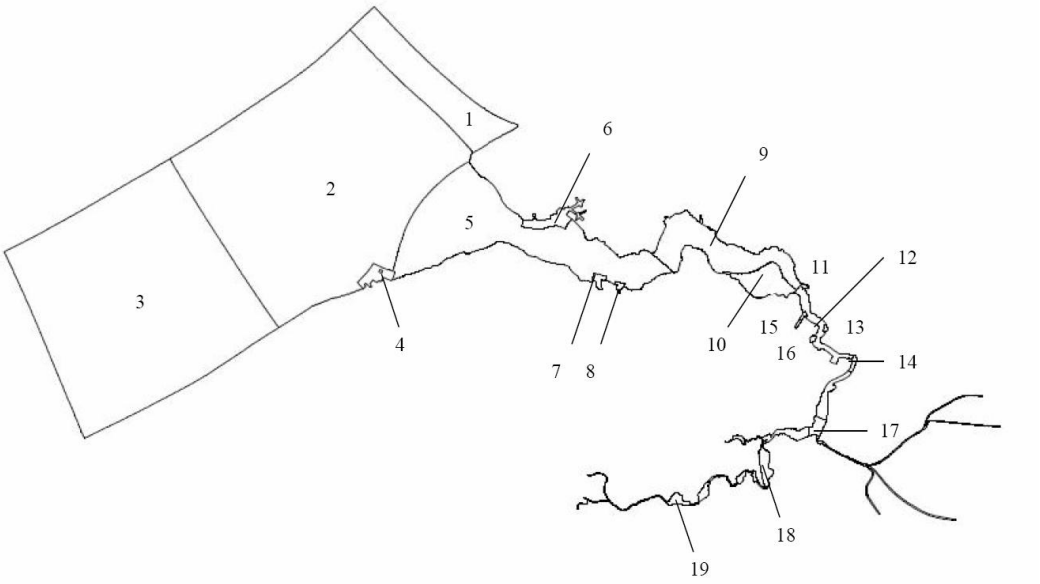

Figure 5.4: Overview of defined areas in silt transport model.

location	kton/y	location	kton/y
W01Koop_eb	0	W16TerneuzenKanaal	0
W02Koop_vloed	0	W17Breskens_1	75
W03HWeert	200	W18Breskens_2	0
W04HWeert2e	200	W19Hoedekens	0
W05Breskens_eb	122	W20EPZ_1	10
W06Breskens_vloed	122	W21EPZ_2	10
W07Terneuzen	125	W22Walsoorden	8
W08Terneuzen2e	125	W24BreskensJacht_vl	75
W09VlisB_eb	90	W25Axel	0
W10VlisB_vloed	90	W29Hansweert	0
W11VlisO_1	309	V26Vlakte Hoboken	0
W12VlisO_2	309	V25Plaat van Boomke	833 (f)
W13VlisW	0	V23Punt van Merelse	1248 (f)
W14TerneuzenVeer	24	V21Schaar Ouden Doel	0
W15_5w	406	N15Schaar Noord	0
W15_5o	406	ZBO Zeebrugge	3154

Table 5.2: Overview of mud discharges from harbour dredging. See also Fig. 5.3. (f) = fluvial mud. All other discharges are assumed to be of marine origin. Source: RWS Directie Zeeland and Dienst Maritieme Toegang. N.B. The loads at V23 and V25 have been increased with 1 MT/y to take into account the siltation at Deurganckdock, which is not yet included into the historic loads.

5.3 Formulations used

The bed of the Scheldt estuary is represented by two layers. Conceptually, the first layer is the thin fluffy fine sediment layer deposited during slack water. At high current velocity, most or nearly all of this layer is resuspended into the water column. The critical shear stress for resuspension τ_{crit1} of this layer is low and its erosion constant M is high. If less than a certain mass $m_{1\rightarrow 0}$ per unit area of fine sediment is available in layer 1, it may well be assumed that the surface coverage of the underlying bed forms is not complete. In this case, the resuspension constant M will become dependent on the percentage of surface coverage. A transition between zeroth order and first order resuspension behaviour occurs. The expression for the erosion flux from layer 1 F_{ero1} now reads:

$$F_{ero1} = \min (M_0, m\, M_1) \times \max (0, (\tau/\tau_{crit1} - 1)), \qquad (5.1)$$

where M_0 and M_1 are the zeroth and first order resuspension constants, respectively and m the available sediment mass per unit area in layer 1. By definition, $M_0 = m_{1\rightarrow 0}\, M_1$.

Conceptually, the second bed layer with user-defined thickness d represents the sand bed which prevails in the Scheldt estuary. The erosion flux of fine sediment present in the pores of the sand bed is expressed as:

$$D_* = D_{50}\left((s-1)g/\nu^2\right)^{1/3}$$
$$F_{ero2} = pM_2\rho_s\left((s\text{-}1)gD_{50}\right)^{0.5} D_*^{0.3}\left(\tau/\tau_{crit2}-1\right)^{1.5} \quad pM_2'\left(\tau/\tau_{crit2}-1\right)^{1.5}, \tag{5.2}$$

where $M_2' = 333M_2$ throughout the present study. The value of 333 follows from the standard values of ρ_s = 2600 kg/m³, s = ρ_s/ρ_w = 2.5, D_{50} = 3 10^{-4} m. The power of 1.5 appears in expression (5.2) because of the Van Rijn type of erosion function used. The erosion rate increases linearly with the mud fraction p.

The sedimentation flux is split into two fractions. Parameter α steers the sedimentation towards layers 1 and 2:

$$F_{sed1} = (1\text{-}\alpha)\, w_s\, C;\ F_{sed2} = \alpha\, w_s\, C. \tag{5.3}$$

As $\alpha << 1$, the rate of sediment exchange between the water column and the first layer is much higher than the rate of exchange with the second layer. In combination with a much higher typical sediment mass per unit area in layer 2 compared with layer 1, the residence and response times of sediment in layer 2 are much longer. Whereas layer 1 responds on the tidal time scale (hours), layer 2 responds on the seasonal scale (months to years). The neap-spring tidal cycle (14 days) may influence both layers.

The formulations for layer 2 discussed above were developed on the framework of the MER sand mining study for Maasvlakte-2 (Van Ledden *et al.*, 2006). Also the first order erosion concept was applied to layer 1 herein. The transition between first and zeroth order erosion for layer 1 is a new concept introduced in the present study. The rationale behind this transition is the much higher mud content of the Scheldt estuary compared with the North Sea, as the first order erosion concept becomes unrealistic for areas with a high availability of mud.

As the model consist of two mud fractions (of fluvial and marine origin), the material parameters have to be specified for both fractions. No sand transport is modelled; the sand layer (layer 2) is assumed to be passive with constant thickness d, but contains a variable mud fraction.

To conclude, the following parameters have to be specified:

Water column:

Settling velocity fraction 1:	w_{sF1} (m/s)
Settling velocity fraction 2:	w_{sF2} (m/s)
Partition coefficient fraction 1:	α_{F1} (–)
Partition coefficient fraction 2:	α_{F2} (–)

Layer 1:

Critical shear stress for erosion fraction 1: $\tau_{crit1F1}$ (Pa)
Critical shear stress for erosion fraction 2: $\tau_{crit1F2}$ (Pa)
1st order resuspension parameter fraction 1: M_{1F1} (1/s)
1st order resuspension parameter fraction 2: M_{1F2} (1/s)
0th order resuspension parameter fraction 1: M_{0F1} (kg/m^2/s)
0th order resuspension parameter fraction 2: M_{0F2} (kg/m^2/s)

Layer 2:

Layer thickness: d (m)
Critical shear stress for erosion: τ_{crit2} (Pa)
Resuspension parameter M_2 (kg/m^2/s)

Note that only the mud fraction p may be eroded from layer 2. The sand layer will always remain in place with constant thickness d, as the present mud transport model is not a morphological model in which bed level changed are computed.

5.4 Limitations

The proposed model formulations do NOT include the following phenomena:

- fluid mud dynamics
- flocculation: constant settling velocity:
- biology-driven seasonal dynamics
- biological production of SPM from algal growth
- consolidation (strength increase in time)
- sand/mud behaviour
- sediment-water interaction (*i.e.* no influence of sediment on water motion)

These phenomena may be included in a later phase of the project (after 2006) if the analysis of the model performance suggests that one or more of the effects mentioned above are the key towards improvement.

5.5 Calibration

5.5.1 Method

The calibration has been carried out according to the following steps:

1. Determine from the literature the proper sediment concentration boundary conditions and loads. Also the dredging and dumping activities within the model domain should be considered.
2. Use a point model in combination with the datasets from Terneuzen and Boerenschans (having a high temporal resolution) to obtain optimal settings for the model parameters such as w_s, τ_{crit} and M. Ideally, these settings should be within the typical range mentioned in the literature. If not so, it should be investigated why.

3. Assuming a typical spatial concentration distribution in the Scheldt, compute the location of the isolines for $\int [M_E (\tau - \tau_{crit}) - w_s C]dt = 0$. These isolines designate the transition between sandy soil without net mud accumulation (but with thin temporary mud deposits during slack water and with a mud percentage in the sand bed in equilibrium with the mud supply and local shear stress conditions) and muddy soil with, on the long term, net accumulation of mud. Note that muddy soils subject to net long-term erosion will eventually (*i.e.* in equilibrium with the long-term average conditions regarding sediment supply and bed shear stress) become sandy soils.
4. Bring the magnitude of the vertical exchange in accordance with field observations by changing τ_{crit} and M_E such that the equilibrium set under 3) does not change. Field data on net sediment accumulation (*e.g.* the evolution of tidal flats and dredging volumes in harbour basins) and on the suspended sediment concentration variation over the tide in shallow areas (where the sediment concentration is steered by local vertical exchange processes) are useful input to optimize vertical exchange. Some iteration between steps 2, 3 and 4 may be required.
5. The next step is to apply these parameters settings to the 3D numerical mud transport model. During this step, a further optimisation in parameter settings may be required because of the limitation of the point model, which neglects both variations in sediment supply and local horizontal concentration gradients which may show up in the SPM time signal caused by advection (N.B. it is therefore recommended to apply the point model preferably in spatially uniform areas. The data from the DOW jetty inside the main channel near Terneuzen is therefore potentially more suitable for analysis with the point model than the data from Baalhoek or Boerenschans, which were measured in a side channel close to a tidal flat and salt marsh).
6. Two versions of the mud transport model are used: one version with a coarse grid that can be used for long-term simulations (months to years) and a second version with a fine grid for short-term simulations (days to weeks). The coarse version can supply the initial conditions for the fine version. The coarse version can be used to investigate the effects of seasonal dynamics and peaks in river discharge, whereas the fine version is meant to investigate the more local behaviour on the tidal scale (25h, preferably also 14d). Ideally, the fine and coarse model should have the same equilibrium conditions regarding SPM distribution, bed composition and accumulation rates. Otherwise, the fine model migrates towards new equilibrium conditions after a restart from initial conditions. Typically, the simulation time with the fine model is much too short to reach the new equilibrium. It is remarked that the coarse and fine versions are based on the same fine hydrodynamic model, but for the coarse version the hydrodynamic data are aggregated 2×2 prior to the sediment transport computations.
7. Initially, the model has been set-up with two sediment fractions: a marine fraction and a fluvial fraction. At a later stage, more fractions may be included, such as a very fine fraction with a low settling velocity. This fraction may not be so important for the sediment balance of the estuary, but may be important if the model is used as an engineering base for light climate simulations.
8. Having followed the procedure described above, the model performance is evaluated based on the list of desiderata. The strong and weak points of the model are determined. It is discussed for what type of management issues to model is already fit for use and for what type of questions further improvements are required and how these improvements might be achieved.

More details on the calibration method are discussed in Appendix B, especially regarding the transition between sandy and muddy areas.

5.5.2 Point model

Using the SPM data at Terneuzen (DOW jetty), a point model was applied to investigate to what extent vertical exchange of sediment dominates the SPM time series and to determine typical parameter settings for the Scheldt estuary. Figure 5.5 shows the results of the first calibration session.

The preliminary conclusion is that intra-tidal and neap/spring inter-tidal SPM fluctuation can be reproduced reasonably well with a local point model, although the neap-spring trend is somewhat overestimated. Seasonal fluctuations (*i.e.* high SPM concentration in winter, low SPM concentration in summer) can not be reproduced by the local point model, as seasonal trends are absent in the local bed shear stress, which is the forcing mechanism of the point model.

The point model has also been applied to the measurements at Boerenschans (part of the dataset from the Liefkenshoek tunnel project), which is equivalent with the dataset from the DOW jetty at Terneuzen. The same parameter settings are applied as for the Terneuzen point model. In such a way can be determined to what extent the parameter settings are location specific. Figure 5.6 shows the results at Liefkenshoek. It is concluded that the point model is not able to reproduce the highest concentration peaks, which may be caused by advection from tidal flats. The secondary maxima and the minima are reasonable reproduced, however.

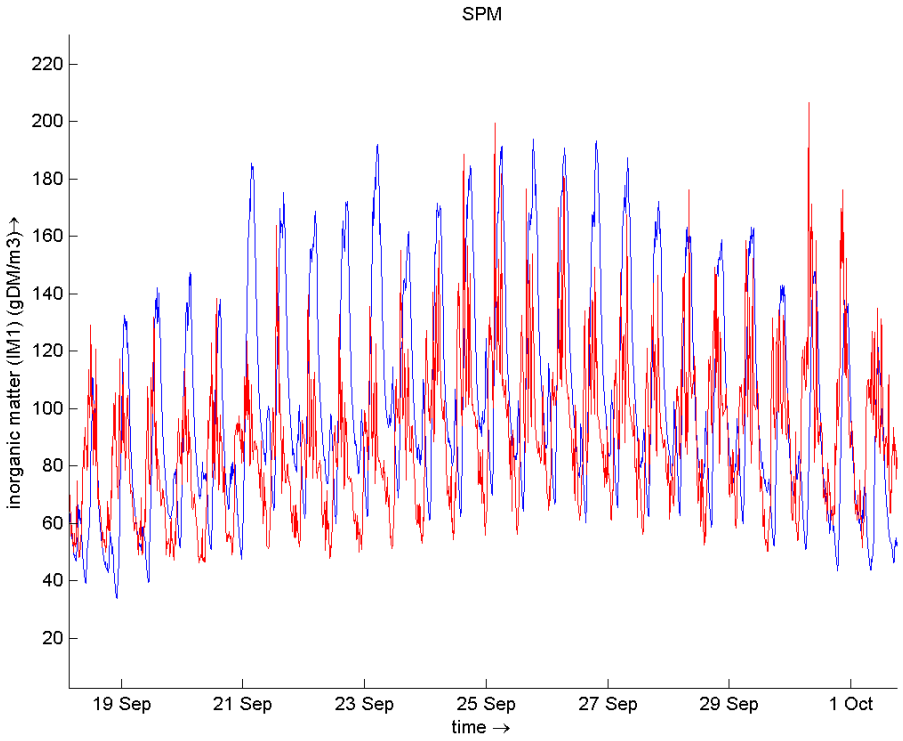

Figure 5.5: Measured (red) and computed (blue) SPM concentration at Terneuzen, depth = –17 m NAP. Computation based on a local (point) model with vertical exchange between water column and sea bed only. For parameter settings see Table 5.3.

parameter	value	units
w_s	0.5	mm/s
α	0.3	–
τ_{crit1}	0.4	Pa
M_1	1.2×10^{-5}	s^{-1}
d	0.1	m
τ_{crit2}	1.0	Pa
M_2	$3.5\ 10^{-7}$	$kg/m^2/s$

Table 5.3: Parameter settings from point model.

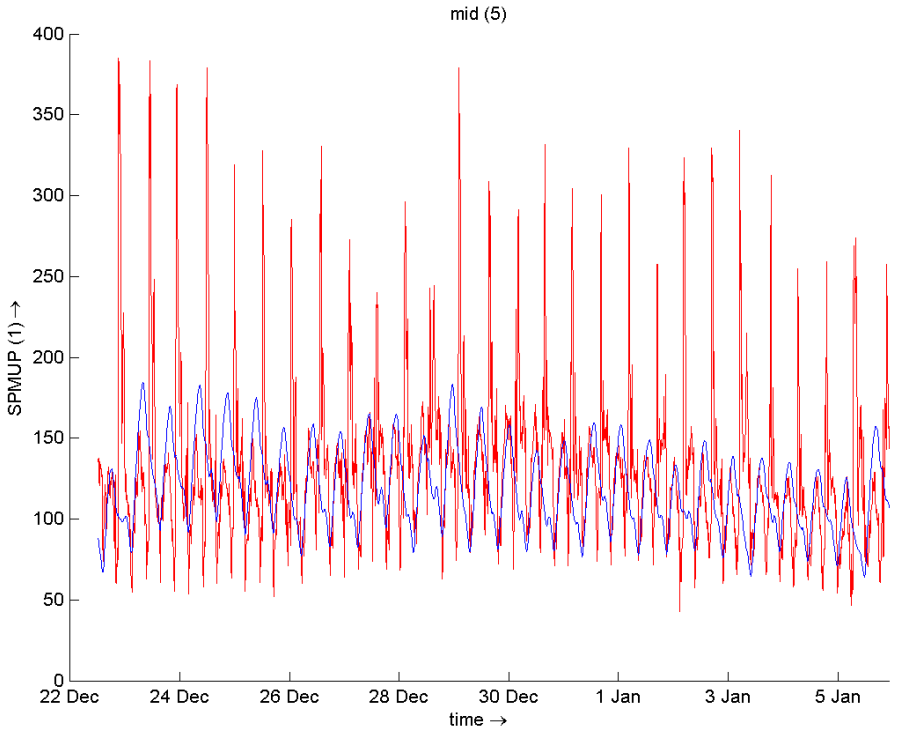

Figure 5.6: Measured (red) and computed (blue) SPM concentration at Boerenschans. Computation based on a local (point) model with vertical exchange between water column and sea bed only. For parameter settings see Table 5.3.

It is expected that seasonal trends do appear in the Scheldt model, as the seasonal trend in SPM concentration is related with the trend in average wind speed and salinity. The observed higher average wind speed in winter will result in more resuspension and therefore a larger supply of SPM in shallow areas, especially in the Western Scheldt outer delta. The observed lower salinity in winter will result in a stronger salinity gradient enhancing the estuarine circulation. Also, the higher freshwater discharge of the river Scheldt, which causes the salinity decrease, will result in a higher fluvial sediment supply in winter. These mechanisms steering seasonal variations are not available in the point model, but are included in the Scheldt model.

Would the simulated seasonal variation nevertheless be too small, an option is to make the critical shear stress for erosion time-dependent, with a lower value in autumn/winter and a higher value in spring/summer. This would reflect the stabilising effect of biological activity in spring/summer. However, it is decided to start with purely physical forcing factors first.

5.5.3 3D Scheldt model

For the first simulation with the 3D model, the parameter settings from the point model are applied (see Table 5.3). In the 3D model two fractions are included, *i.e.* the marine and fluvial fraction. For a start, both fractions have the same parameter settings. Based on the first simulation, a sensitivity analysis is made by a variation of the following parameters:

- settling velocity: **0.5**, 1 and 2 mm/s
- critical shear stress for resuspension from layer 1: 0.1, 0.2 and **0.4** Pa
- critical shear stress for resuspension from layer 2: 0.5 and **1** Pa
- thickness layer 2: 0.05 and **0.1** m
- the exchange rate between layer 2 and the water column by a simultaneous variation of M_2 and α: doubled or halved.

The bold values are the values from the point model. From the sensitivity analyses, the following is concluded:

1. For w_s = 0.5 mm/s the vertical concentration is much too uniform compared with field observations, whereas for w_s = 2 mm/s the system becomes too stratified. A setting of w_s = 1 mm/s is a good compromise, showing reasonable agreement with the ratio between observed near-surface and near-bottom SPM concentrations.
2. For τ_{crit1} = 0.1 Pa, the modelled harbour siltation is too low, whereas the SPM concentration becomes rather high. For τ_{crit1} = 0.4 Pa too much sediment is lost towards the bed, resulting in a too low SPM concentration, especially farther up-estuary. The setting of τ_{crit1} = 0.2 Pa forms a good compromise, with both reasonable siltation volumes and SPM concentrations.
3. For τ_{crit2} = 1.0 Pa the equilibrium mud fraction in layer 2 is very low in dynamic areas (<< 0.01), but becomes very high (close to unity) in semi-sheltered areas, where the sand fraction is still dominant according to the McLaren soil data. In order to reduce the strong sensitivity of the equilibrium mud fraction on the bed shear stress climate, τ_{crit2} was reduced to 0.5 Pa (half of the original value).
4. The short-term SPM concentration fluctuations are virtually independent from the assumed thickness d of layer 2. However, the response time to long-term changes (for example changes in boundary conditions on a seasonal scale) is sensitive to second layer thickness. A thinner layer results in a faster system response. To be able to reach equilibrium conditions within the simulation time frame envisaged (maximal 2 years), the layer thickness was pragmatically reduced to 0.05 m. Would field observations demonstrate the necessity of a longer response time, this can be easily taken into account in the model, however.

5. The last aspect of the sensitivity study is the exchange rate between layer 2 and the water column. The higher the exchange rate, the more sensitive layer 2 becomes for short-term (*e.g.* neap-spring) variations. A smaller exchange reduces the model's too strong response to neap-spring forcing.

Table 5.4 shows the final parameter settings which are chosen based on the sensitivity calculations. With these settings all simulations discussed in Section 5.6 and 5.7 are carried out. Note that the settings for marine and fluvial sediment are equal, apart from α. To enhance the fluvial SPM concentration with respect to the marine concentration, α_2 has been reduced twofold, which implies that the fluvial fraction less easily penetrates into the sandy bed layer (in the model). The reduced value for α compared with the settings from the point model is explained for the major part by the doubled settling velocity. To maintain an equal flux towards the second bed layer, α should be halved.

parameter	**value**	**units**	**value**	**units**
	fraction 1: marine		*fraction 2: fluvial*	
w_s	1.0	mm/s	1.0	mm/s
α	0.1	–	0.05	–
τ_{crit1}	0.2	Pa	0.2	Pa
M_1	2.3×10^{-5}	s^{-1}	2.3×10^{-5}	s^{-1}
d	0.05	m	0.05	m
τ_{crit2}	0.5	Pa	0.5	Pa
M_2	$3.5\ 10^{-7}$	$kg/m^2/s$	$3.5\ 10^{-7}$	$kg/m^2/s$

Table 5.4: Final parameter settings used in 3D model. Note that the settings for the marine and fluvial fraction are equal apart from α.

5.6 Overview of model simulations

The following simulations have been made with the settings displayed in Table 5.4 (unless indicated otherwise):

runID	**description**
w15	winter simulation, $Q_{riv} = 200\ m^3/s$
w15s12	winter simulation with numerical scheme 12[1], simulation period 3 months
w15 1×1	winter simulation with scheme 12 and unaggregated grid (i.e. most accurate); simulation period 2 weeks; restart from w15.

[1] *Scheme no. 12 in DELWAQ uses a FCT-method (Boris and Book, 1973) in the horizontal and is implicit in time and centrally discretised in the vertical. The less accurate scheme no. 16 in DELWAQ is implicit upwind in the horizontal and centrally discretised in the vertical. The latter schema is able to handle much larger time steps.*

w17	winter simulation with 2× slower response time (α and M_2 ×0.5 for both fractions)
z15	summer simulation, Q_{riv} = 76 m^3/s
ws15	year simulation (based on 14-day winter hydrodynamics with varying boundary concentrations and fluvial loads). On 1/1 the winter conditions are applied, on 7/1 the summer conditions. Between these dates a linear interpolation is applied
ws16	same as ws15, but with 2× faster response time (α and M_2 ×2 for both fractions)
ws18	same as ws15, but without sediment loads from dumping activities

Apart from simulation w15_1×1, all simulations were carried out on a 2×2 aggregated grid to reduce CPU time. All simulations except z15 were based on the 14-day winter hydrodynamics discussed in Chapter 4. As the water levels at the start and the end of this simulation, which is used 26 subsequent times to compute a full year of sediment transport, do not match well, the last 2 hours are not used in the sediment computations. The overall volume closure error is just under 1%. In shallow areas, the error may be substantially larger. To avoid a concentration jump at the transition from the last time stored in the hydrodynamic database to the first time, DELWAQ adds or removes mass with a direct relationship with the local volume correction. The amount of mass added or removed appears in the sediment budget discussed in Section 5.7. In the major part of the model domain, the error is small or even very small compared with the other terms in the mass balance. However, the error may become very large in shallow areas, mainly up-estuary.

These errors may be reduced or even completely removed if the period of the hydrodynamic simulation is increased or if only harmonic water level components are used that fit within the simulation period (*e.g.* M_2, S_2 and their higher harmonics for a single neap-spring period).

It is remarked that wave effects are taken into account in a parameterised form only. This is done as follows. From the observed waves at location Scheur west Wandelaar (depth 15 m) the bed shear stress is calculated for the period 1979 – 2003 (n_{obs} = 70128, every 3h). The average wave-induced bed shear stress in the winter months (Dec, Jan and Feb) is about 0.5 Pa. This value is added as a constant to the current induced bed shear stress calculated by DELWAQ. This addition is applied to the North Sea area of the model domain only. Inside the Scheldt area, the equilibrium wave height was calculated as a function of water depth for a winter-averaged wind speed of 7 m/s and a fixed fetch length of 25 km using the Bretscheider formulation. Figure 5.7 shows the resulting bed shear stress as a function of water depth h. The wave-induced bed shear stress τ_{wav} may be approximated with:

$$\tau_{wav} = \tau_0 \exp(-ah)$$

with τ_0 = 0.47 Pa and a = 0.185 1/m. The resulting constant wave-induced bed shear stress covering the whole model domain is shown in Figure 5.8.

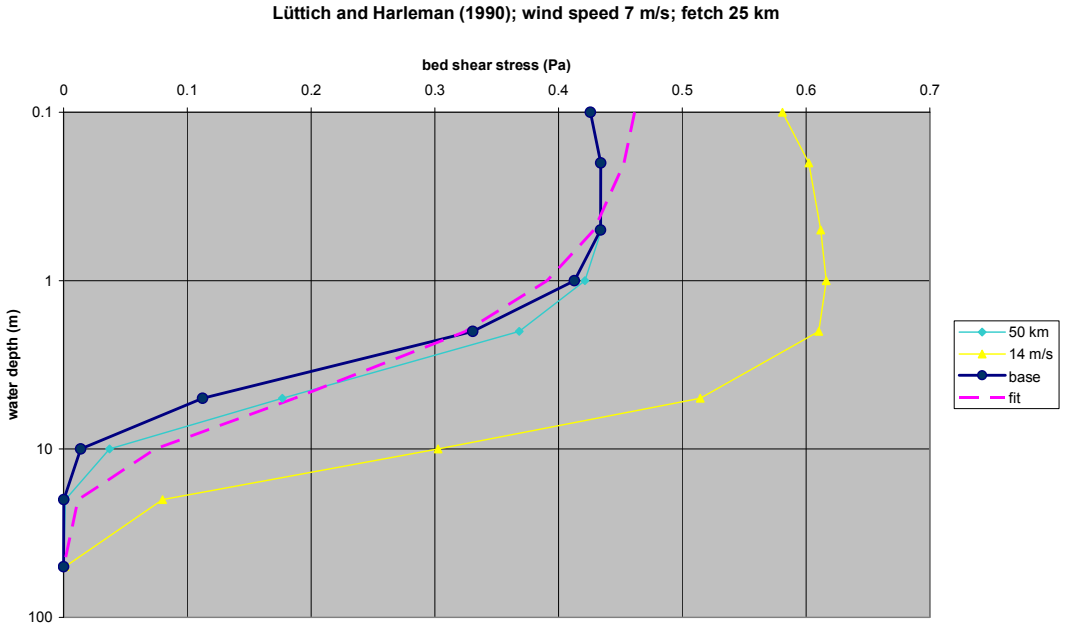

Figure 5.7: Wave induced bed shear stress as function of water depth for equilibrium waves. Wind speed 7 m/s, fetch 25 km. Wave height and period calculation according to Bretschneider, bed shear stress according to Lüttich and Harleman (1990).

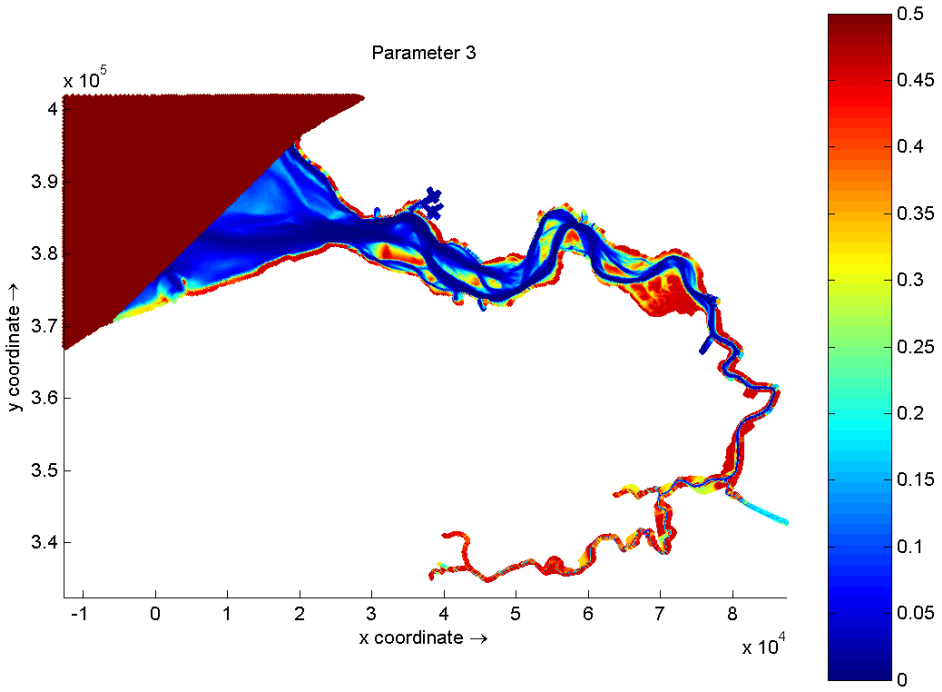

Figure 5.8: Applied constant wave-induced bed shear stress (Pa).

5.7 Results and discussion

The results for simulations **w15** (winter, S1), **z15** (summer, S2), **w17** (winter with changed settings, S3), **ws15** (year, S4), **ws16** (year with changed settings, S5) and **ws18** (year without dumping of dredged material, S6) are shown in Appendix S.

For each simulation *i*, the following figures are presented:

S*i*.1: 14-day mean SPM concentration in the surface layer and the concentration ratio between surface and bottom. For the year simulations a = winter conditions and b = summer conditions
S*i*.2: net siltation over 1 month and mud fraction in bottom (layer 2)
S*i*.3: fraction marine mud in the water column and in the bottom
S*i*.4: 14-day mean SPM concentration along Scheldt estuary, total and marine fraction
S*i*.5: surface and bottom SPM time series at DOW jetty and Boerenschans.
S*i*.6: surface and bottom SPM time series at Doel, Zuidergat, Honte and Wielingen, including observed long-time average concentration and 10 and 90 percentile values
S*i*.7: net mud balance of the Scheldt area in kton/year

Based on these figures, the following observations are made:

- Typical concentrations in the western part of the Western Scheldt are predicted reasonably well: winter concentrations are high, summer concentrations are low (see **w15** and **z15**). In the western part of the Western Scheldt, SPM levels are sensitive to the applied concentration boundary conditions. Presently, the Appelzak transect has been used as a proxy for the southern model boundary, but this may be refined with more field data if available. Remote sensing data may provide a better estimate on seasonal SPM levels at the southern model boundary.
- Typical concentrations near Antwerp tend to be too low. This can be improved by increasing the boundary concentration at sea, but this results in much too high concentrations in the estuary mouth. The measurements show a gradual concentration decrease from the estuary mouth towards Terneuzen, which is reproduced by the model. However, the subsequent concentration increase towards the estuarine turbidity maximum (ETM) near Antwerp is not reproduced by the model. This is a major deviation which needs attention, as the ETM forms one of the essences of the Scheldt estuary.
- The vertical stratification is quite well reproduced by the model. The stratification increases towards the estuary mouth, which agrees with observations (see Chapter 3). The stratification level depends strongly on the settling velocity and can be easily modified in the model if required. As the settling velocity also affects the deposition rate, it may be required to change other parameters also, such as α or M.
- The tidal concentration variation is approximately a factor 2, which matches with observations.
- The neap-spring concentration variation is approximately a factor 3, which is too much compared with observations (factor 1.5 – 2). The neap-spring variation increases towards the mouth. It is expected that this aspect can be improved by applying variable wave forcing and by reducing the rate of exchange with the second bottom layer.

- The computed mud percentage in the bed agrees reasonably well with the observed mud percentage (McLaren). However, the dependency of the equilibrium mud percentage on the local bed shear stress climate is still too pronounced. In sheltered areas the mud percentage tends to be too high. This may be further improved by reducing the power in Eq. (5.2), reducing τ_{crit2} (at the same time, M_2 should be reduced to maintain the exchange rate at a high shear stress at the same level), or improving the realism of the wave-induced bed shear stress, which is presently just a constant contribution.
- The model shows distinct seasonal dynamics (**ws15**), but these results require a careful interpretation. The seasonal dynamics are presently caused by the variation in boundary conditions, both up-estuary and down estuary. Internally, there is not yet any seasonal forcing, as the wave effects and the river discharge are still constant. Also the critical shear stress for erosion, which may have a seasonal trend in shallow and intertidal areas caused by biological activity, is kept constant. From the boundaries, sediment penetrates the system like a 'tidal wave' with a period of 1 year. The farther from the boundaries, the more the seasonal variation is dampened and the larger is the phase lag. This response can be optimised by changing the buffer capacity of the system (*i.e.* the equilibrium mass of sediment). The higher is the buffer capacity, the slower and more dampened is the system response. This type of seasonal dynamics forces the sediment concentration to change concurrently in the water column and in the bottom. However, locally-induced seasonal dynamics (waves, biology) would show the reverse pattern: a decrease in bottom concentration in combination with an increase in SPM levels and vice versa. One should be cautious that the model does not well predict the seasonal dynamics based on the wrong mechanism.
- The model does show most siltation were it is observed: in the harbour basins bordering the Scheldt estuary. Siltation volumes have the right order of magnitude at Zeebrugge, Vlissingen and Terneuzen, but are much too low at Antwerp. This is attributed to the too low SPM levels, as no clear ETM is modelled. If the predicted SPM levels near Antwerp would improve, also the modelled siltation volumes will improve. Hardly any permanent siltation occurs in shallow areas or intertidal flats. This is caused by two aspects:
  1. The applied mean wave-induce bed shear stress in shallow areas (ca. 0.4 Pa, see Fig. 5.7 exceeds the critical shear stress for erosion (0.2 Pa). However, some areas will in reality experience much less wave activity, making permanent mud accumulation possible. A more accurate wave forcing will probably improve this.
  2. By definition, the mud percentage in the sand layer is in equilibrium with the long-term mud supply and bed shear stress climate, unless the supply is so high or the average bed shear shear stress is so low that the soil becomes muddy. In the modelled sandy part of the estuary, no net long-term mud accumulation is possible (notwithstanding seasonal dynamic etc.). In reality, new sand banks do catch fines until their local equilibrium composition is reached. As the present model does not include morphological changes, this sediment sink is excluded. The related source term (mud from eroding sand banks) is also neglected, however. For a system with a constant sand volume, the resulting net error is therefore small.
- The alongshore flux along the Belgium coast is unrealistically high (> 100 MT/y for winter conditions). As observed typical summer and winter concentrations are applied to the boundaries, this may be partly caused by an overestimation of the residual current along the coast. Also, the use of observed concentrations at Appelzak for boundary conditions may result in an overestimation of the alongshore flux, as Appelzak is

located in a turbidity maximum. As the estimated sediment flux along the coast is large (also for more realistic numbers of 10 – 20 MT/y) compared with the net import towards the Scheldt, the too high supply in terms of net flux probably does not much affect the model performance in the Scheldt estuary, as the sediment supply in terms of SPM concentration is realistic.

- The strongest gradient in the ratio between fluvial and marine mud occurs near the Dutch-Belgium border for the winter simulation **w15**. This is in agreement with observations from Verlaan (1998). The ratio between the fluvial and marine mud fraction is quite insensitive to model parameter setting (but maintaining equal settings for both fractions). Apparently, this is caused by the local strong widening of the estuarine cross-section. However, the ratio is quite sensitive to the up-estuary freshwater discharge (simulation **z15**). During summer conditions, the marine fraction migrates up-estuary.
- For the present model settings, loads and boundary conditions, a temporary cease of sediment dumping during one year results in significantly lower SPM concentrations (Fig. S6.8). However, the model should be further improved —especially regarding the ETM near Antwerp and the long-term balance between harbour siltation and dumping— prior to drawing final conclusions. It is remarkable that the computed effect near Antwerp is much less pronounced than in the Western Scheldt. This requires further attention.

Figure 5.9 shows time series of the SPM concentration at Terneuzen Boei 20 (surface) for identical simulations apart from the numerical scheme and grid resolution. The simulation with the unaggregated grid and solving Scheme 16 (blue line) is expected to be most accurate.

Based on Figs. 5.9, S7.1 and S7.2 (see appendix) it is concluded that the difference between 1×1 and 2×2 aggregation is small apart from regarding very local concentration patterns. The difference between Scheme 12 and Scheme 16 is substantial. Schema 16 results in higher surface concentrations and much more diffuse spatial patterns. It is therefore recommended to use Scheme 12 in future calculations. However, for simulations of one year or more this is an unattractive option, with required simulation times of one week or more.

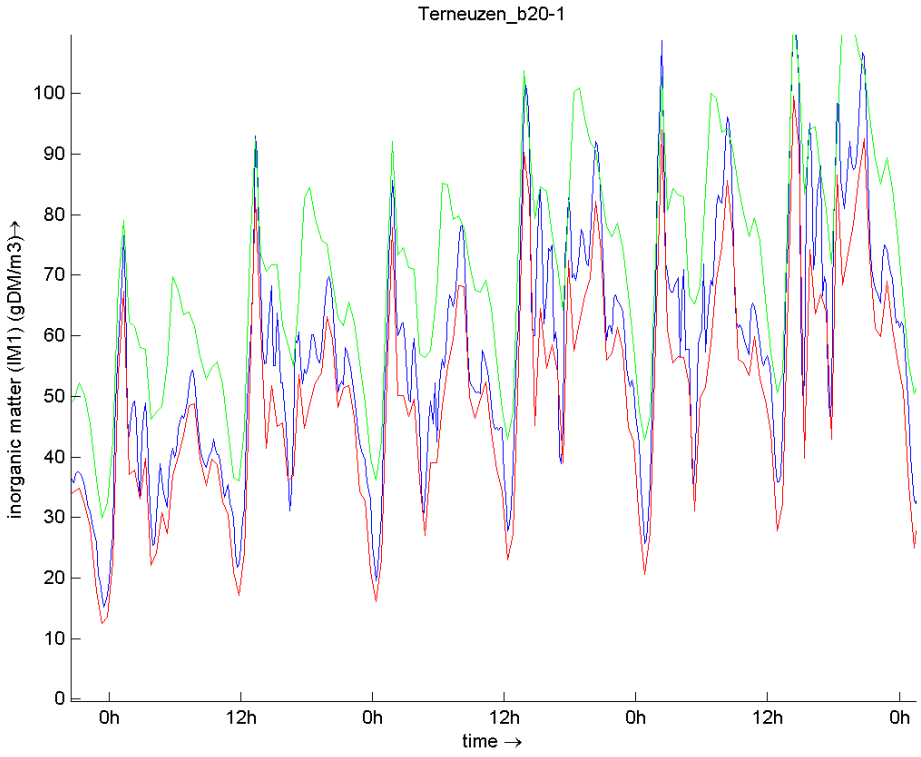

Figure 5.9: SPM concentration at Terneuzen Boei 20 for simulations with Scheme 16 (green), Scheme 12 (red) (both with 2×2 aggregated grid) and with Scheme 12, unaggregated grid.

The absence in the model of a distinct ETM near Antwerp should be investigated first prior to further other optimisation. It may be caused by:

1. an improper residual current distribution in the hydrodynamics
2. a too high vertical eddy diffusivity from the hydrodynamics
3. the number of horizontal layers (5) may be too small
4. the applied numerical scheme 16 in the silt transport computation may be too diffusive

Warner *et al.* (2006) investigated the sensitivity of an ETM to settling velocity, tidal mixing and sediment supply. They present some dimensionless numbers with values favouring the generation of an ETM. Their analysis can be helpful in an investigation on the cause(s) for the absence of an ETM in the present model.

5.8 Conclusions and recommendations

The developed mud model shows already a realistic behaviour in the western part of the Western Scheldt. Tidal, fortnightly and seasonal trends are reproduced with some success, although further improvements are definitely within reach. The most important flaw of the present model is its lack of an ETM near Antwerp. Here the concentration remains too low, resulting in too low siltation volumes in the harbour docks and access channels. The absence of an ETM near Antwerp may be caused by, amongst others:

- insufficient realism on the residual bottom currents in the hydrodynamic model;
- a too low level of accuracy in the hydrodynamic model regarding tidal asymmetry;
- the absence of flocculation in the mud model (the settling velocity is assumed to be constant);
- too much dispersion, either regarding physical parameter settings or numerical diffusion;
- insufficient vertical detail with 5 layers;
- inaccuracies in the data on the mud dumping volumes at Antwerp or on the fluvial sediment load upstream;

Sufficient data are available to calibrate the model on short-term fluctuations. The model response to long-term fluctuations depends on the assumed buffer capacity of the bed. Data for the calibration on long term trends are very scarce, unfortunately.

It is recommended to pay more attention to seasonal trends that do not originate from fluctuations in sediment supply (these have already been considered), but from variations in freshwater discharge, wind and wave climate and the seasonal (de)stabilisation of mudflats. To this order, the applied wind and wave climate should be more refined and the hydrodynamics of periods much longer than a fortnight should be modelled. This is essential for modelling sediment accumulation at upper intertidal and supra-tidal mudflats. Also, the boundary condition at the SW sea boundary should be refined.

6 Overall conclusions

In the framework of the present study (phases 1 and 2 of LTV-slib), the following tasks have been performed:

1. System description and literature study
2. Data analysis
3. Development of hydrodynamic model
4. Development of mud transport model
5. Management issues

The first four items are reported in the present report. The last item is reported in a separate note. As such, the targets set for phases 1 and 2 for the LTV-slib project have been realised.

Both the hydrodynamic and the mud transport model are technically completed and operational and show already sensible results. However, the calibration can not be considered as 'finished', as the model behaviour is not yet fully satisfactory. This was expected at the start of the study, however.

Regarding the hydrodynamics, more work is required on for example:

- analysis of the residual current distribution along in coast and in the estuary, especially near the observed estuarine turbidity maximum (ETM) near Antwerp
- analysis of the transient behaviour of the longitudinal salinity distribution in response to changing freshwater discharge

Also, it is recommended to store a much longer period than 14 days in the hydrodynamic database used by the mud transport model. This reduces repeated mass corrections and introduces more realism regarding natural variability. Grid aggregation may be required to arrive at realistic simulation times and disk storage requirements.

Regarding the mud transport model, more work is required on:

- the reproduction of the ETM near Antwerp
- a more realistic wave forcing
- refinement of concentration boundary conditions and sediment loads
- determination of the optimal equilibrium sediment mass in the estuary
- correct siltation volumes in harbours in balance with mud dumping from harbour maintenance.

7 References

WLB (2004) 2Dh NEVLA-Scheldemodel. Bouw en afregeling stromingsmodel. Model 753-01

Alkyon (2005) Evaluatie van Hydraulische modellen voor operationele getijvoorspellingen. In opdracht van de Vlaamse Overheid, afdeling Kust.

Bruens, A., J. Vanlede, T. van Kessel (2006). Notitie beheersvraagstukken LTV-slibmodel. WL | Delft Hydraulics Report Z4210.75 (in Dutch).

Chen, M.S., S. Wartel, B. van Eck and D. van Maldegem (2005). Suspended matter in the Scheldt estuary. *Hydrobiologia* 540, pp. 79–104.

Claessens, J. (1988). Het hydraulische regime van de Schelde, *Water* 43, pp. 163–169 (in Dutch).

Eck, G.T.M. van, N. de Pauw, M. van Langenbergh and G. Verreet (1991). Emissies, gehalten en gedrag van effecten van (micro)verontreinigingen in het stroomgebied van het Schelde-estuarium. *Water* 60, pp. 164–181 (in Dutch).

Fettweis, M., M. Sas, J. Monbaliu (1998). Seasonal, neap-spring and tidal variation of cohesive sediment concentration in the Scheldt Estuary, Belgium. Estuarine, Coastal and Shelf Science 47, 21–36.

IMDC (1998). The Scheldt Estuary: Physical, Navigational and Dredging Aspects. Report I/R/11128/98.024/MFE, May, 1998 (prepared by M. Fettweis and M. Sas).

IMDC (1998b). Container Dock West. Hydraulic-sedimentological investigation. End report. Antwerp, Belgium.

IMDC *et al.* (2004). Feasibility study 2D nutrient- and sediment transport modelling for the Scheldt estuary and GOG KBR. Specifications 16EB/01/23; Part 2: Inventarisation. Report I/RA/11214/04.018/MBO, October, 2004 (author: M. Bollen) (in Dutch).

Lacroix, G., Kevin Ruddick, José Ozer, Christiane Lancelot (2004). Modelling the impact of the Scheldt and Rhine/Meuse plumes on the salinity distribution in Belgian waters (southern North Sea). *J. Sea Research* 52, pp. 149–163.

Ledden, M., B. van Prooijen, T. van Kessel, A. Nolte, H. Los, J. Boon, W. de Jong (2006). Impact sand extraction Maasvlakte 2. Royal Haskoning Report 9P7008.O9.

Maldegem D. van (2002). Overzicht gegevens voor LTV-slibmodel Schelde-estuarium. Werkdocument RIKZ/AB/2004.821x. RIKZ.

Maren, B. van and T. van Kessel (2006). Sensitivity analysis and calibration of the 3D mud model for the Sea Scheldt. WL | Delft Hydraulics Report Z3824.55.

McLaren (1994). Sediment transport in the Western Scheldt between Baarland and Rupelmonde. Report prepared for the Antwerp Harbour Authorities.

Nihoul, J.C.J.F., F. Ronday, J.J. Peters, A. Sterling (1978). Hydrodynamics of the Scheldt estuary. In: J.C.J.F. Nihoul (ed.), Hydrodynamics of Estuaries and Fjords, Elsevier, Amsterdam, pp. 27–53.

Pawlowicz R., B. Beardsley, and S. Lentz (2002) Classical tidal harmonic analysis including error estimates in MATLAB using T_TIDE, *Computers and Geosciences 28*, 929-937.

Peters, (1975). Les mechanismes de mélange des eaux dans l'estuaire de l'Escaut. Tijdschrift der Openbare Werken van België 2, pp. 101–119.

RIKZ (2005) Technical documentation TRIWAQ (v.2.4)

RIKZ (2005) User's guide WAQPRE (v.10.41)

RIKZ (2005) User's guide WAQUA: general information (v.10.41)

RWS/RIKZ (1995). Analysis 13-hour vertical measurements in the Western Scheldt for silt transport modelling. Note RIKZ/OS-95.615.x, November 1995 (author: H.P.J. Mulder) (in Dutch).

RWS/RIKZ (2002) Overview of data for LTV mud model Scheldt estuary. Work document RIKZ/AB/2004.821.x, December 2002 (author: D. van Maldegem) (in Dutch).

RWS/RIKZ (2004a). Monitoring and research programme for mud; Part: budget knowledge 2004. Work document RIKZ/ABD/2004, January 2004 (author: D. van Maldegem) (in Dutch).

RWS/RIKZ (2004b). Monitoring and research programme for mud; Part: overview literature and executed projects. Work document RIKZ/ABD/2004xxx, January 2004 (author: D. van Maldegem) (in Dutch).

Smith and Banke (1975) Variation of the sea surface drag coefficient with wind speed. Quart. J. Roy. Meteorol. Soc. Vol.101 - 665:673.

Suijlen, J.M. and Duin, R.N.M. (2001). Variability of near-surface total suspended matter concentrations in the Dutch coastal zone of the North Sea. Climatological study on the suspended matter concentrations in the North Sea. Report RIKZ/OS/2001.150X.

Toorman, E. (1997) Containerdok West. Hydraulisch en sedimentologisch onderzoek. Erosiegevoeligheid van de bodemsedimenten. Laboratoriumproeven. Rapport KUL-HYD/ET97.3

Temmerman, S. (2003). Sedimentation on tidal marshes in the Scheldt estuary. Ph.D. thesis Katholieke Universiteit Leuven, Belgium.

Verlaan, P.A.J. (1998). Mixing of marine and fluvial particles in the Scheldt estuary. Ph.D. thesis Delft University of Technoloy, The Netherlands

Warner, J.C., C.R. Sherwood and W.R. Geyer (2006). Sensitivity of estuarine turbidity maximum to settling velocity, tidal mixing and sediment supply. In: Maa, J.P.-Y. *et al.* (Eds) Estuarine and Coastal Fine Sediment Dynamics INTERCOH 2003. Proceedings in Marine Science 8, Elsevier, Amsterdam.

Wartel, S., G.T.M. van Eck (2000). Mud budget of the Scheldt estuary (2000). Koninklijk Belgisch Instituut voor Natuurwetenschappen, Brussel / Rijksinstituut voor Kust en Zee, Middelburg (in Dutch).

WL | Delft Hydraulics (2004). Field data Scheldt estuary. Note 6 April 2004 (authors: M. van Helvert, A. van der Weck *et al.*) (in Dutch).

A Comparison of peak flows

Flows are indicated in m^3/s. Positive flows are flood, negative flows are ebb.

Transect 5a		Zuidergat	% of total	SvW	% of total
measurement	max ebb	-16843	56%	-13195	44%
	max flood	22923	55%	18926	45%
winter	max ebb	-17110	59%	-12110	41%
	max flood	21970	60%	14870	40%
summer	max ebb	-17300	59%	-12170	41%
	max flood	21530	59%	14690	41%
Transect 7		pas v Terneuzen	% of total	Everingen	% of total
Measurement	max ebb	-27399	46%	-31946	54%
	max flood	32050	42%	44499	58%
winter	max ebb	-27430	45%	-33210	55%
	max flood	29420	41%	41810	59%
summer	max ebb	-28270	45%	-34210	55%
	max flood	28750	41%	41400	59%
Transect 9		Vaarwater langs Hoofdplaat	% of total	Honte / Schaar v Spijkerplaat	% of total
Measurement	max ebb	-8918	15%	-51916	85%
	max flood	13108	16%	66893	84%
winter	max ebb	-8698	11%	-71070	89%
	max flood	9619	10%	83800	90%
summer	max ebb	-8929	11%	-72590	89%
	max flood	9235	10%	82320	90%
Transect 10		Vaarwater langs Hoofdplaat	% of total	Honte / Schaar v Spijkerplaat	% of total
measurement	max ebb	-8948	11%	-73332	89%
	max flood	11535	12%	87428	88%
winter	max ebb	-9829	11%	-80310	89%
	max flood	10700	10%	94430	90%
summer	max ebb	-10160	11%	-81690	89%
	max flood	10380	10%	92690	90%

Table A.1: comparison of peak flows

B Details on calibration method

Adapted from Van Maren and Van Kessel (2006):

An important pivot point is the shear stress level at which the erosion rate exactly balances the deposition rate. This balance occurs for $\int [M_E (\tau - \tau_{crit}) - w_s C]dt = 0$, where C is a typical mud concentration. At both sides around this pivot point the following occurs:

1. $\int [M_E (\tau - \tau_{crit}) - w_s C]dt < 0$: the available mass of sediment on the bed is large and becomes never depleted over the tide;
2. $\int [M_E (\tau - \tau_{crit}) - w_s C]dt > 0$: the available mass of sediment is small and becomes depleted for periods with a high bed shear stress. Because of this depletion, the erosion formulation shifts from zeroth order to first order: $E = M_{1E} C_{bed} (\tau - \tau_{crit})$, where M_{1E} is the first order resuspension parameter and C_{bed} the sediment mass per unit area on the bed. By definition, this results in a dynamic equilibrium between sedimentation and erosion: $\int [M_{1E} C_{bed} (\tau - \tau_{crit}) - w_s C]dt = 0$.

The first situation will occur in a low-energy environment and the second situation in a high-energy environment (*e.g.* tidal channels). For the first case the mass of eroded sediment is determined by the erosion rate, but for the second case the eroded mass is determined by the sedimentation rate, as the erosion is supply-limited. For the first case the sediment mass on the bed tends to increase in time (*i.e.* net deposition). A decrease would, after some time, inevitably cause a transfer to situation 2, whatever be the initial condition. In the Scheldt river, areas of type 1 and type 2 can be discerned based on their bed composition. Type 1 areas will be muddy, whereas type 2 areas will be sandy, possibly with a thin and weak temporary mud layer on top.

It is remarked that for situation 1, the average residence time of sediment on the bed tends to be long and consolidation may therefore occur. The dominant erosion process is surface erosion (although some very weak, fresh deposits may still be subject to mass erosion, even in a low-energy environment). For situation 2, however, the average residence time of sediment on the bed may be only a few hours or less. Consolidation is insignificant and mass erosion therefore prevails.

The target for the calibration is to determine a set of (τ_{crit}, M_E) that results in a proper-sized area for cases 1 and 2 with respect to observations and a sediment accumulation rate in area 1 that meets the sediment balance of the system. The bed shear stress level at which sedimentation and erosion are in equilibrium (averaged over time) can be realised with different sets of (τ_{crit}, M_E): low values for both τ_{crit} and M_E may result in the same equilibrium bed shear stress as high values. The difference between these settings shows up in the sedimentation-erosion dynamics: high values for both τ_{crit} and M_E cause more erosion at high shear stress levels and more sedimentation at low shear stress levels. Note that the erosion and deposition rates as a function of the bed shear stress cannot be set independently, as no critical shear stress for deposition is used.

Of course, another important target for the calibration is to realise a good reproduction of the observed suspended sediment concentration over the tide. For an *a-priori* estimate of realistic parameter settings, a local balance between sedimentation and resuspension may be assumed (neglecting advection). For areas where the sediment mass on the bed never becomes depleted, the sediment concentration increase ΔC in the water column during flood (or ebb) is then directly related to the eroded mass from the bed:

$$\Delta C\, h = \int_{t\text{flood}} [M_E\, (\tau - \tau_{\text{crit}}) - w_s\, C]\mathrm{d}t,$$

where h is water depth. The second term in the integral signifies the continuous deposition flux reducing the net erosion flux.

In the main channel, where the eroded mass is limited by the available mass of sediment, the following expression may be used as an estimate for the concentration decrease during slack water (still neglecting advection):

$$\Delta C\, h = w_s\, C t_{\text{slack}},$$

where t_{slack} is the period that $\tau < \tau_{\text{crit}}$. This concentration decrease, which approximately equals the concentration increase during accelerating flow after the turn of the tide (for all deposited mud tends to be resuspended for case 2), can be optimised with respect to field observations by optimising w_s and τ_{crit} (determining t_{slack}).

The time scale for model spin-up starting with an empty bottom can be estimate according to $t/t_{\text{tide}} = m / C_b\, \Delta V$, where ΔV is the tidal volume, C_b the concentration at the boundary and m the mass in the model domain at when a dynamic equilibrium has been attained. Note that m still gradually increases at equilibrium because of net deposition in low-energetic areas. The required spin-up time may be reduced by applying an initial sediment mass close to M. As a rule-of-thumb, the initial mass in muddy 'Type 1' areas should be chosen sufficiently large, whereas the initial mass in sandy 'Type 2' areas should be chosen sufficiently small. One should be well aware that putting a large initial mass of mud in a sandy area bordering a muddy area may require a very large spin-up time ($t \sim m_A / (\int [M_E\, (\tau - \tau_{\text{crit}}) - w_s\, C]\mathrm{d}t)$), where m_A is the initial mass per unit area and M_E is the resuspension parameter; note that the denominator is close to zero near the border between sandy and muddy areas). Therefore it is better to underestimate than to overestimate the initial sediment mass.

H Figures Hydrodynamic Model

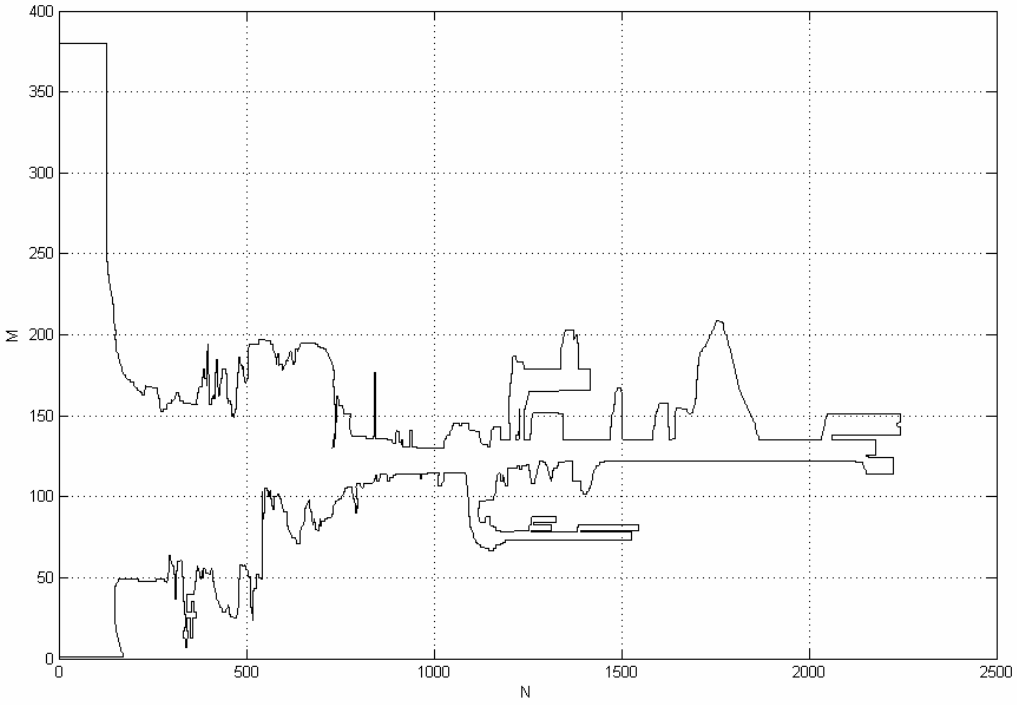

Figure H.2: Matrix view of grid	**M.756/01**
FLANDERS HYDRAULICS RESEARCH / DELFT HYDRAULICS	

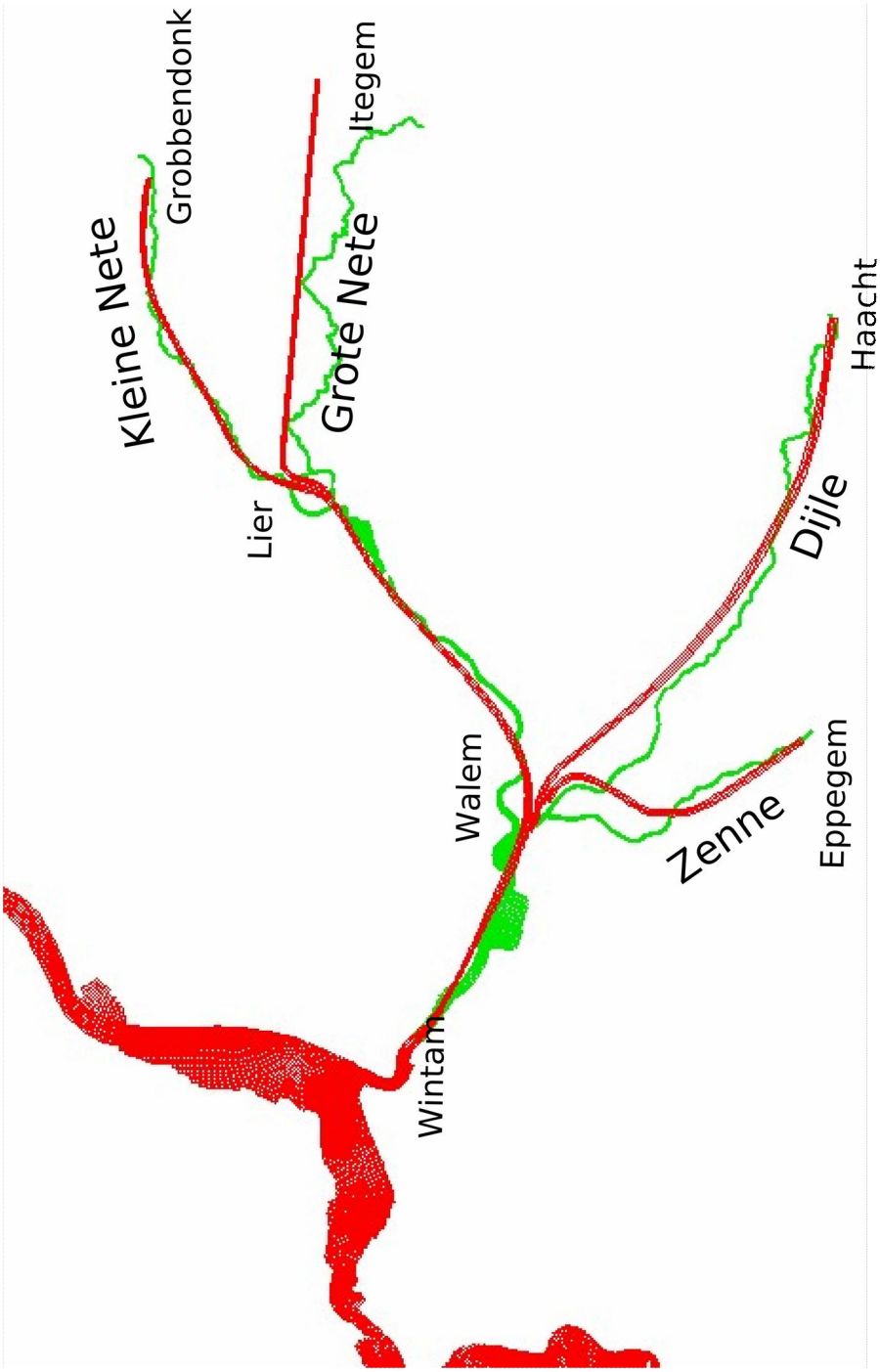

Figure H.3: Grid in Rupel basin. LTV-slib grid (red) and NEVLA grid (green).

M.756/01

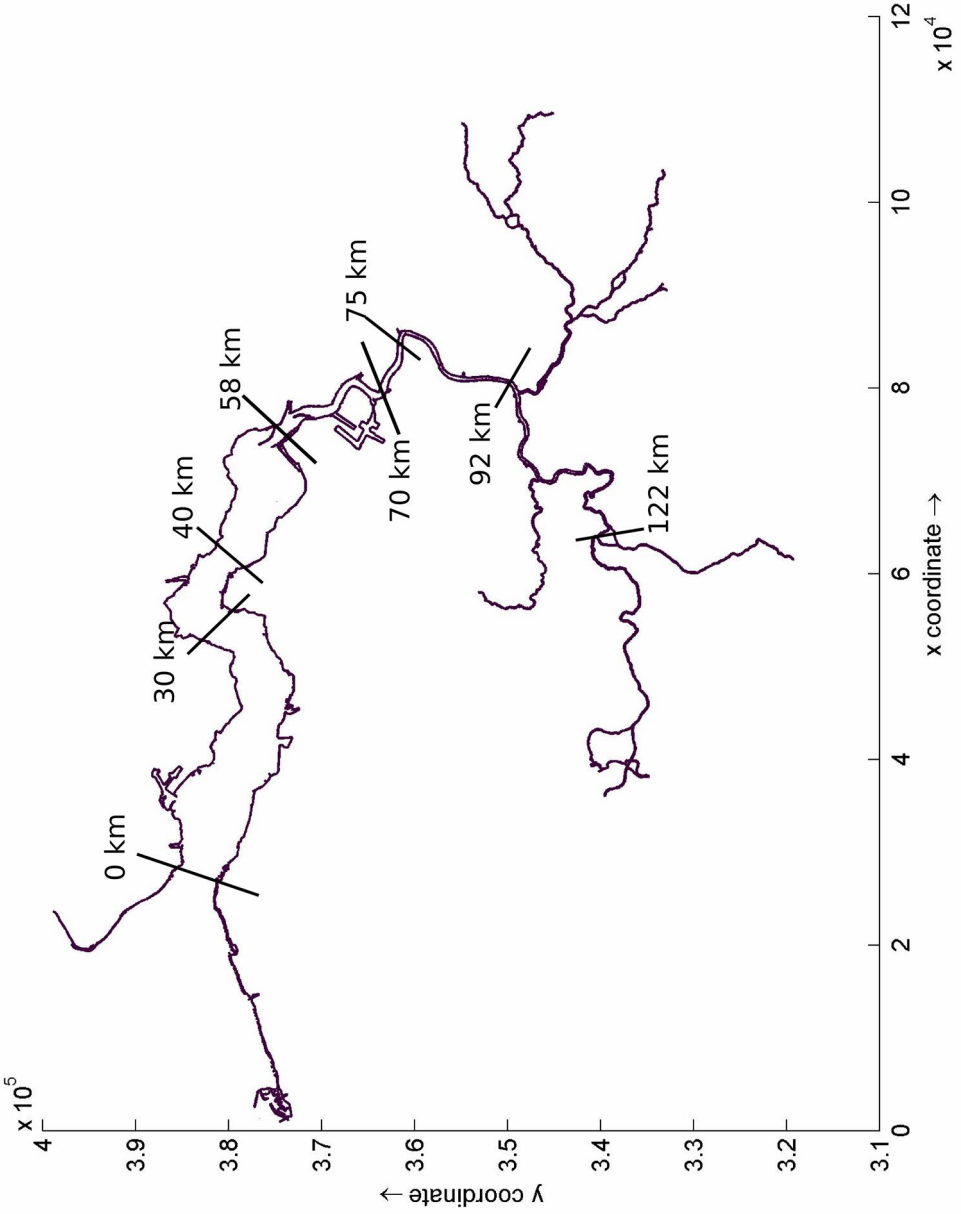

Figure H.4: Distance along estuary (after Chen et al. 2003)	**M.756/01**
FLANDERS HYDRAULICS RESEARCH / DELFT HYDRAULICS	

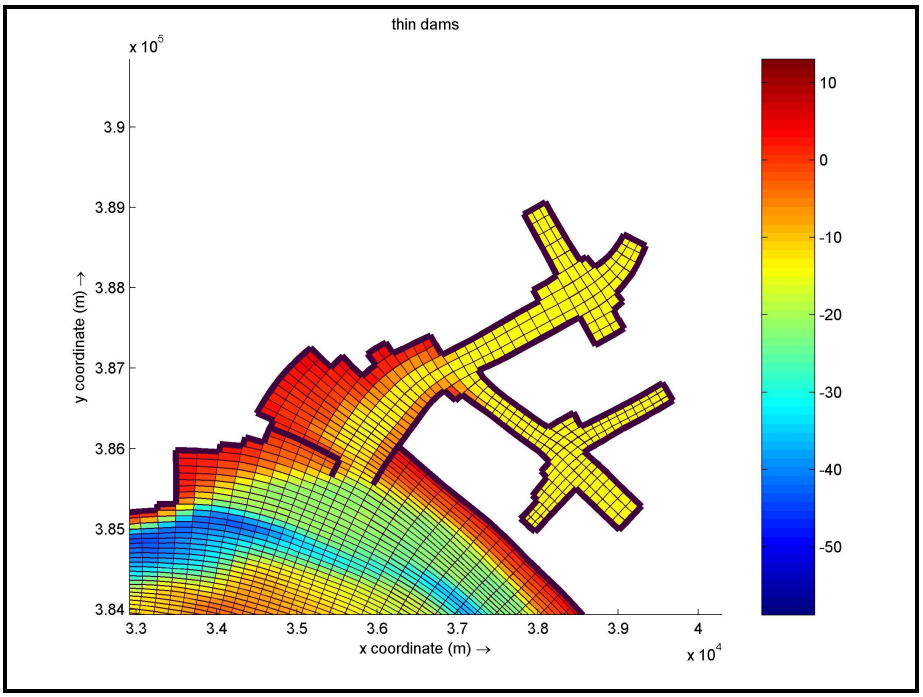

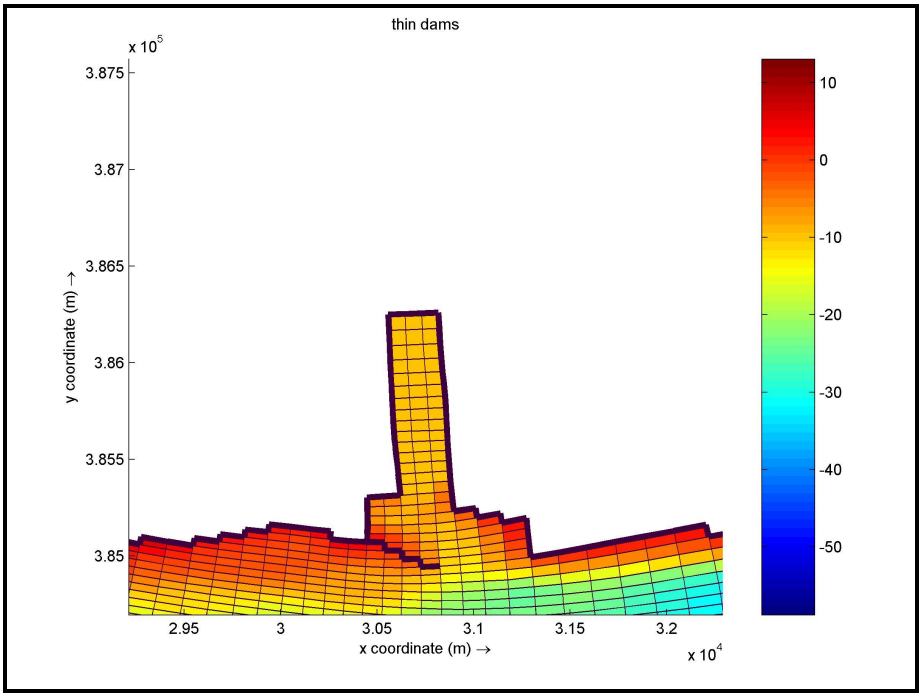

Figure H.5: Thin dams en bathymetrie in de harbour of Vlissingen (east and west)

M.756/01

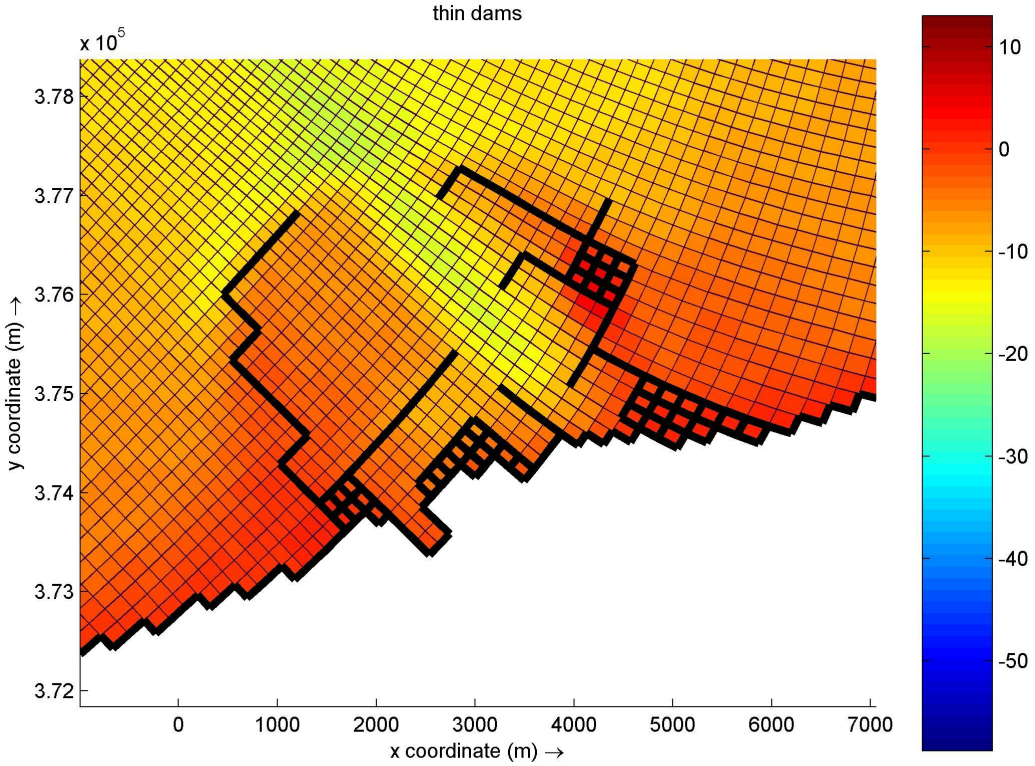

Figure H.6: Thin dams en bathymetrie around the harbour of Zeebrugge.
Dampoints are indicated by for thin dams (one on each side)

M.756/01

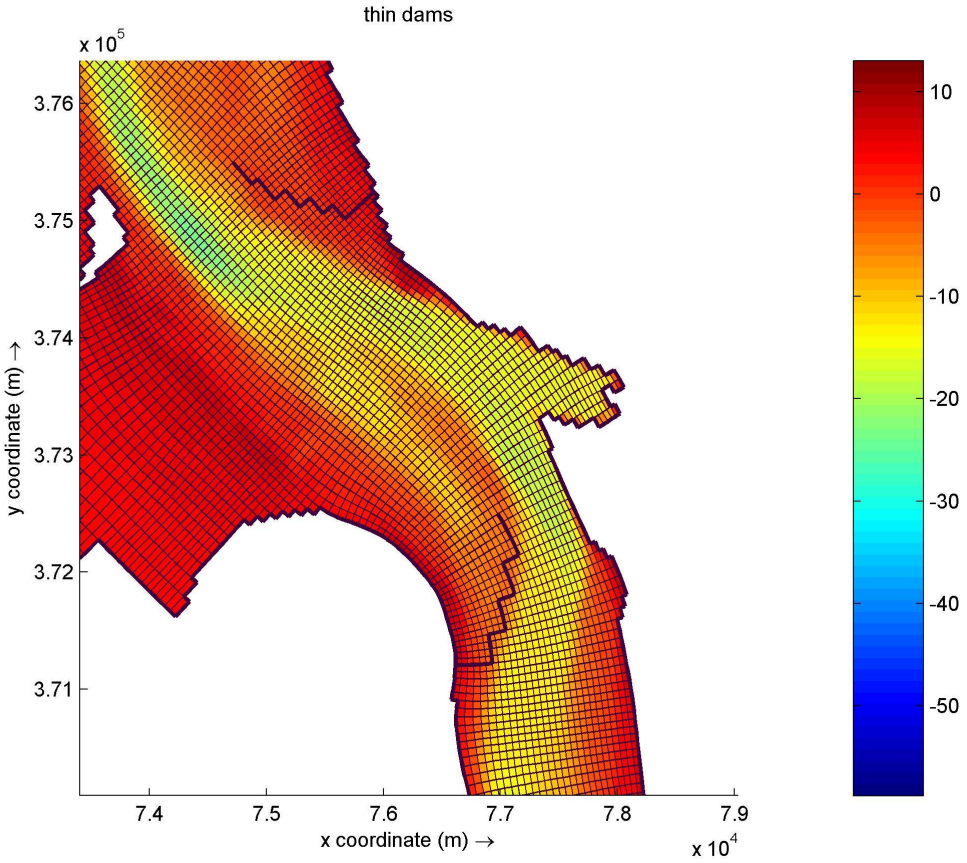

Figure H.7: Strek- en leidam: schematization in thin dams	**M.756/01**
FLANDERS HYDRAULICS RESEARCH / DELFT HYDRAULICS	

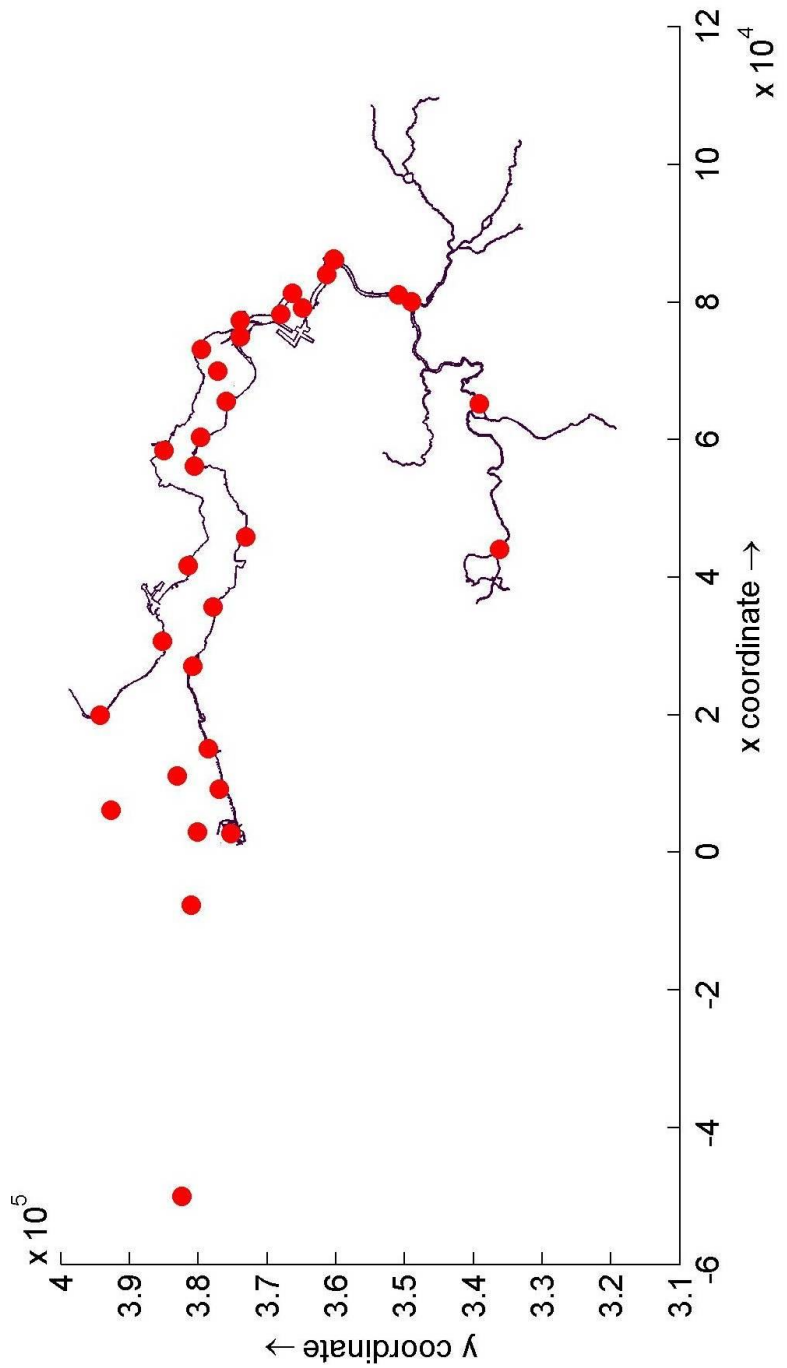

Figure H.8: Definition of output points in the model	**M.756/01**	
FLANDERS HYDRAULICS RESEARCH / DELFT HYDRAULICS		

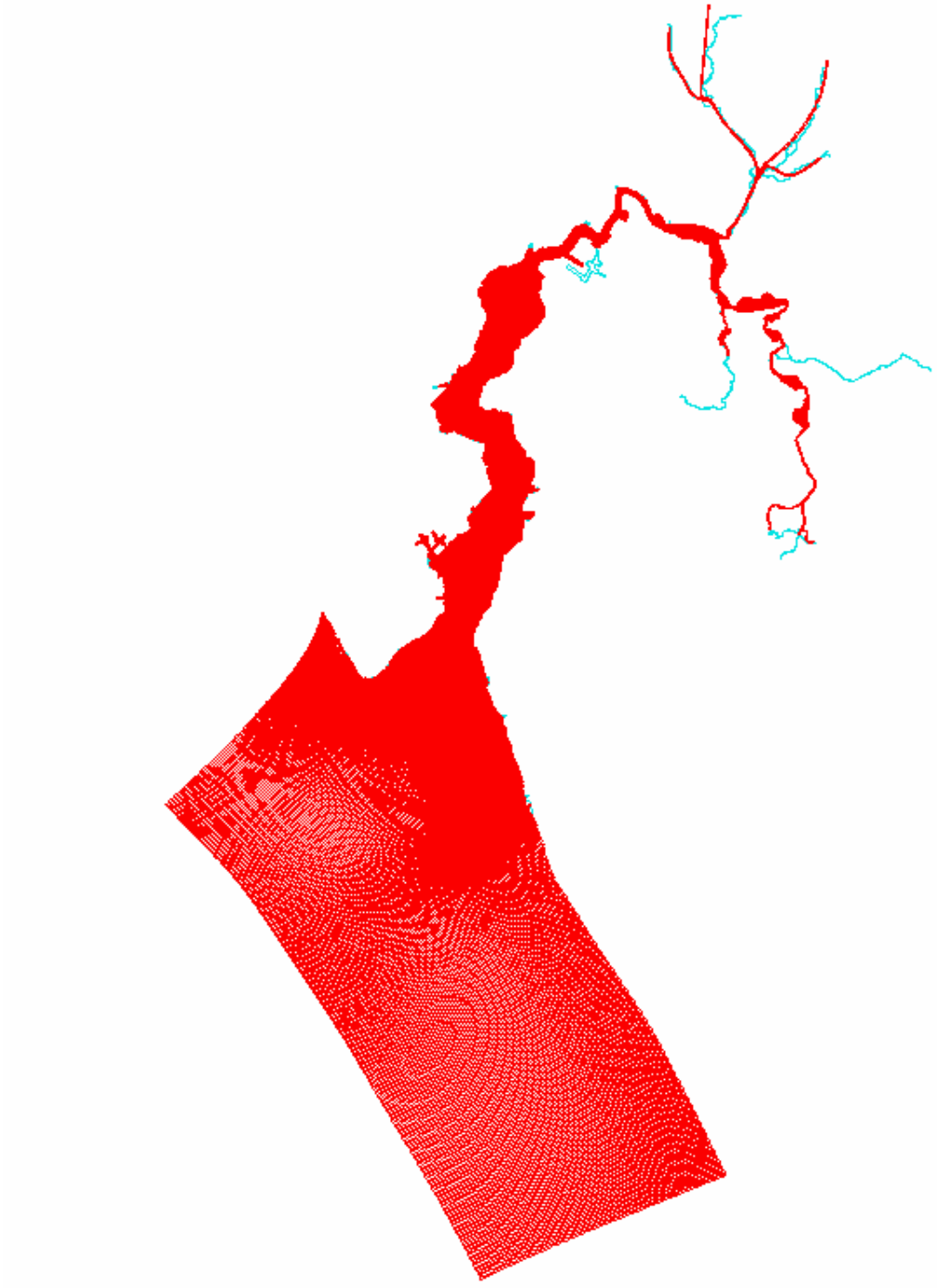

Figure H.9: Hydrodynamic grid	**M.756/01**	
FLANDERS HYDRAULICS RESEARCH / DELFT HYDRAULICS		

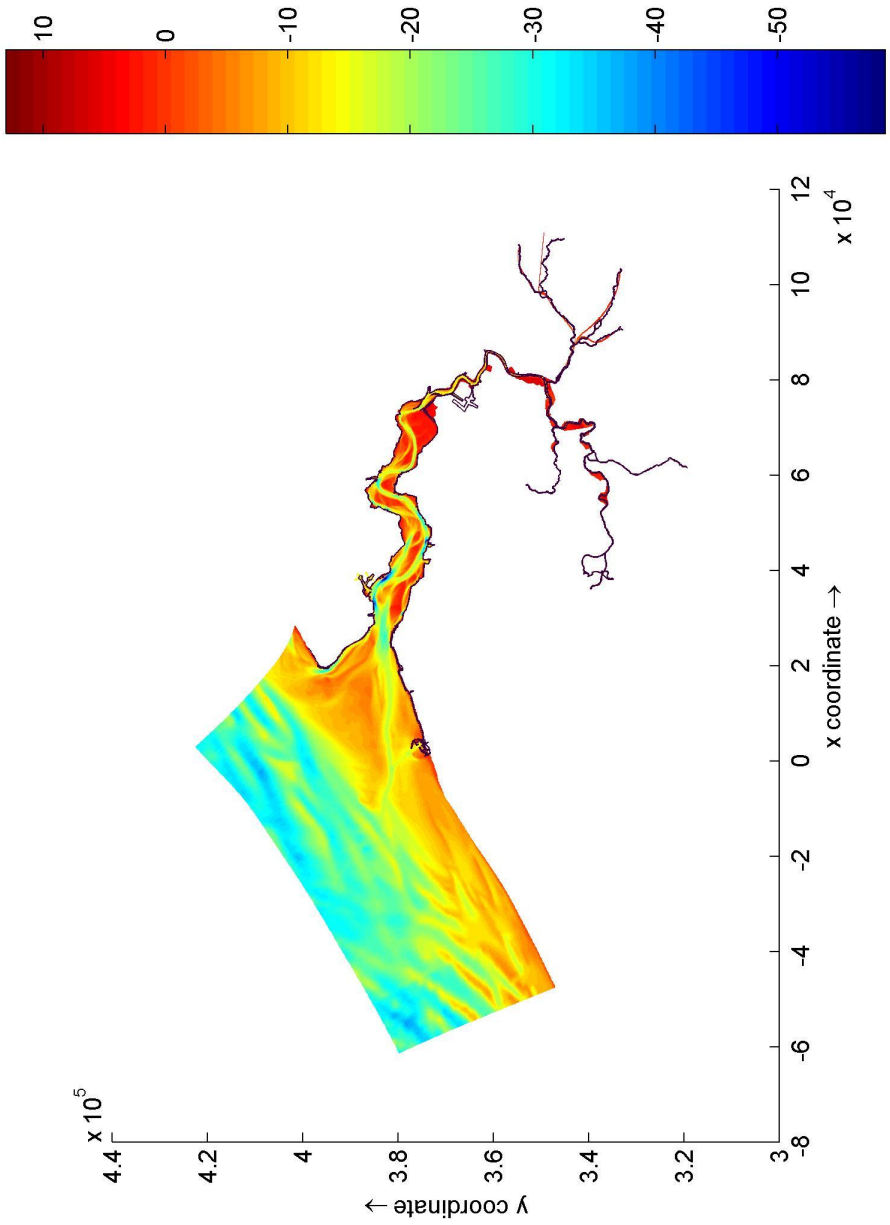

Figure H.10: Bathymetry

M.756/01

FLANDERS HYDRAULICS RESEARCH / DELFT HYDRAULICS

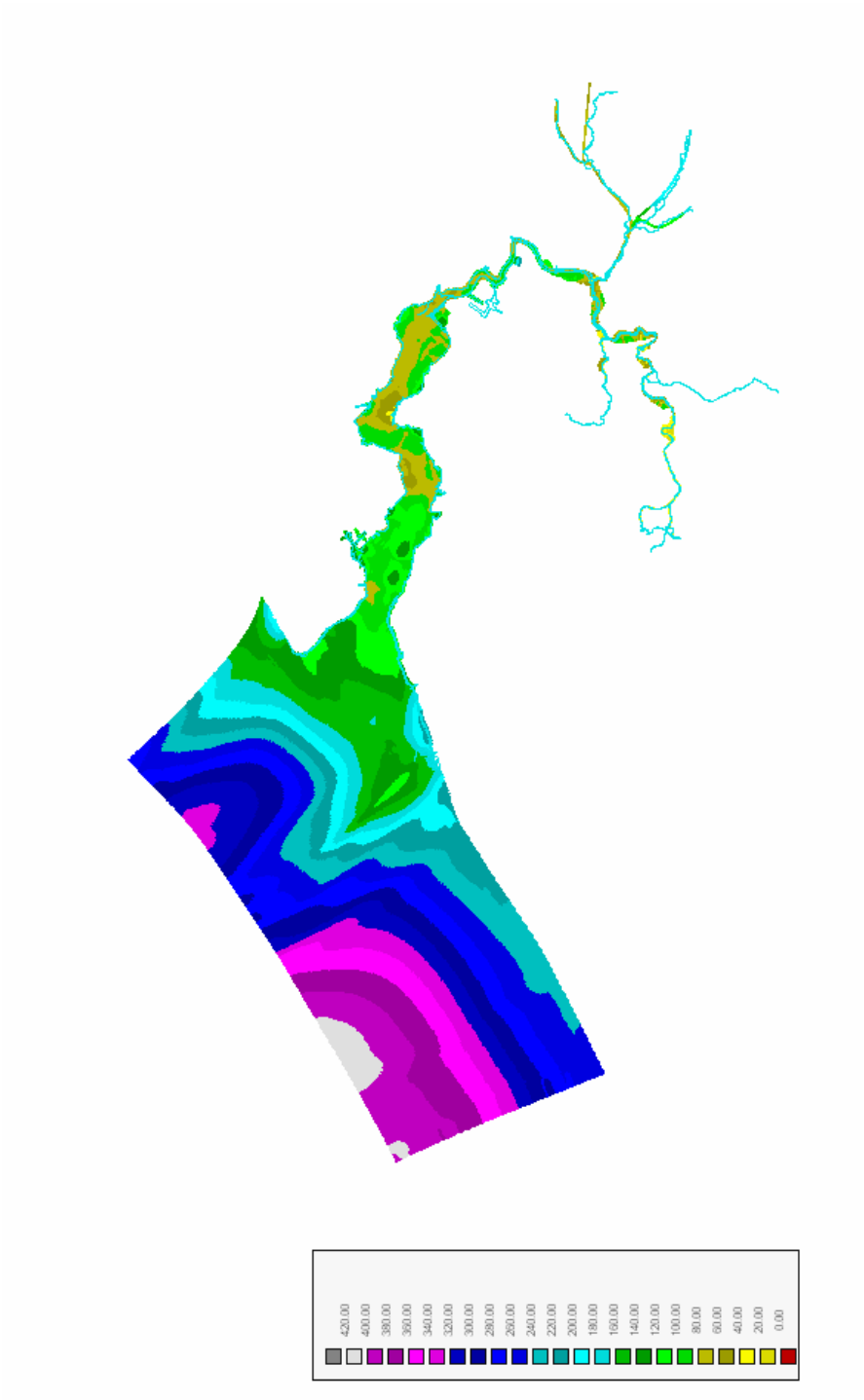

Figure H.11: Hydrodynamic grid: resolution	**M.756/01**	
FLANDERS HYDRAULICS RESEARCH / DELFT HYDRAULICS		

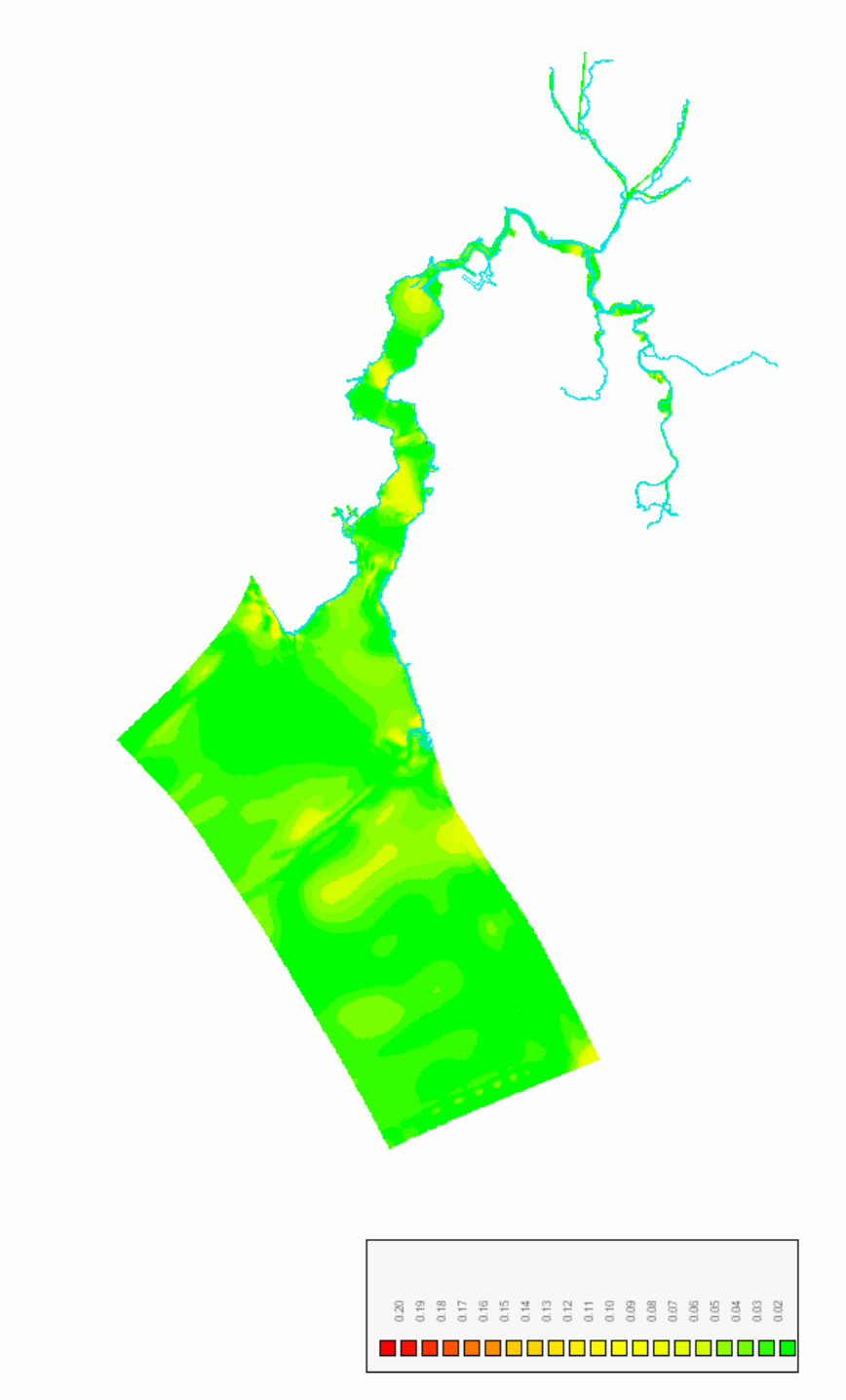

Figure H.12: Hydrodynamic grid: orthogonality	**M.756/01**
FLANDERS HYDRAULICS RESEARCH / DELFT HYDRAULICS	

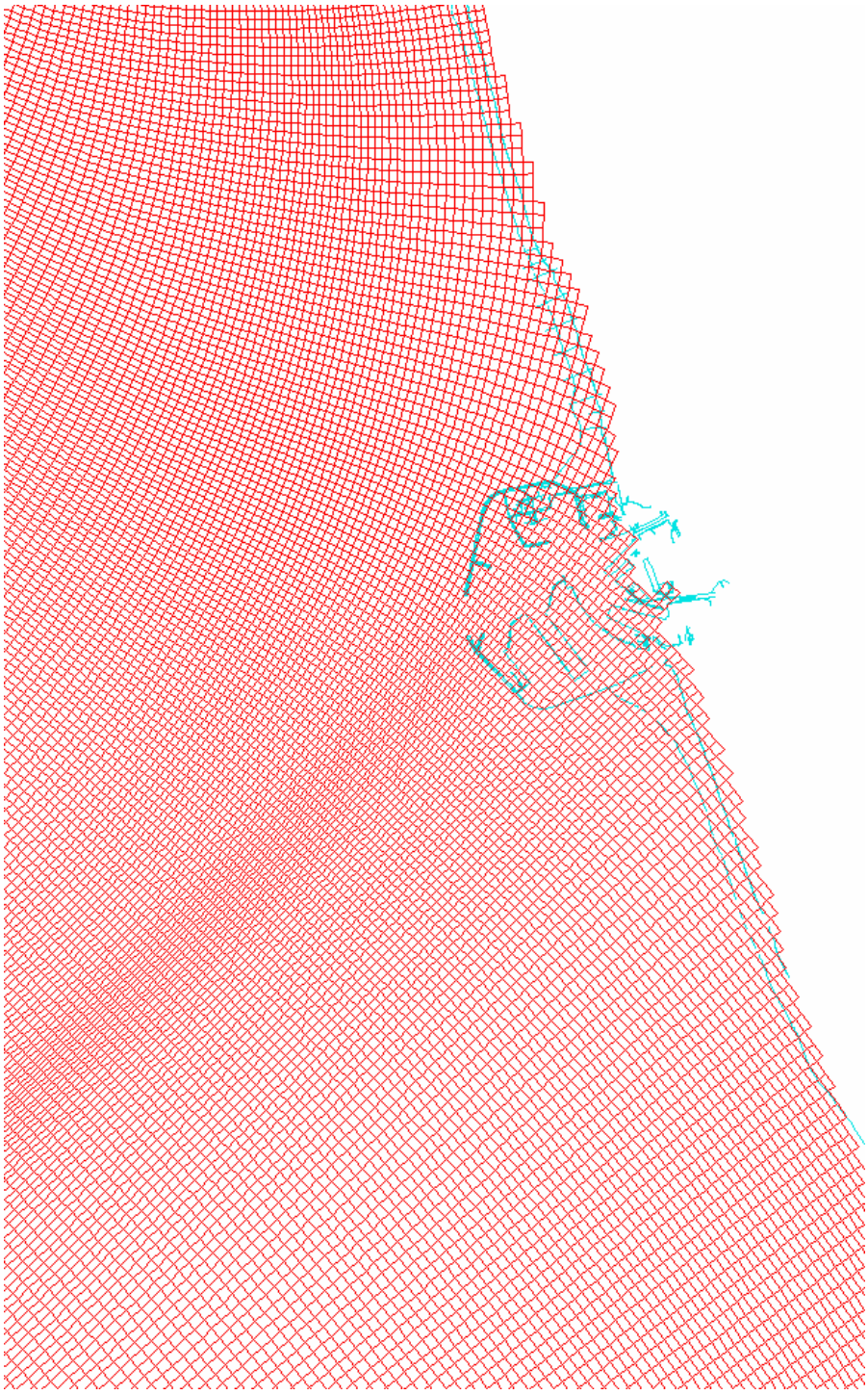

Figure H.13: Grid (detail Zeebrugge)	**M.756/01**
FLANDERS HYDRAULICS RESEARCH / DELFT HYDRAULICS	

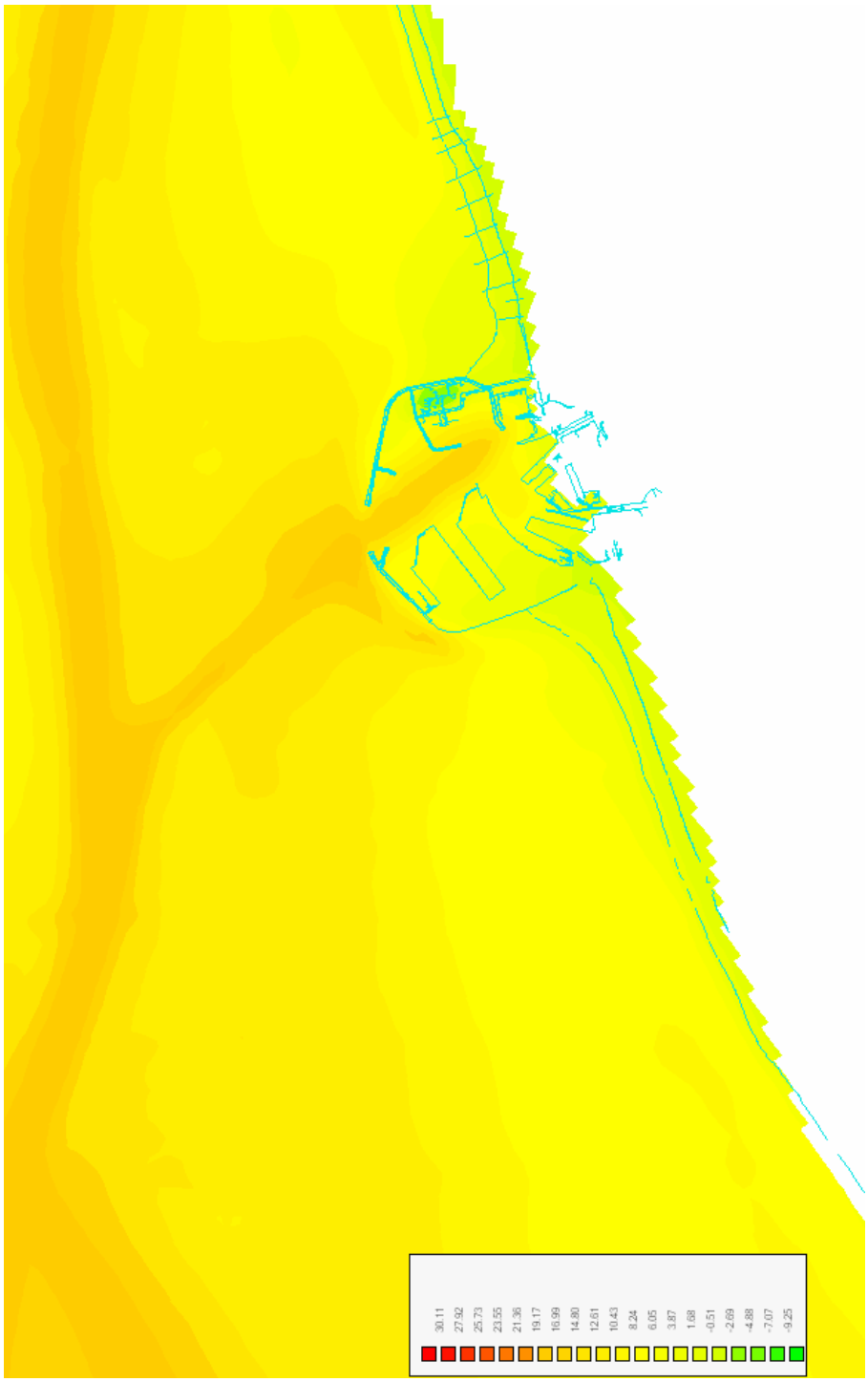

Figure H.14: Bathymetry (detail Zeebrugge)

M.756/01

FLANDERS HYDRAULICS RESEARCH / DELFT HYDRAULICS

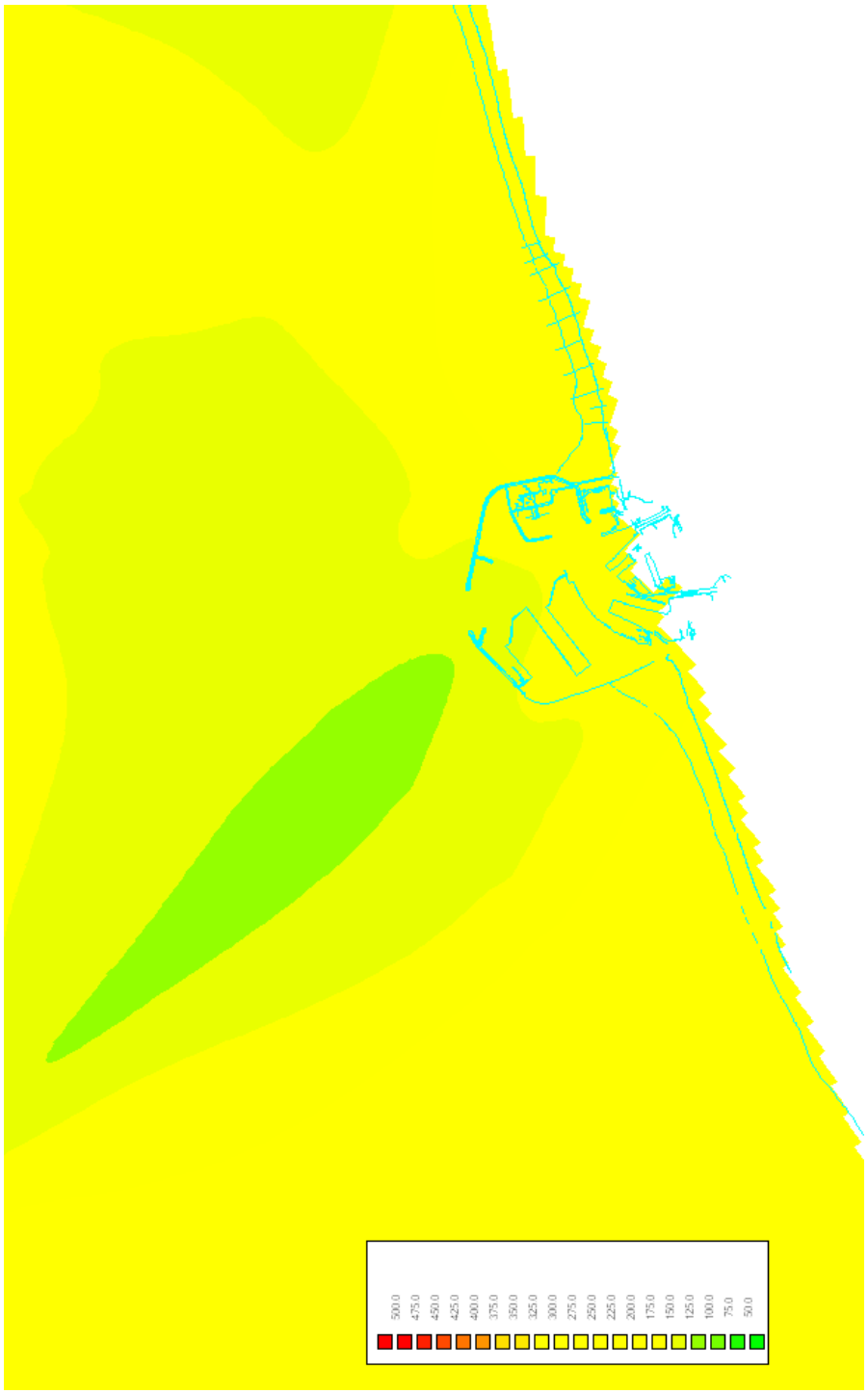

Figure H.15: Grid (detail Zeebrugge): resolution	**M.756/01**
FLANDERS HYDRAULICS RESEARCH / DELFT HYDRAULICS	

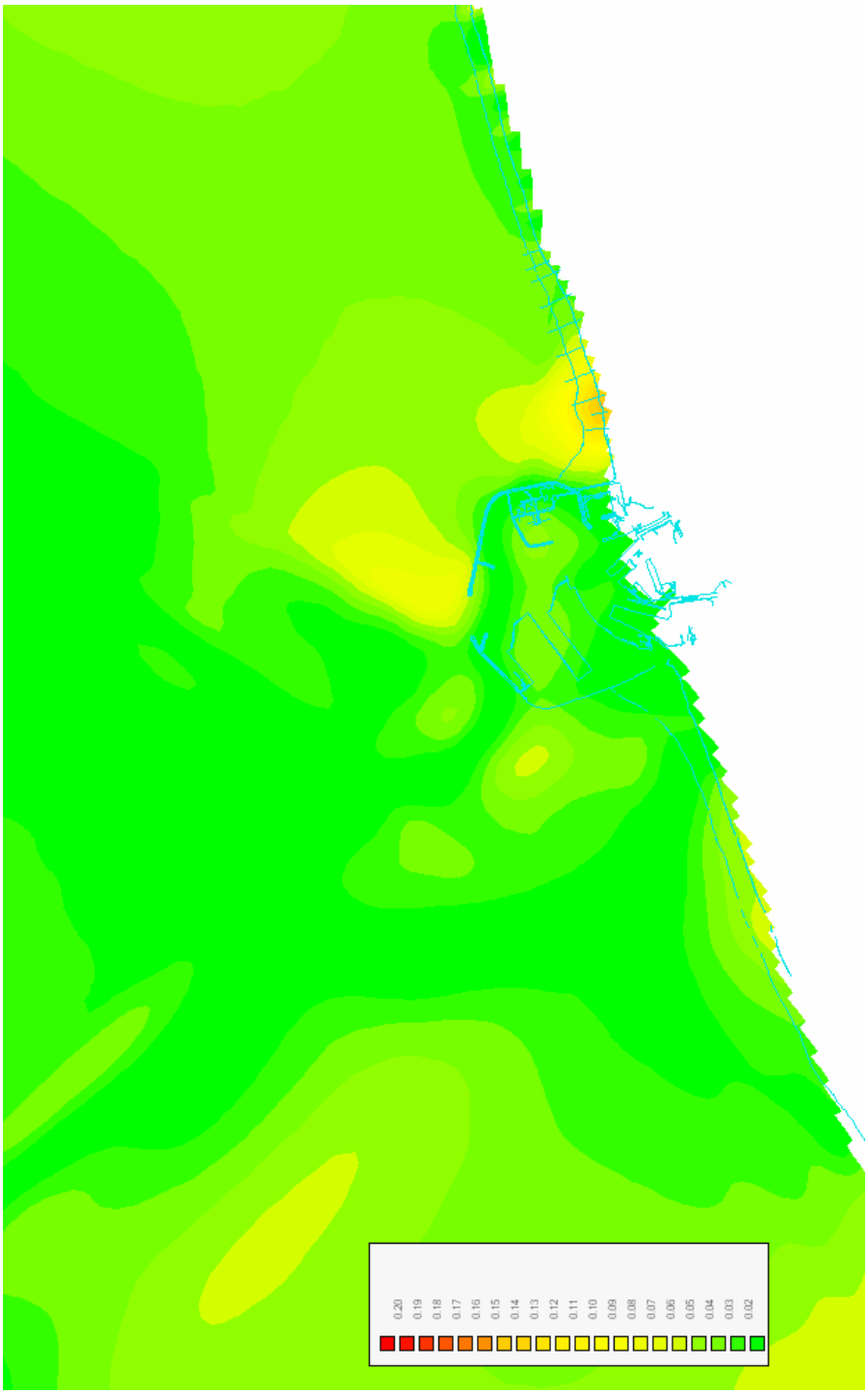

Figure H.16: Grid (detail Zeebrugge): orthogonality

M.756/01

Figure H.17: Grid (detail Western Scheldt)	**M.756/01**
FLANDERS HYDRAULICS RESEARCH / DELFT HYDRAULICS	

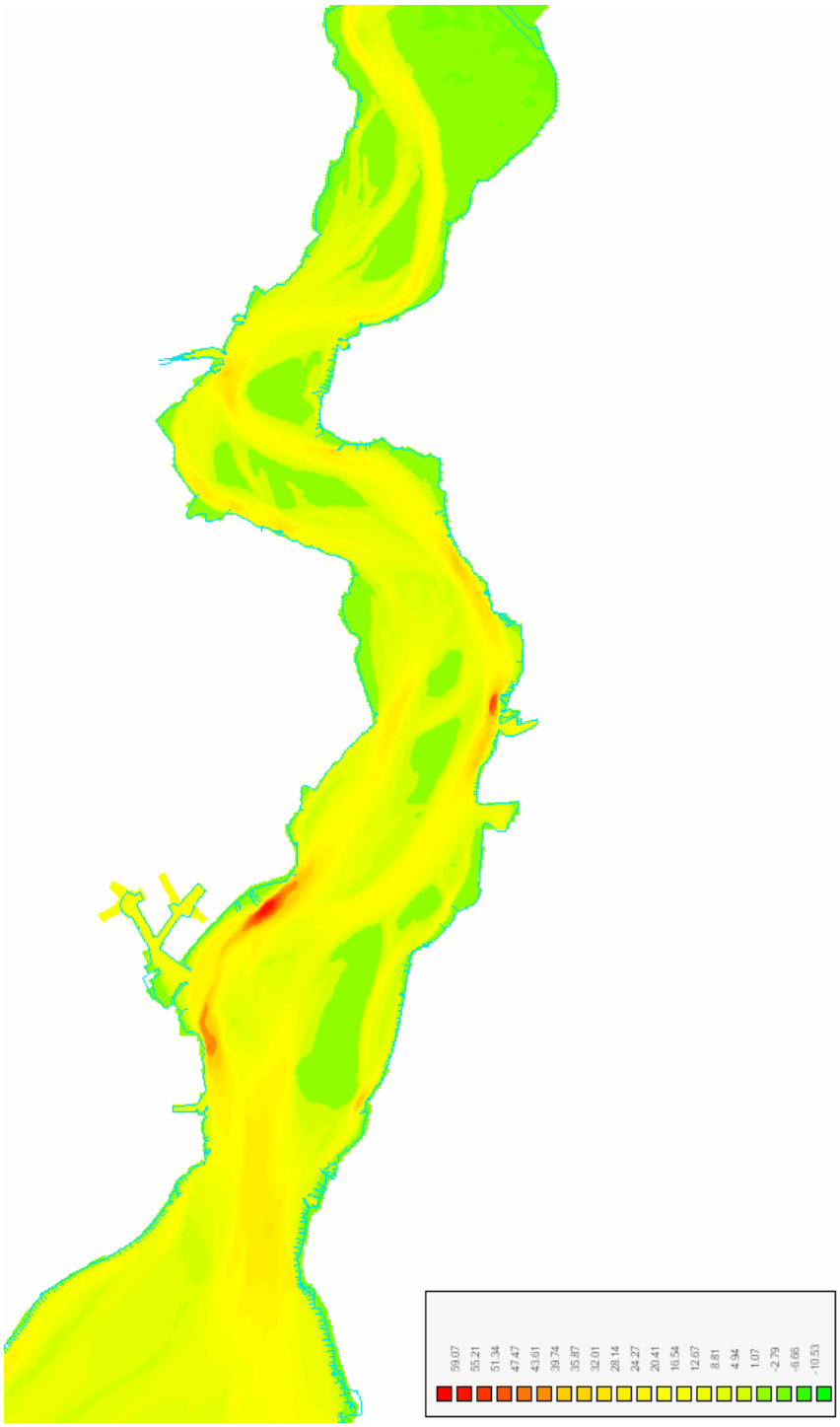

Figure H.18: Bathymetry (detail Western Scheldt)	**M.756/01**
FLANDERS HYDRAULICS RESEARCH / DELFT HYDRAULICS	

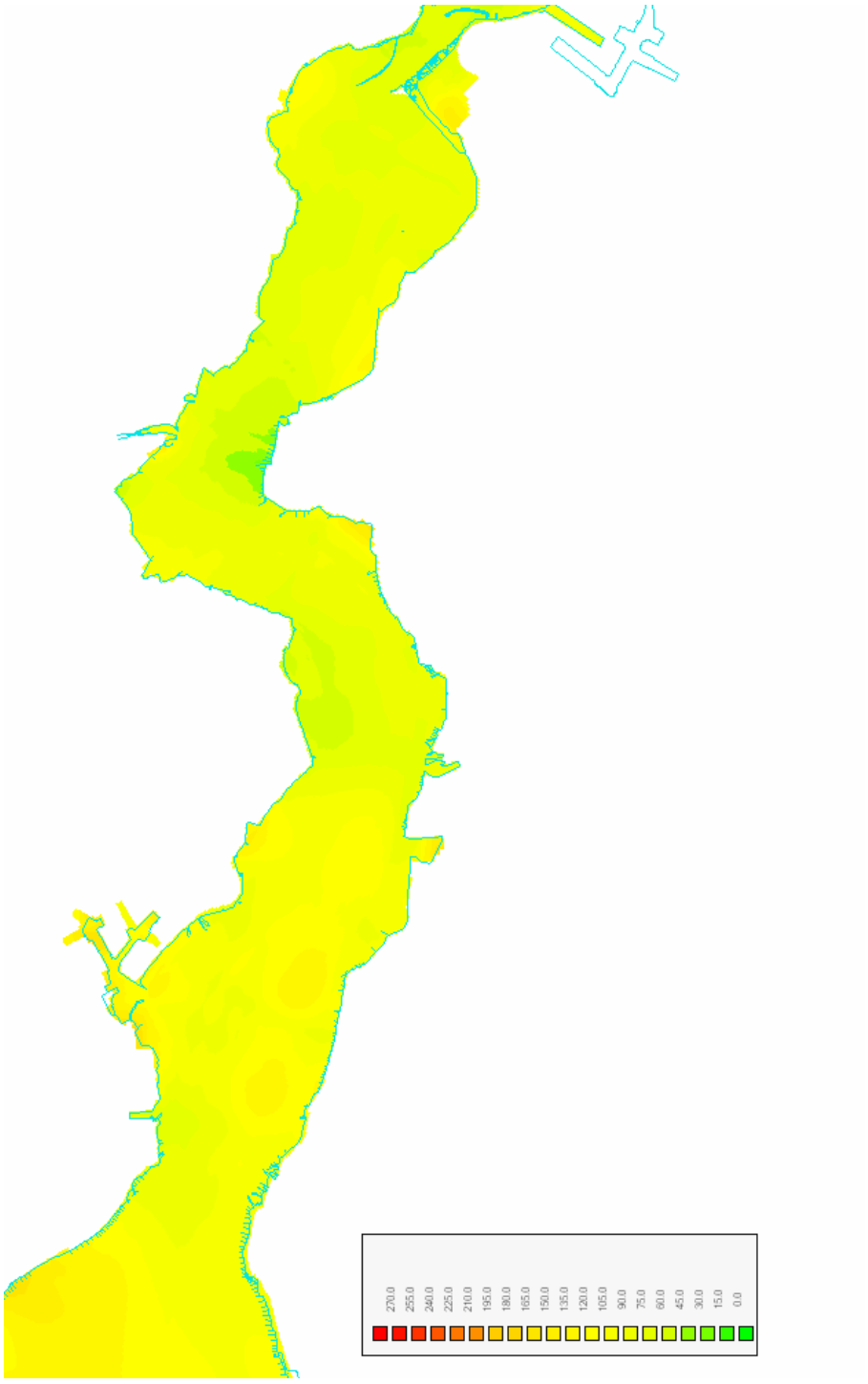

Figure H.19: Grid (detail Western Scheldt): resolution	**M.756/01**
FLANDERS HYDRAULICS RESEARCH / DELFT HYDRAULICS	

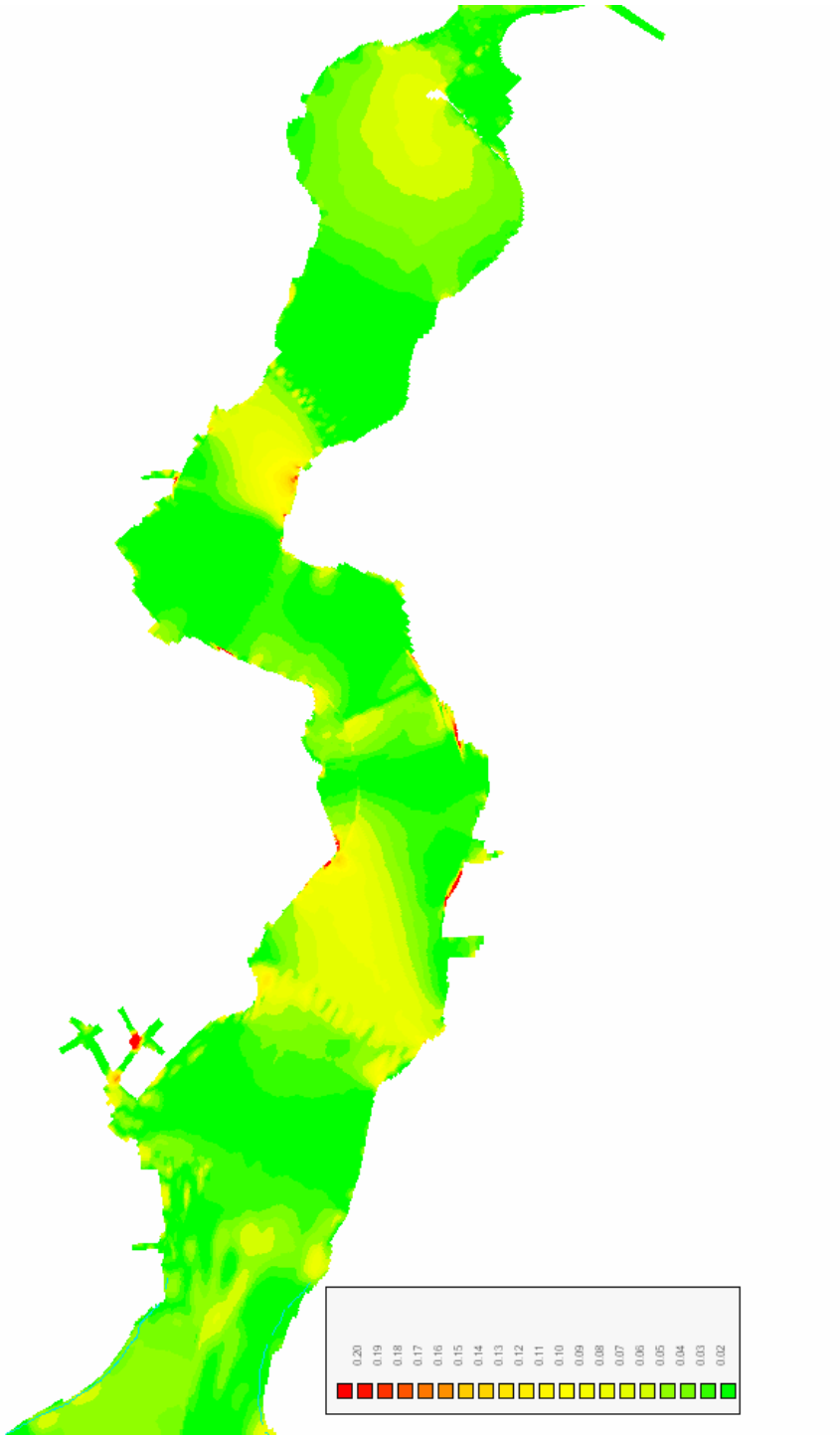

Figure H.20: Grid (detail Western Scheldt): orthogonality	**M.756/01**
FLANDERS HYDRAULICS RESEARCH / DELFT HYDRAULICS	

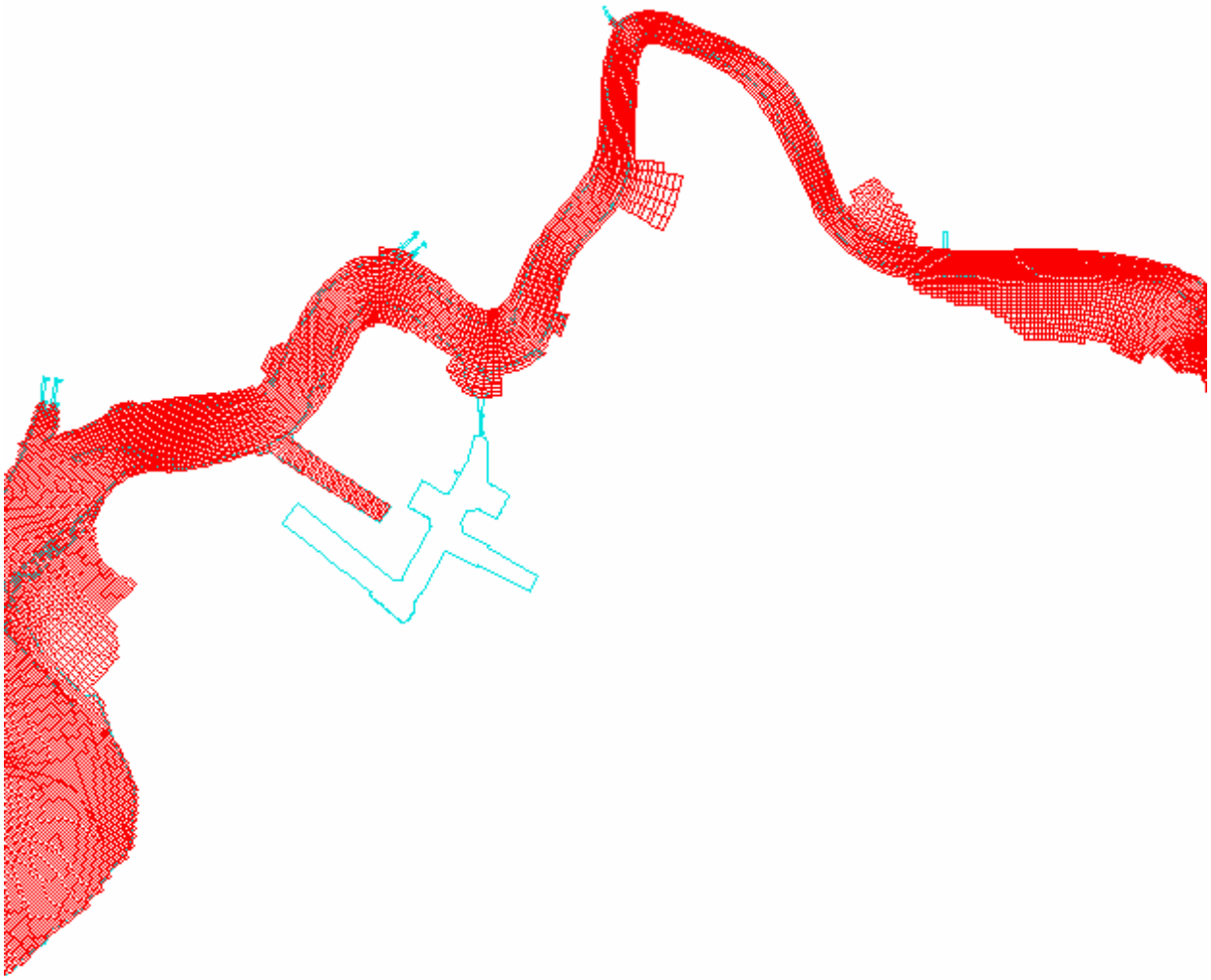

Figure H.21: Grid (detail Sea Scheldt)	**M.756/01**	
FLANDERS HYDRAULICS RESEARCH / DELFT HYDRAULICS		

Figure H.22: Bathymetry (detail Sea Scheldt)	**M.756/01**
FLANDERS HYDRAULICS RESEARCH / DELFT HYDRAULICS	

Figure H.23: Grid (detail Sea Scheldt): resolution	**M.756/01**
FLANDERS HYDRAULICS RESEARCH / DELFT HYDRAULICS	

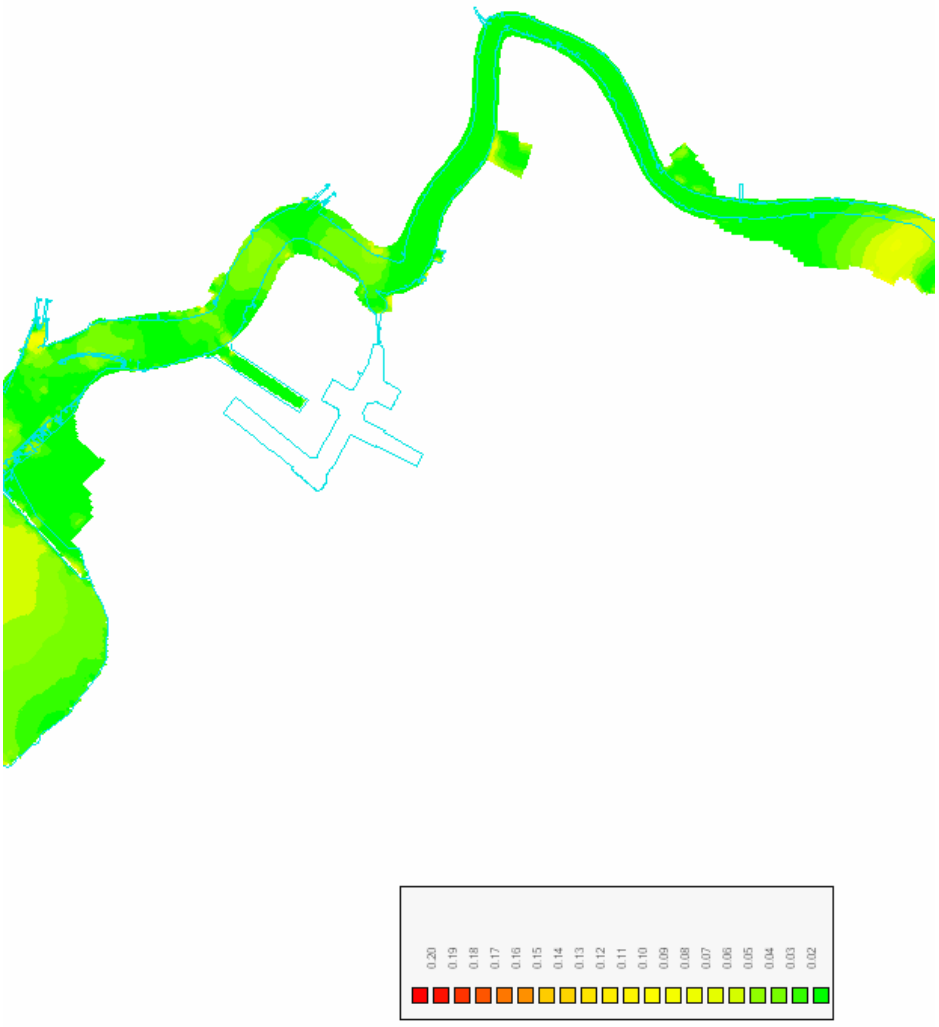

Figure H.24: Grid (detail Sea Scheldt): orthogonality	**M.756/01**
FLANDERS HYDRAULICS RESEARCH / DELFT HYDRAULICS	

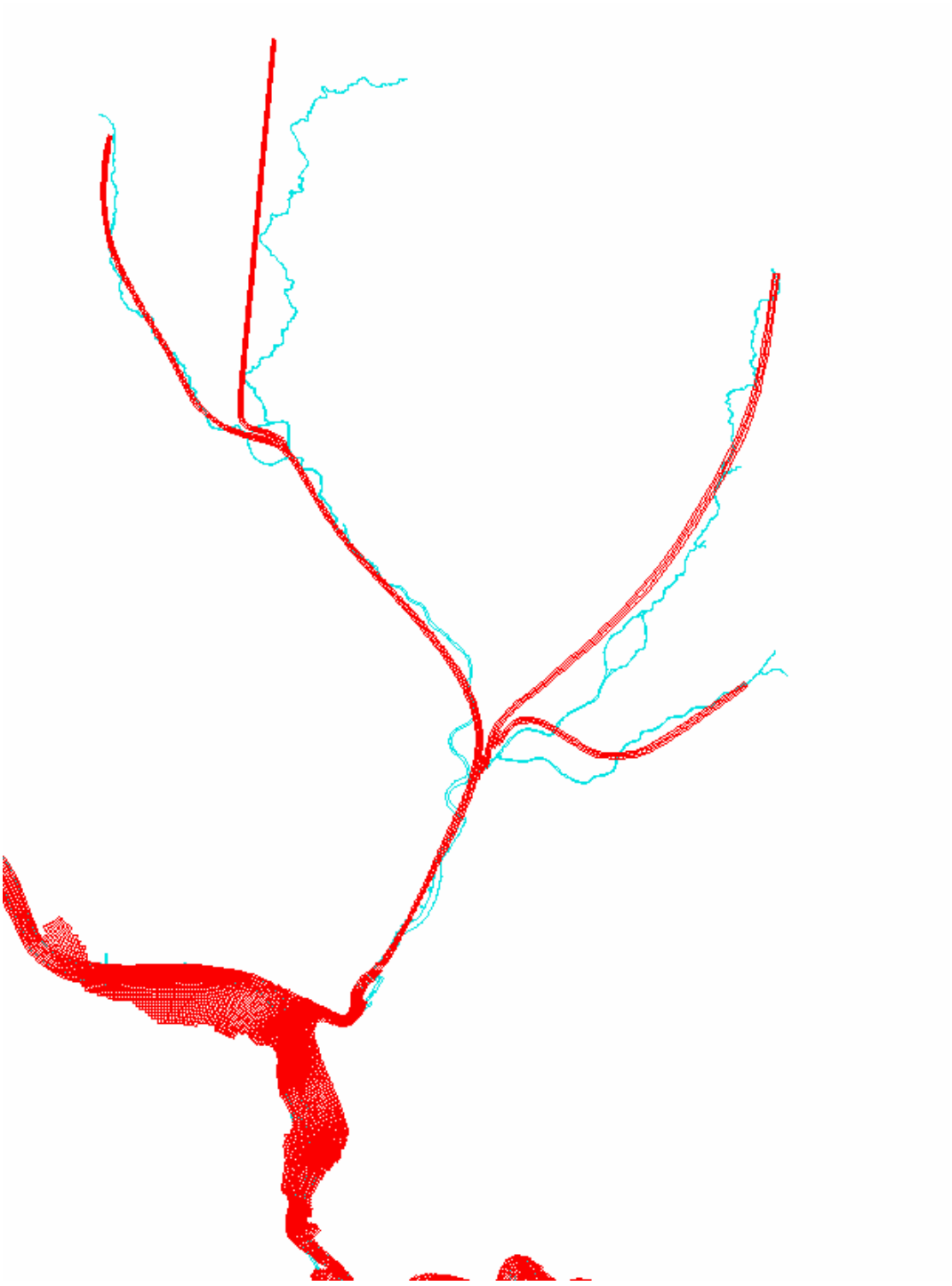

Figure H.25: Grid (detail Rupel basin)	**M.756/01**	
FLANDERS HYDRAULICS RESEARCH / DELFT HYDRAULICS		

Figure H.26: Bathymetry (detail Rupel basin)

M.756/01

FLANDERS HYDRAULICS RESEARCH / DELFT HYDRAULICS

Figure H.27: Grid (detail Rupel basin): resolution	**M.756/01**
FLANDERS HYDRAULICS RESEARCH / DELFT HYDRAULICS	

Figure H.28: Grid (detail Rupel basin): orthogonality	**M.756/01**
FLANDERS HYDRAULICS RESEARCH / DELFT HYDRAULICS	

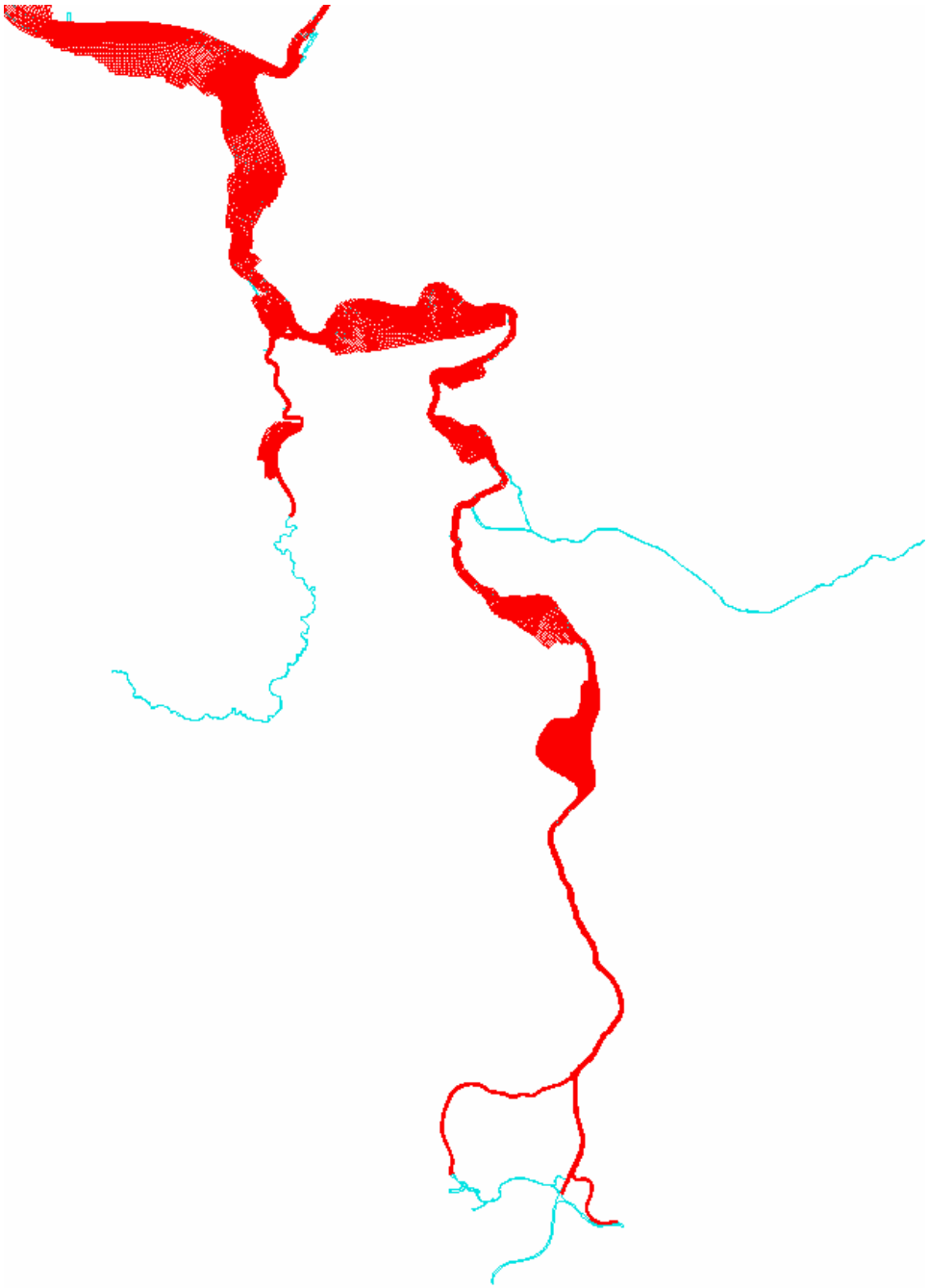

Figure H.29: Grid (detail Upper Scheldt)	**M.756/01**	
FLANDERS HYDRAULICS RESEARCH / DELFT HYDRAULICS		

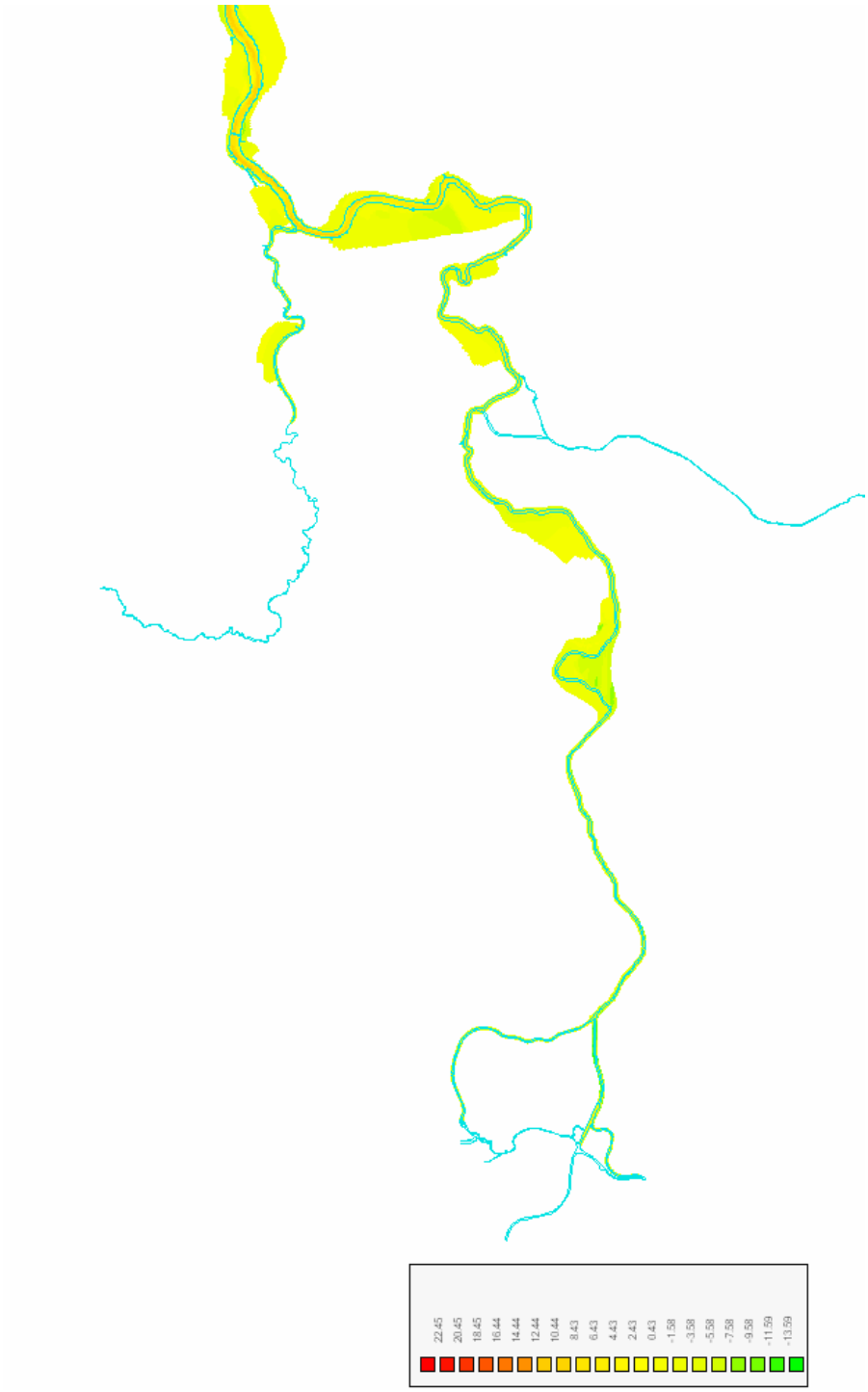

Figure H.30: Bathymetry (detail Upper Scheldt)	**M.756/01**	
FLANDERS HYDRAULICS RESEARCH / DELFT HYDRAULICS		

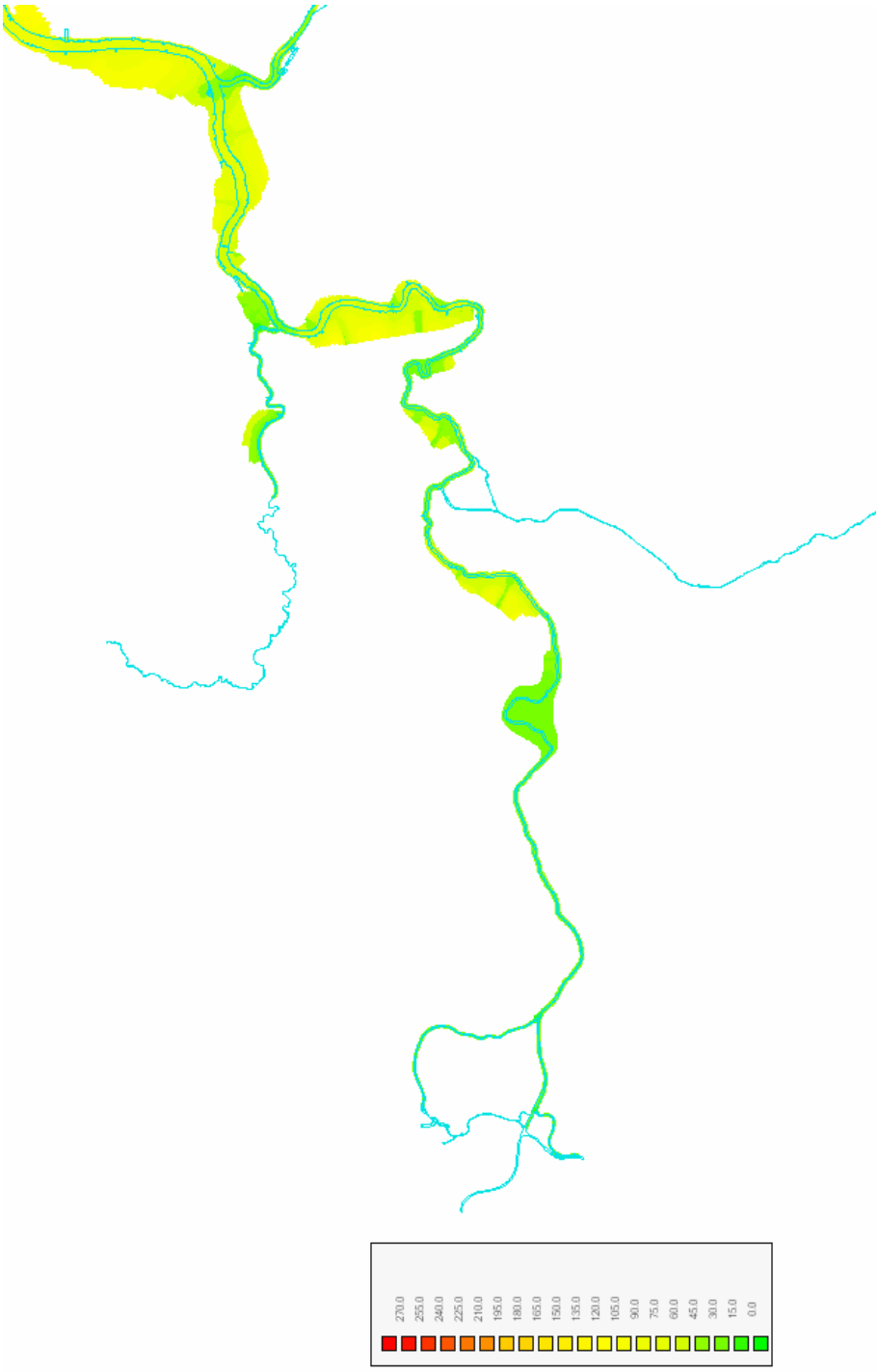

Figure H.31: Grid (detail Upper Scheldt): resolution	**M.756/01**
FLANDERS HYDRAULICS RESEARCH / DELFT HYDRAULICS	

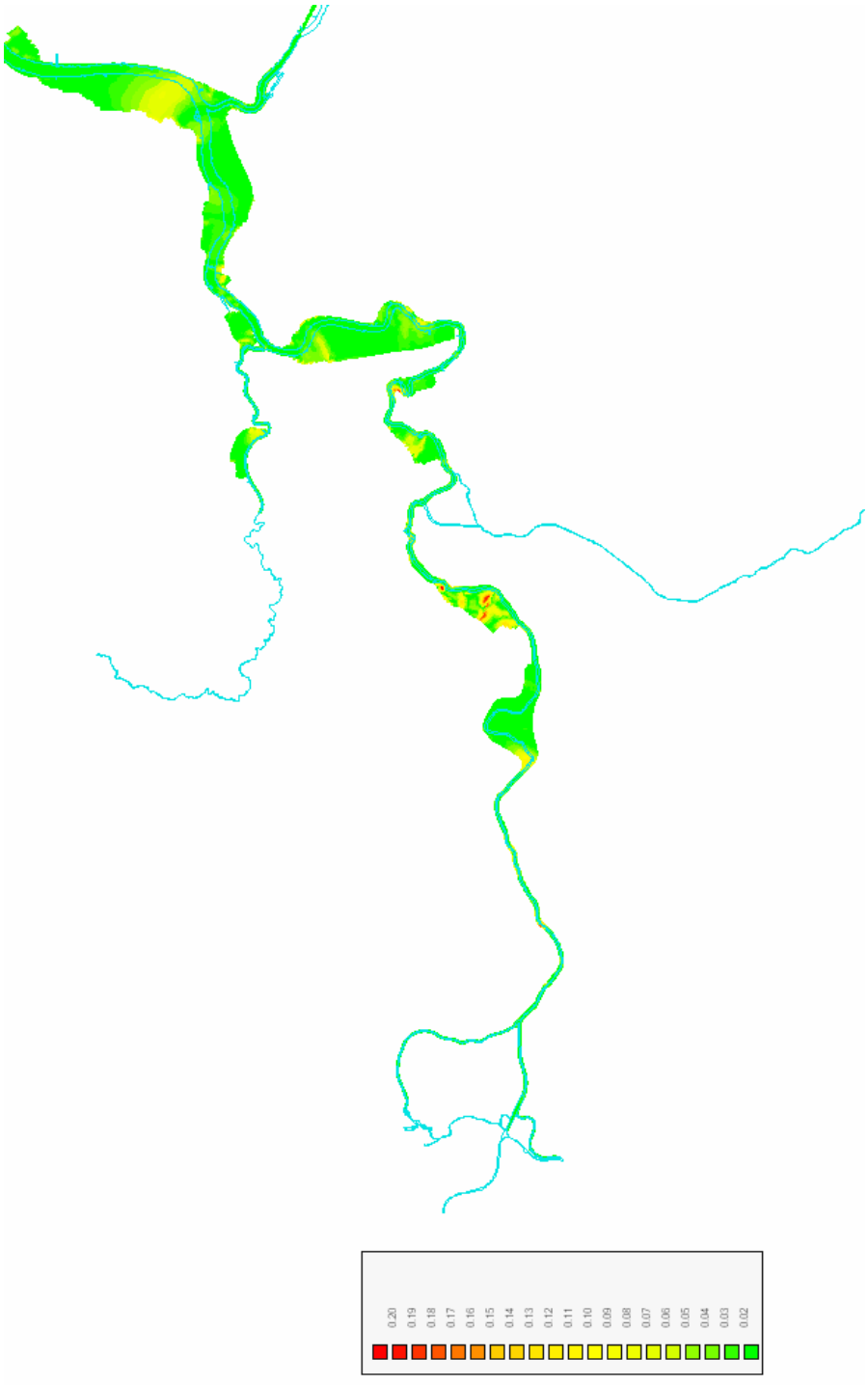

Figure H.32: Grid (detail Upper Scheldt): orthogonality	**M.756/01**
FLANDERS HYDRAULICS RESEARCH / DELFT HYDRAULICS	

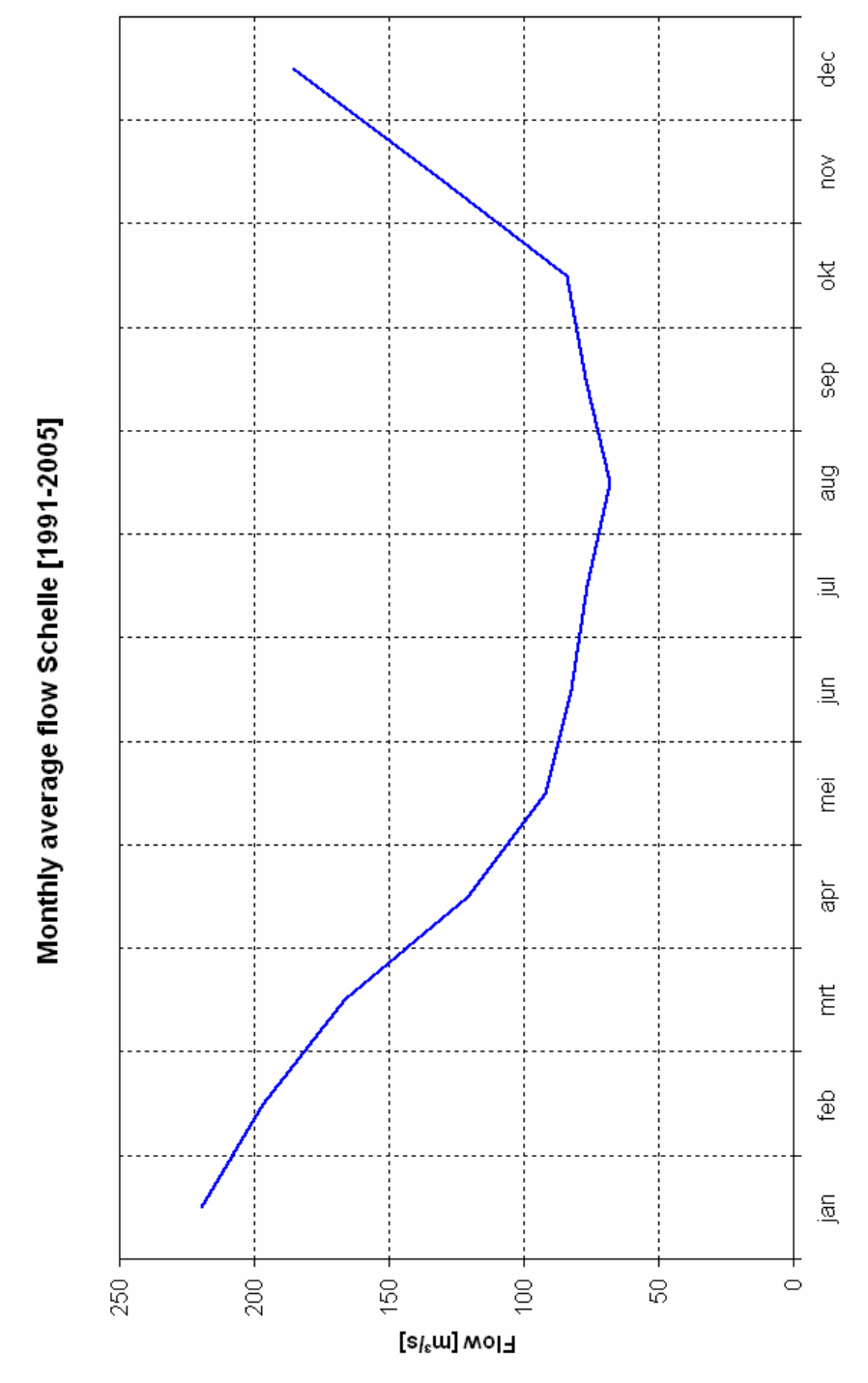

Figure H.33: Monthly average flow Schelle (1991 – 2005)

M.756/01

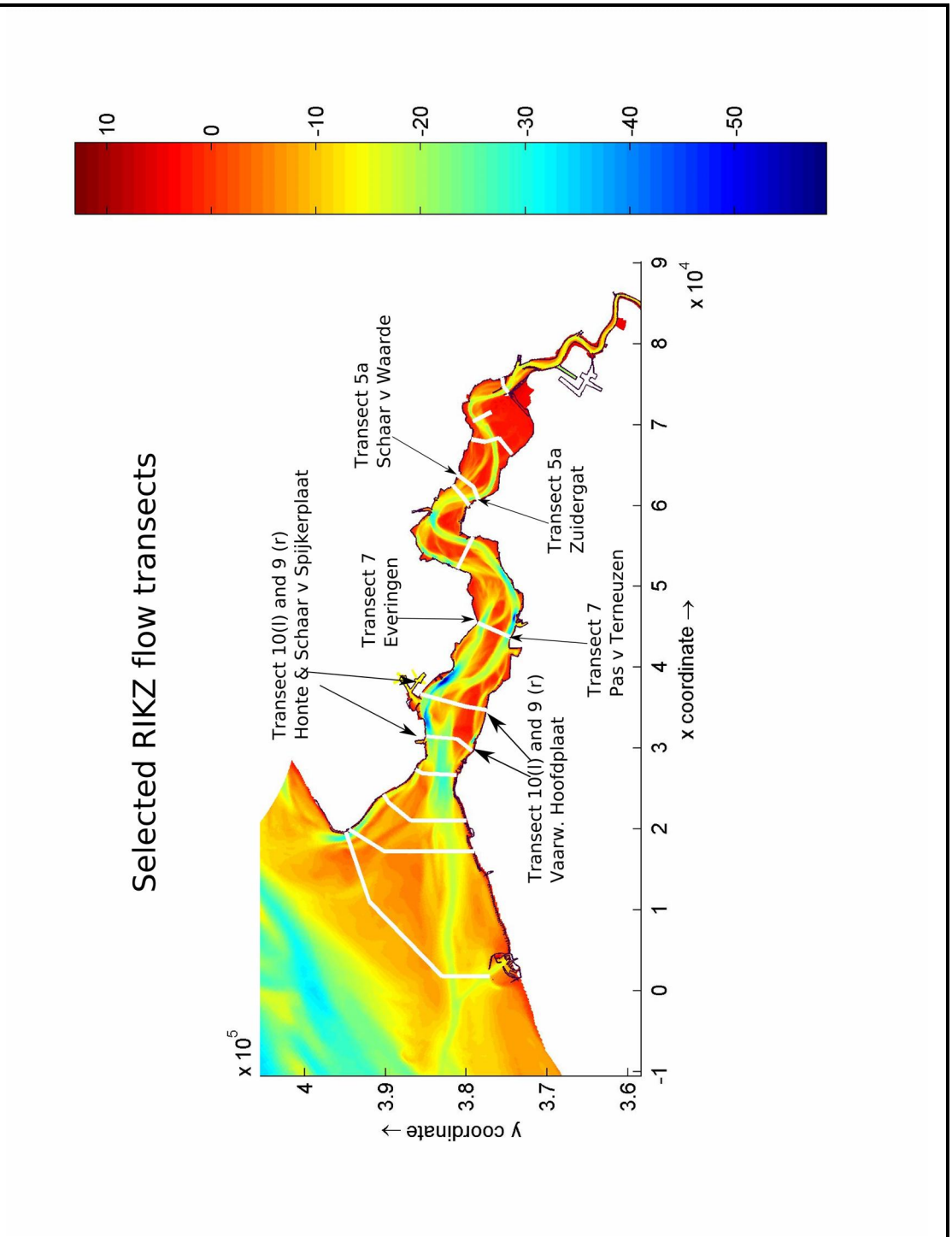

Figure H.34: Position of RIKZ flow transects

M.756/01

FLANDERS HYDRAULICS RESEARCH / DELFT HYDRAULICS

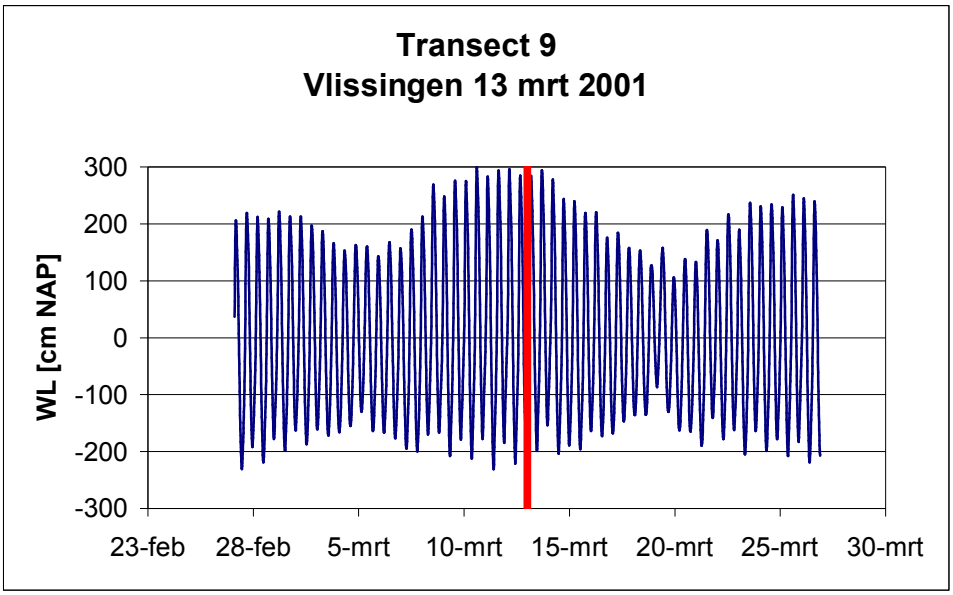

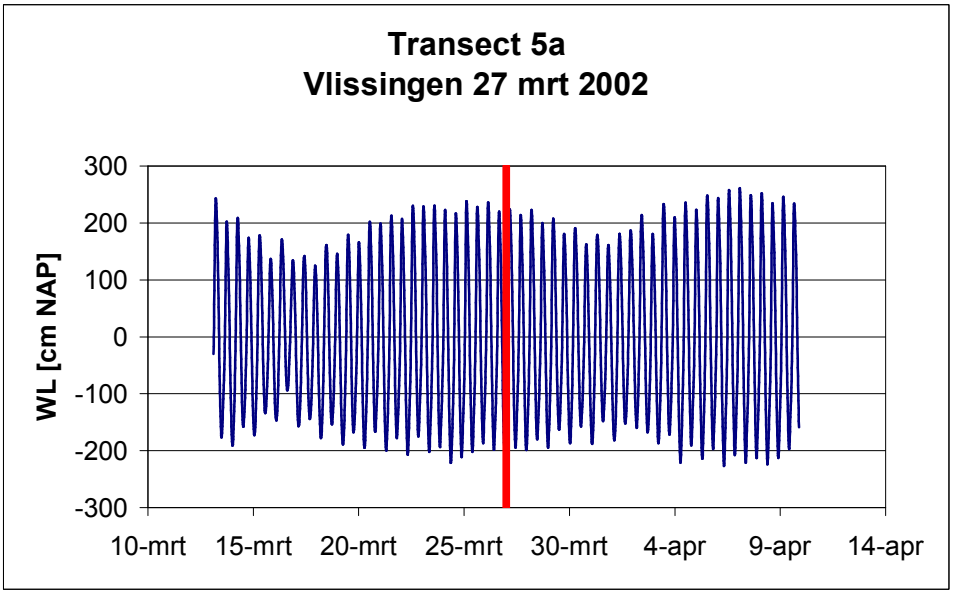

Figure H.35: Tidal condition RIKZ transects 9 and 5a
Red line indicates moment of transect

M.756/01

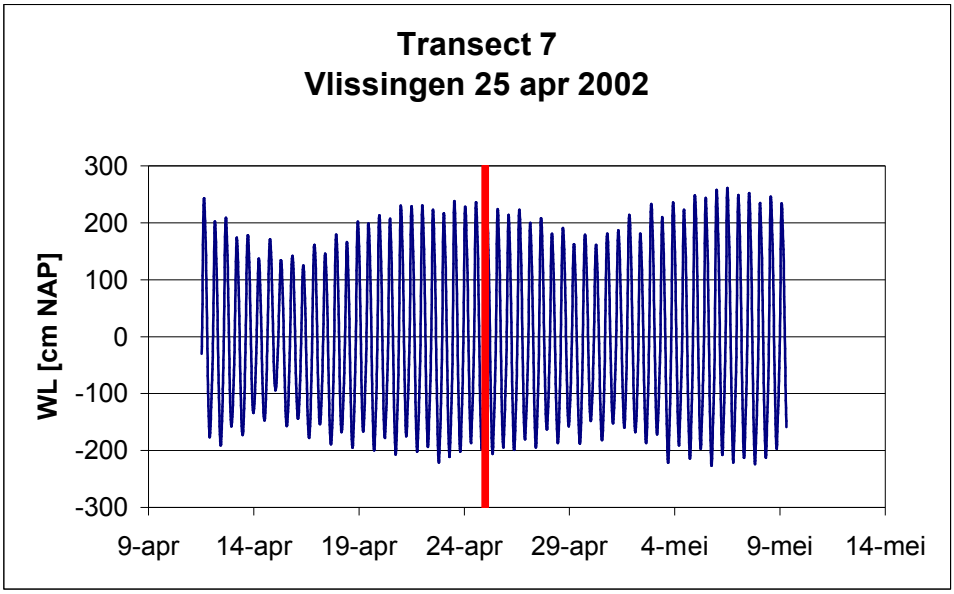

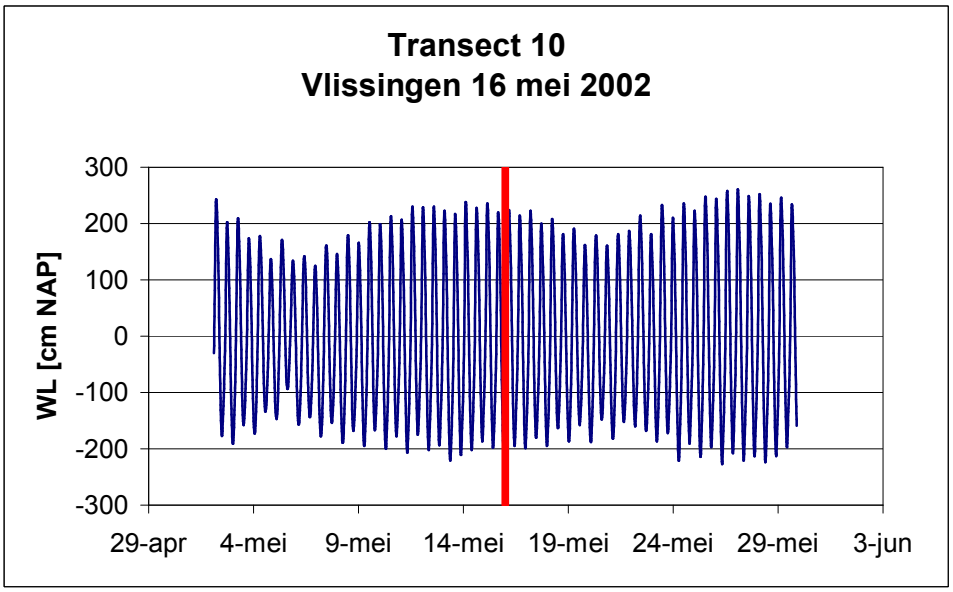

Figure H.36 Tidal condition RIKZ transects 7 and 10
Red line indicates moment of transect

M.756/01

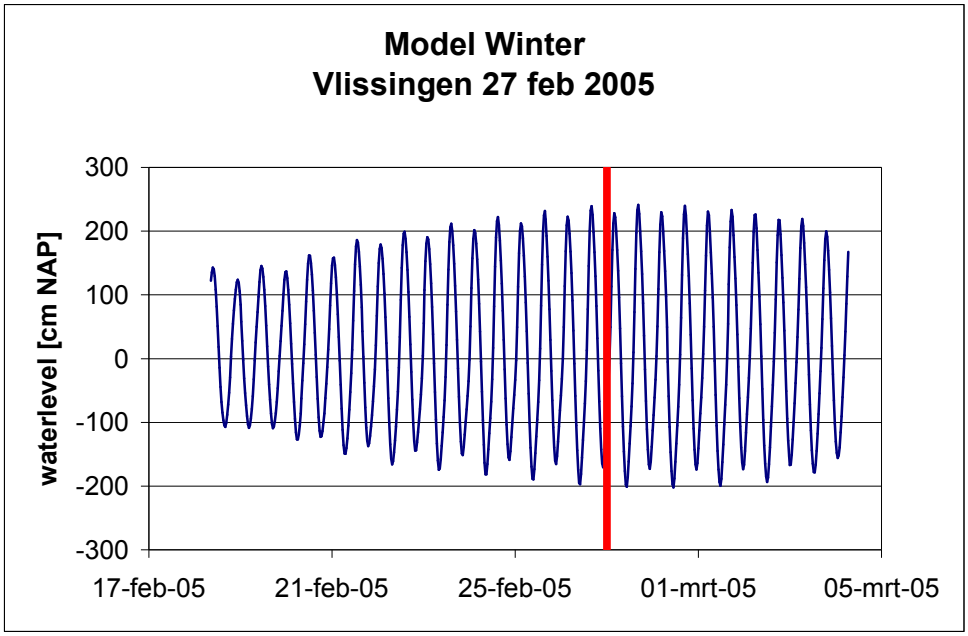

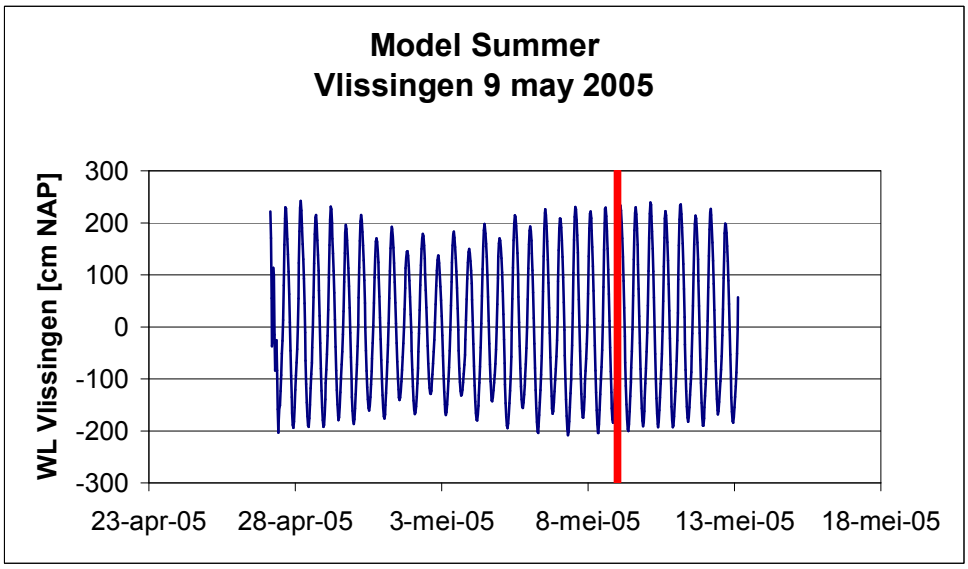

Figure H.37: Tidal conditions winter & summer run
Red line indicates spring tide

M.756/01

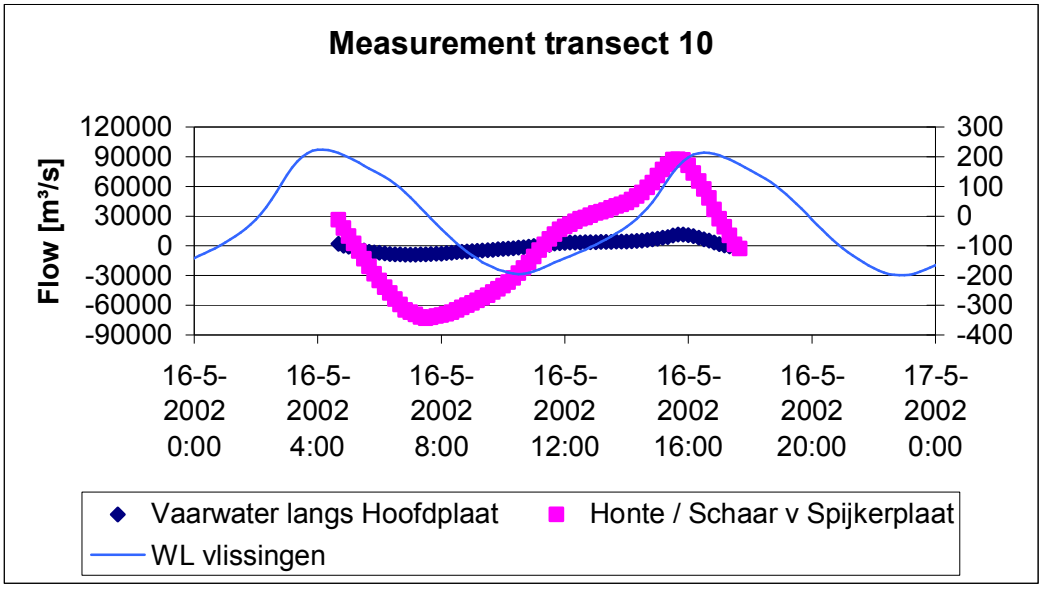

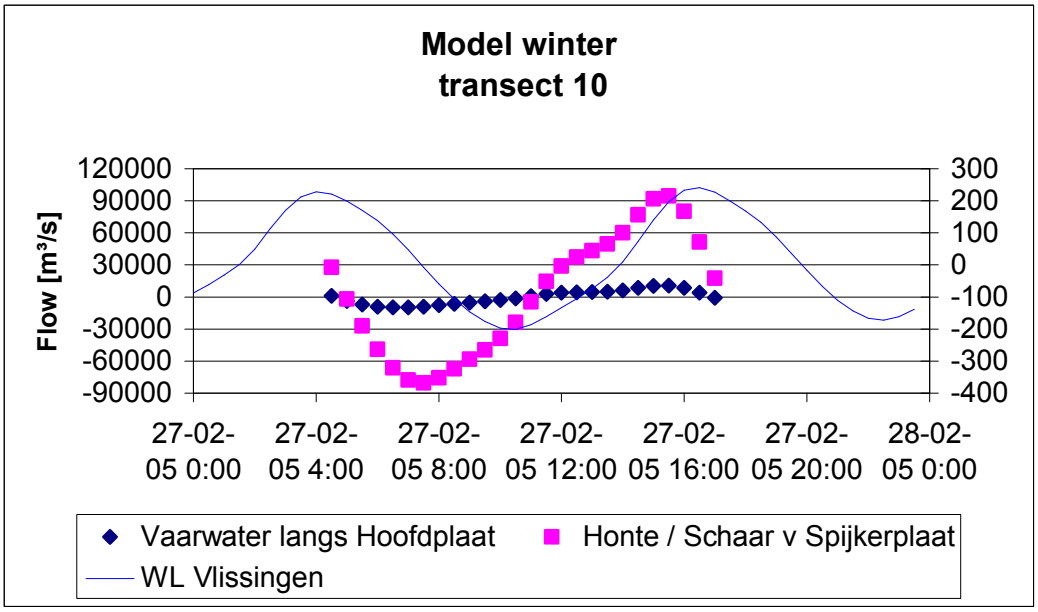

Figure H.38: RIKZ Measurement transect 10
Model result (winter) transect 10

M.756/01

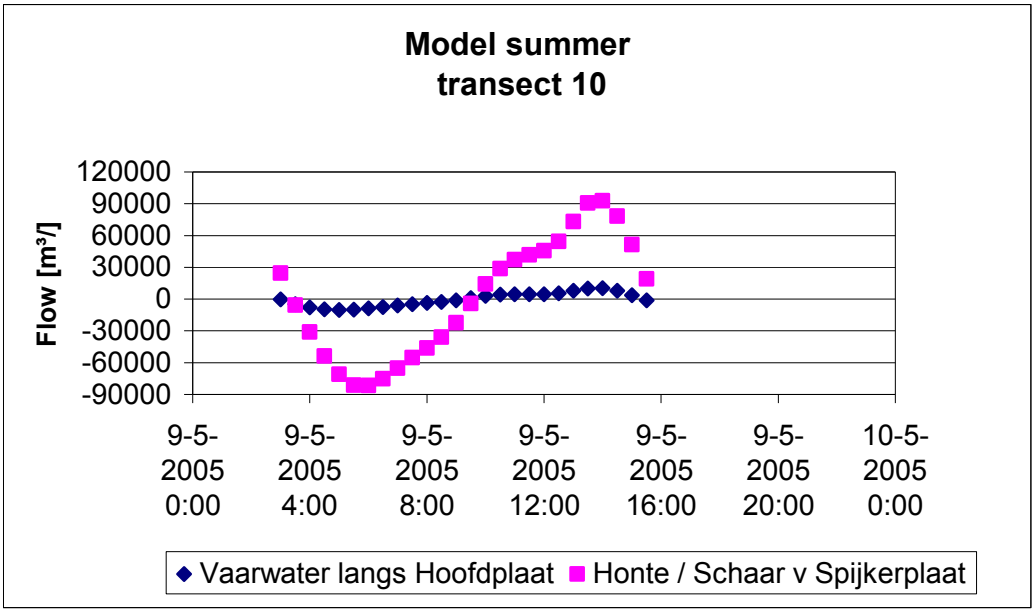

Figure H.39: Model result (summer) transect 10

M.756/01

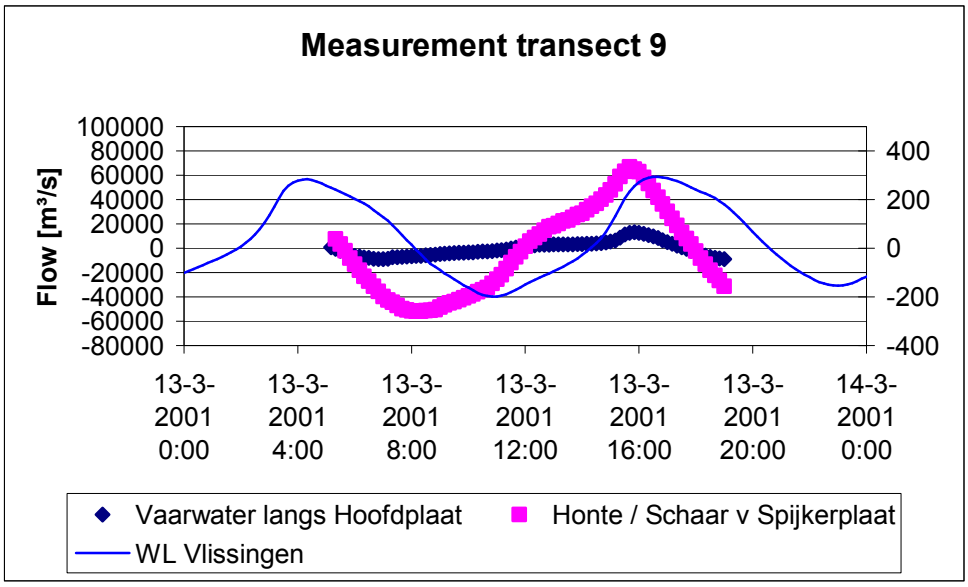

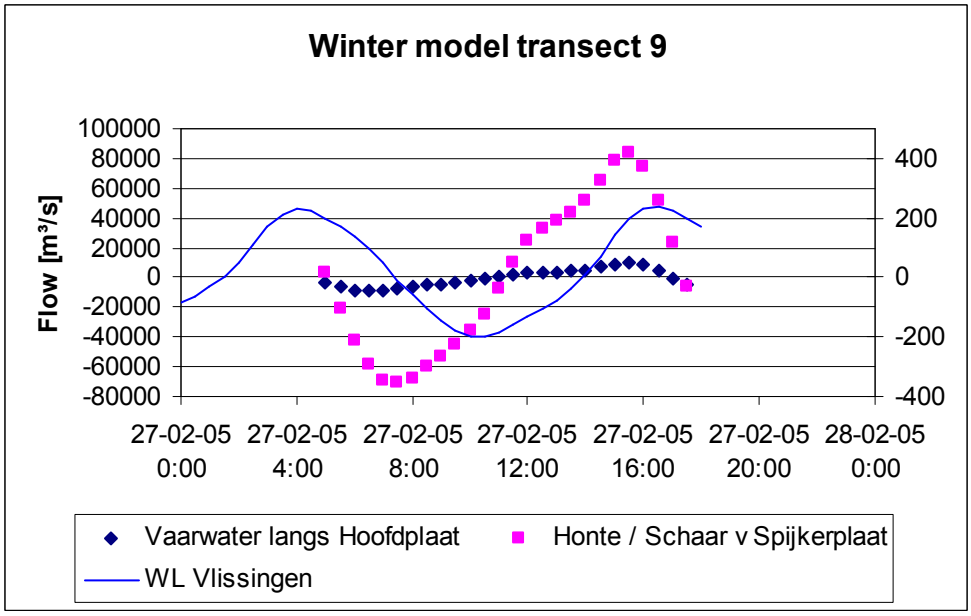

Figure H.40: RIKZ Measurement transect 9
Model result (winter) transect 9

M.756/01

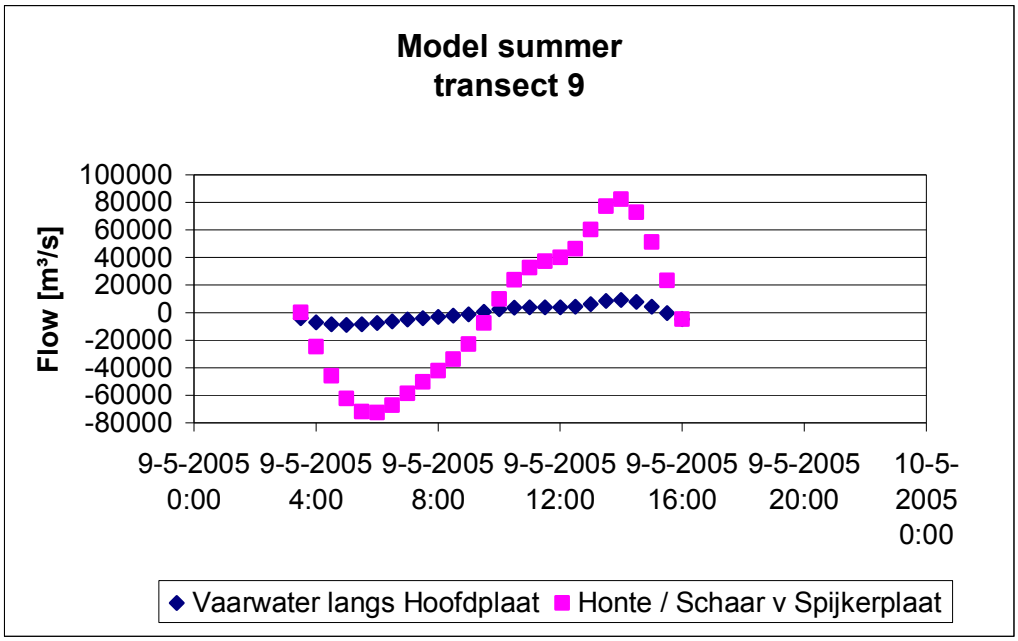

Figure H.41: Model result (summer) transect 9

M.756/01

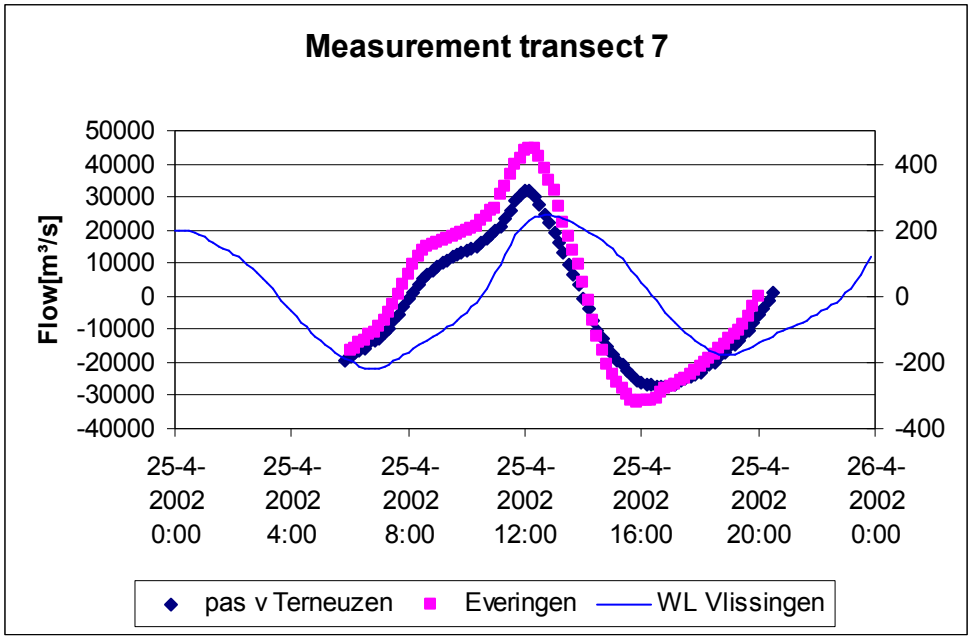

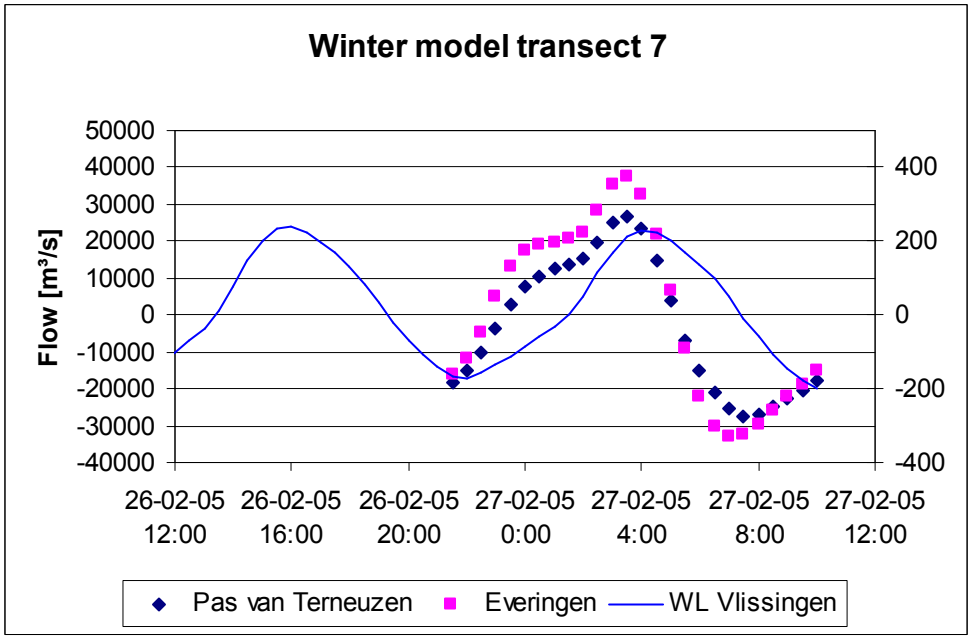

Figure H.42: RIKZ Measurement transect 7
Model result (winter) transect 7

M.756/01

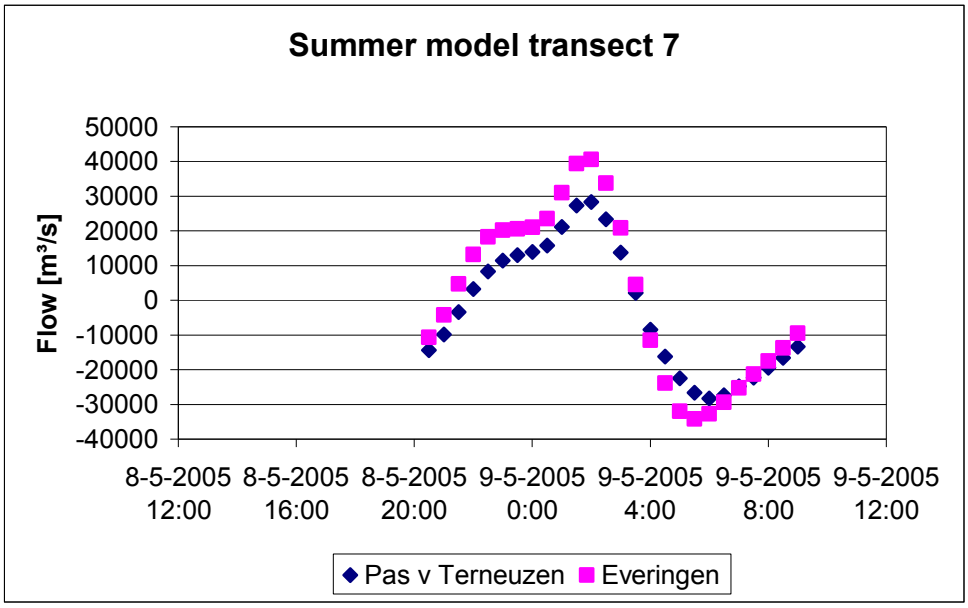

Figure H.43: Model result (summer) transect 7

M.756/01

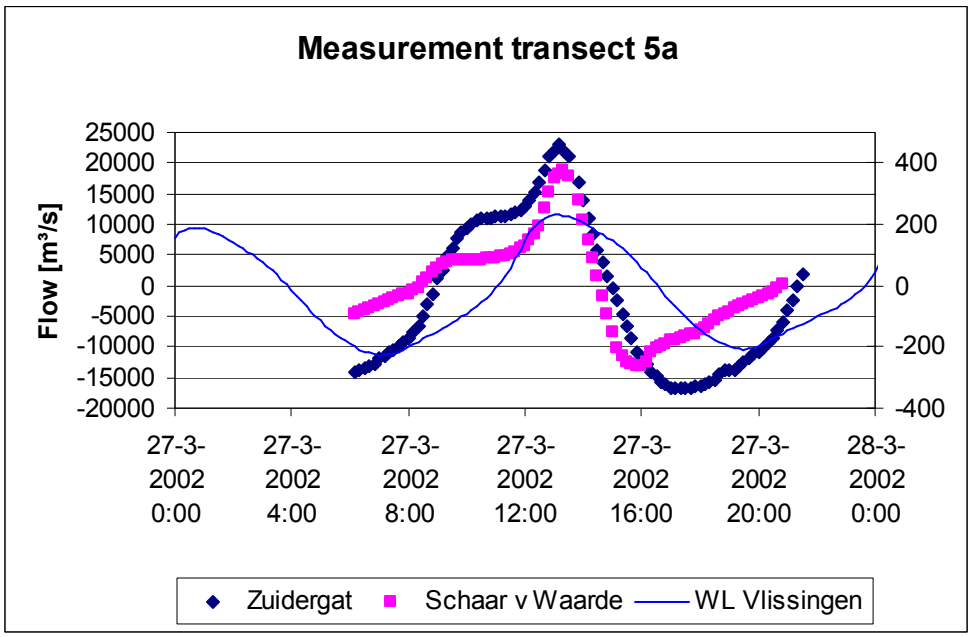

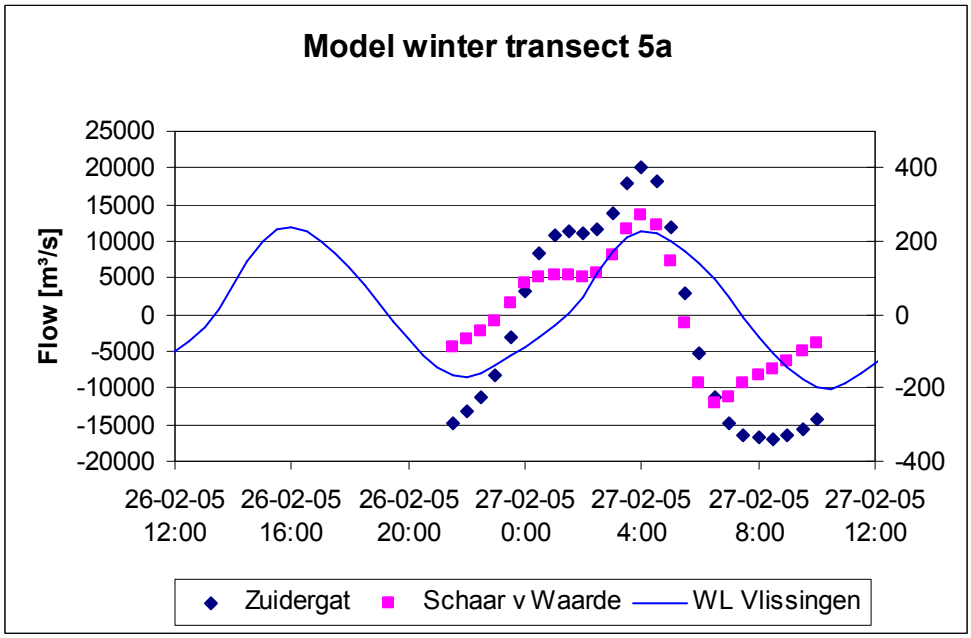

Figure H.44: RIKZ Measurement transect 5a
Model result (winter) transect 5a

M.756/01

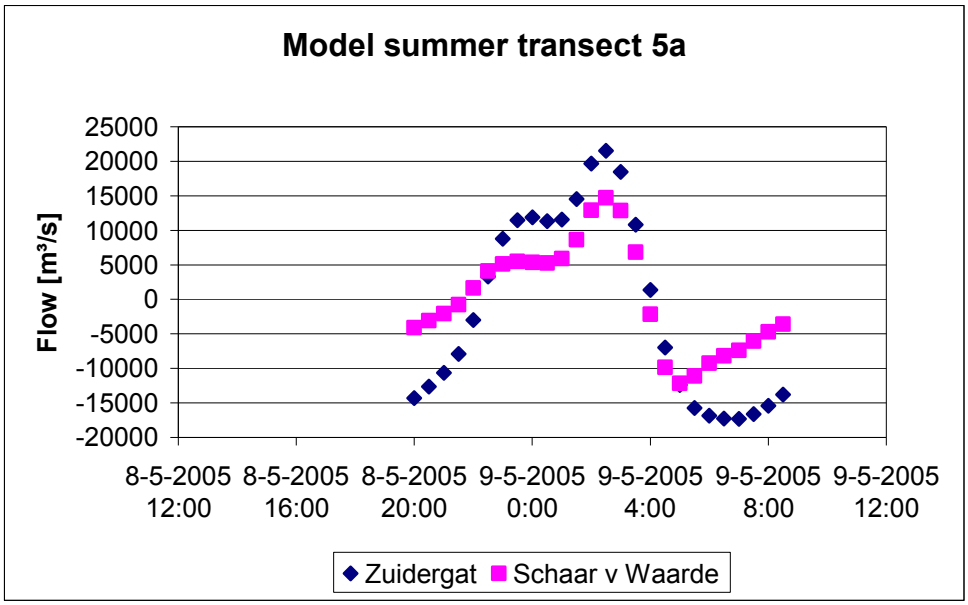

Figure H.45: Model result (summer) transect 5a

M.756/01

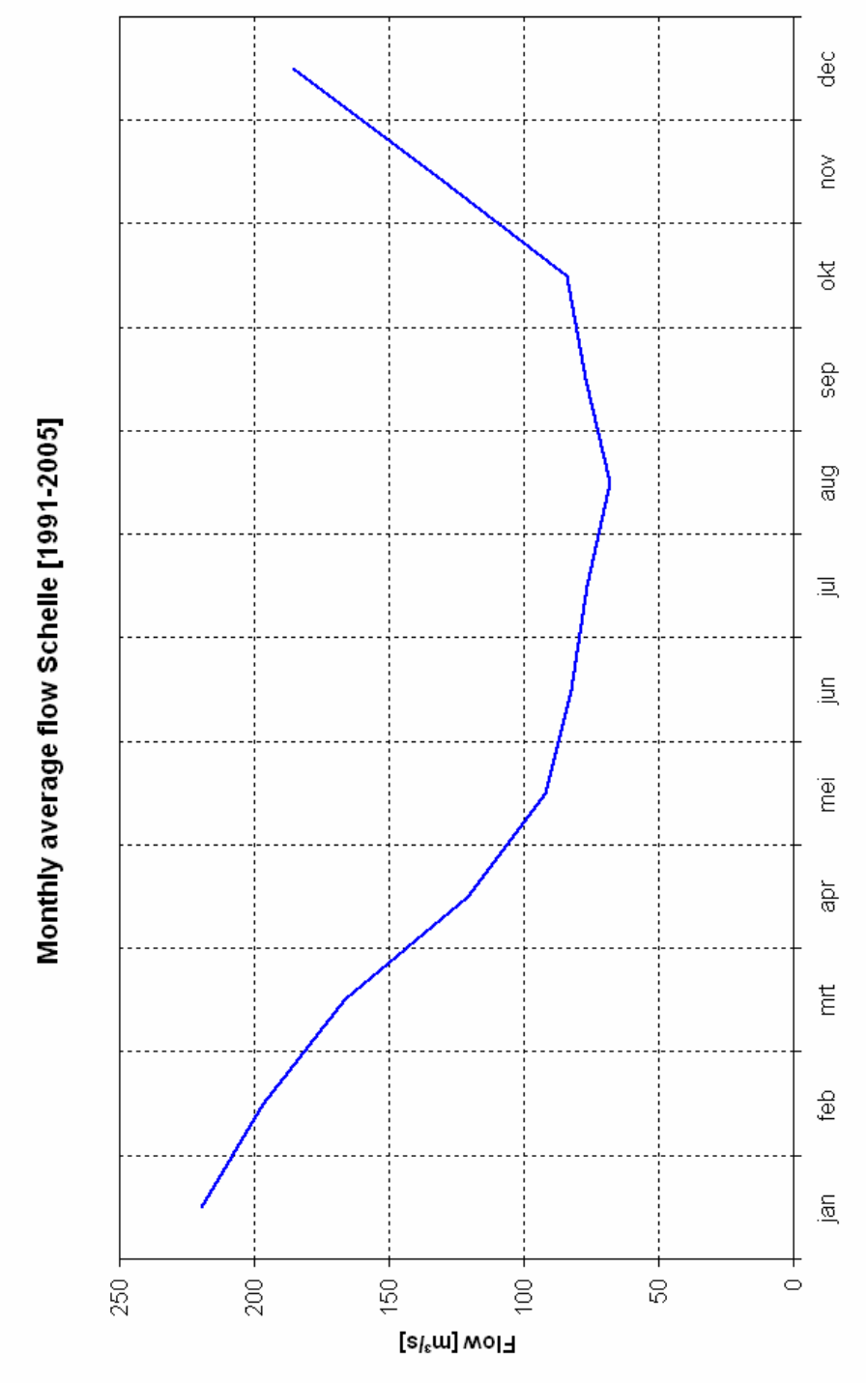

Figure H.46: Monthly average flow at Schelle (1991-2005)
Source: hydrometrie, WLB

M.756/01

FLANDERS HYDRAULICS RESEARCH / DELFT HYDRAULICS

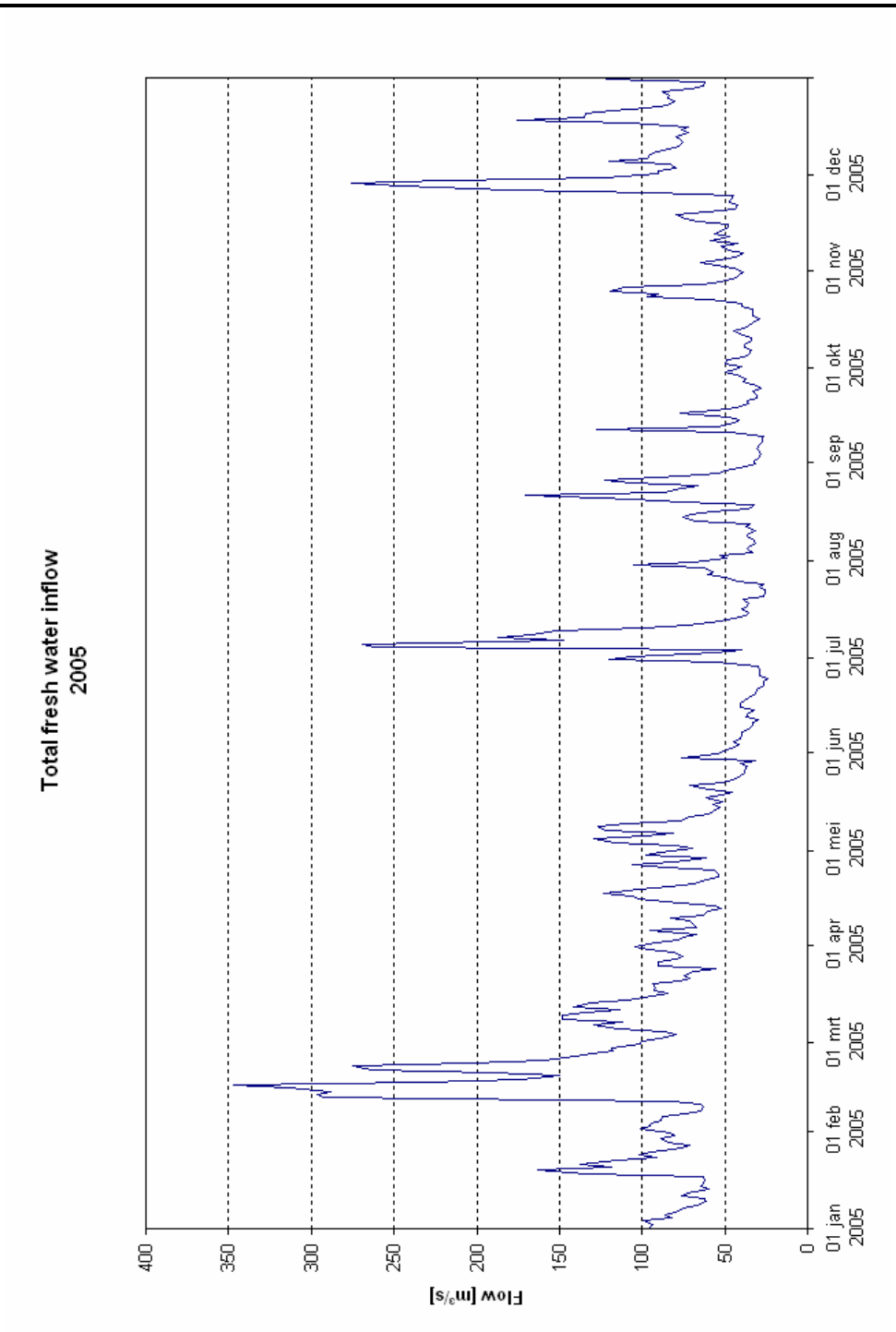

Figure H.47: Total fresh water inflow Scheldt basin (2005)
Source: hydrometrie, WLB

M.756/01

FLANDERS HYDRAULICS RESEARCH / DELFT HYDRAULICS

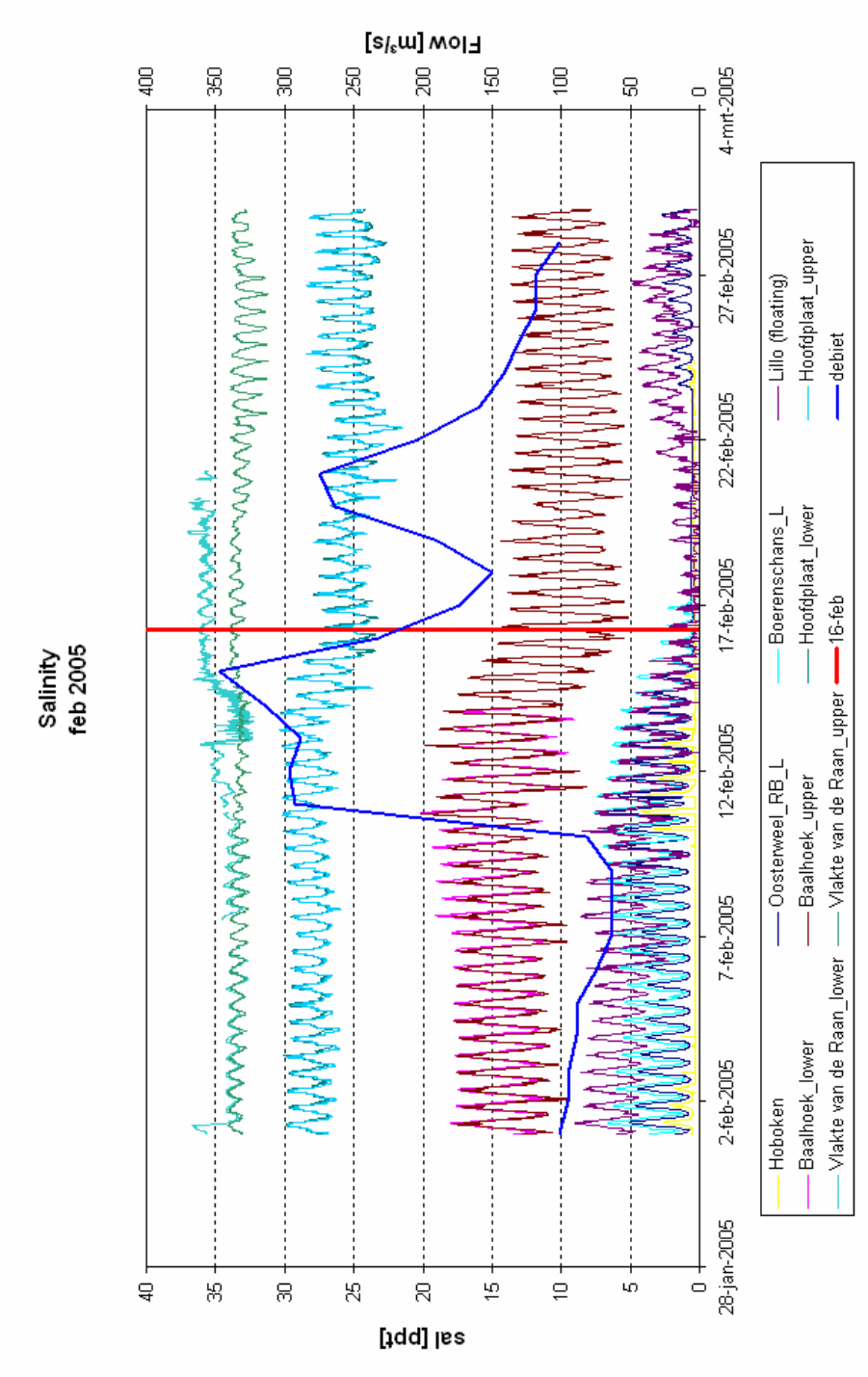

Figure H.48: Measured salinity February 2005
Total fresh water inflow February 2005
HW Westkapelle: 16/02/2005 6u50
Source: ZEGE, WLB-hydrometrie

M.756/01

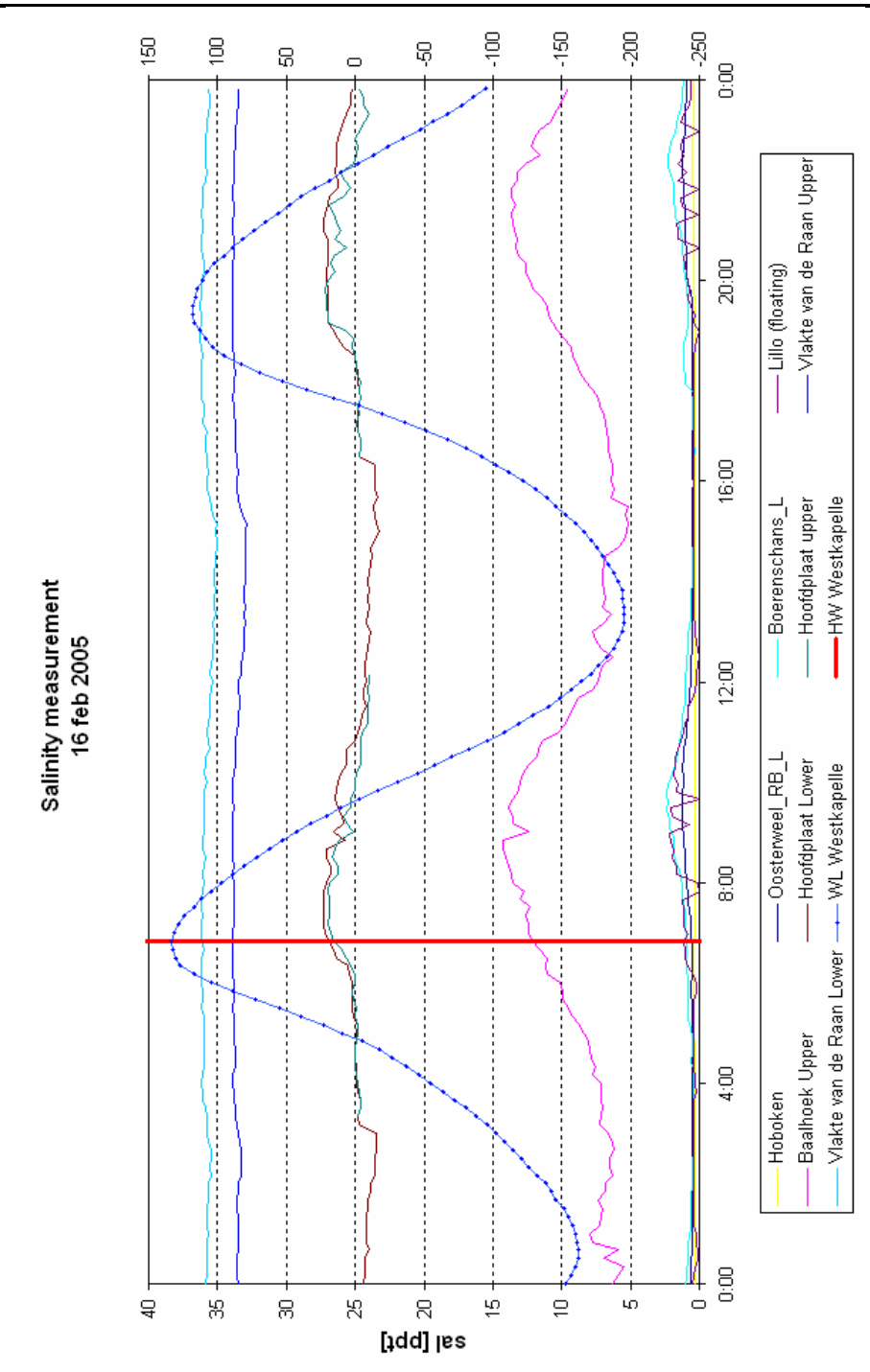

Figure H.49: Selection of initial conditions winter run
HW Westkapelle: 16/02/2005 6u50
Source: ZEGE, WLB-hydrometrie

M.756/01

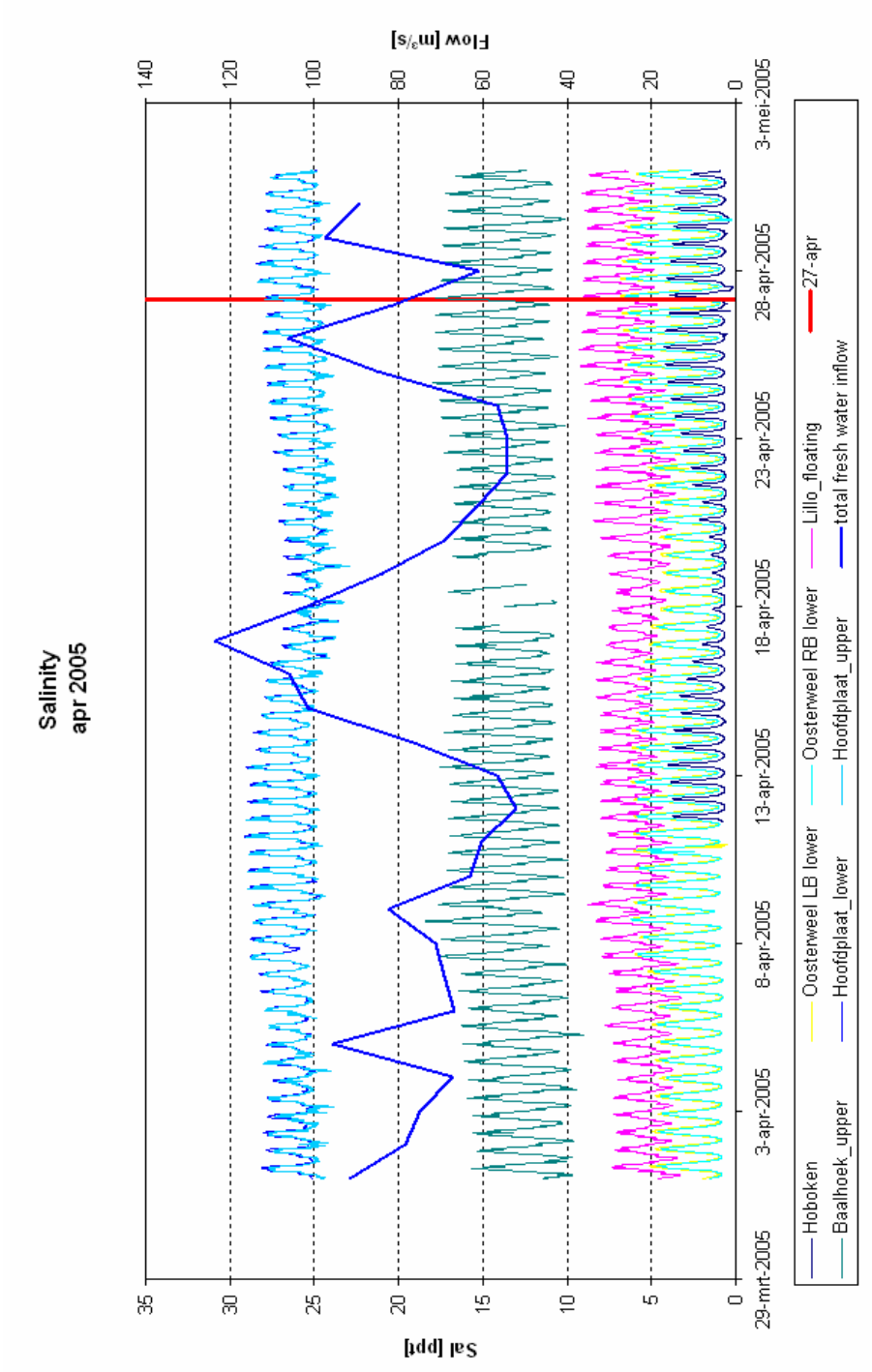

Figure H.50: Measured salinity april 2005
Total fresh water inflow april 2005
HW Westkapelle: 27/04/2005 3u10
Source: ZEGE, WLB-hydrometrie

M.756/01

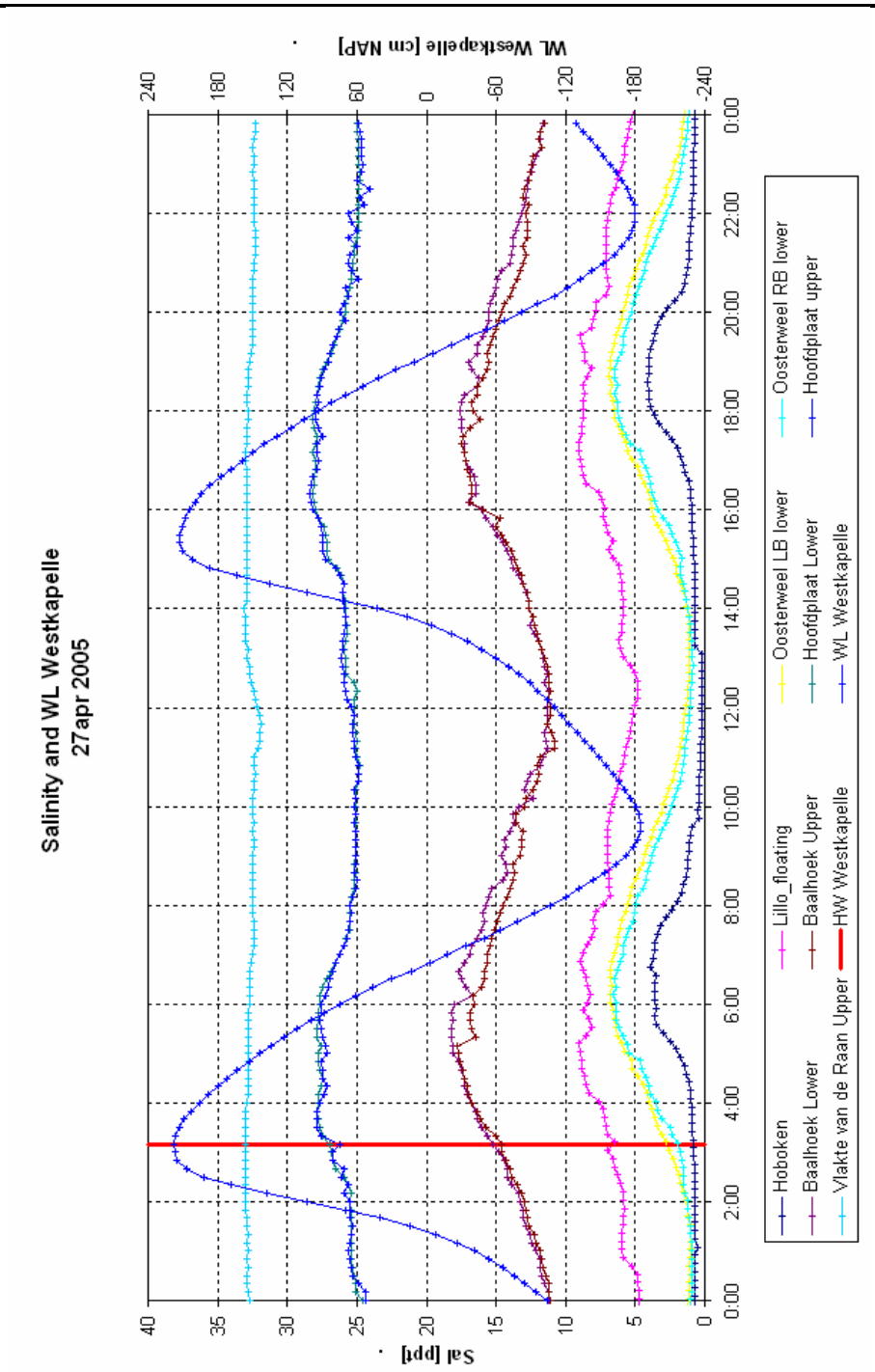

Figure H.51: Selection of initial conditions summer run
HW Westkapelle: 27/04/2005 3u10
Source: ZEGE, WLB-hydrometrie

M.756/01

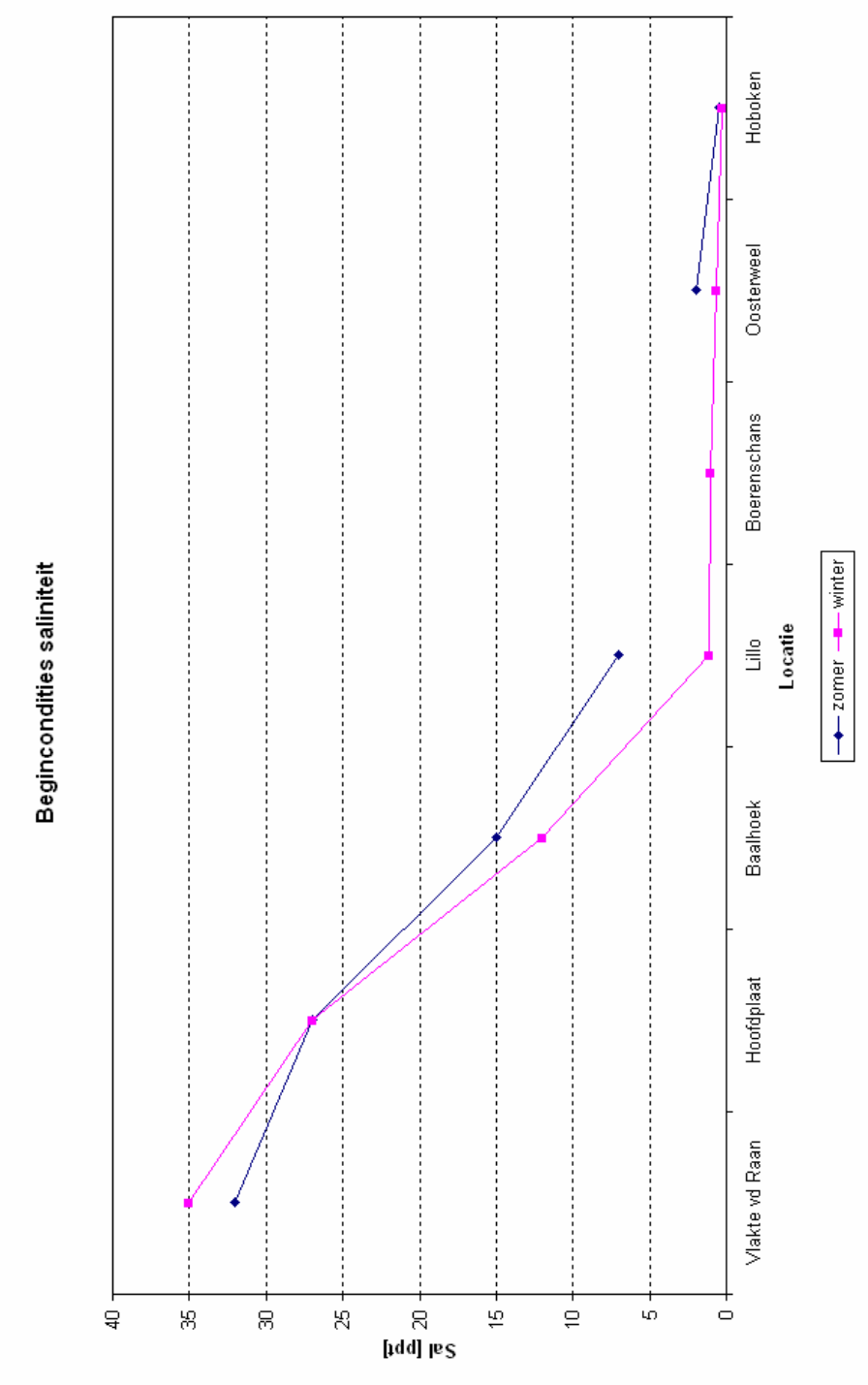

Figure H.52: Initial conditions salinity, winter and summer conditions.

M.756/01

FLANDERS HYDRAULICS RESEARCH / DELFT HYDRAULICS

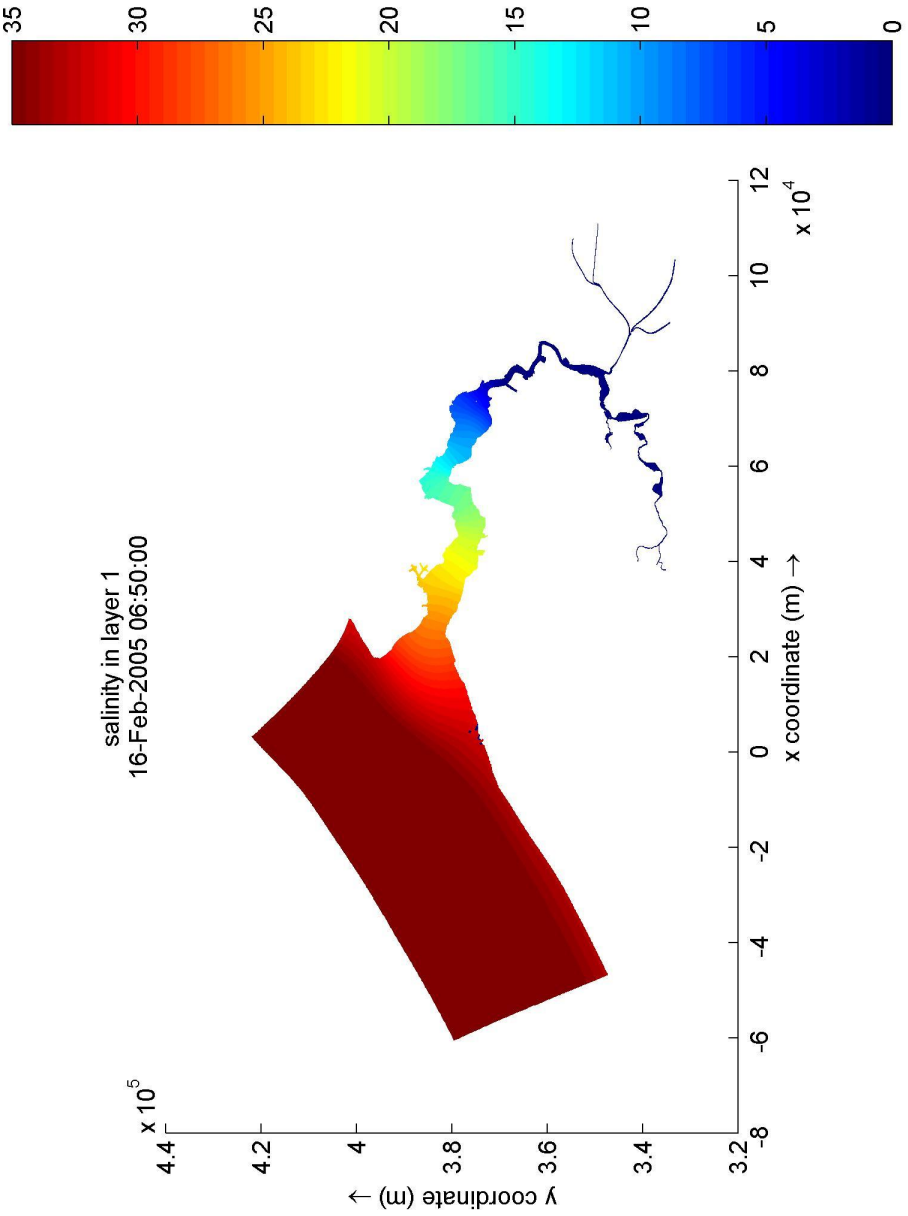

Figure H.53: Initial condition winter run: salinity

M.756/01

FLANDERS HYDRAULICS RESEARCH / DELFT HYDRAULICS

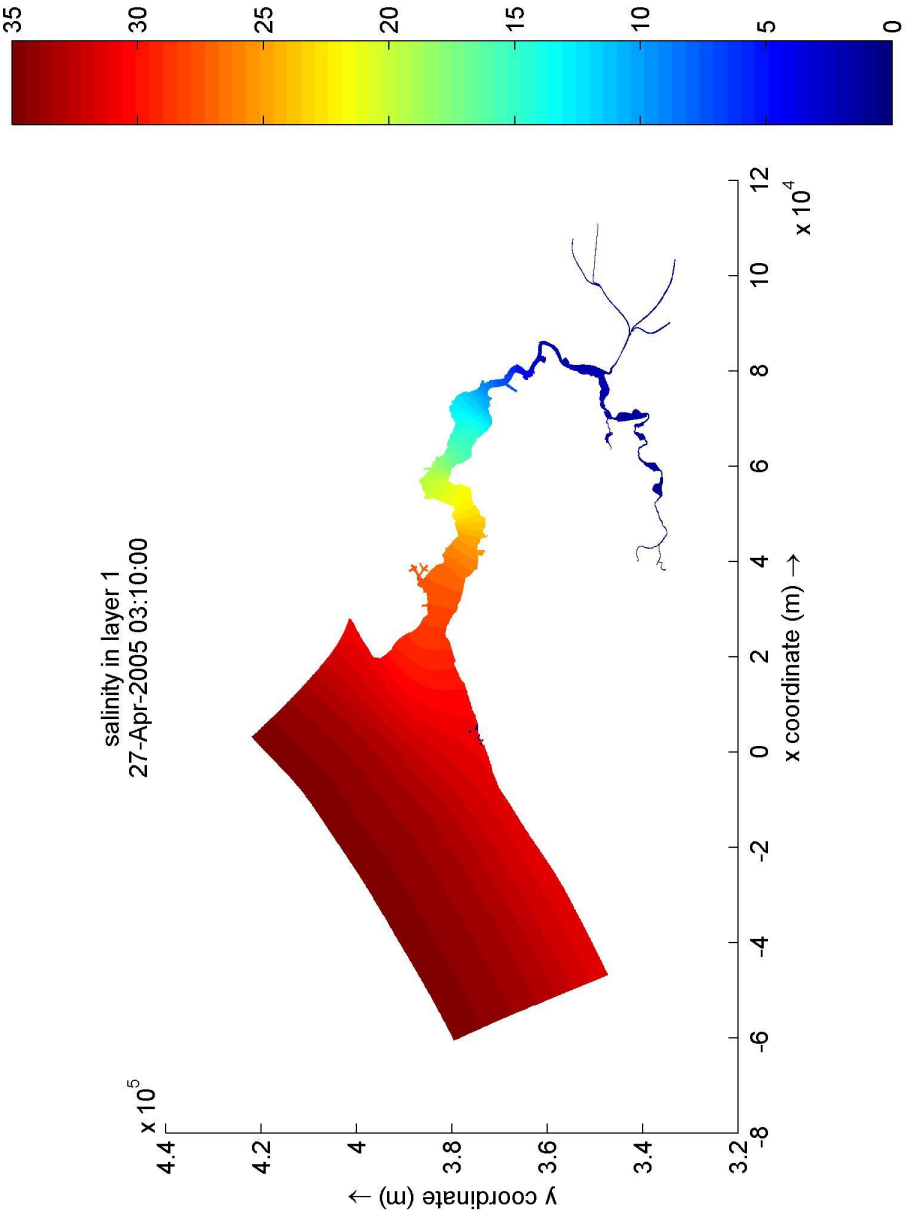

Figure H.54: Initial condition summer run: salinity

M.756/01

FLANDERS HYDRAULICS RESEARCH / DELFT HYDRAULICS

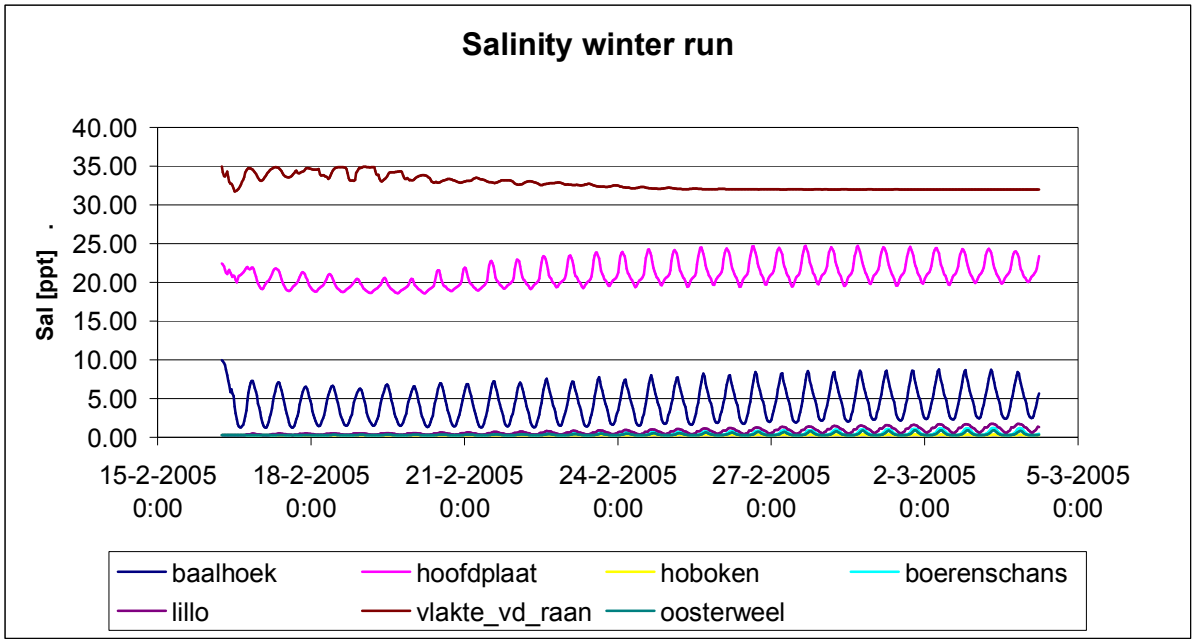

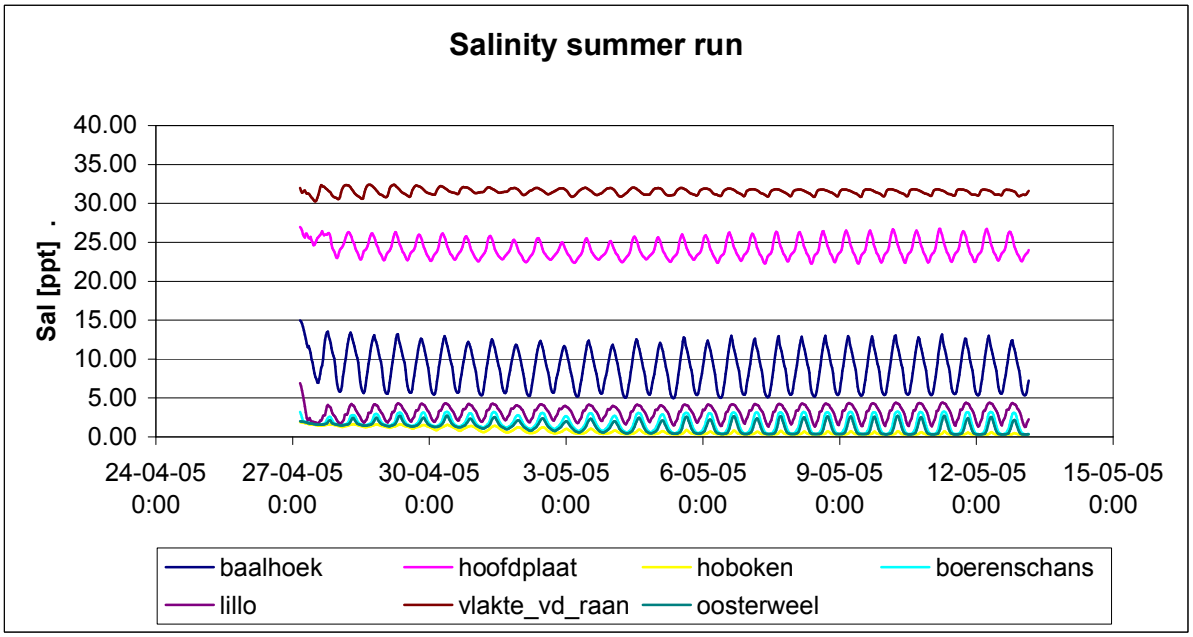

Figure H.55: Salinity in winter and summer model runs

M.756/01

FLANDERS HYDRAULICS RESEARCH / DELFT HYDRAULICS

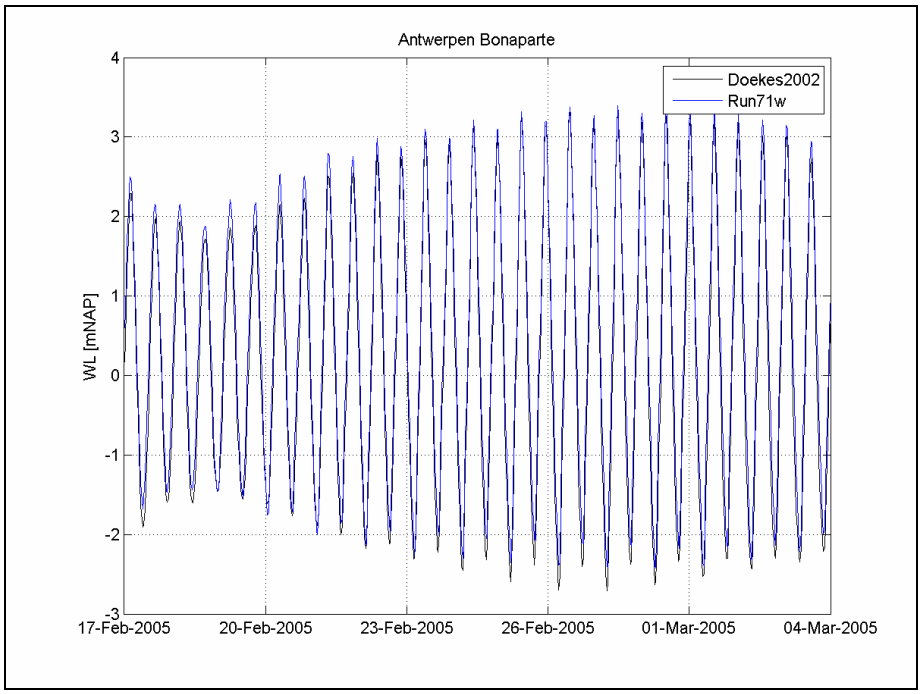

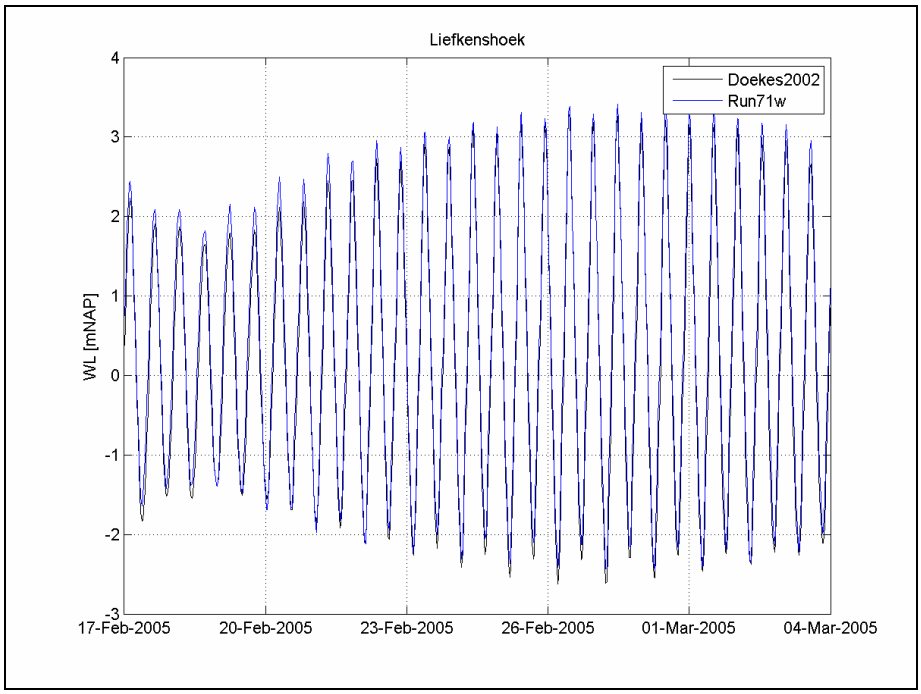

Figure H.56: Water level in winter model, compared to waterlevel out of Doekes (2002) dataset

M.756/01

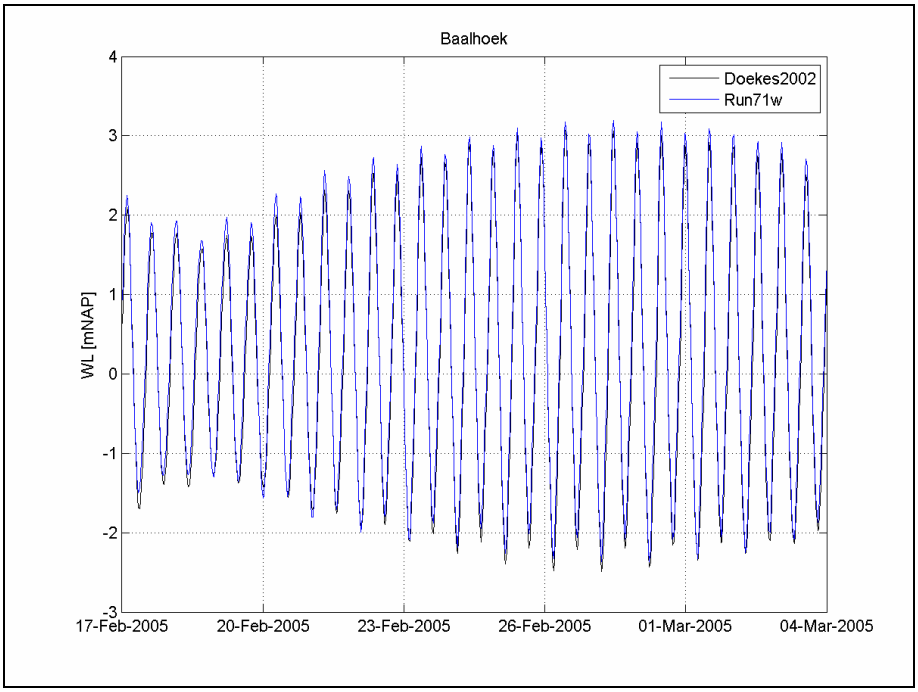

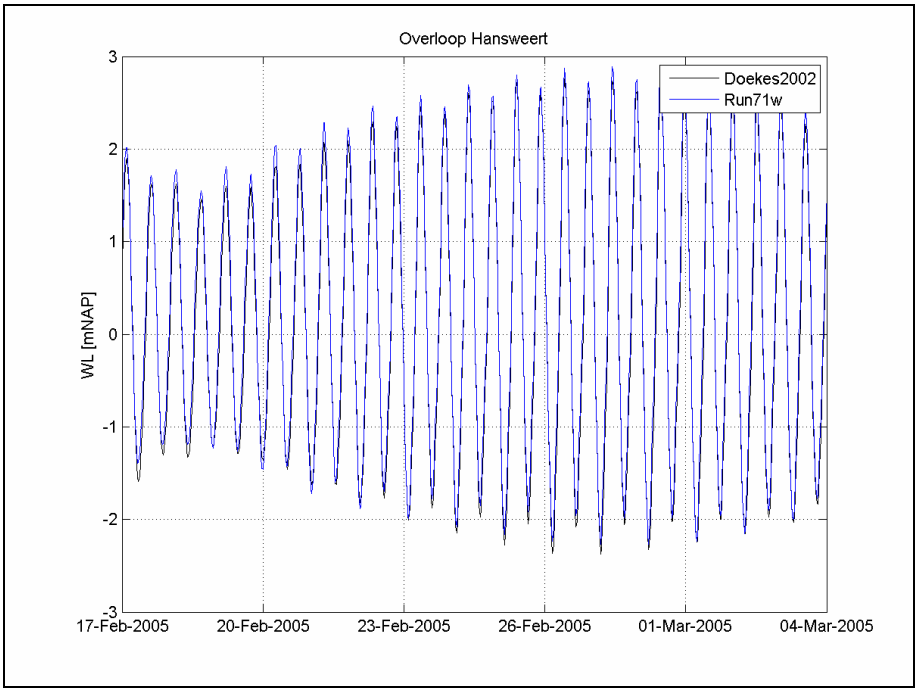

Figure H.57: Water level in winter model, compared to waterlevel out of Doekes (2002) dataset

M.756/01

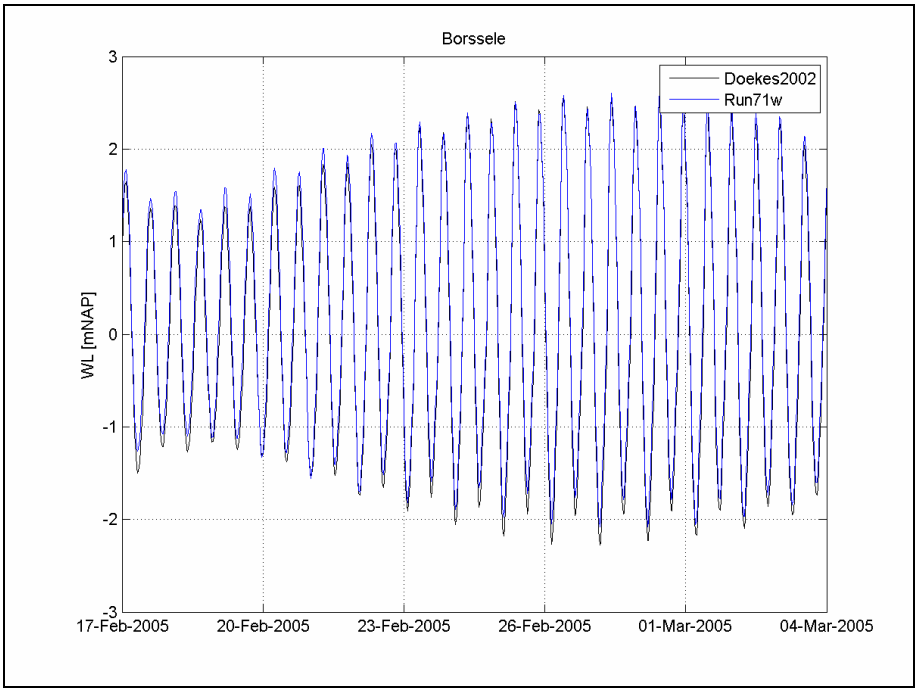

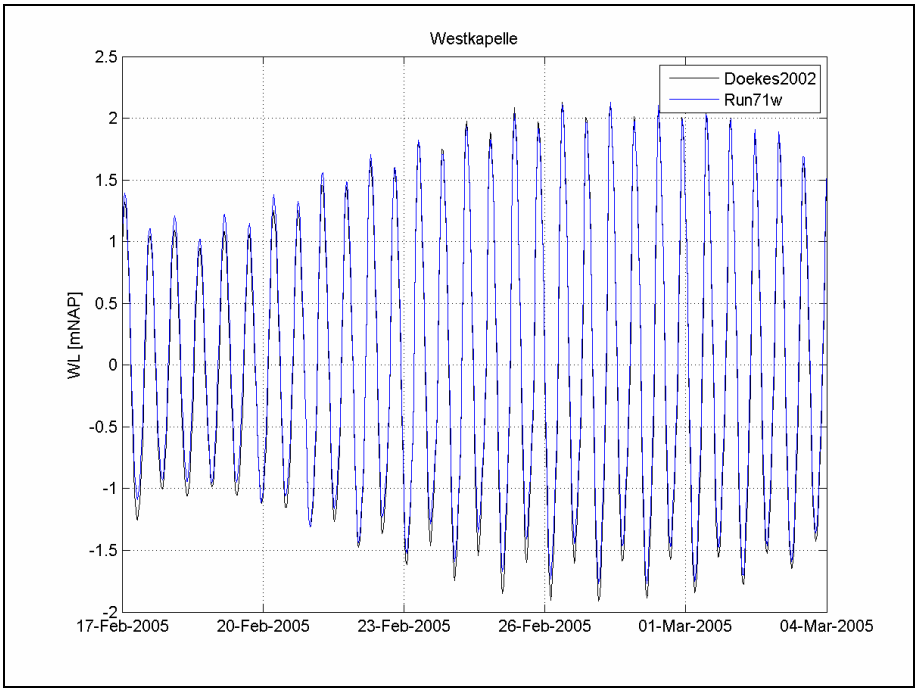

Figure H.58: Water level in winter model, compared to waterlevel out of Doekes (2002) dataset

M.756/01

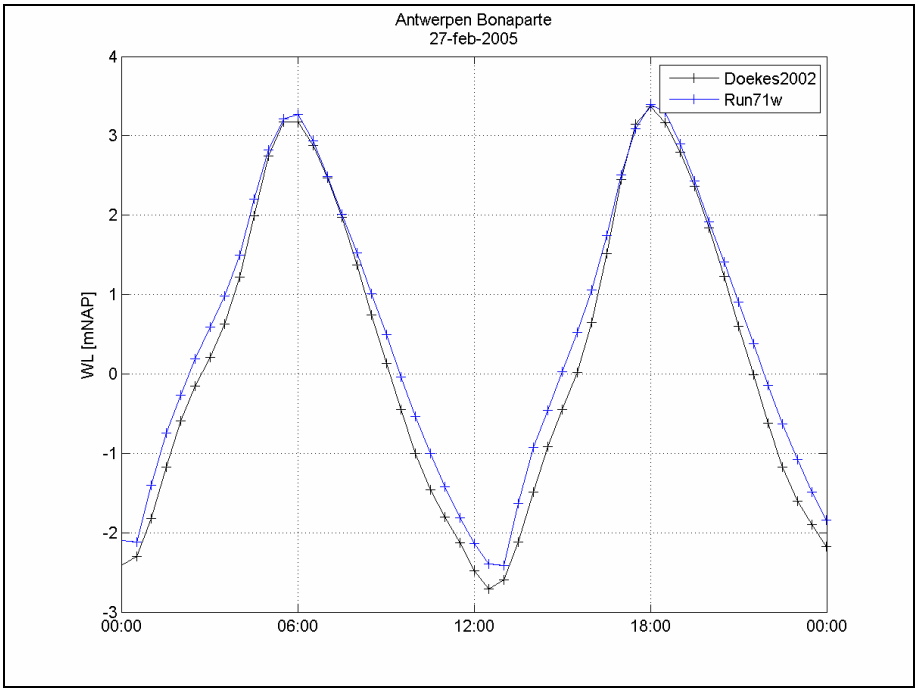

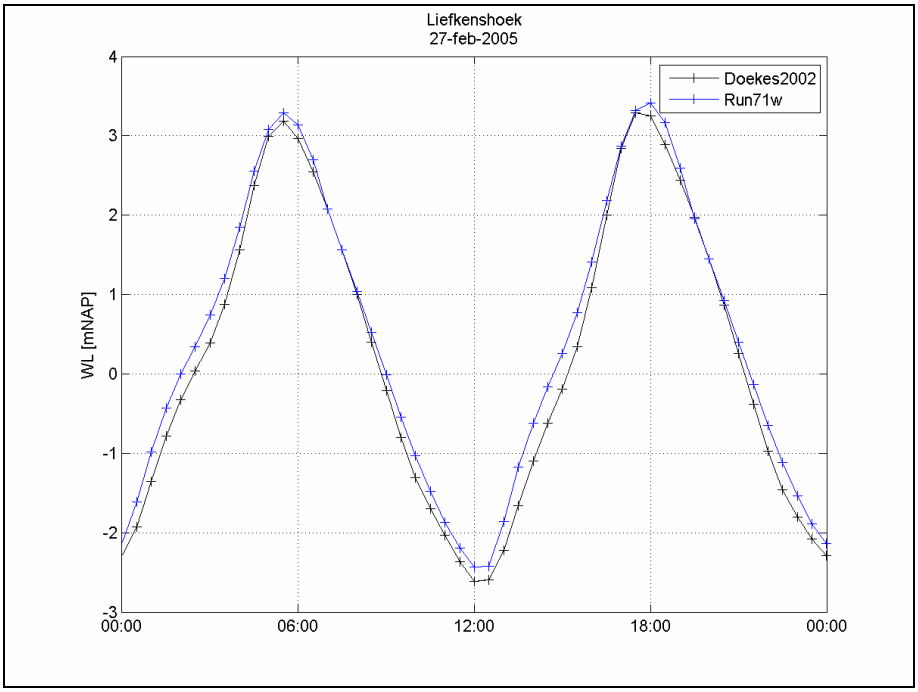

Figure H.59: Water level in winter model, compared to waterlevel out of Doekes (2002) dataset

M.756/01

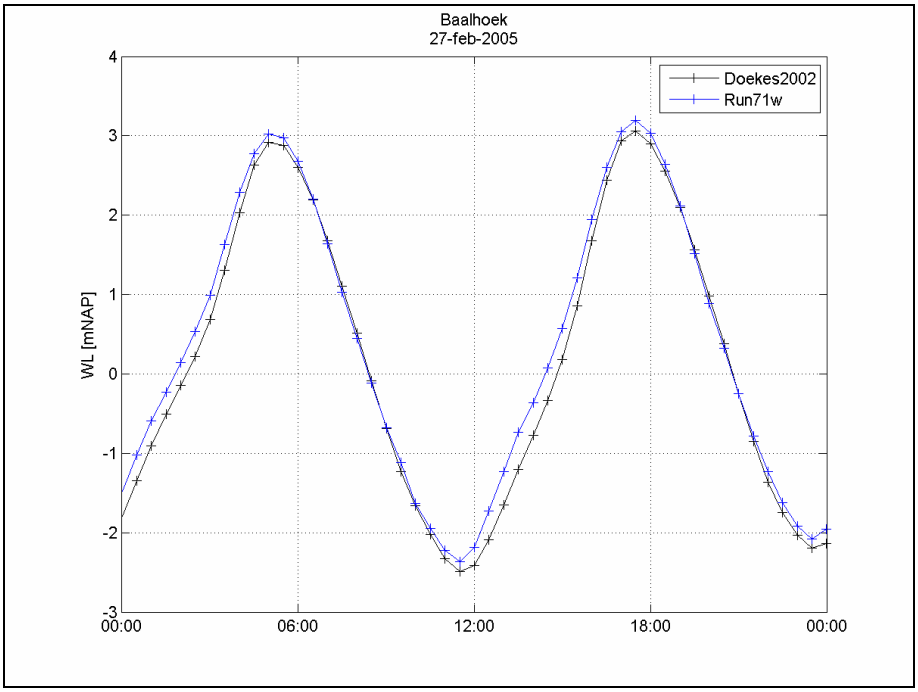

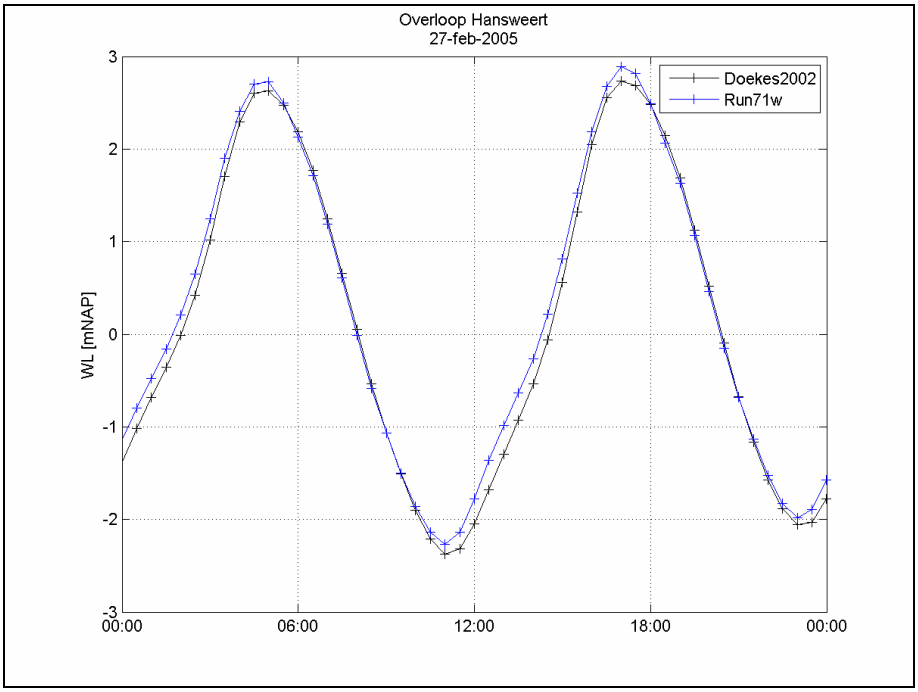

Figure H.60: Water level in winter model, compared to waterlevel out of Doekes (2002) dataset

M.756/01

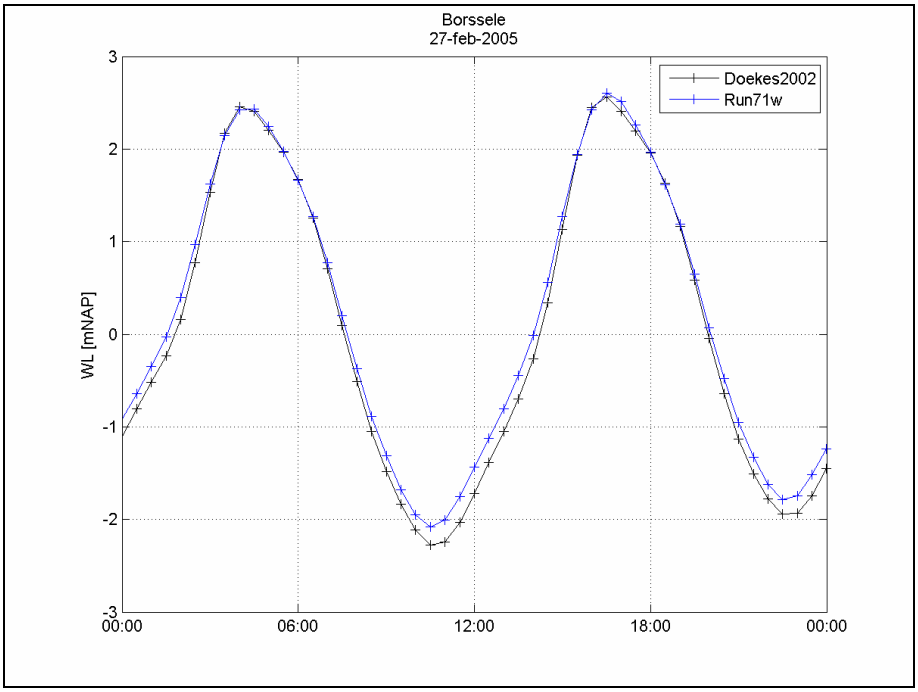

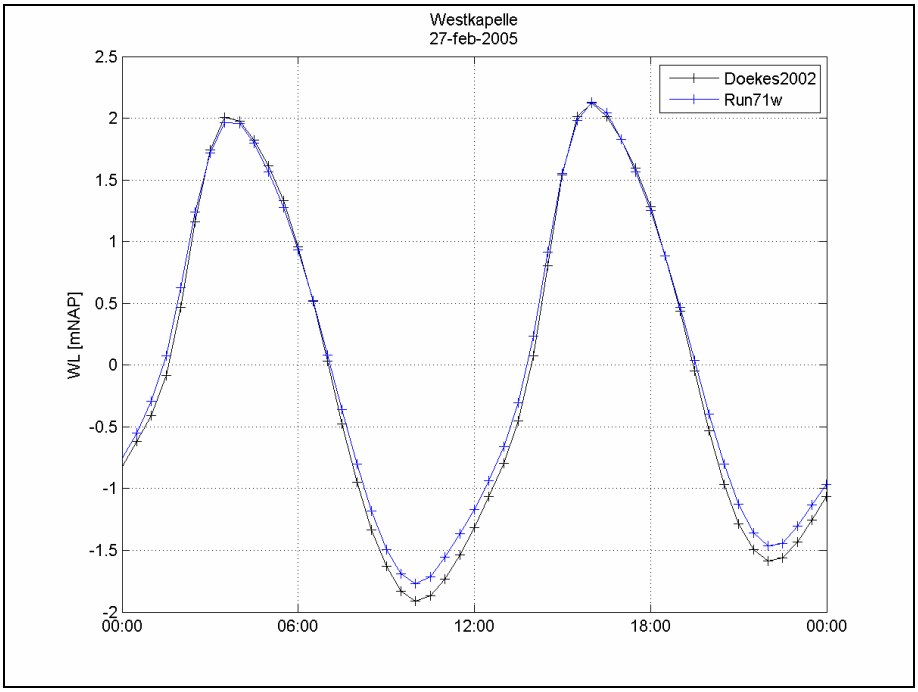

Figure H.61: Water level in winter model, compared to waterlevel out of Doekes (2002) dataset

M.756/01

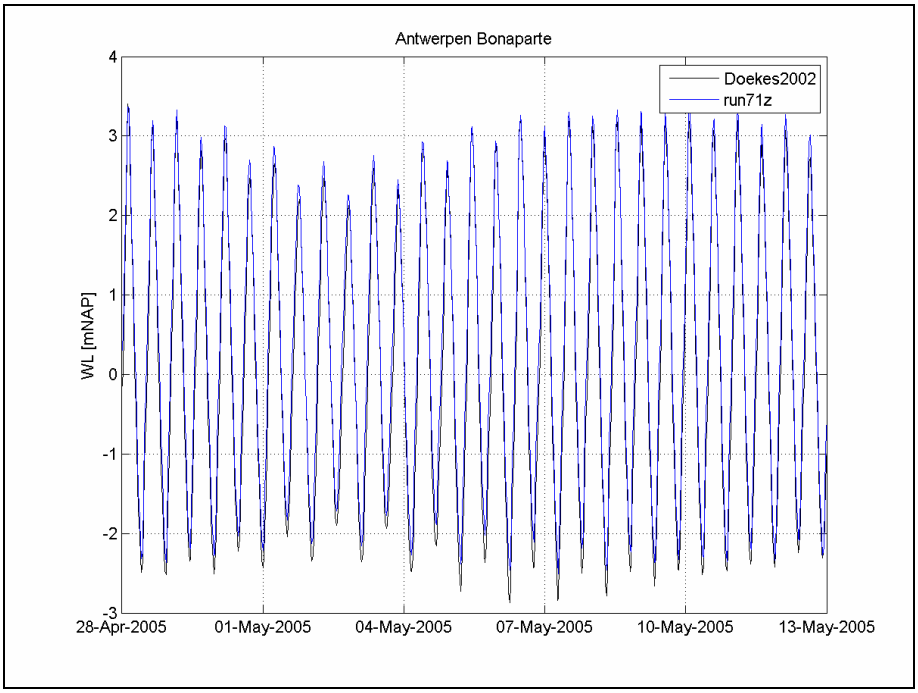

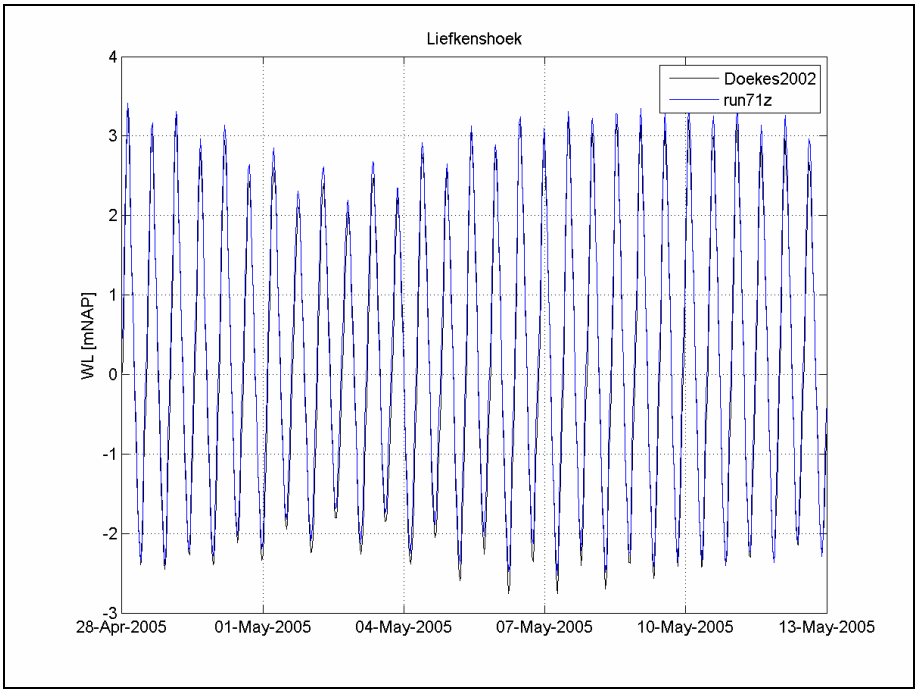

Figure H.62: Water level in summer model, compared to waterlevel out of Doekes (2002) dataset

M.756/01

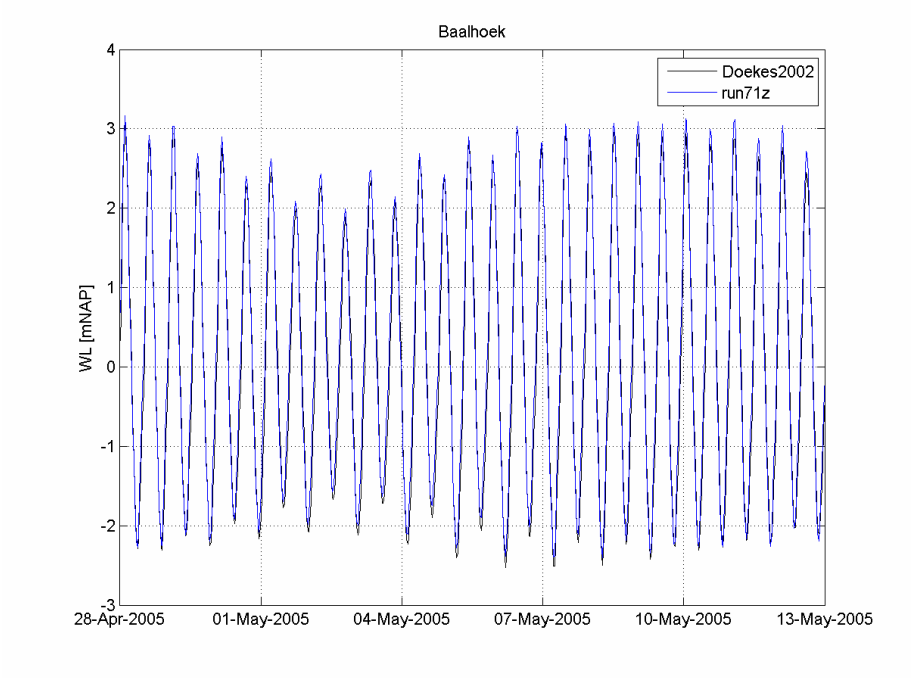

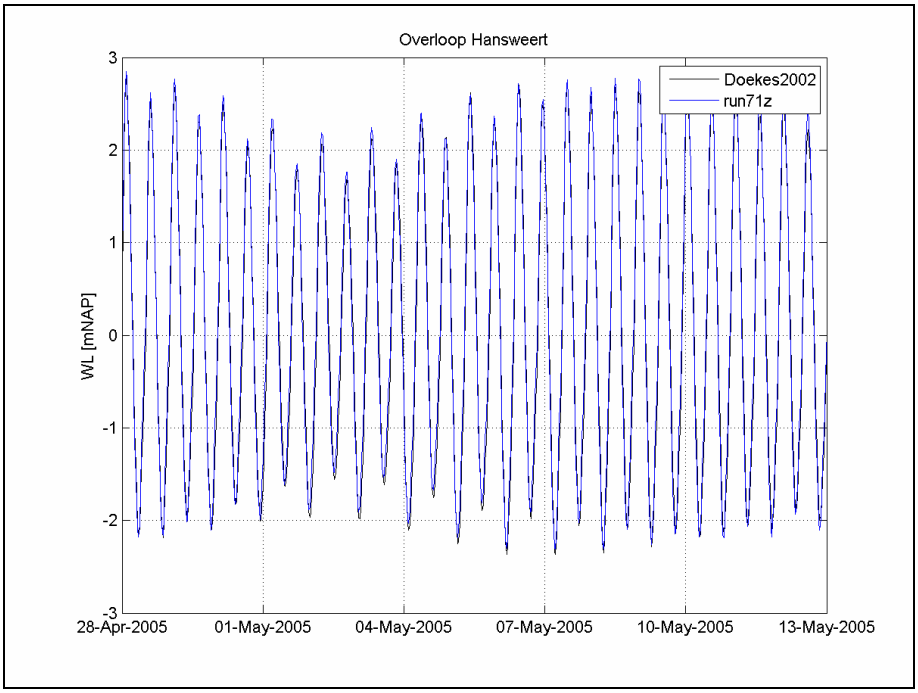

Figure H.63: Water level in summer model, compared to waterlevel out of Doekes (2002) dataset

M.756/01

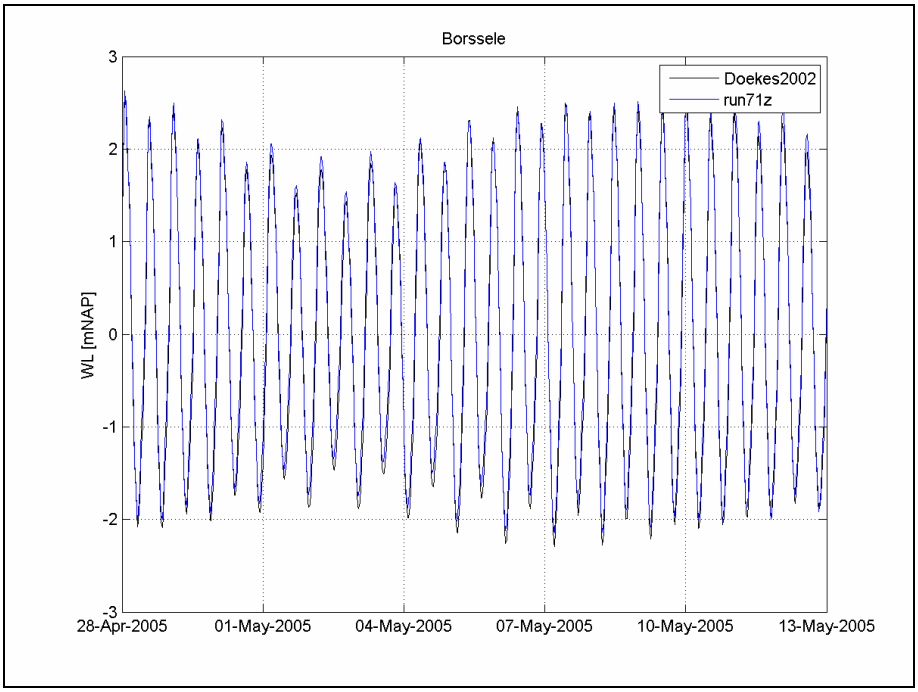

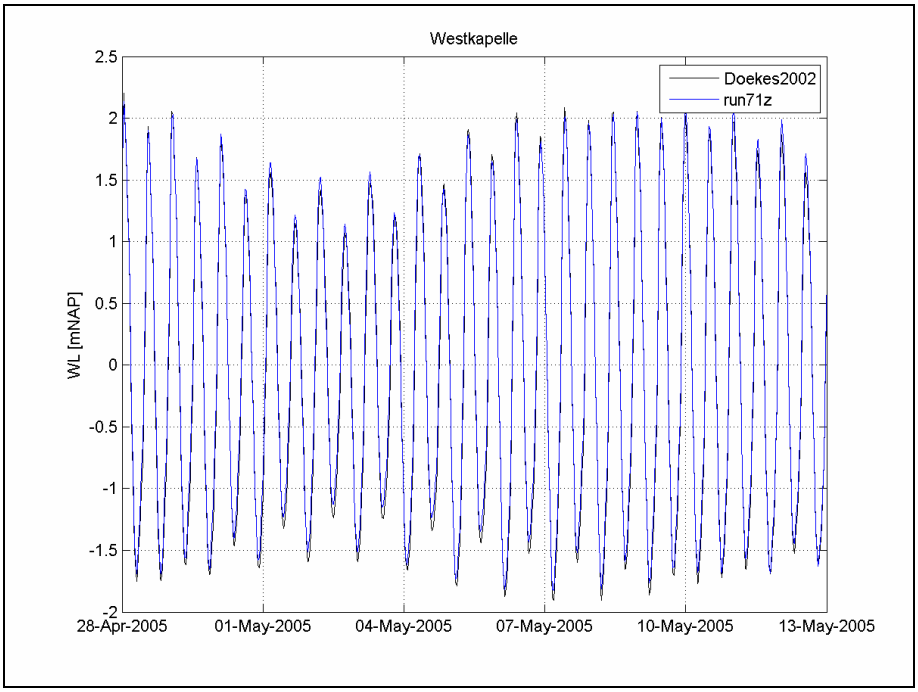

Figure H.64: Water level in summer model, compared to waterlevel out of Doekes (2002) dataset

M.756/01

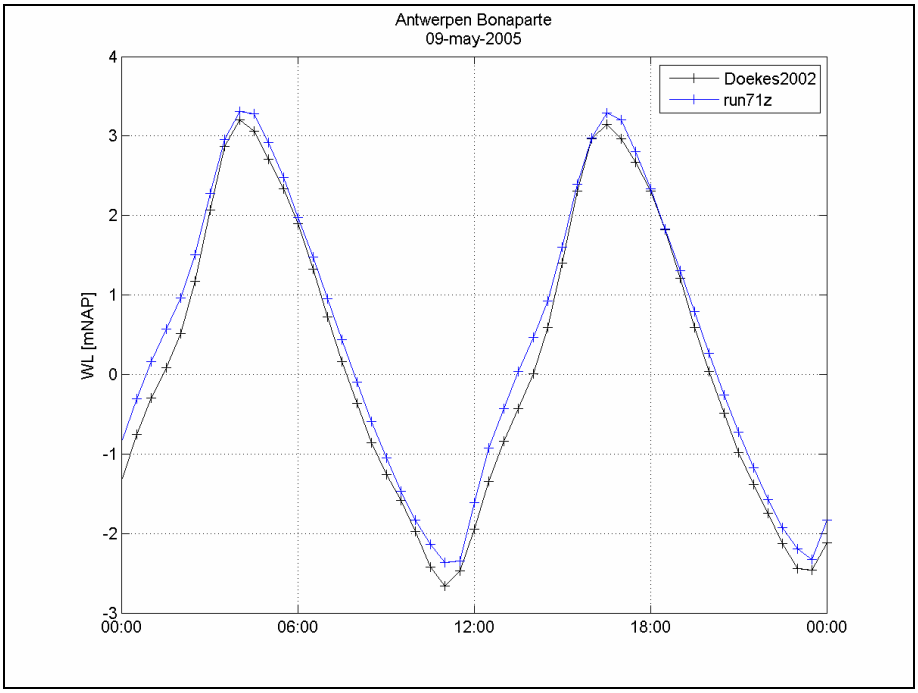

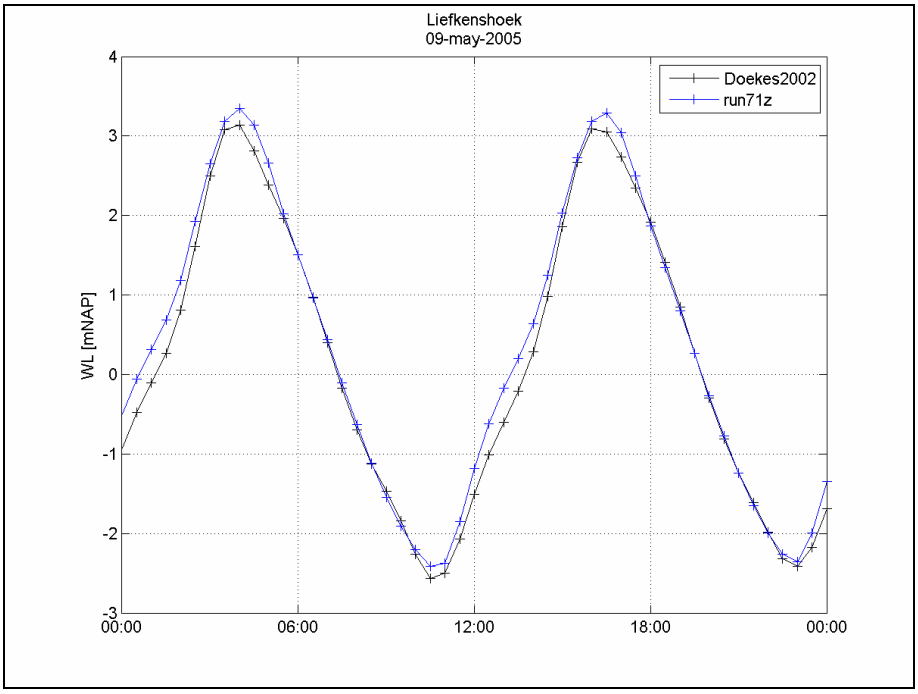

Figure H.65: Water level in summer model, compared to waterlevel out of Doekes (2002) dataset

M.756/01

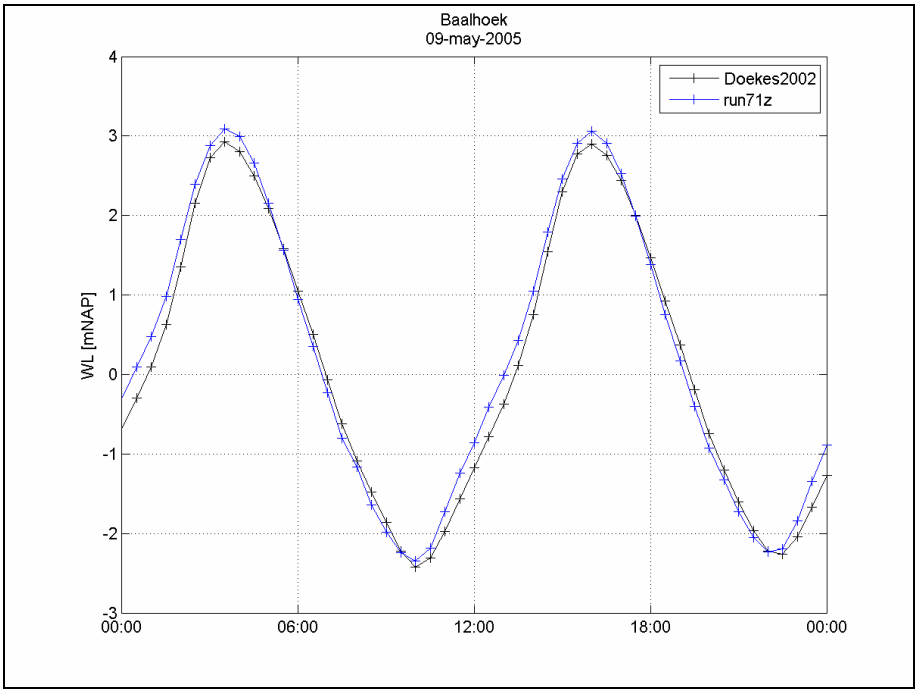

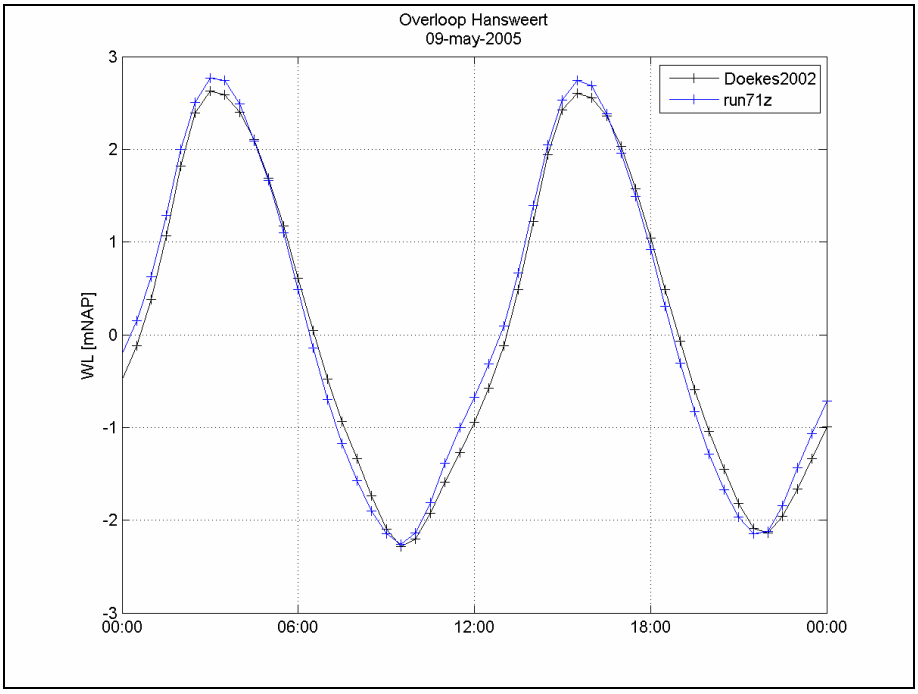

Figure H.66: Water level in summer model, compared to waterlevel out of Doekes (2002) dataset

M.756/01

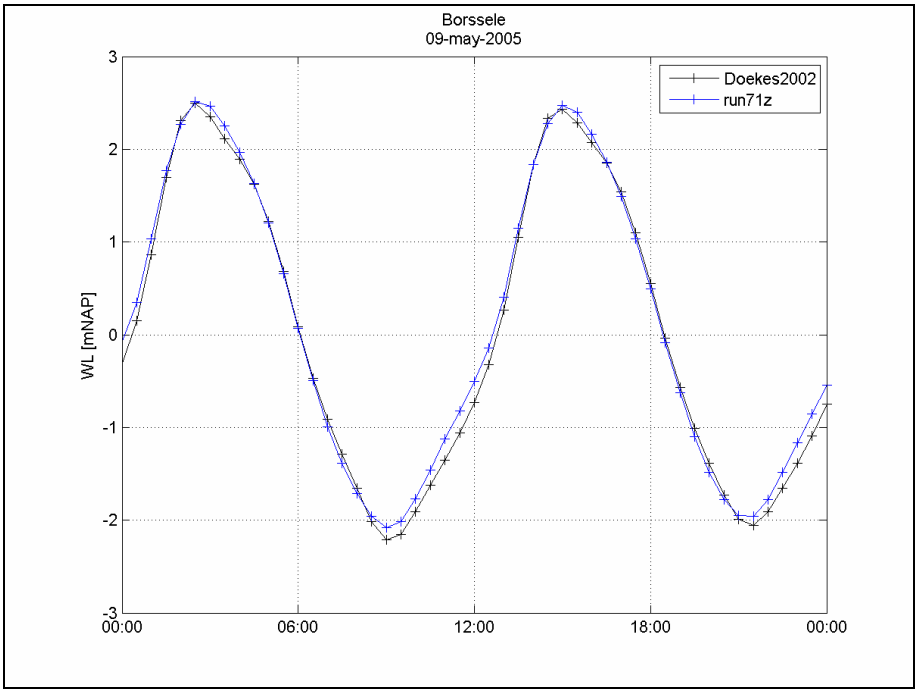

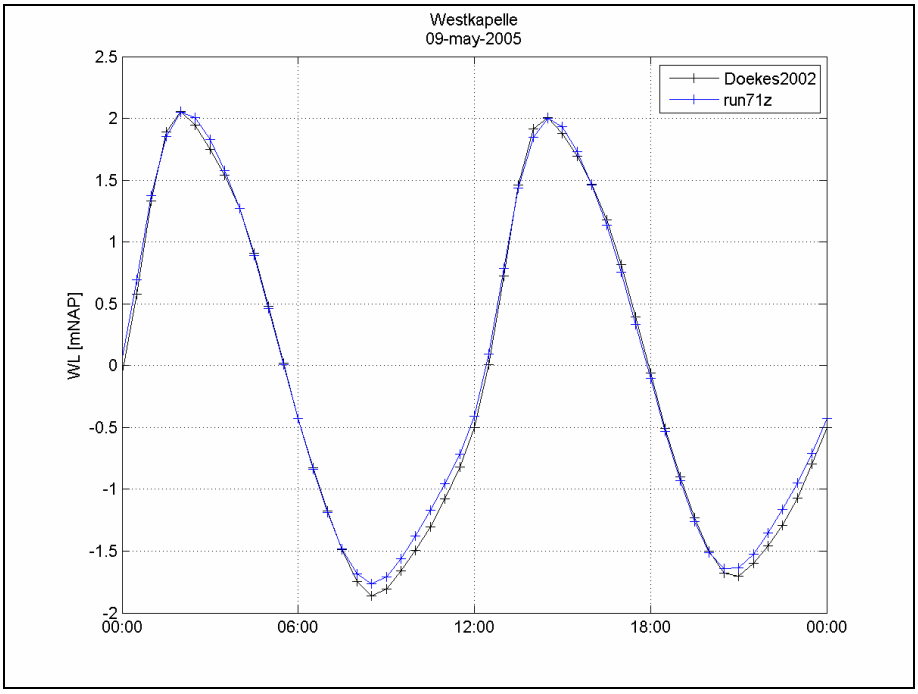

Figure H.67: Water level in summer model, compared to waterlevel out of Doekes (2002) dataset

M.756/01

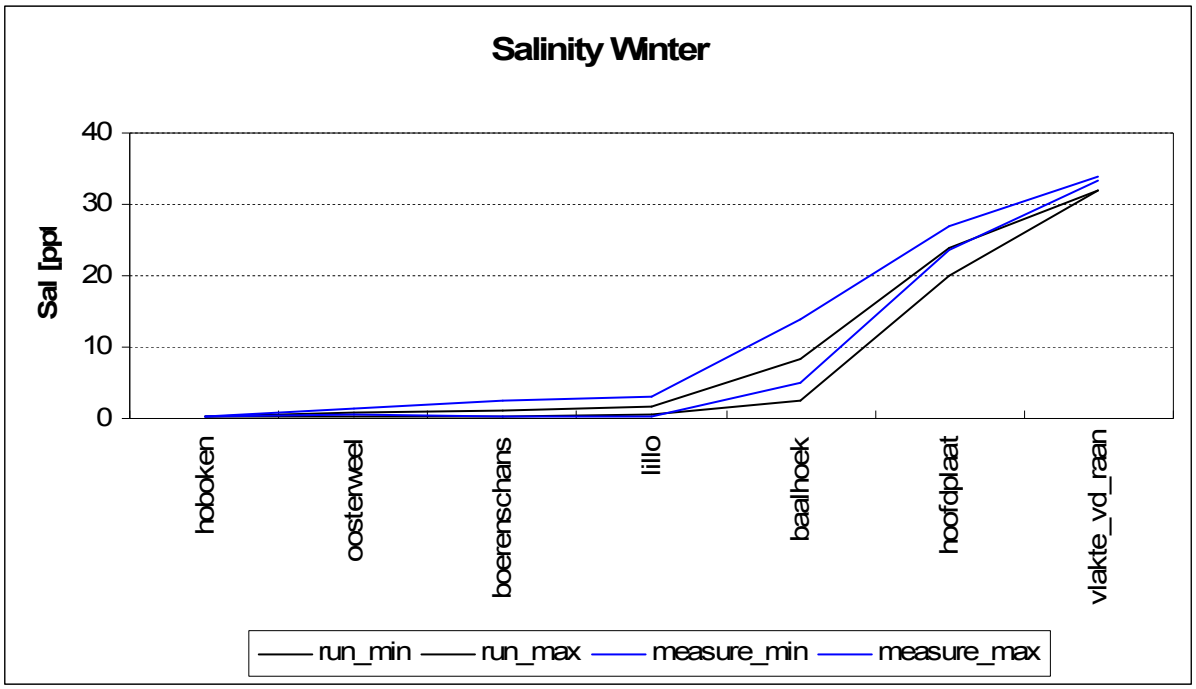

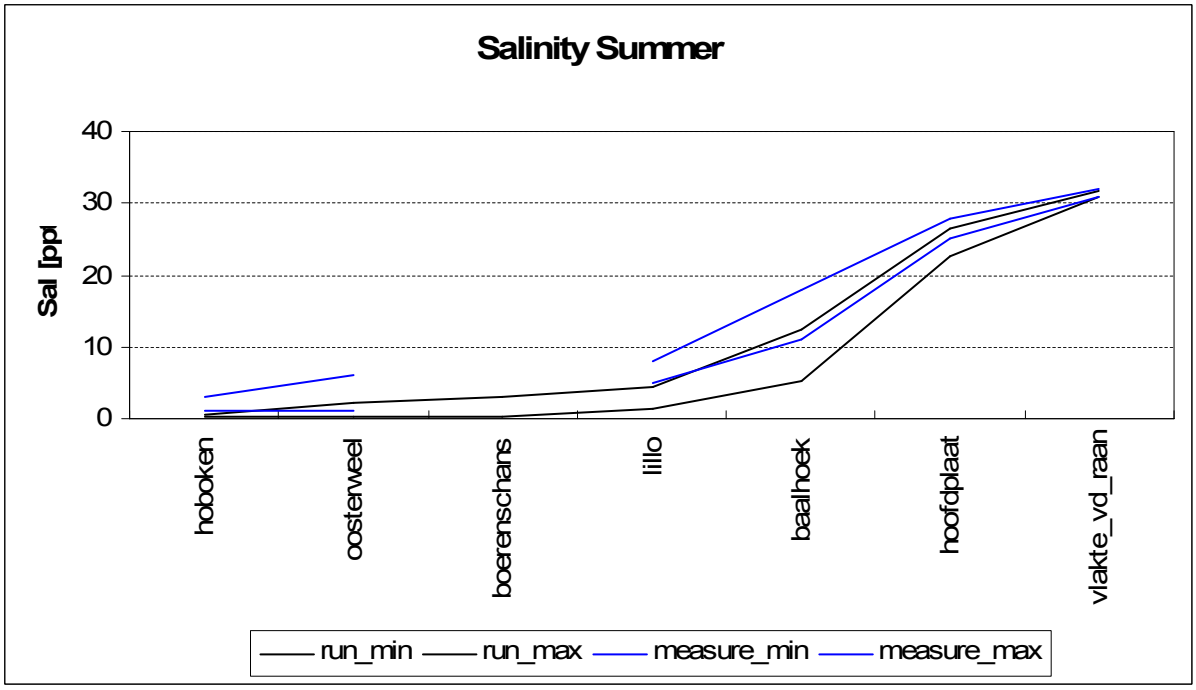

Figure H.68: Salinity minima and maxima along the estuary.
End of both runs and measurements

M.756/01

S Figures Silt Transport Model

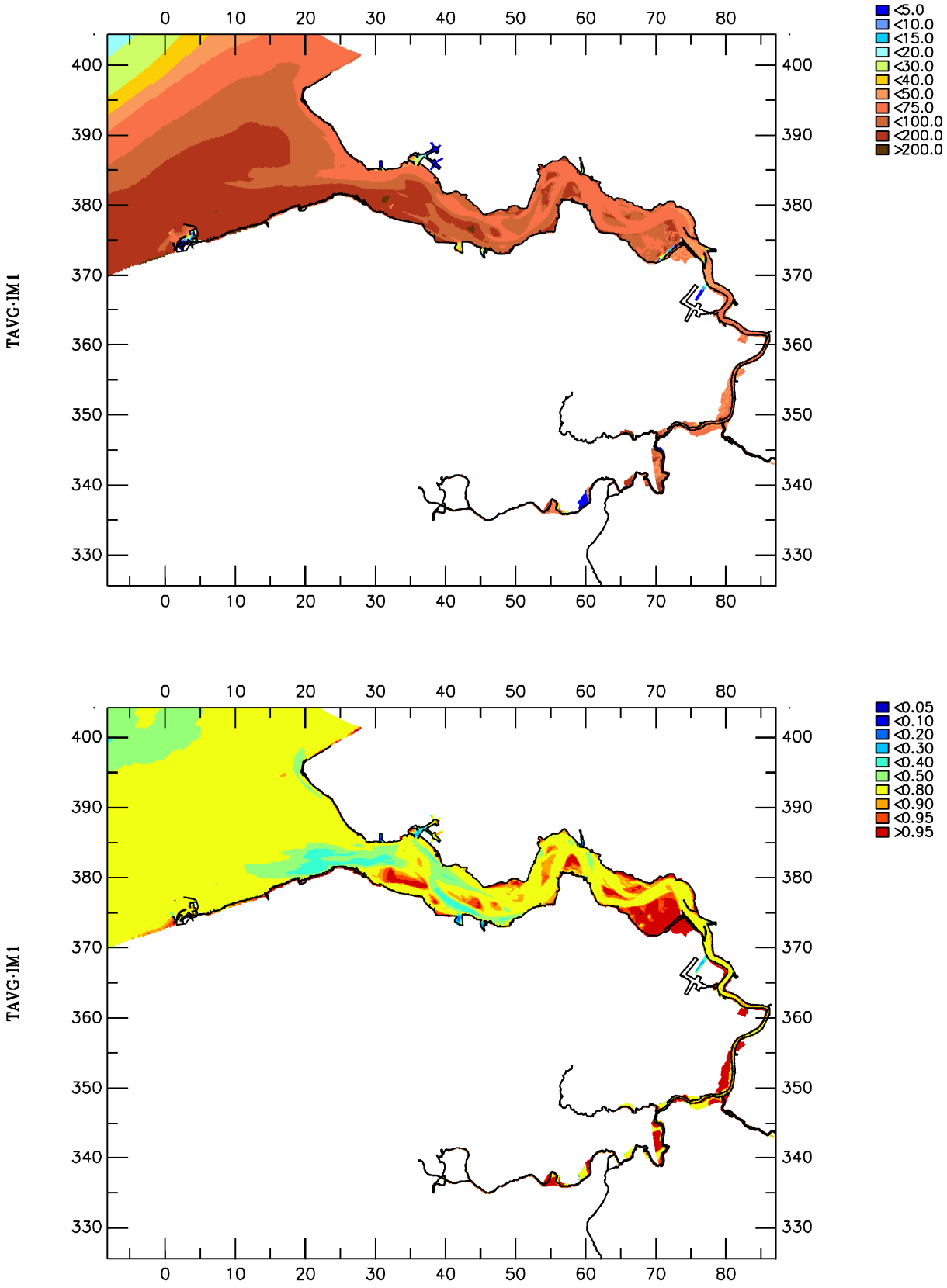

top: SPM concentration in surface layer (mg/l) bottom: concentration ratio surface/bottom (–)	hydro 14dw	w15r
WL | Delft Hydraulics	Z4210	Fig. S1.1

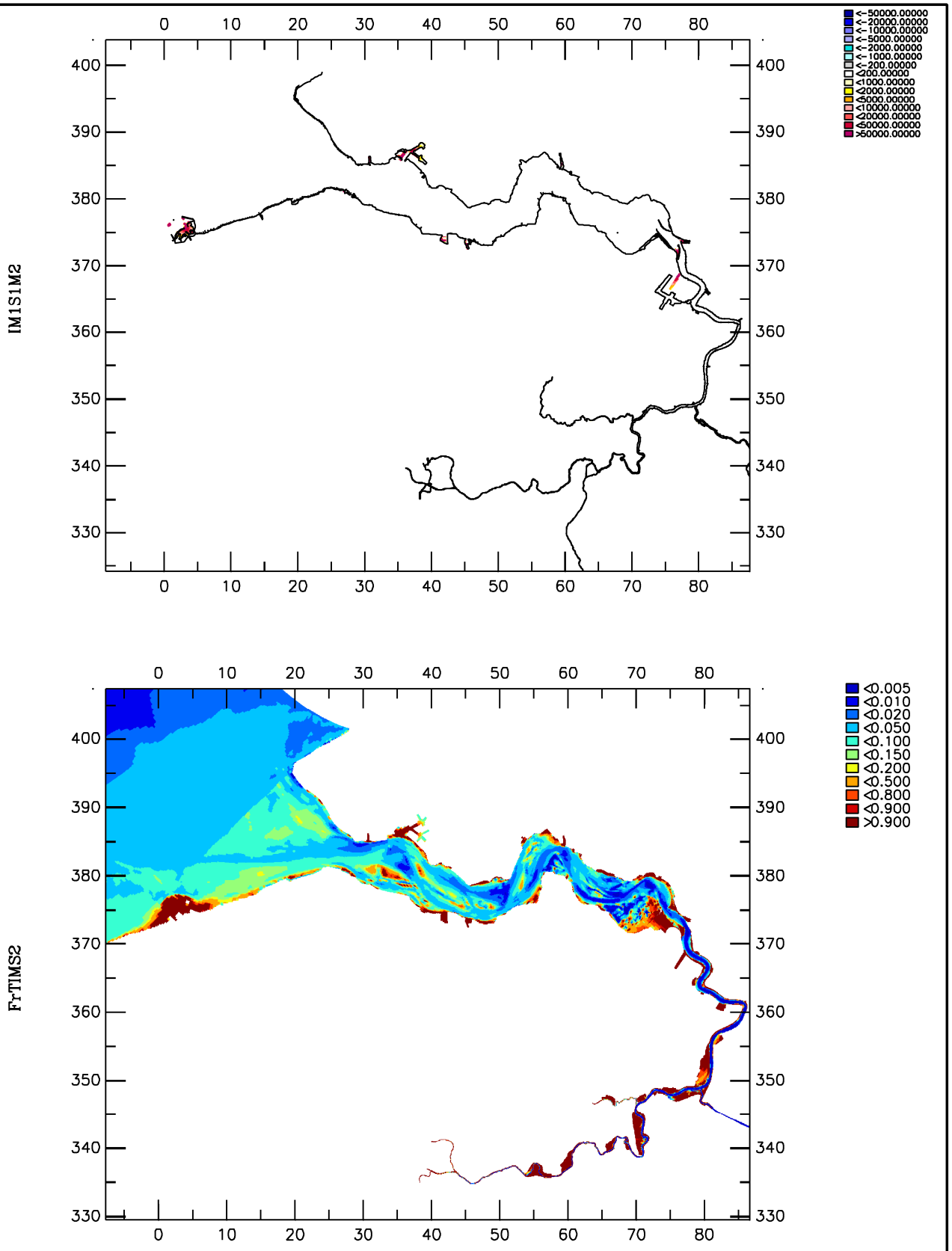

top panel: net siltation over 1 month (g/m2)
bottom panel: mud fraction in bottom

hydro 14dw	w15r

WL | Delft Hydraulics

Fig. S1.2

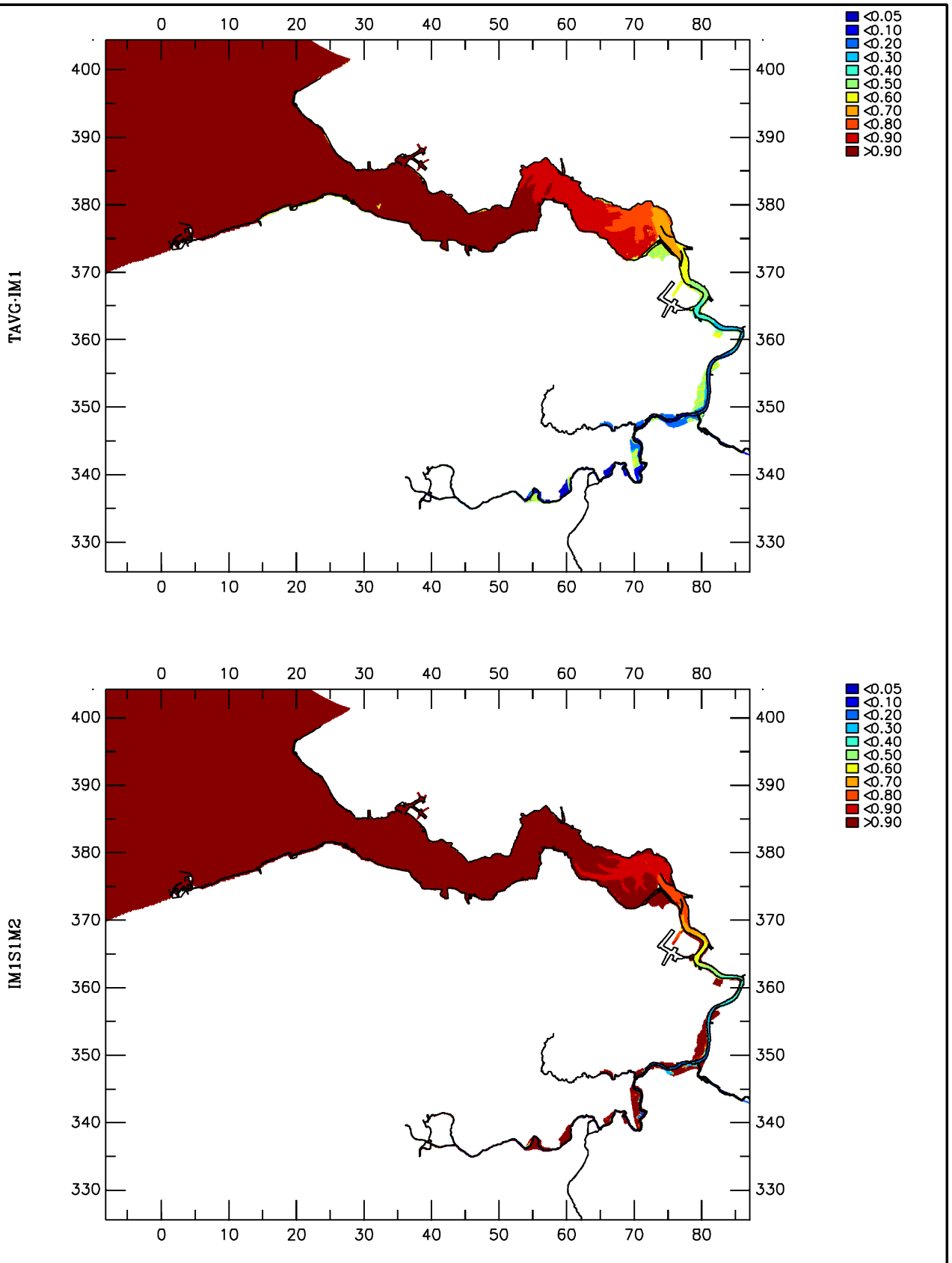

fraction marine mud (–) upper panel: in the water column lower panel: in the bottom	hydro 14dw	w15r
WL | Delft Hydraulics	Z4210	Fig. S1.3

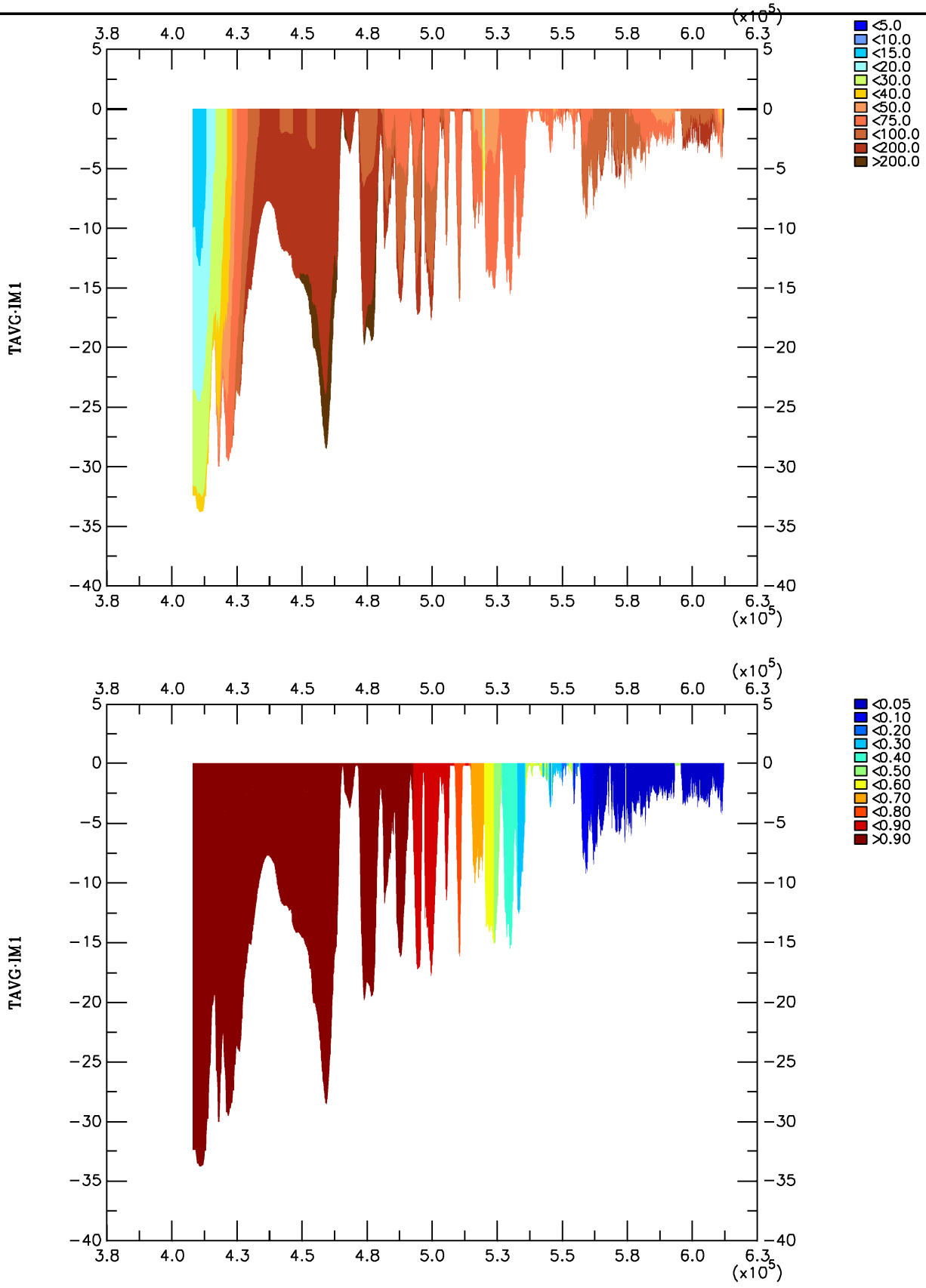

SPM concentration (mg/l) along Scheldt estuary upper panel: fluvial + marine fraction (mg/l) lower panel: marine fraction only (ratio)	hydro 14dw	w15r
WL | Delft Hydraulics		Fig. S1.4

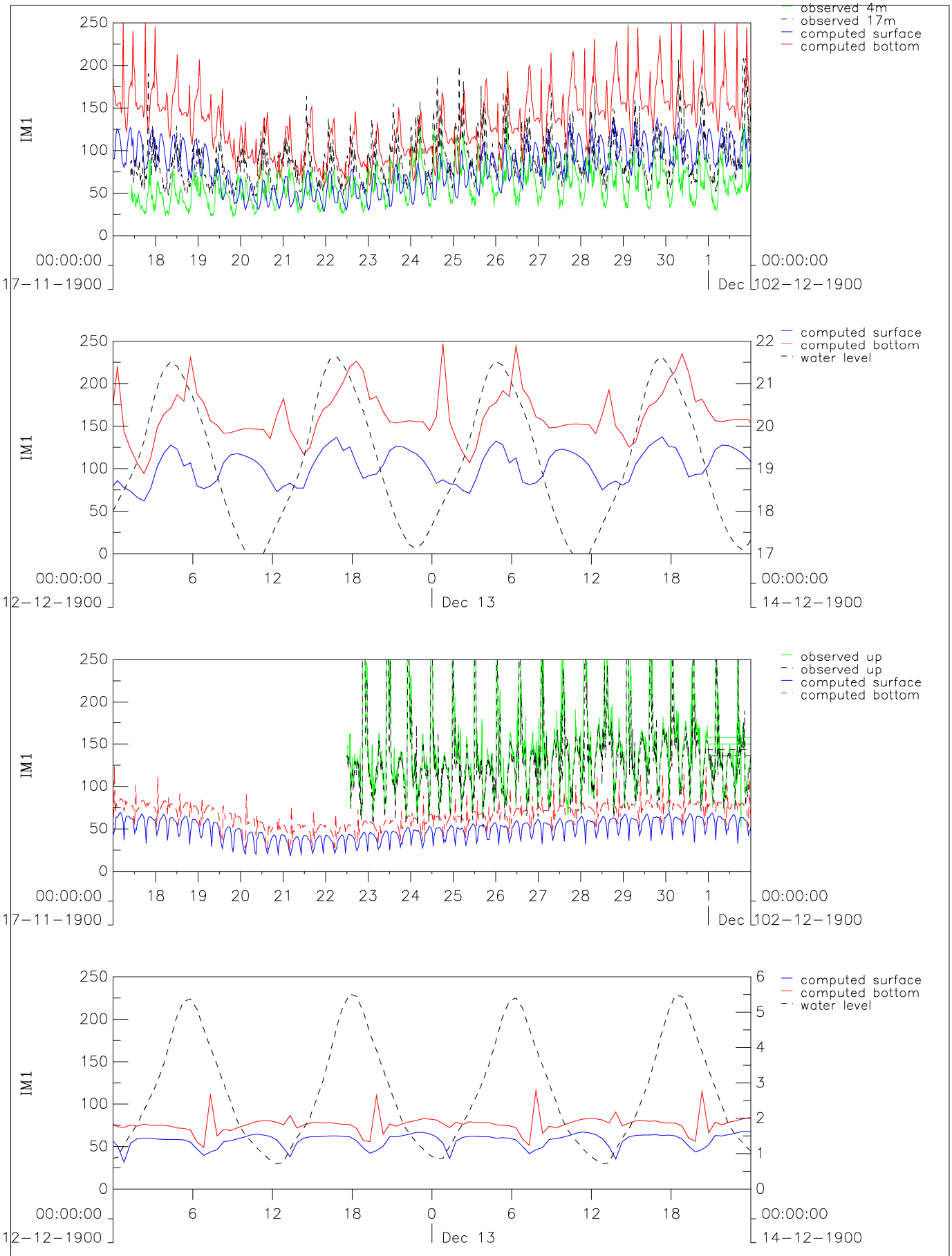

Computed and observed SPM concentration (mg/l)
top panels: Terneuzen DOW jetty neap-spring and daily
bottom panels: Boerenschans neap-spring and daily

hydro 14dw | w15r

WL | Delft Hydraulics

Fig. S1.5

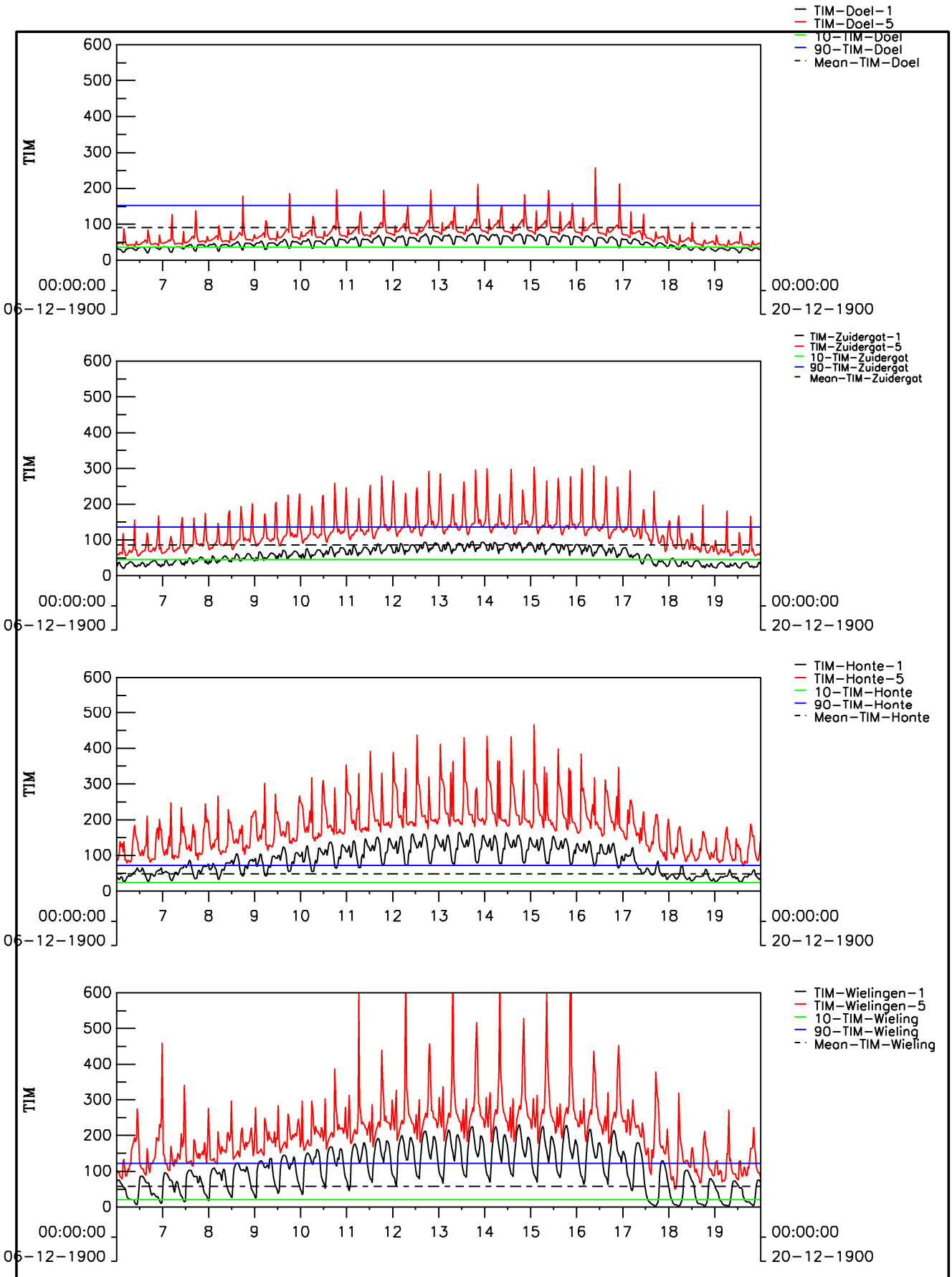

Time series SPM concentration (mg/l)
top panels: Schaar van Doel (top) and Zuidergat neap-spring
bottom panels: Honte and Wielingen (bottom) neap-spring

hydro 14dw | w15r

WL | Delft Hydraulics

Fig. S1.6

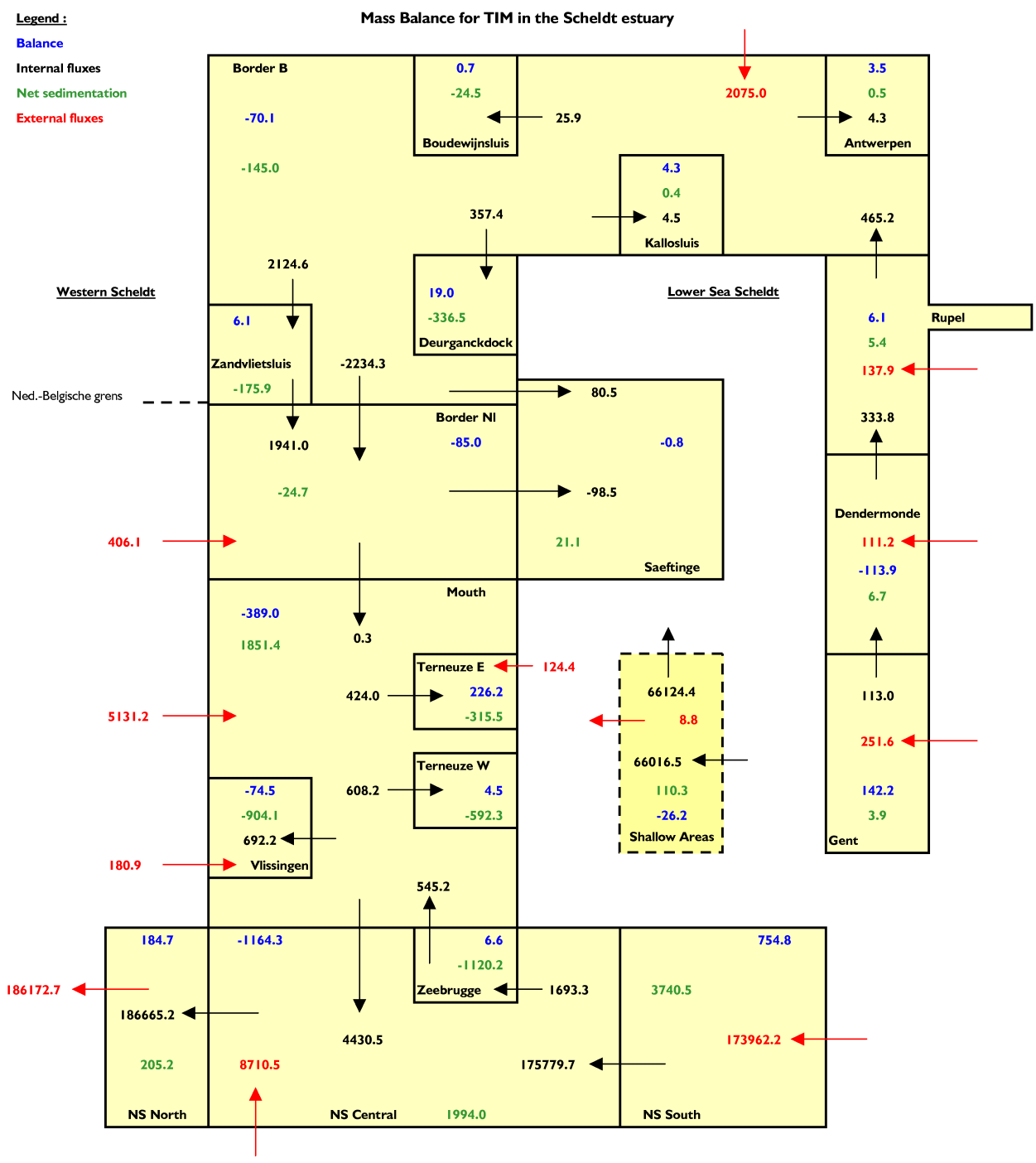

DELWAQ results
Net mud transport, 4th quarter [kT/year]

Z4210

W15Q4

WL | DELFT HYDRAULICS

Fig. S1.7

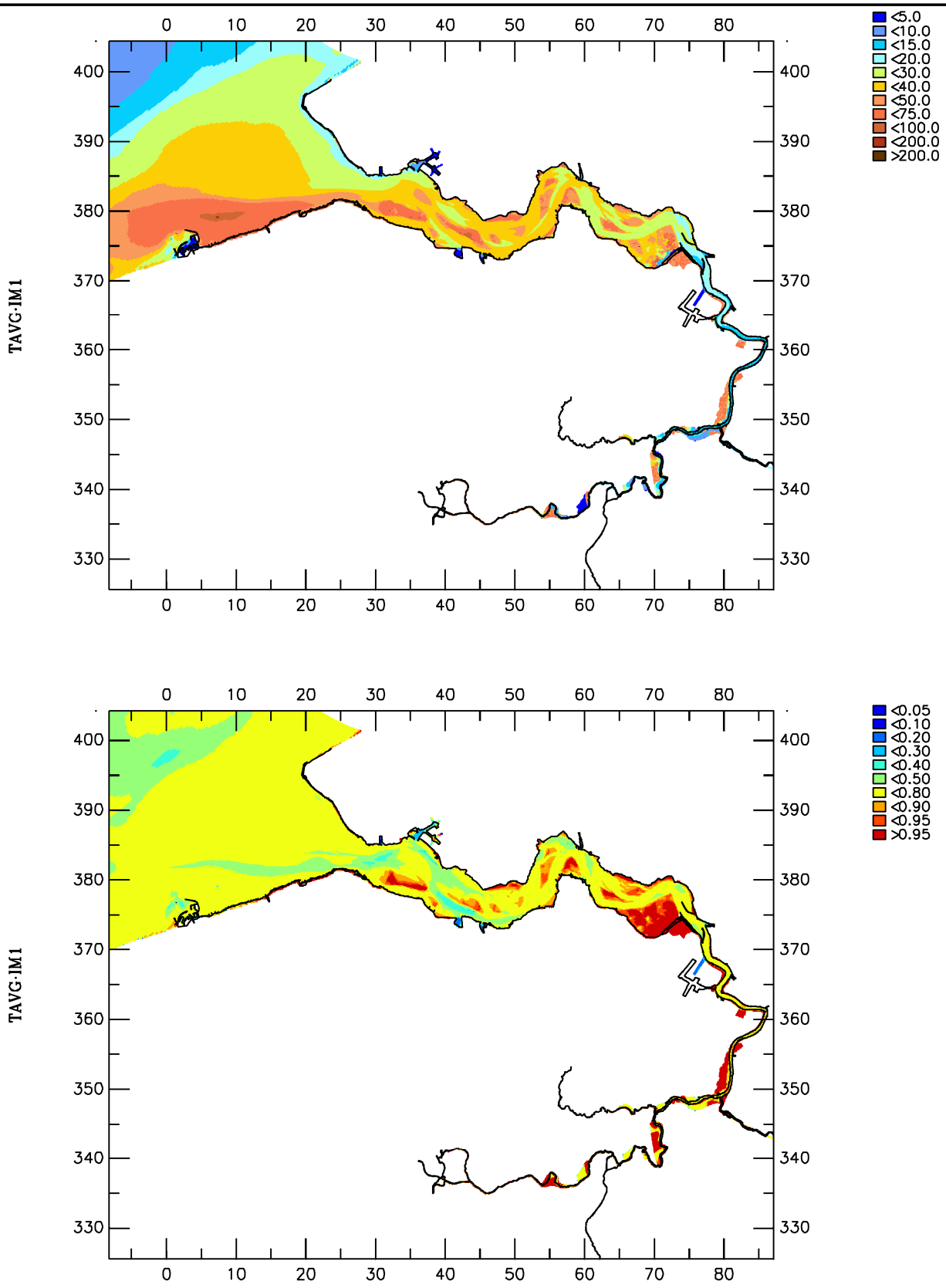

top: SPM concentration in surface layer (mg/l)
bottom: concentration ratio surface/bottom (−)

	hydro 14ds	z15r
WL | Delft Hydraulics	Z4210	Fig. S2.1

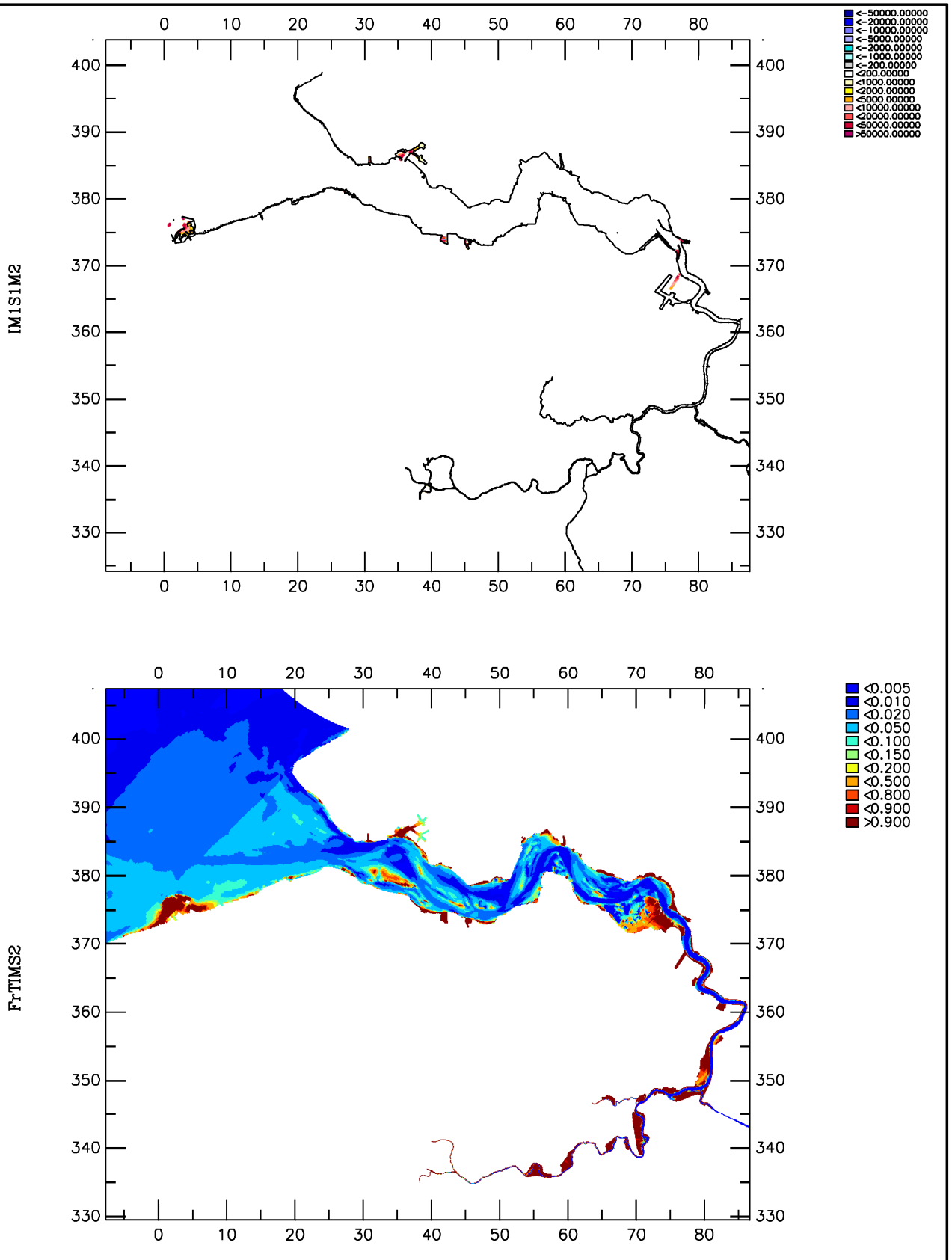

top panel: net siltation over 1 month (g/m2)
bottom panel: mud fraction in bottom

hydro 14ds | z15r

WL | Delft Hydraulics

Fig. S2.2

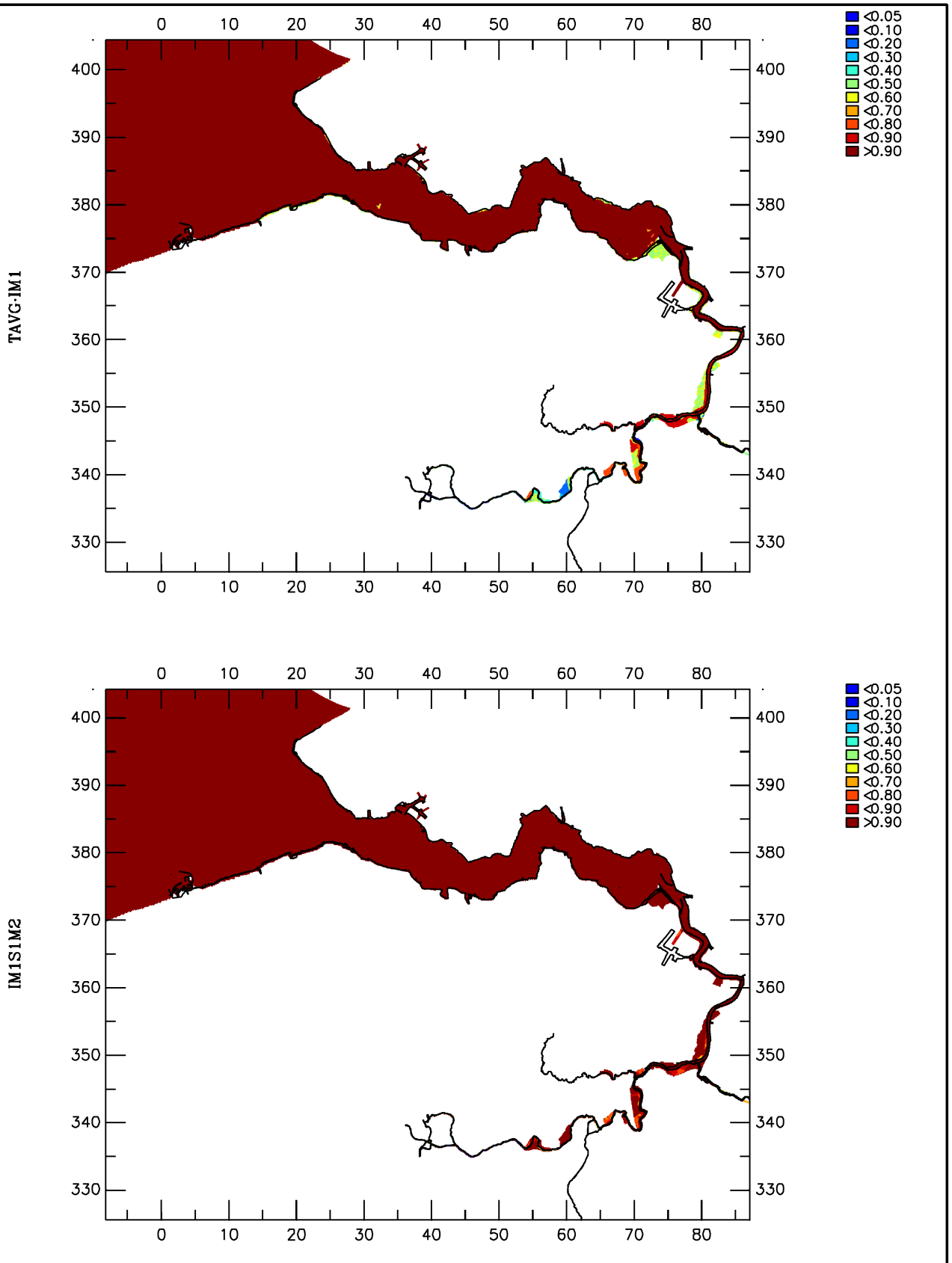

fraction marine mud (–)
upper panel: in the water column
lower panel: in the bottom

hydro 14ds | z15r

WL | Delft Hydraulics | Z4210 | Fig. S2.3

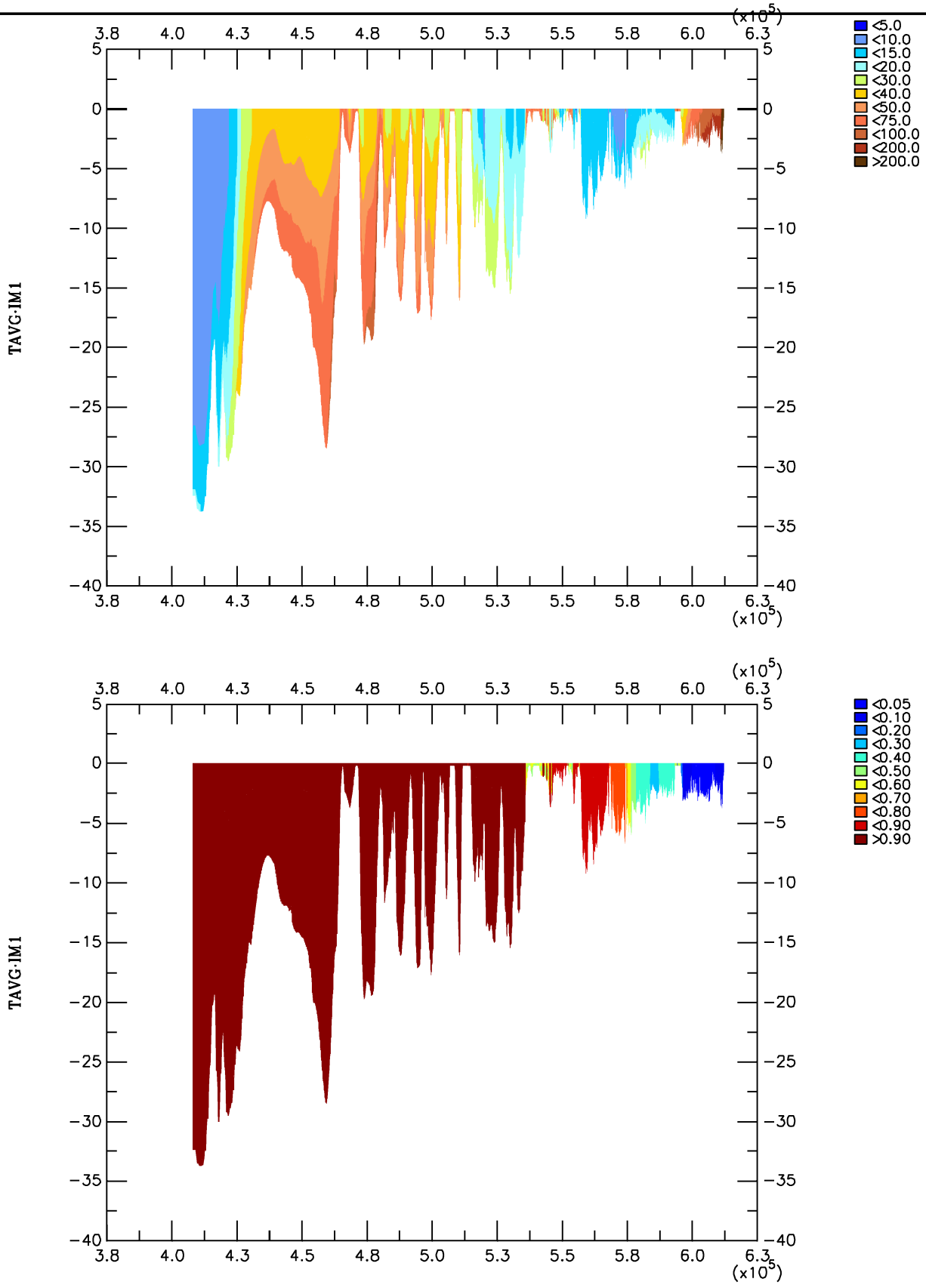

SPM concentration (mg/l) along Scheldt estuary upper panel: fluvial + marine fraction (mg/l) lower panel: marine fraction only (ratio)	hydro 14ds	z15r
WL | Delft Hydraulics		Fig. S2.4

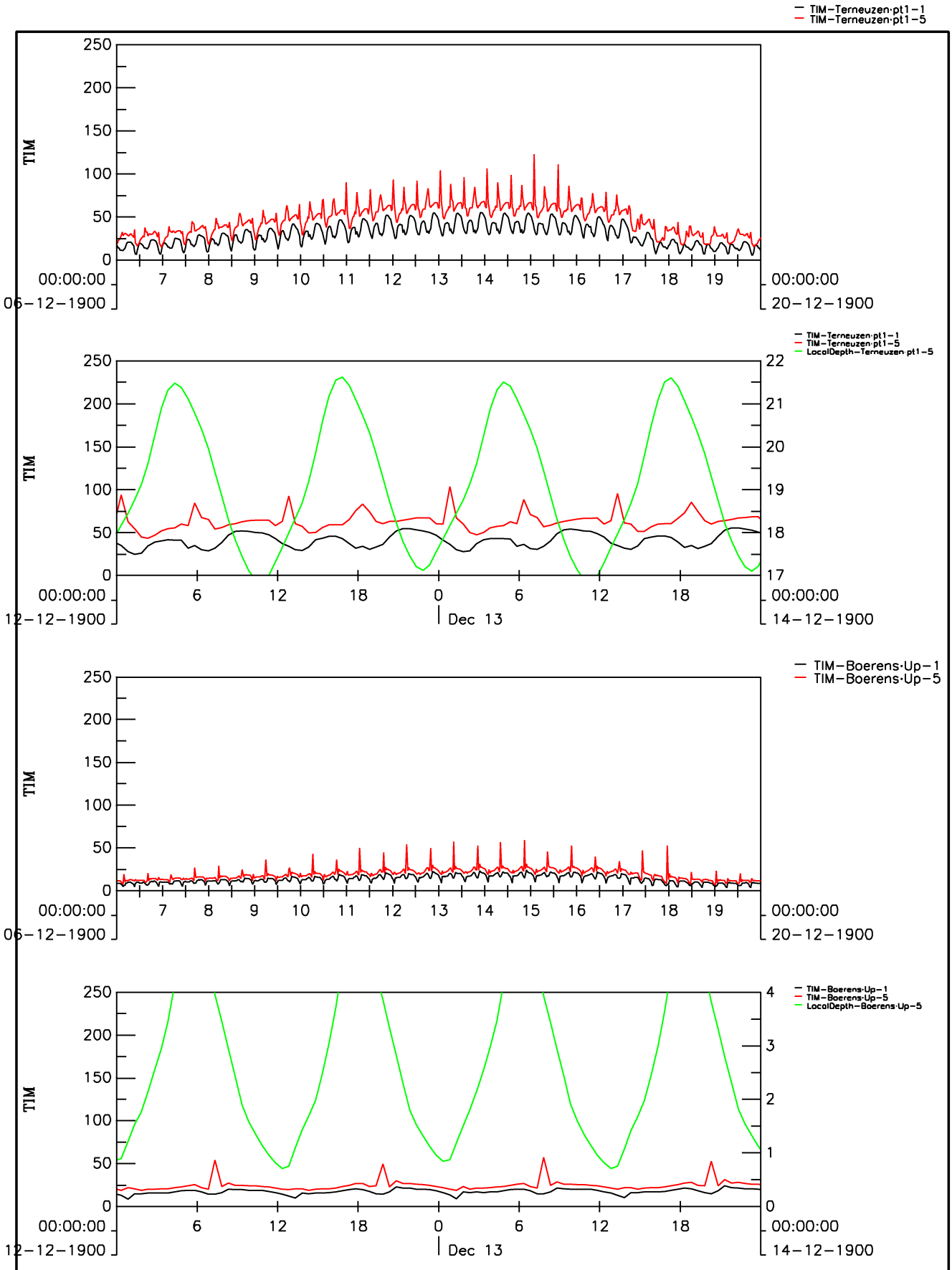

Time series SPM concentration (mg/l) top panels: Terneuzen DOW jetty neap-spring and daily bottom panels: Boerenschans neap-spring and daily	hydro 14ds	z15r
WL | Delft Hydraulics		Fig. S2.5

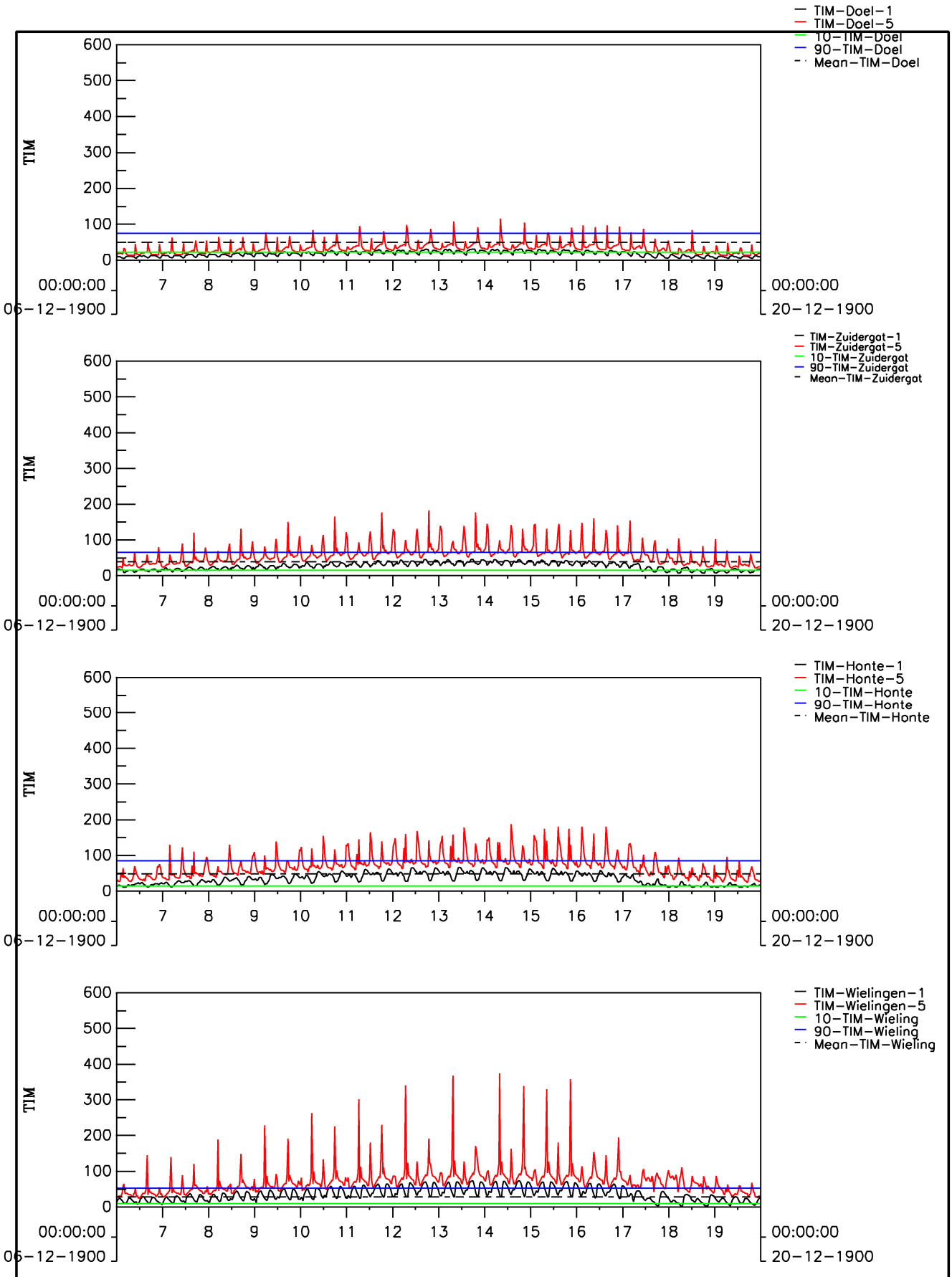

Time series SPM concentration (mg/l)
top panels: Schaar van Doel (top) and Zuidergat neap-spring
bottom panels: Honte and Wielingen (bottom) neap-spring

hydro 14ds | z15r

WL | Delft Hydraulics

Fig. S2.6

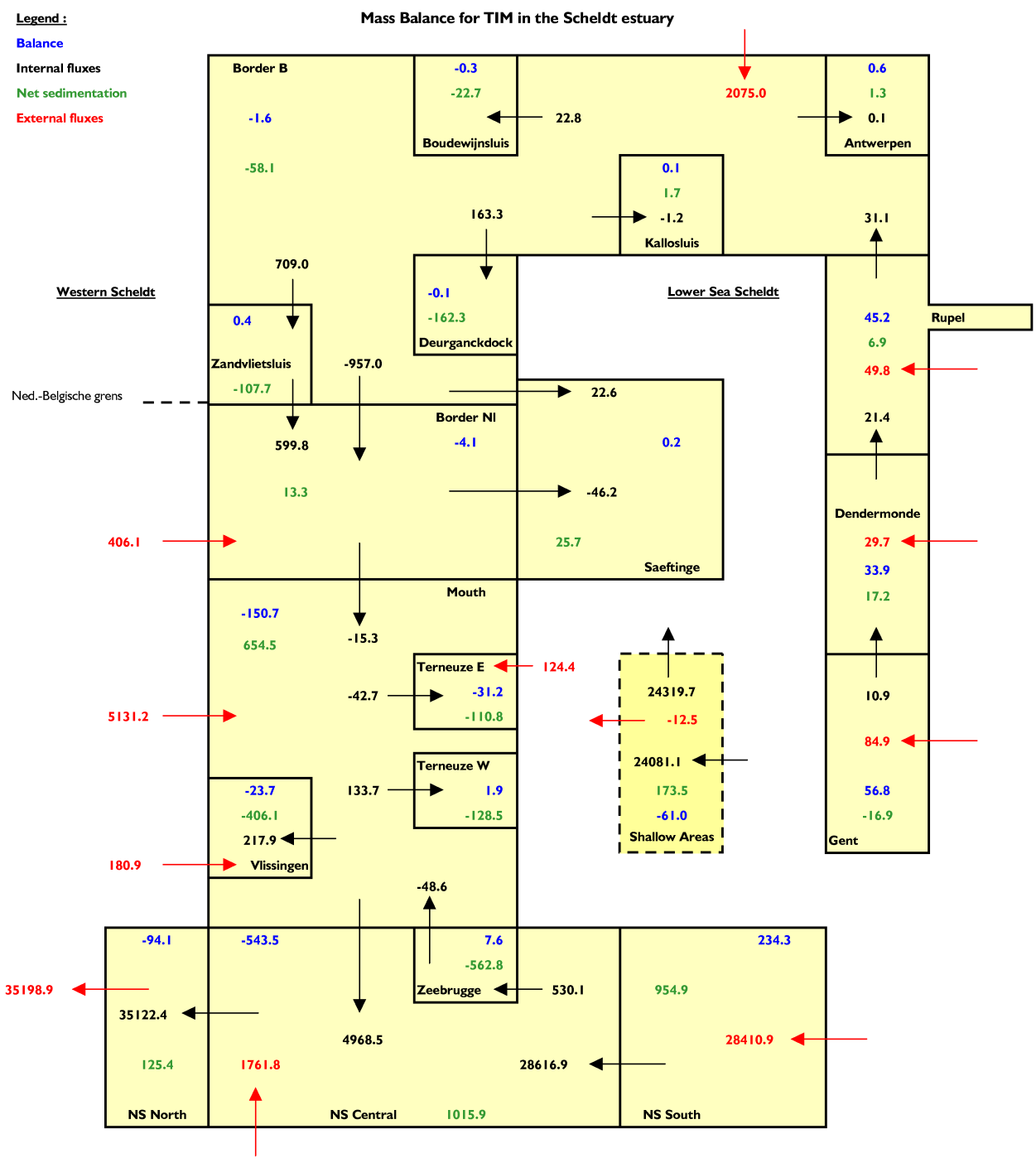

DELWAQ results
Net mud transport, 4th quarter [kT/year]

Z4210

Z15Q4

WL | DELFT HYDRAULICS

Fig. S2.7

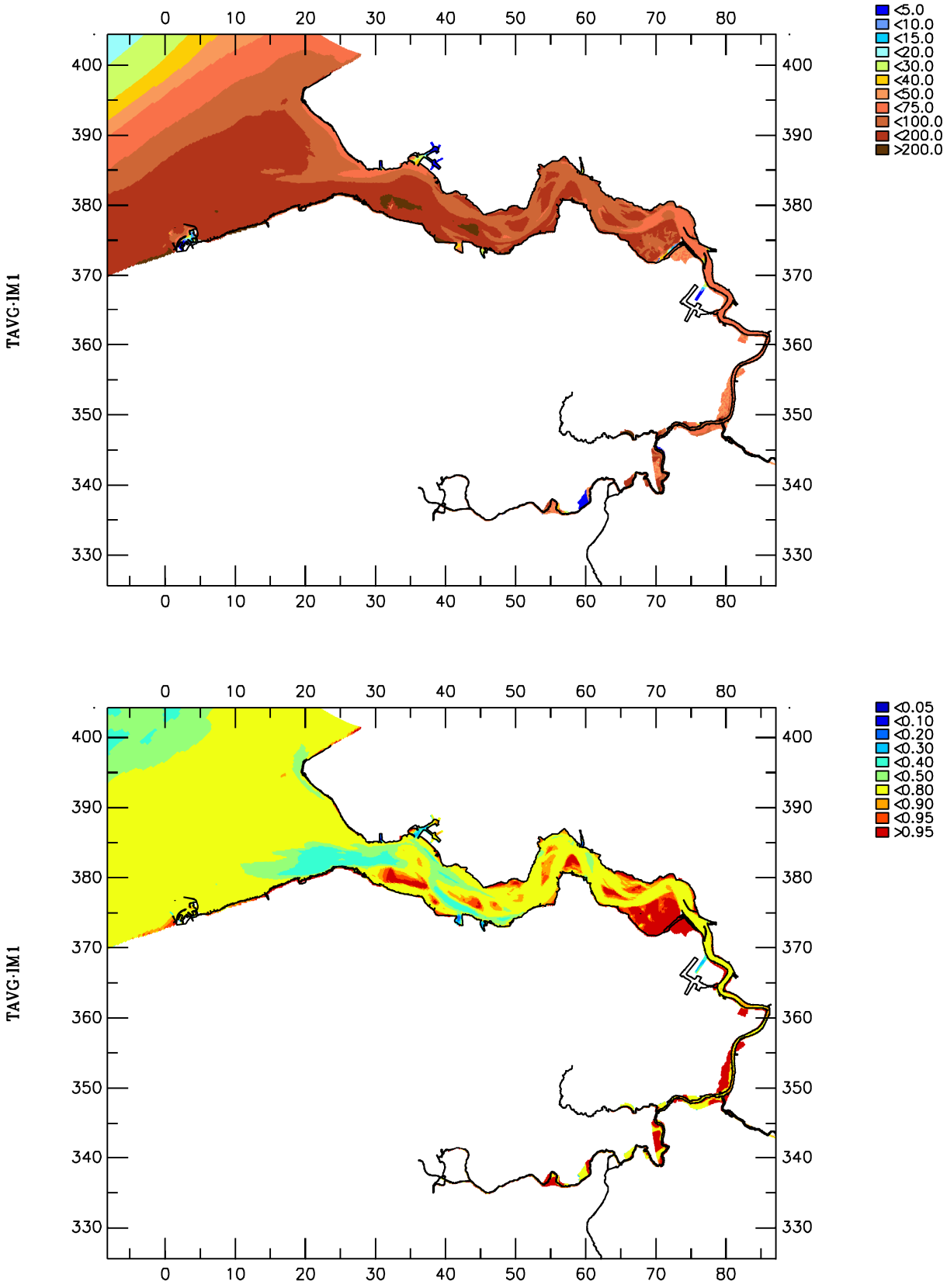

top: SPM concentration in surface layer (mg/l)
bottom: concentration ratio surface/bottom (–)

hydro 14dw	w17r
WL | Delft Hydraulics	Z4210 Fig. S3.1

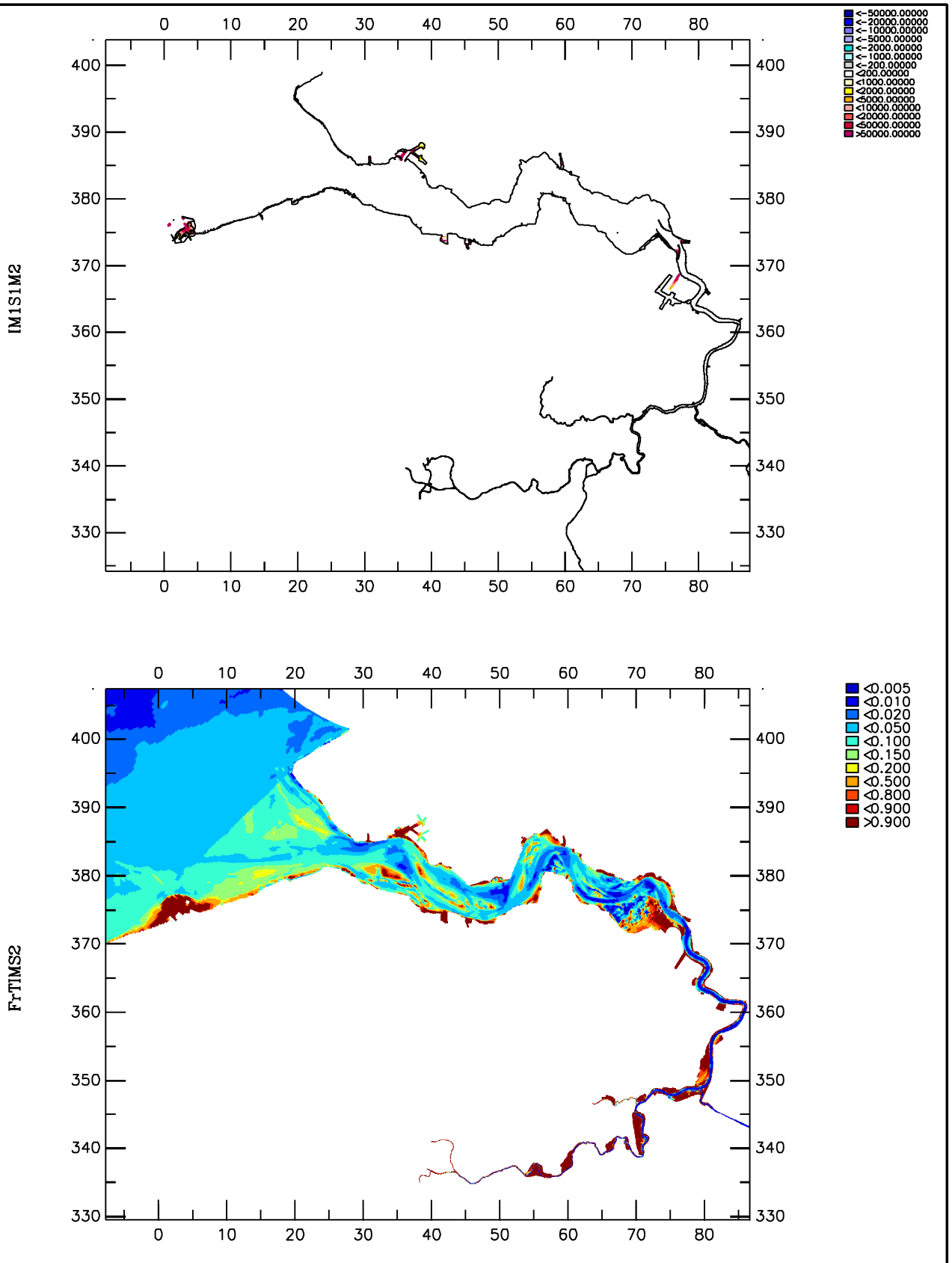

top panel: net siltation over 1 month (g/m2)
bottom panel: mud fraction in bottom

hydro 14dw | w17r

WL | Delft Hydraulics

Fig. S3.2

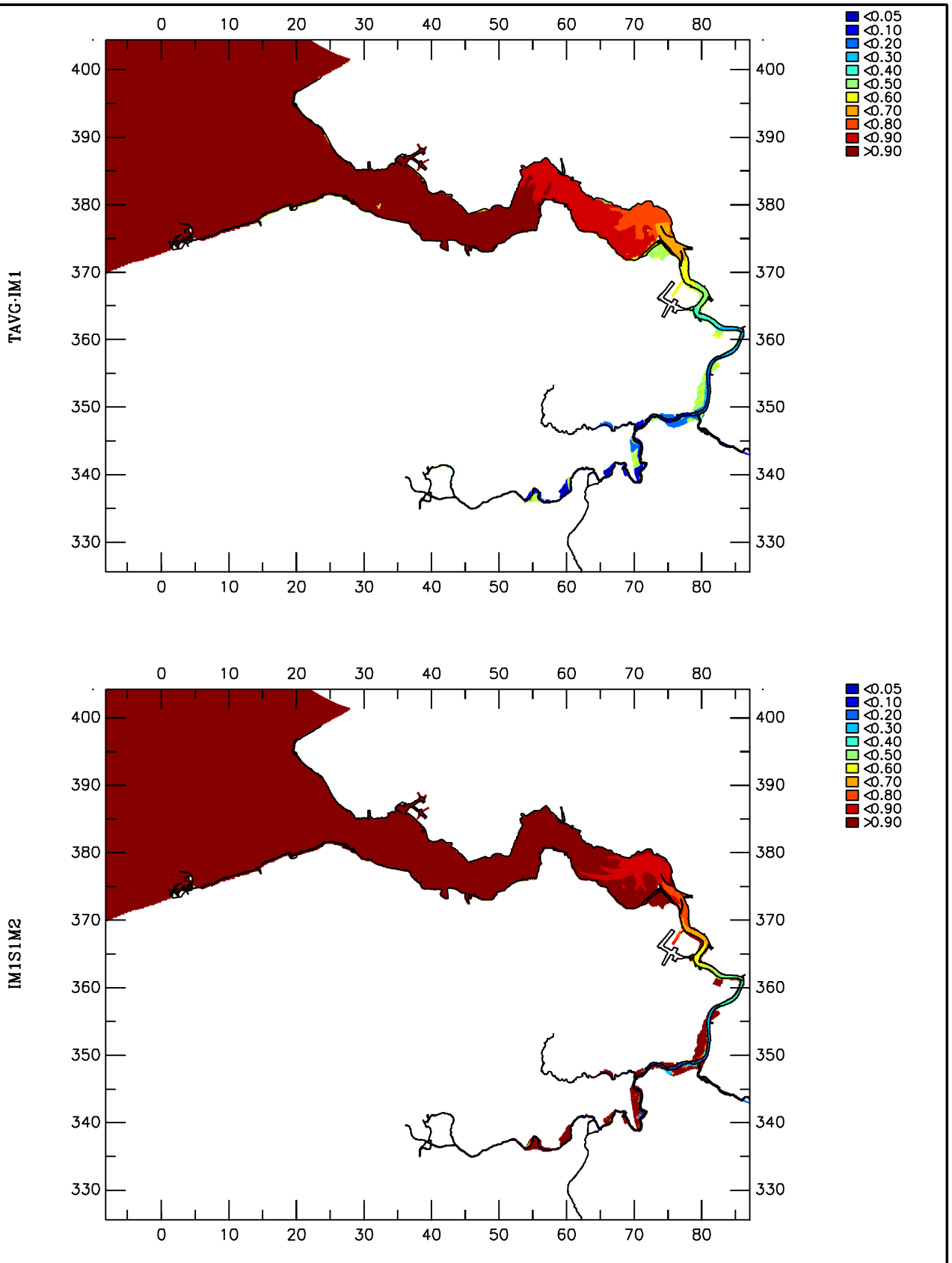

fraction marine mud (–) upper panel: in the water column lower panel: in the bottom	hydro 14dw	w17r
WL | Delft Hydraulics	Z4210	Fig. S3.3

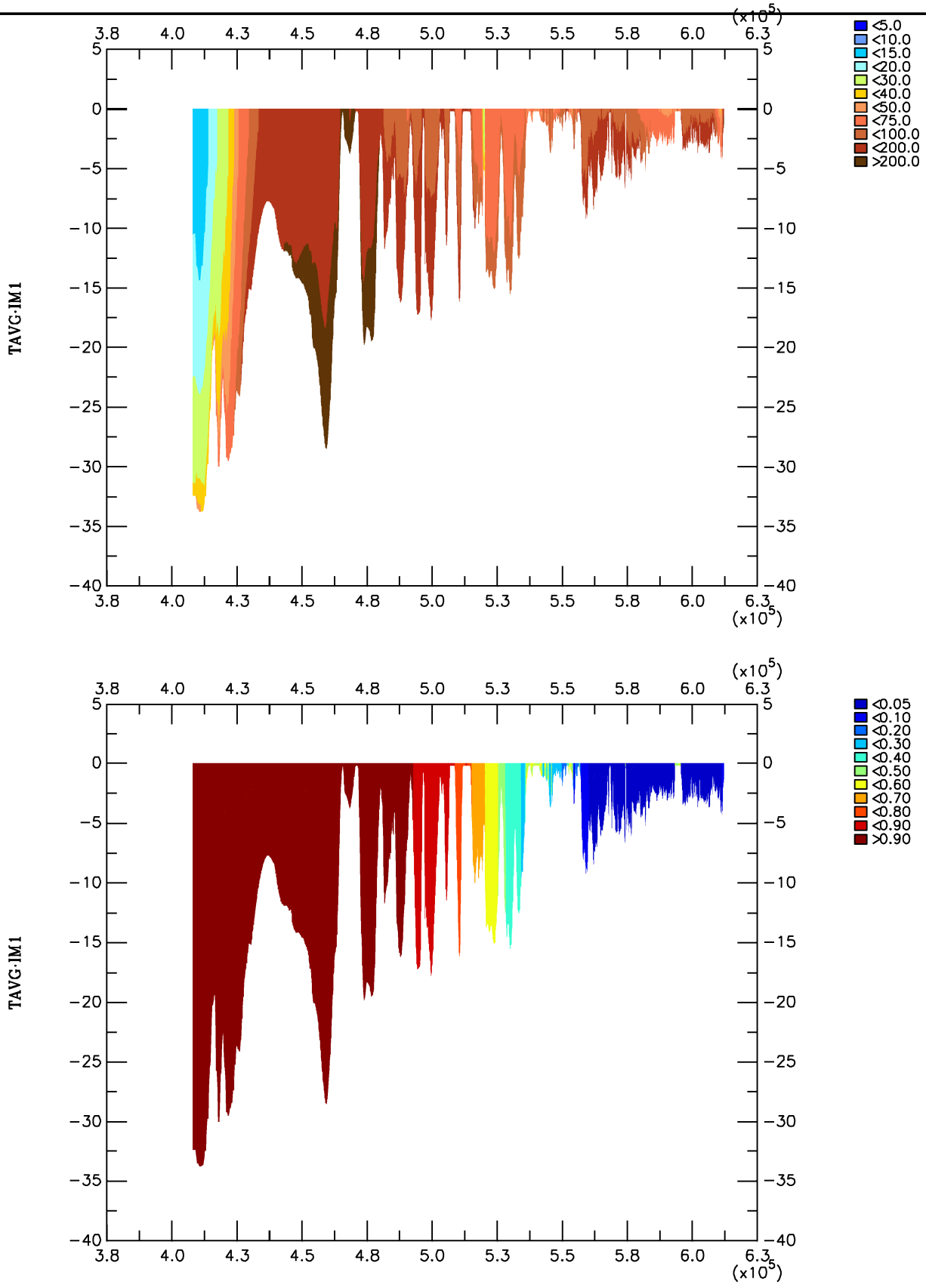

SPM concentration (mg/l) along Scheldt estuary upper panel: fluvial + marine fraction (mg/l) lower panel: marine fraction only (ratio)	hydro 14dw	w17r
WL | Delft Hydraulics		Fig. S3.4

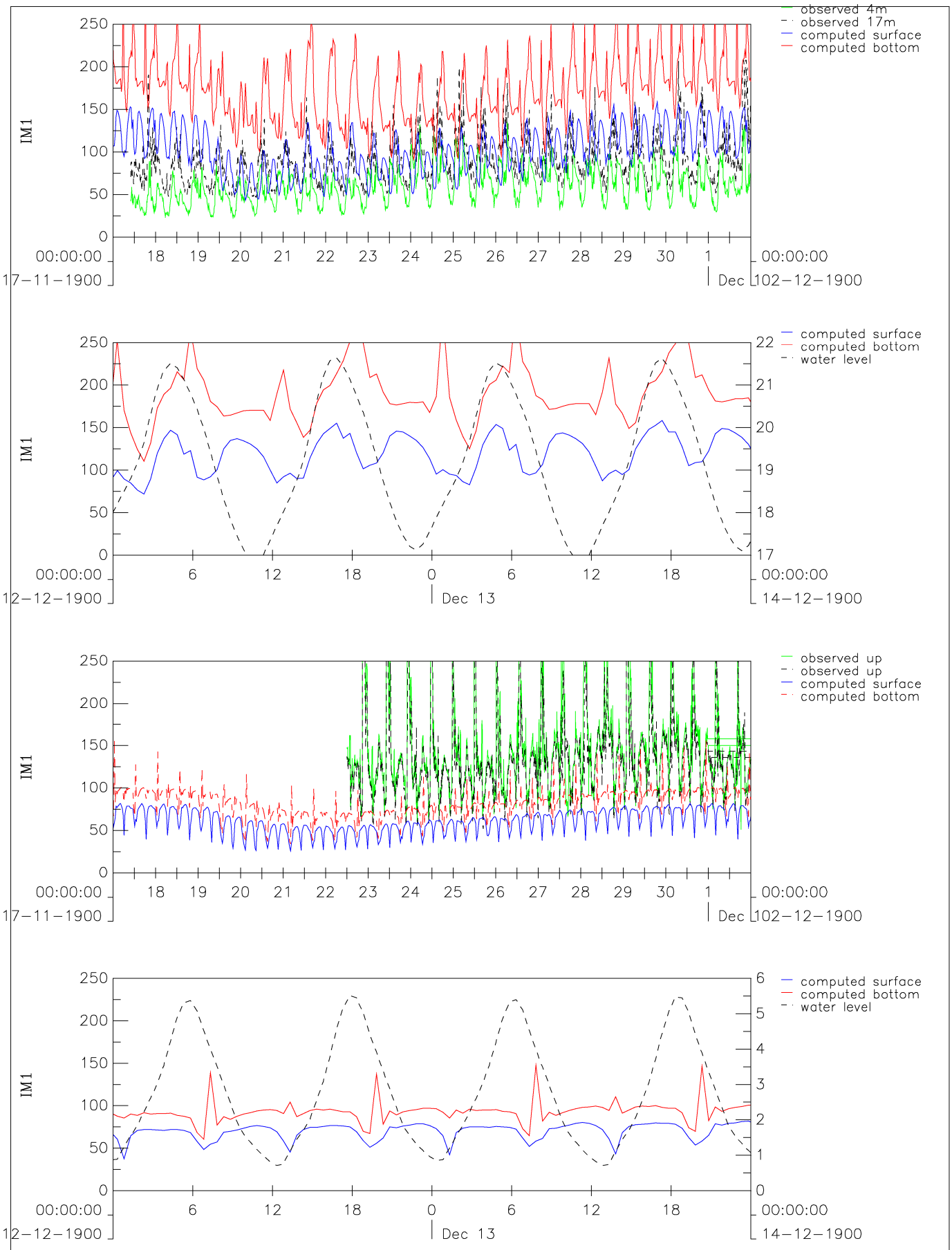

Computed and observed SPM concentration (mg/l) top panels: Terneuzen DOW jetty neap-spring and daily bottom panels: Boerenschans neap-spring and daily	hydro 14dw	w17r
WL | Delft Hydraulics		Fig. S3.5

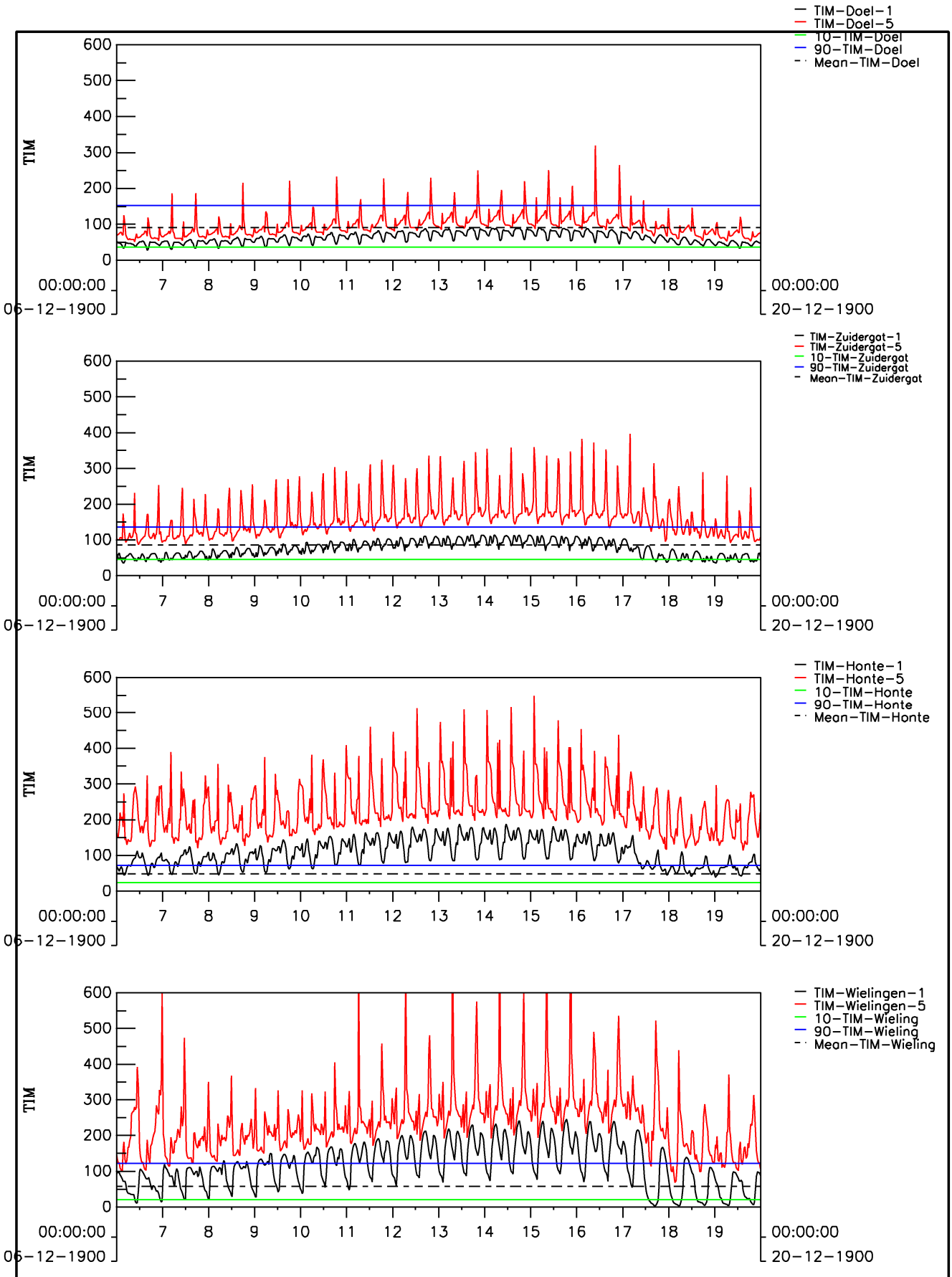

Time series SPM concentration (mg/l)
top panels: Schaar van Doel (top) and Zuidergat neap-spring
bottom panels: Honte and Wielingen (bottom) neap-spring

hydro 14dw | w17r

WL | Delft Hydraulics

Fig. S3.6

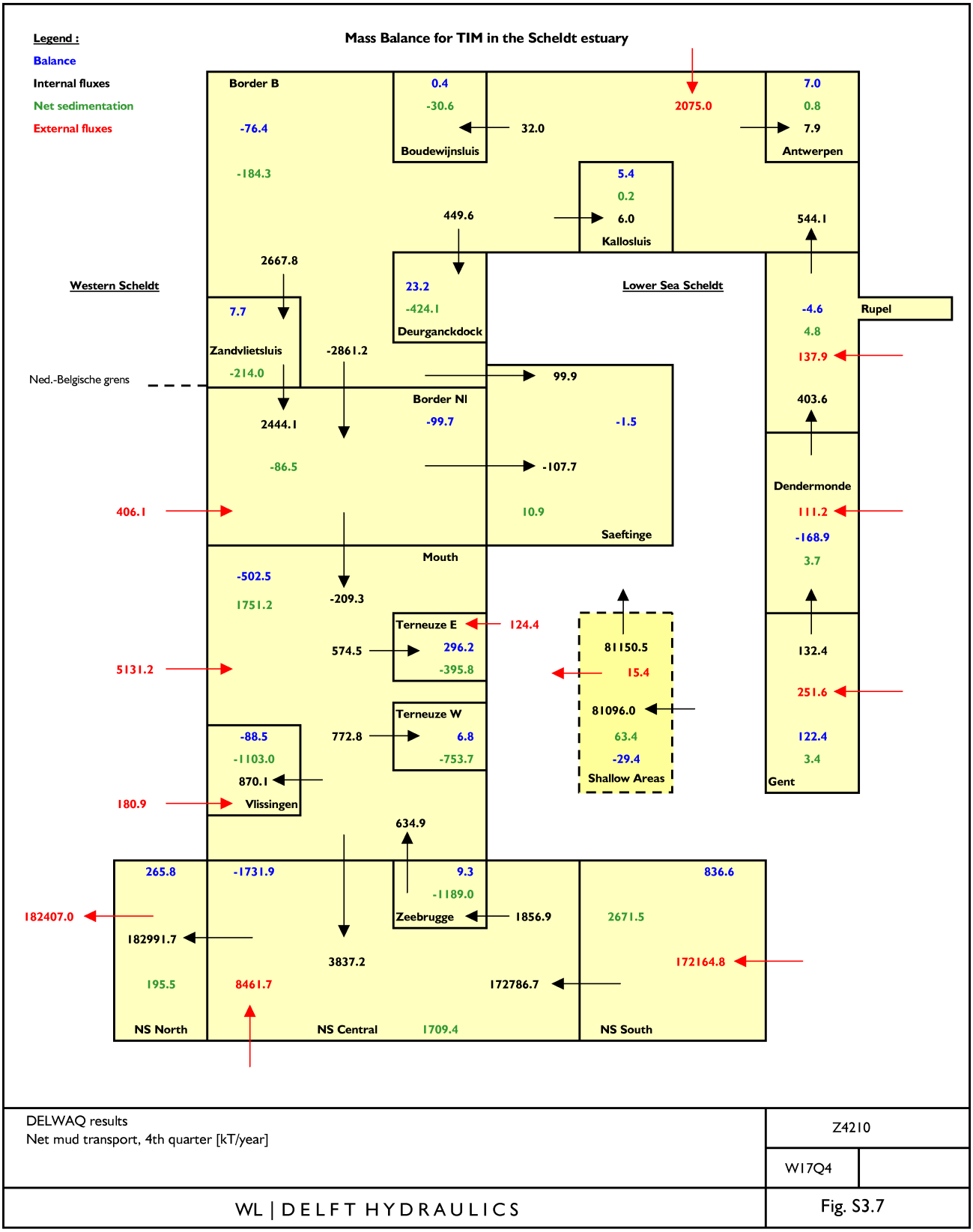

DELWAQ results
Net mud transport, 4th quarter [kT/year]

Z4210

W17Q4

WL | DELFT HYDRAULICS

Fig. S3.7

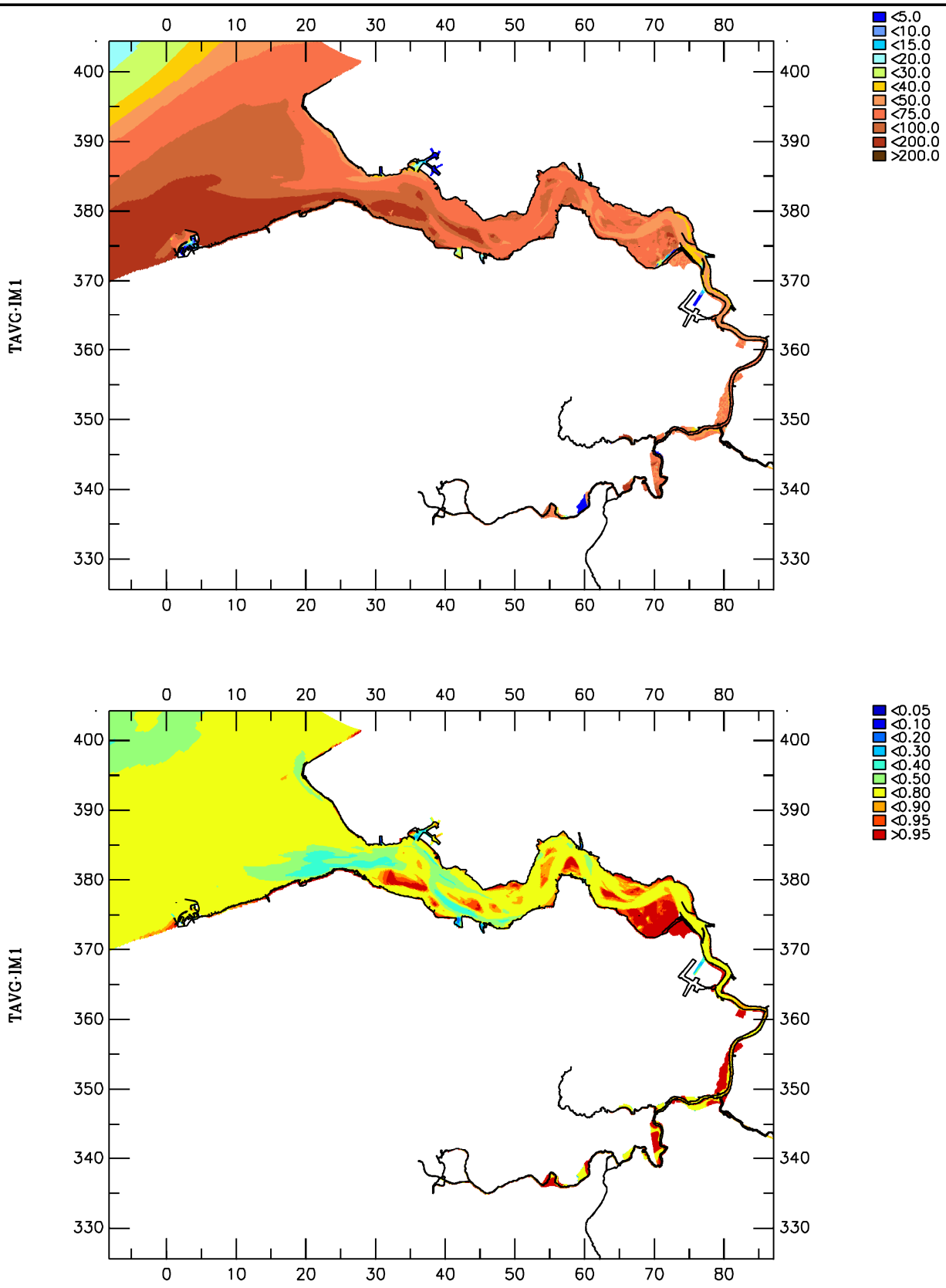

top: SPM concentration in surface layer (mg/l) bottom: concentration ratio surface/bottom (–) winter conditions	hydro 14dw	ws15r
WL | Delft Hydraulics	Z4210	Fig. S4.1a

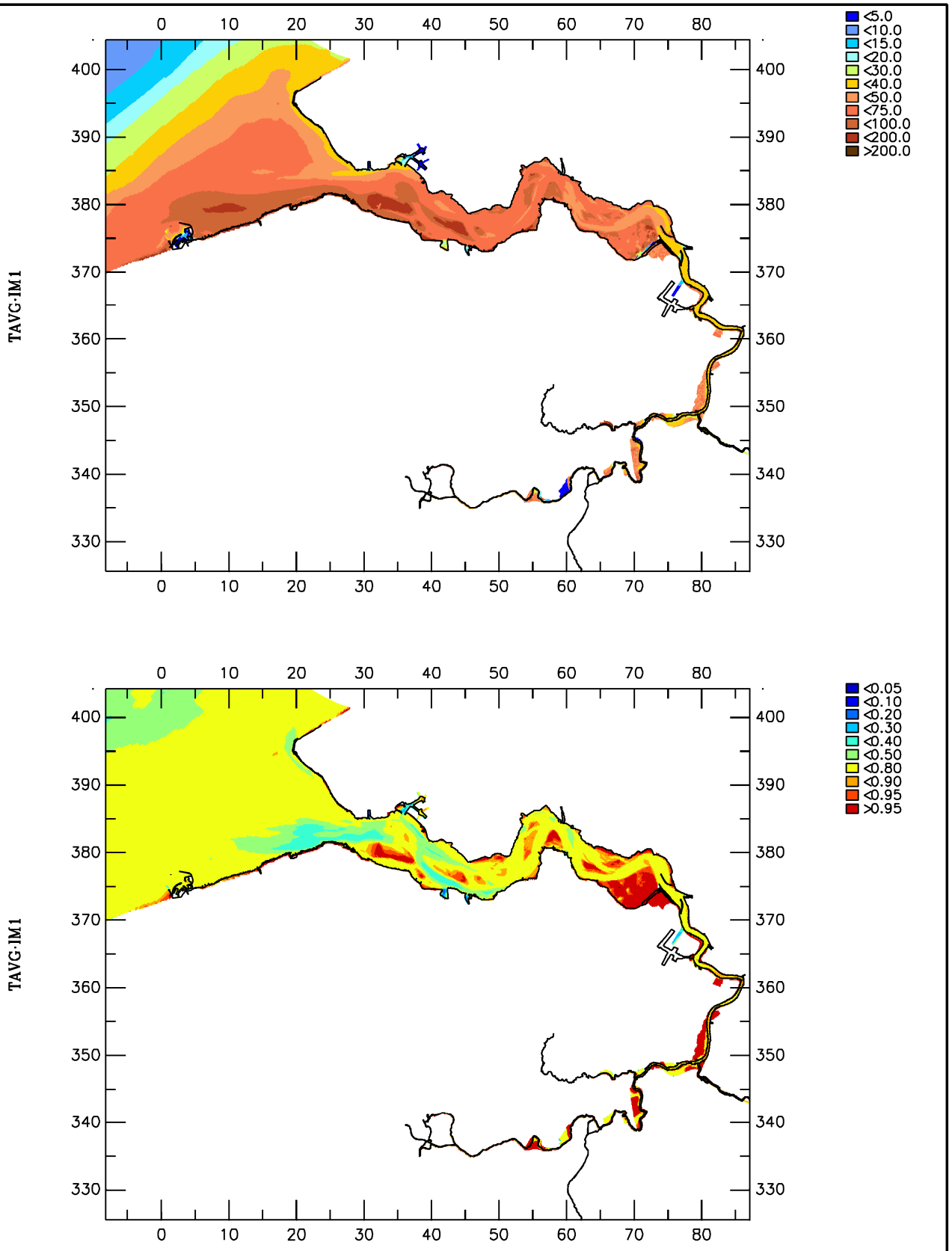

top: SPM concentration in surface layer (mg/l) bottom: concentration ratio surface/bottom (–) summer conditions	hydro 14dw	ws15r
WL | Delft Hydraulics	Z4210	Fig. S4.1b

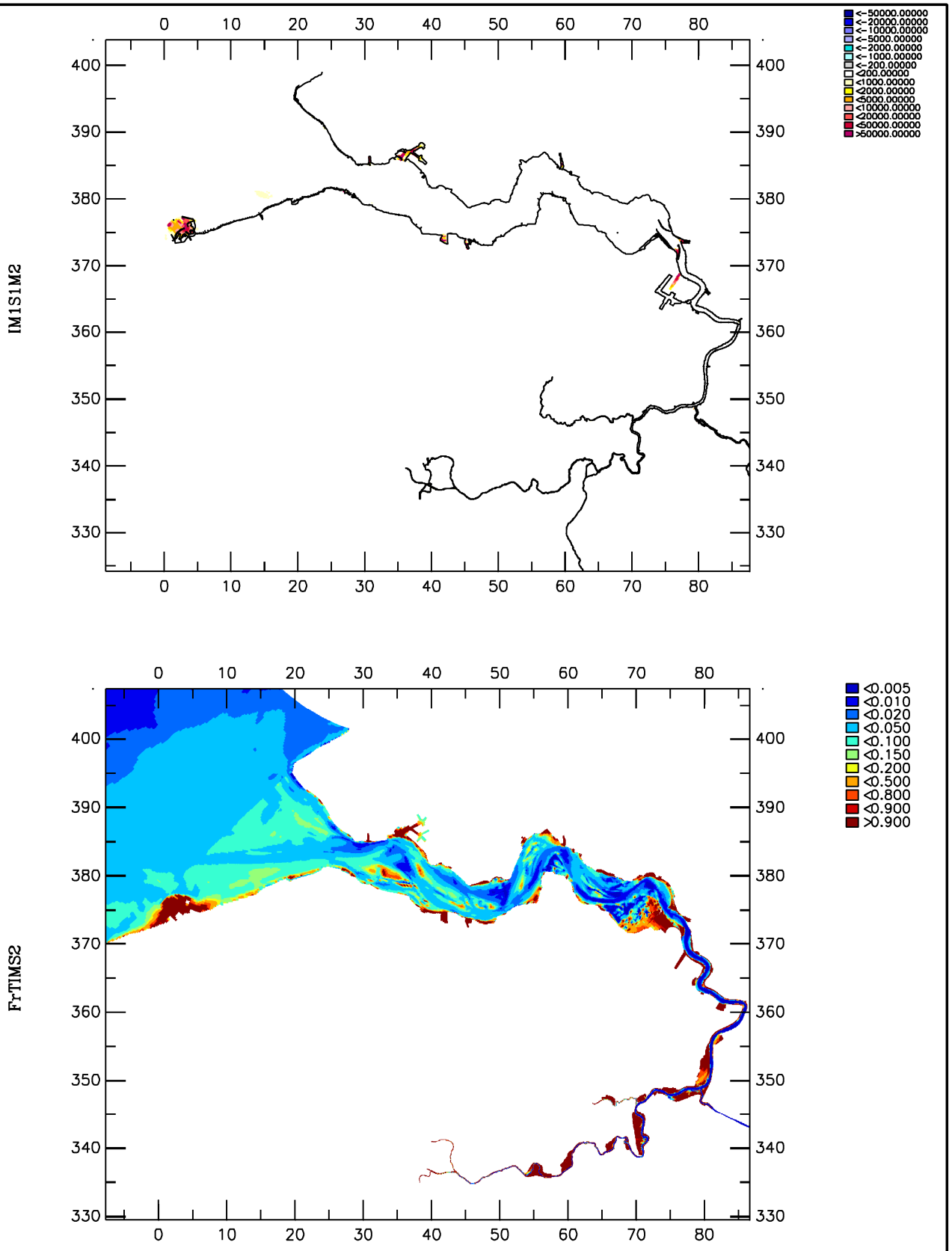

top panel: net siltation over 1 month (g/m2)
bottom panel: mud fraction in bottom
winter conditions

hydro 14dw | ws15r

WL | Delft Hydraulics

Fig. S4.2a

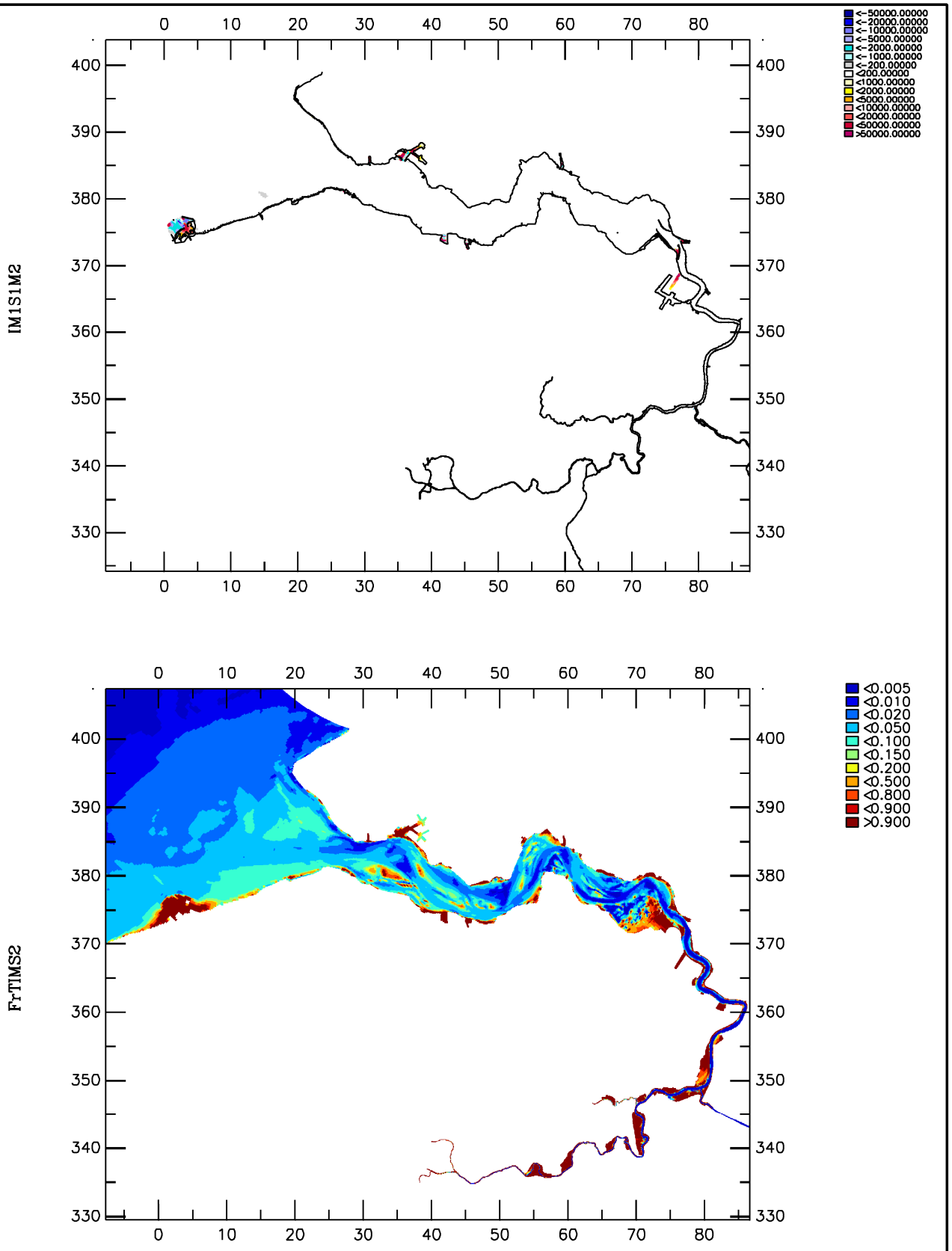

top panel: net siltation over 1 month (g/m2)
bottom panel: mud fraction in bottom
summer conditions

hydro 14dw | ws15r

WL | Delft Hydraulics

Fig. S4.2b

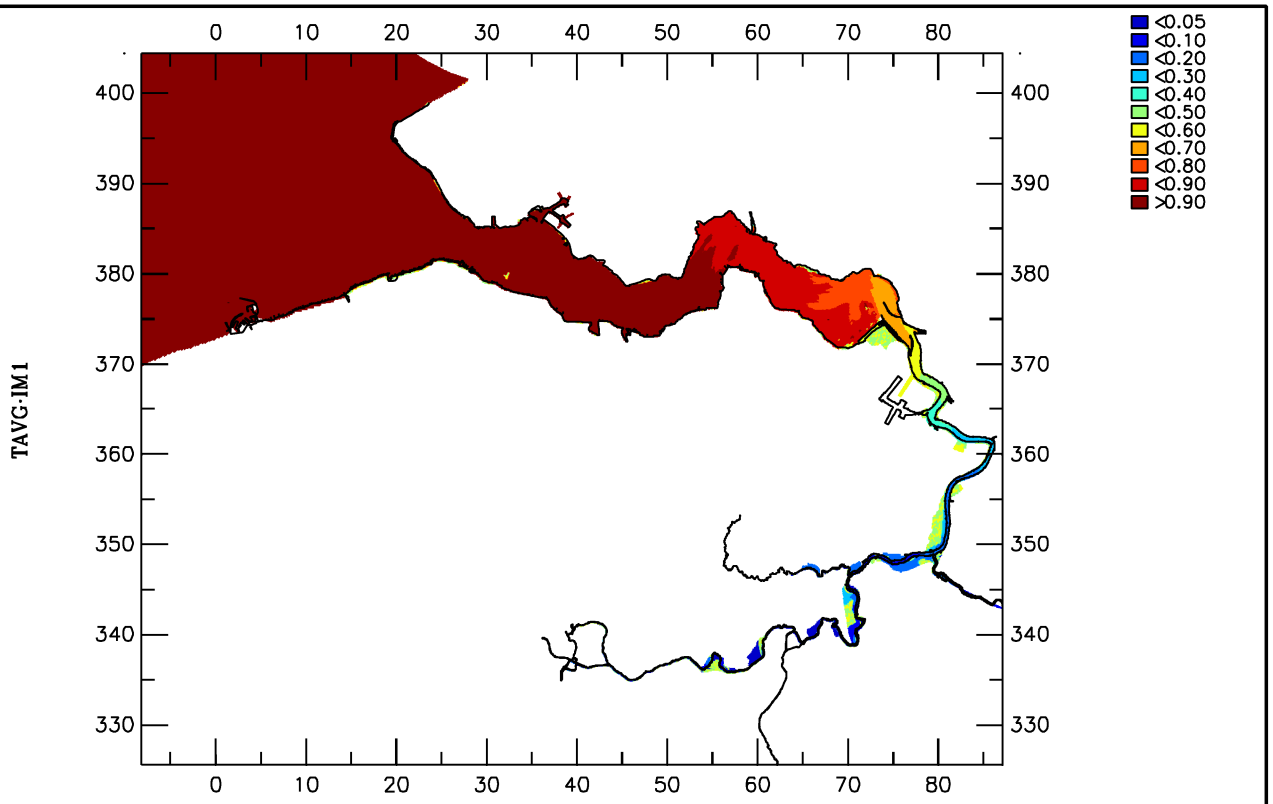

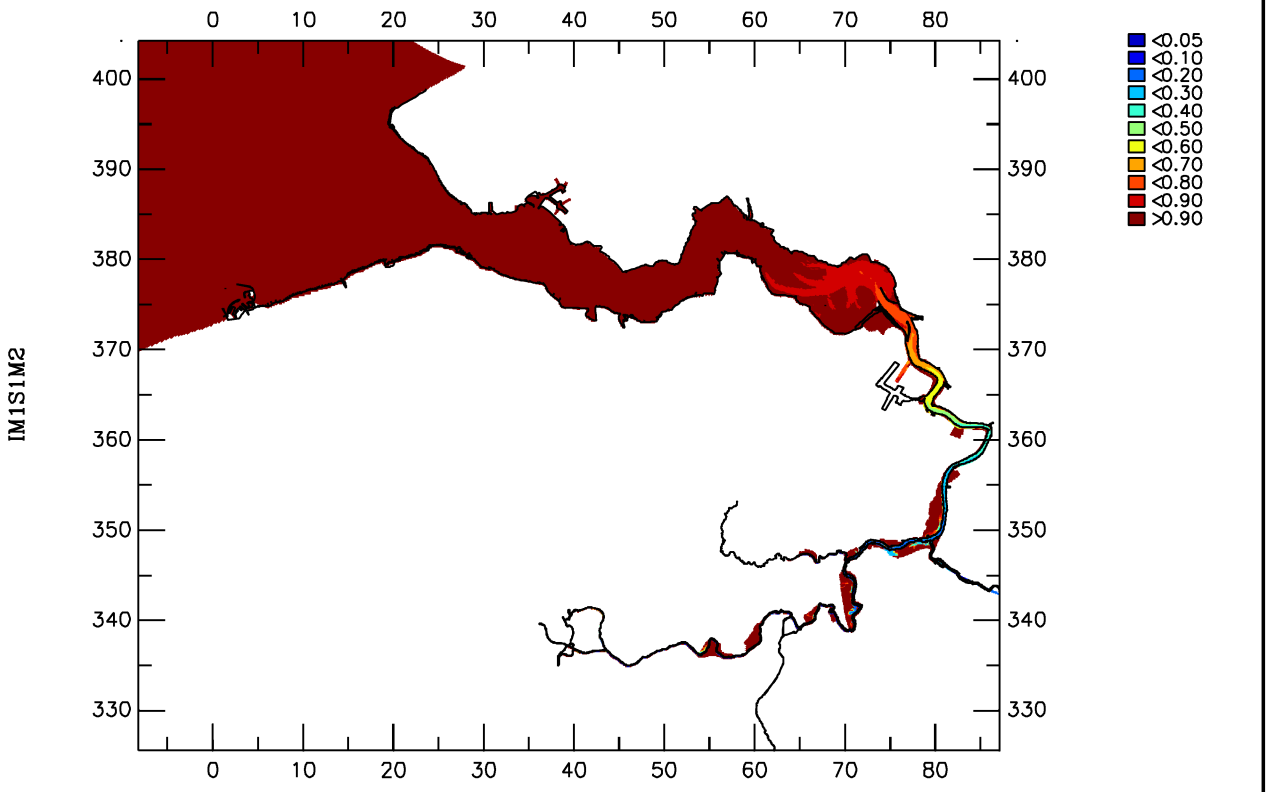

fraction marine mud (–) winter conditions
upper panel: in the water column
lower panel: in the bottom

hydro 14dw | ws15r

WL | Delft Hydraulics | Z4210 | Fig. S4.3a

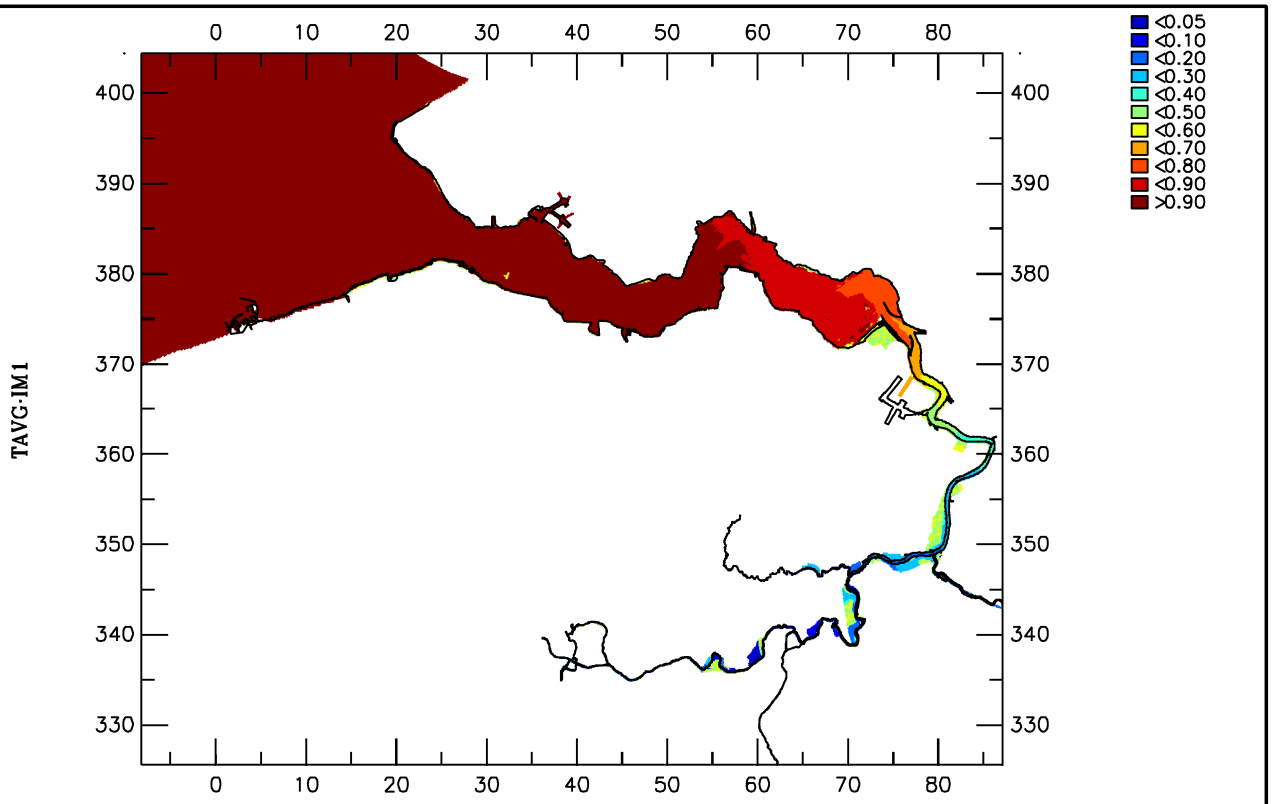

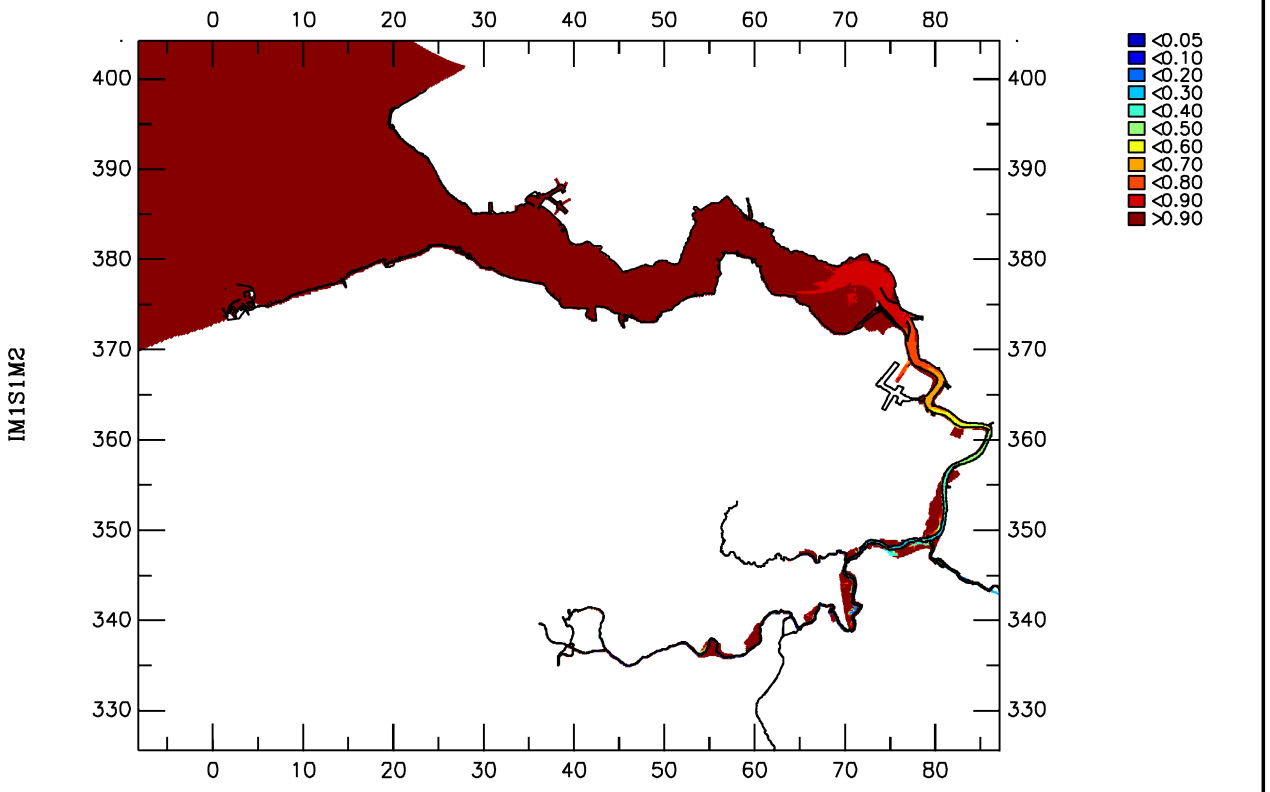

fraction marine mud (–) summer conditions
upper panel: in the water column
lower panel: in the bottom

hydro 14dw	ws15r
WL | Delft Hydraulics	Z4210
	Fig. S4.3b

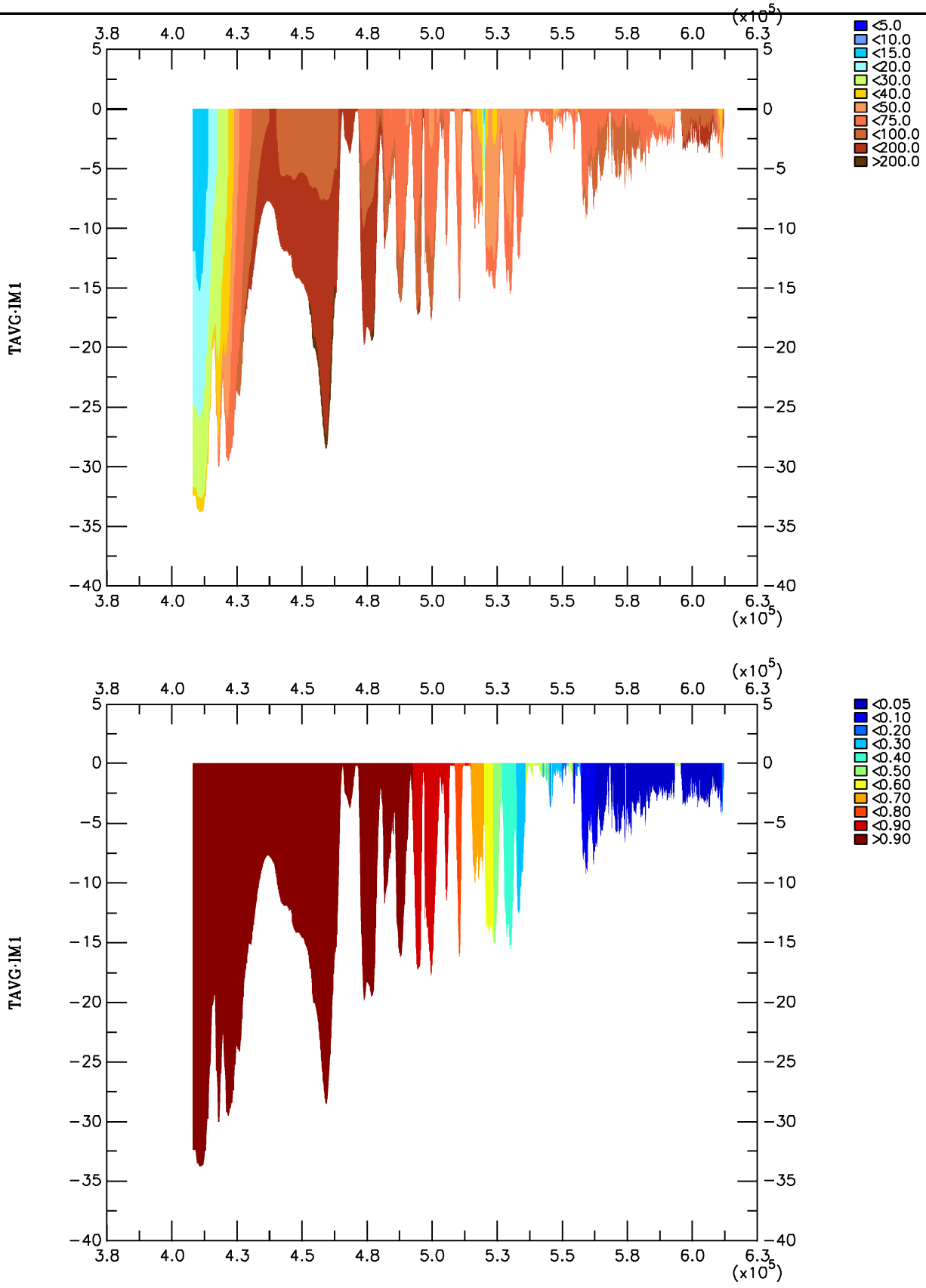

SPM concentration (mg/l) along Scheldt estuary winter upper panel: fluvial + marine fraction (mg/l) lower panel: marine fraction only (ratio)	hydro 14dw	ws15r
WL | Delft Hydraulics		Fig. S4.4a

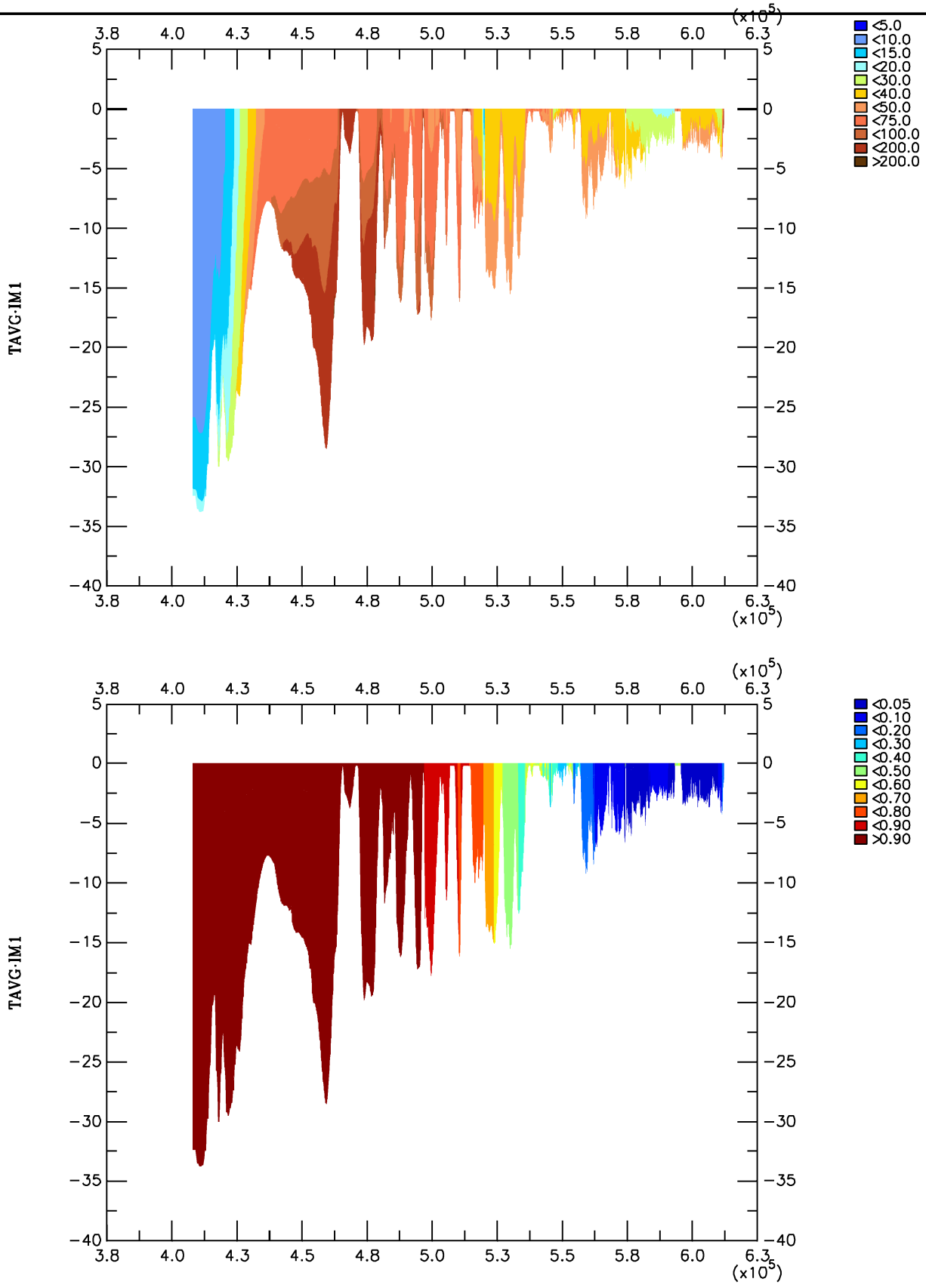

SPM concentration (mg/l) along Scheldt estuary summer upper panel: fluvial + marine fraction (mg/l) lower panel: marine fraction only (ratio)	hydro 14dw	ws15r
WL | Delft Hydraulics		Fig. S4.4b

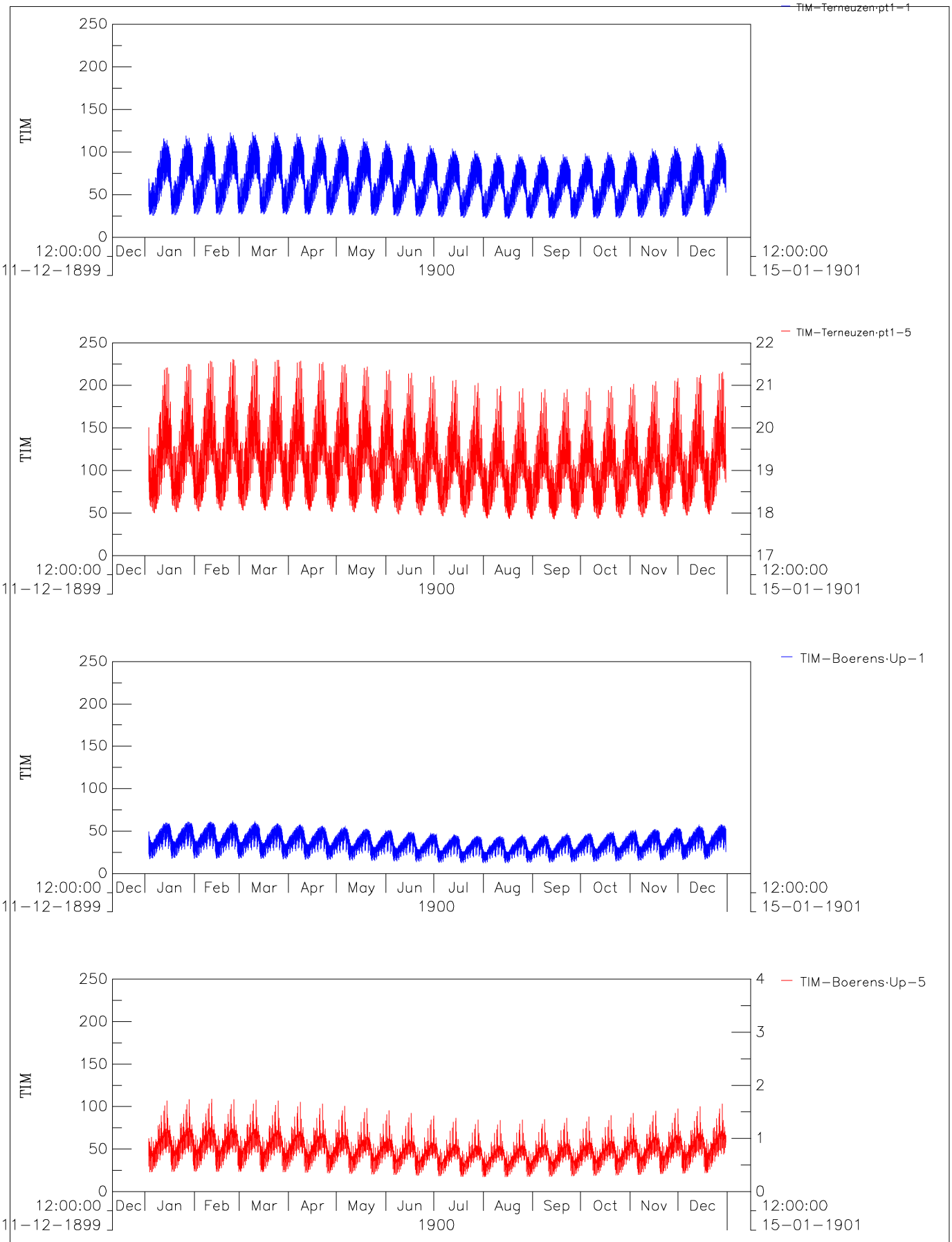

Time series SPM concentration (mg/l) top panels: Terneuzen DOW jetty year surface/bottom bottom panels: Boerenschans year surface/bottom	hydro 14dw	ws15r
WL | Delft Hydraulics		Fig. S4.5

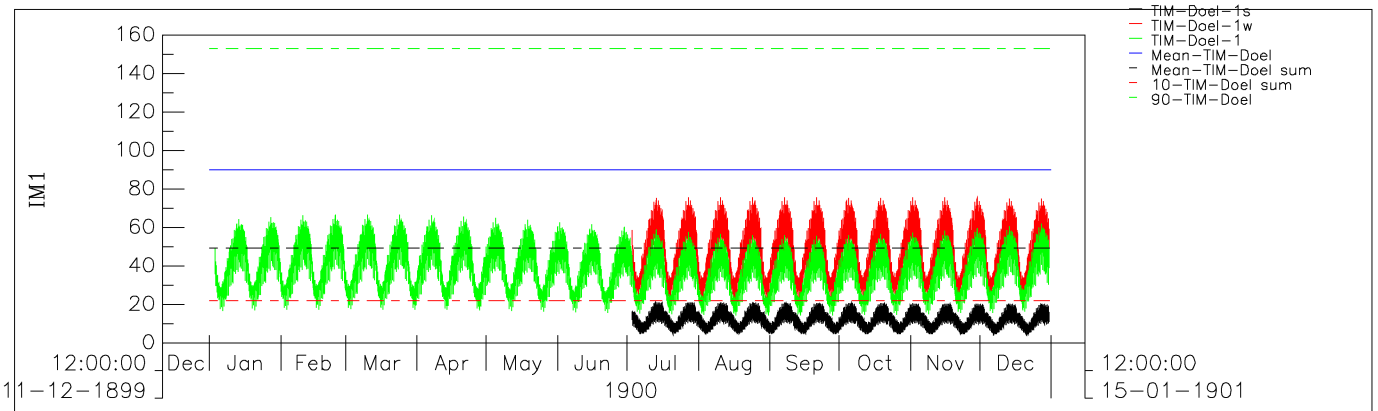

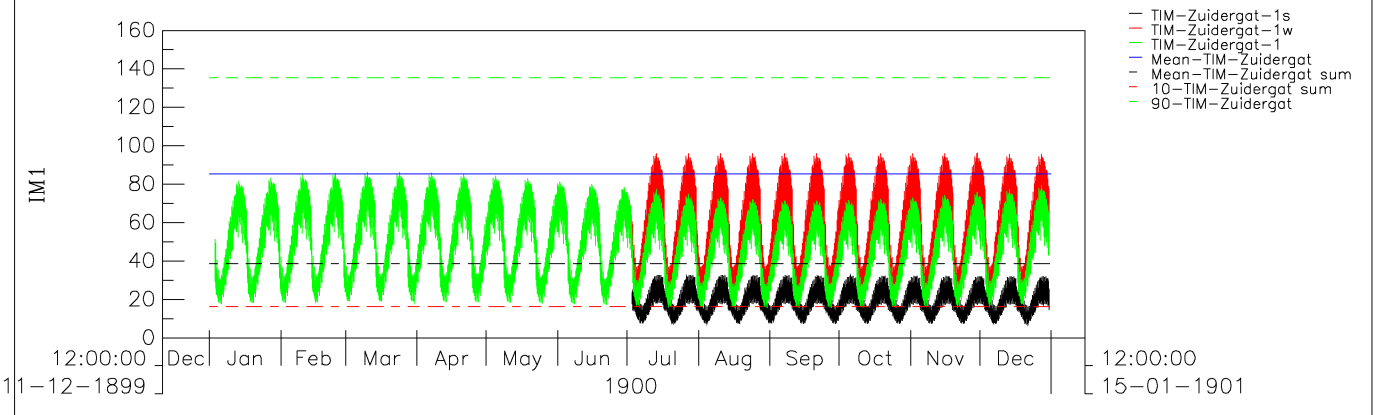

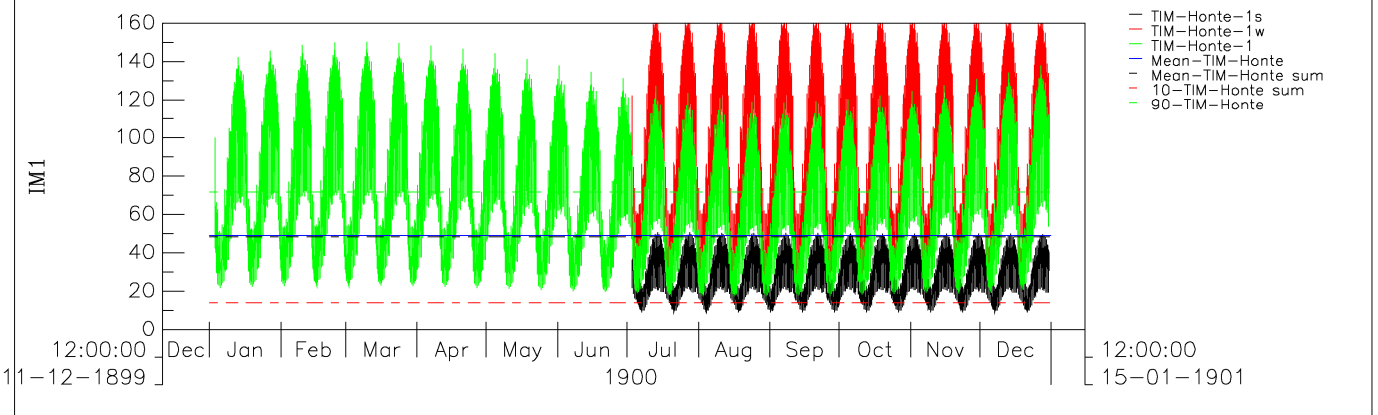

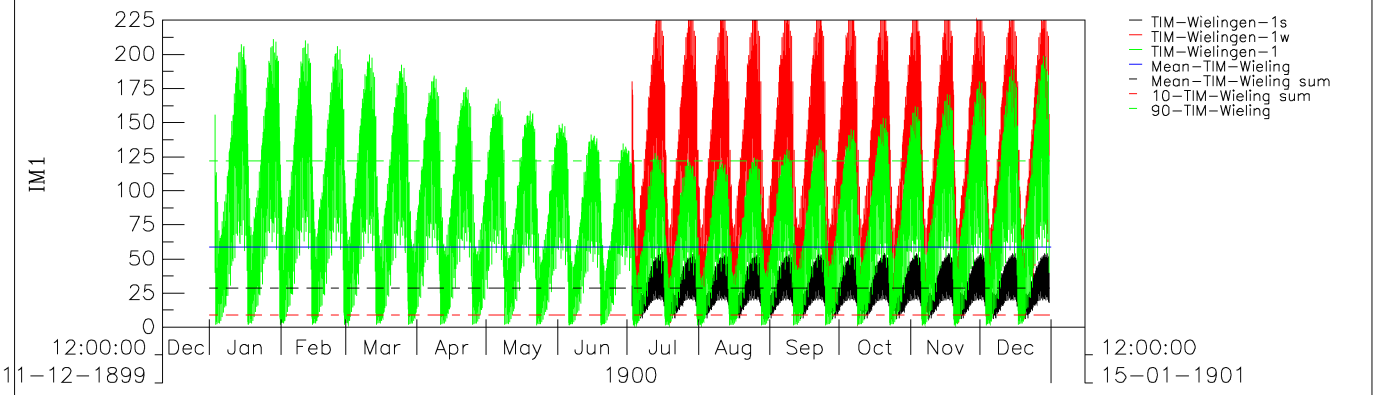

Time series SPM concentration (mg/l)
top panels: Schaar van Doel (top) and Zuidergat neap-spring
bottom panels: Honte and Wielingen (bottom) neap-spring

hydro 14dw | ws15r

WL | Delft Hydraulics

Fig. S4.6b

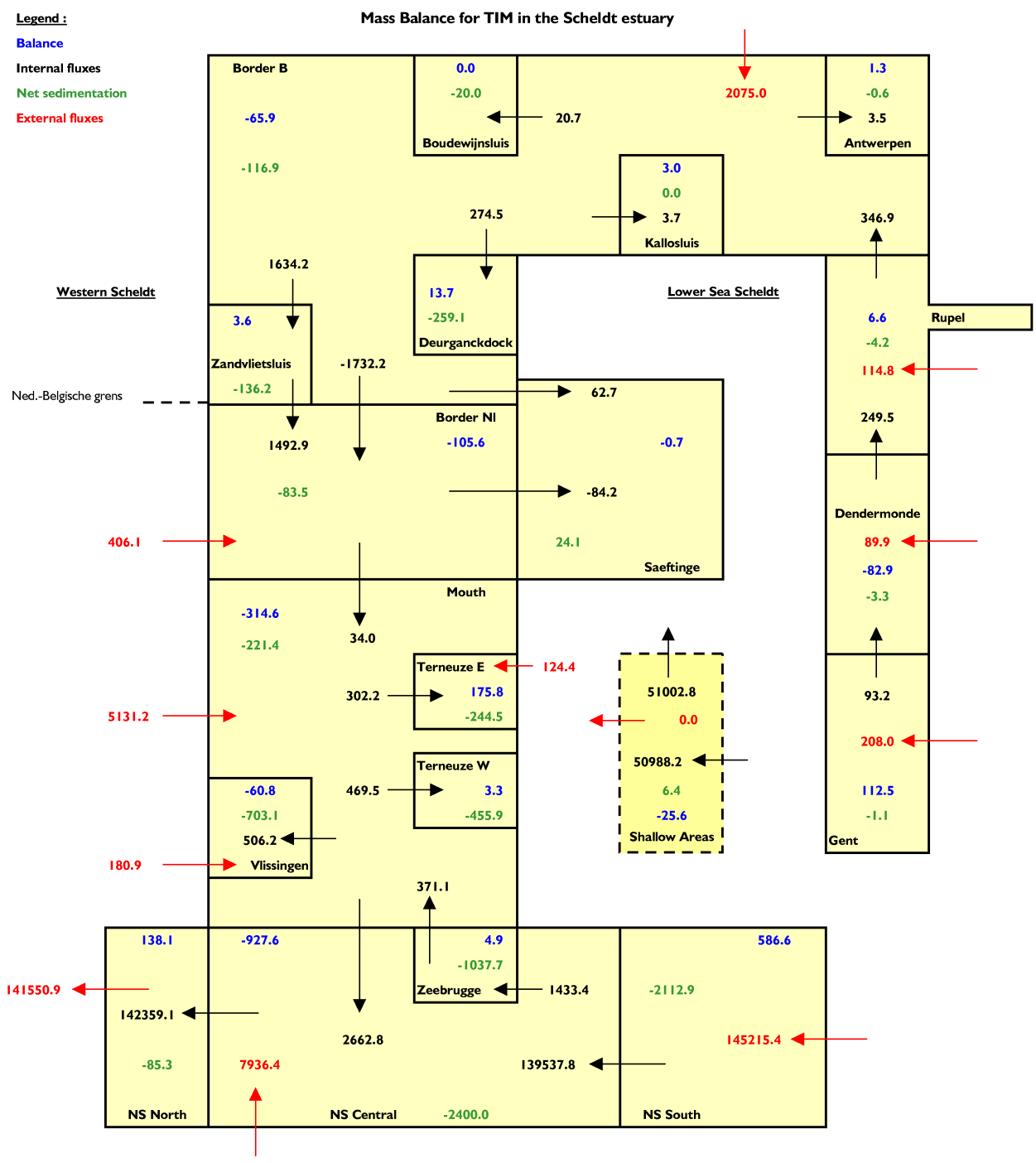

DELWAQ results
Net mud transport, 4th quarter [kT/year]

Z4210

WS15Q4

WL | DELFT HYDRAULICS

Fig. S4.7a

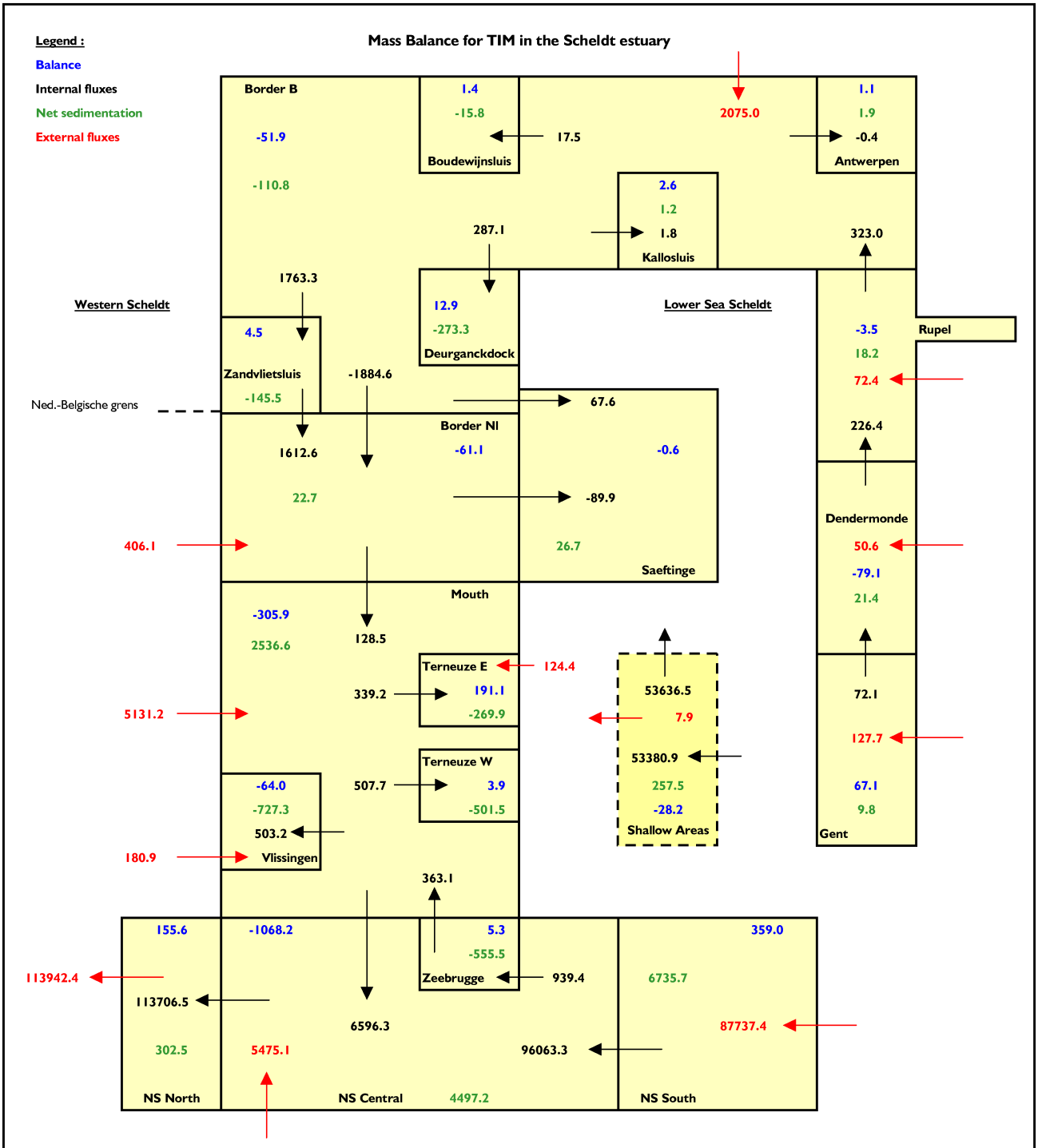

DELWAQ results
Net mud transport, 2nd quarter [kT/year]

Z4210

WS15Q2

WL | DELFT HYDRAULICS

Fig. S4.7b

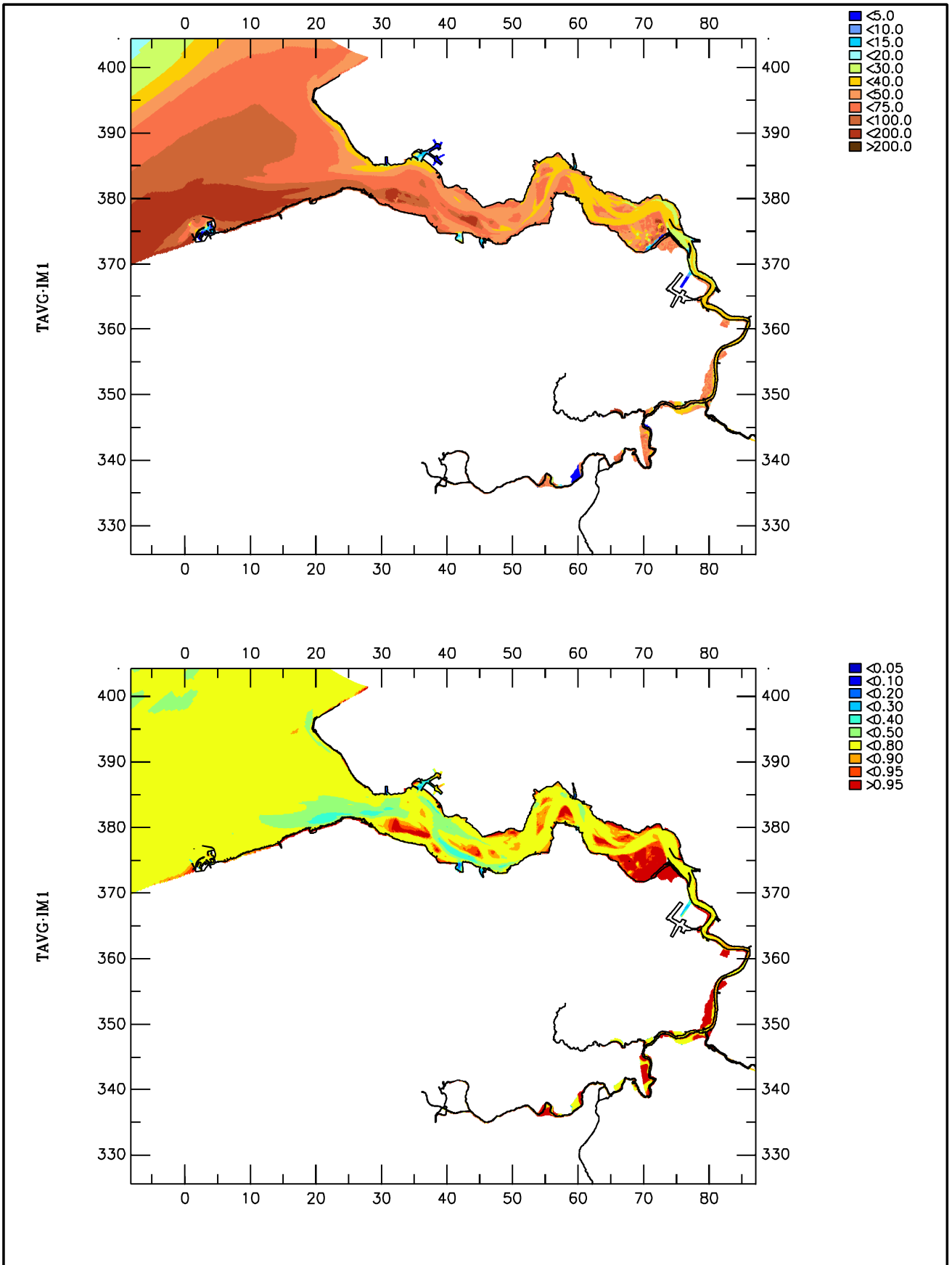

top: SPM concentration in surface layer (mg/l) bottom: concentration ratio surface/bottom (–) winter conditions	hydro 14dw	ws16r
WL | Delft Hydraulics	Z4210	Fig. S5.1a

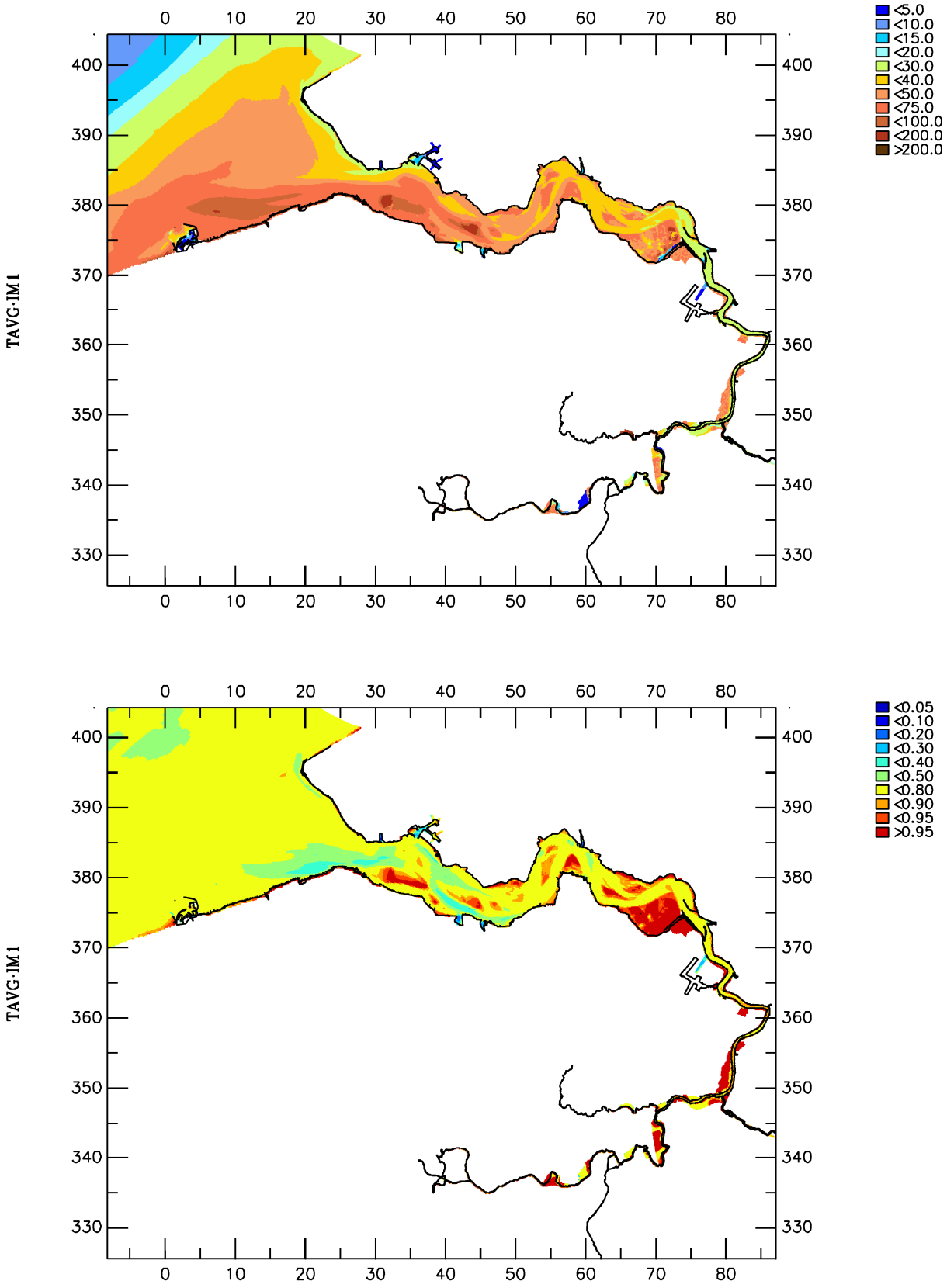

top: SPM concentration in surface layer (mg/l) bottom: concentration ratio surface/bottom (–) summer conditions	hydro 14dw	ws16r
WL | Delft Hydraulics	Z4210	Fig. S5.1b

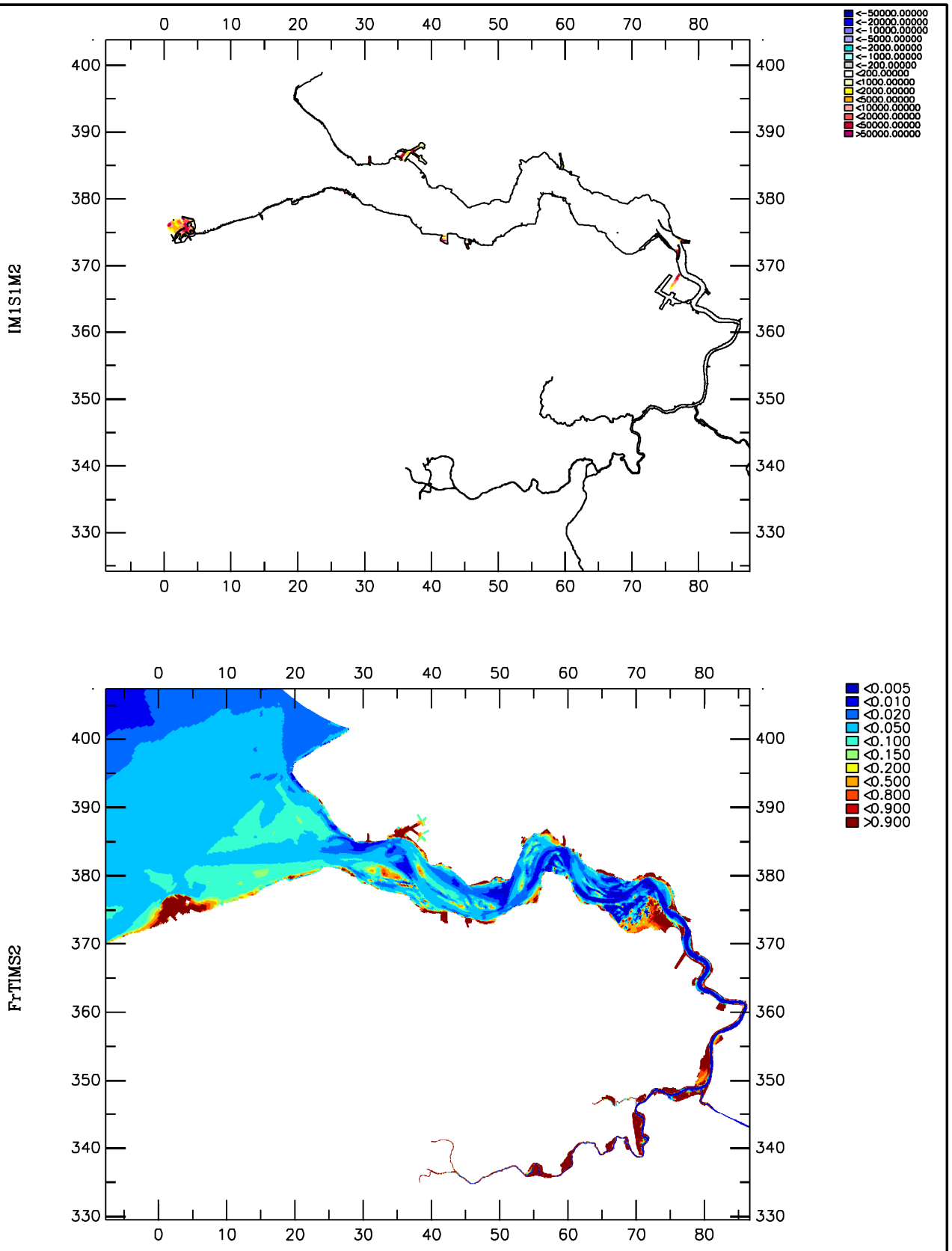

top panel: net siltation over 1 month (g/m2)
bottom panel: mud fraction in bottom
winter conditions

hydro 14dw | ws16r

WL | Delft Hydraulics

Fig. S5.2a

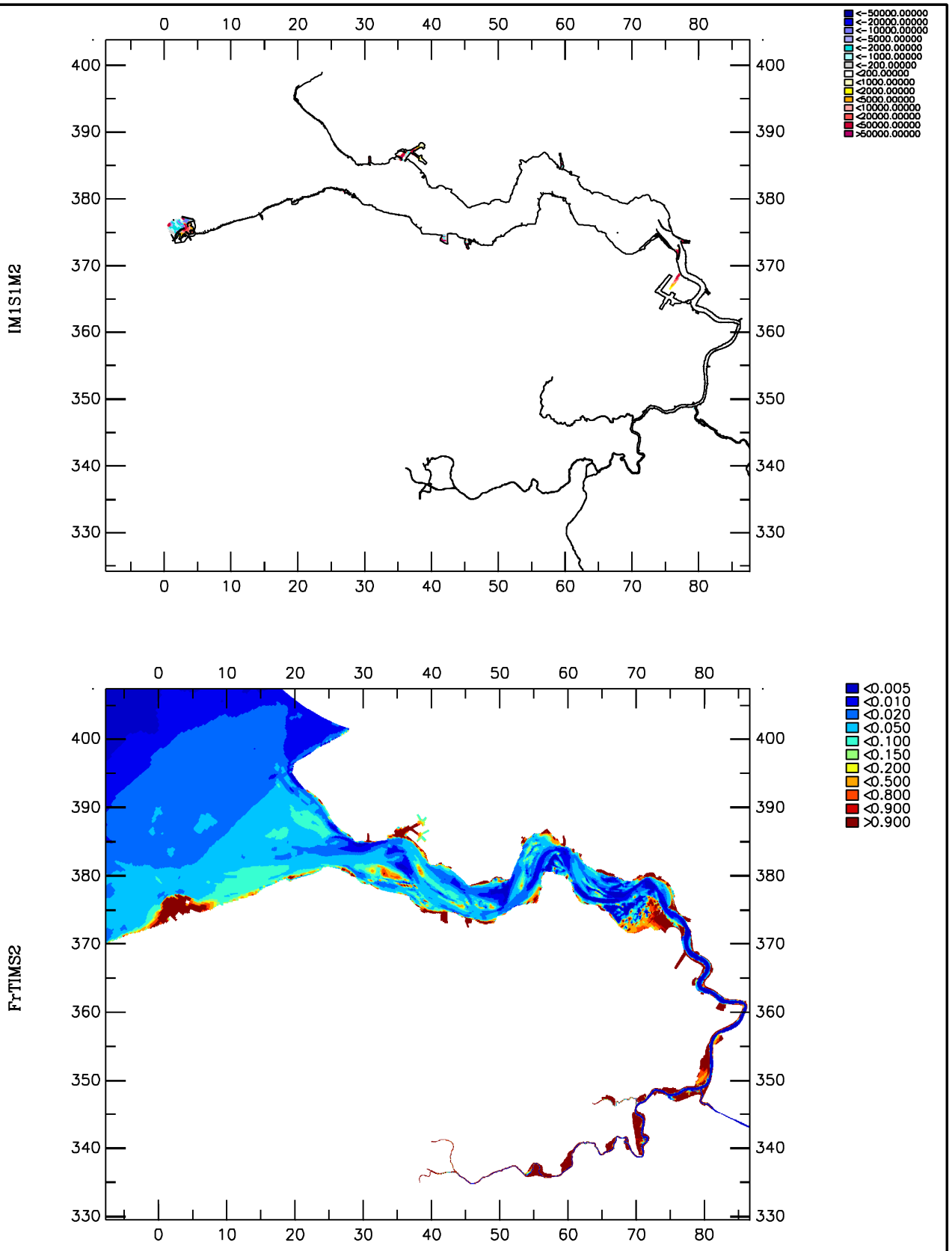

top panel: net siltation over 1 month (g/m2)
bottom panel: mud fraction in bottom
summer conditions

hydro 14dw | ws16r

WL | Delft Hydraulics

Fig. S5.2b

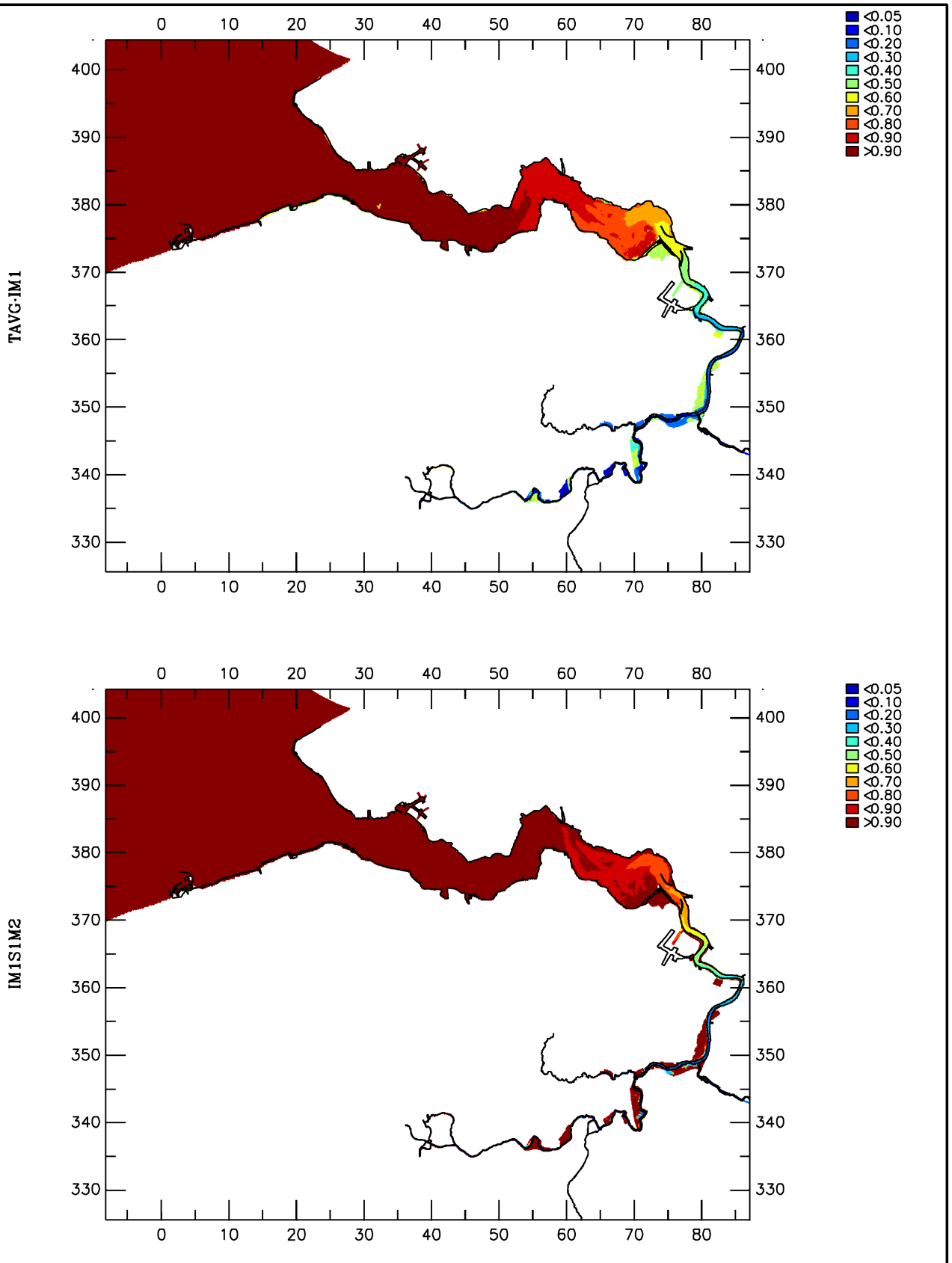

fraction marine mud (–) winter conditions upper panel: in the water column lower panel: in the bottom	hydro 14dw	ws16r
WL | Delft Hydraulics	Z4210	Fig. S5.3a

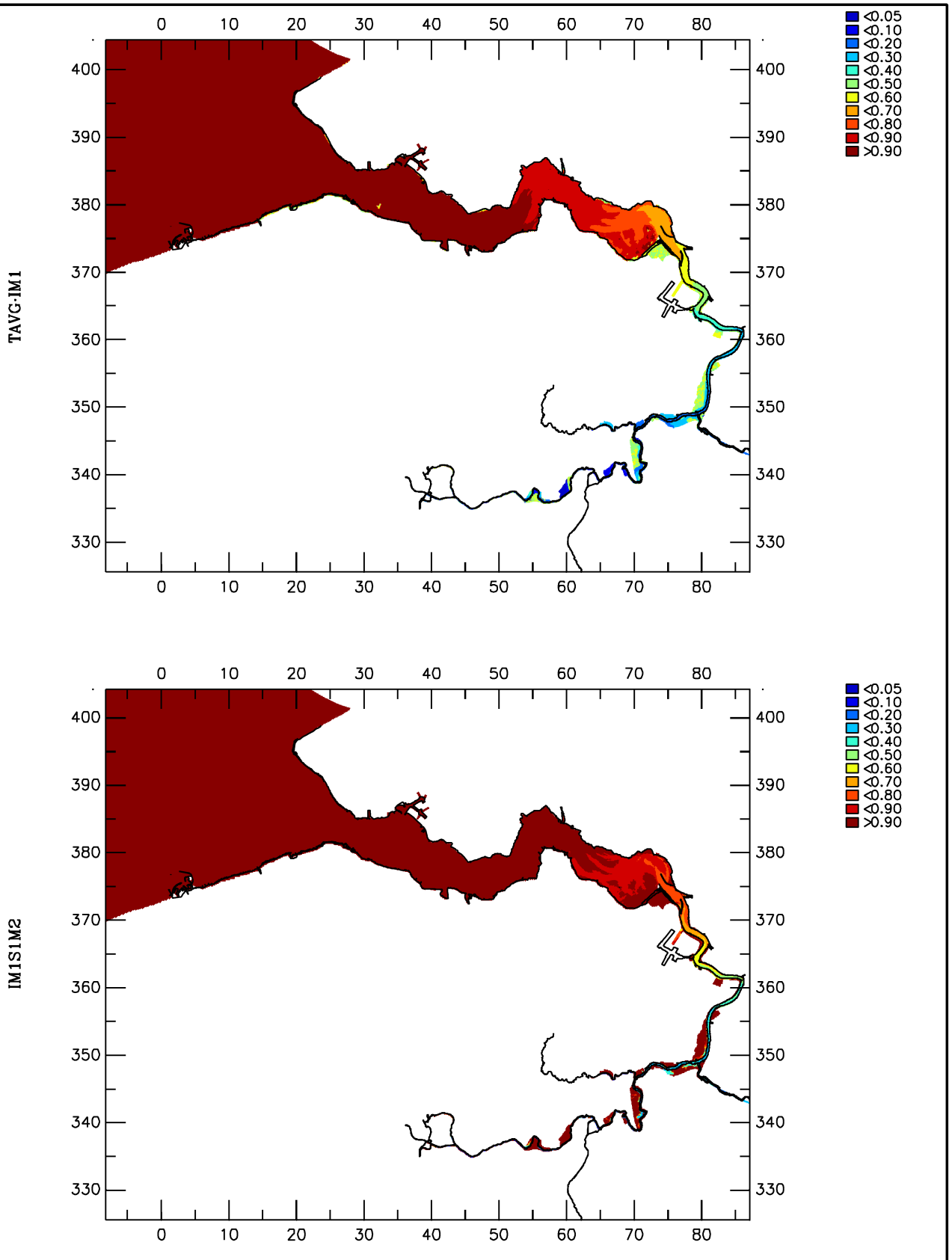

fraction marine mud (–) summer conditions
upper panel: in the water column
lower panel: in the bottom

hydro 14dw | ws16r

WL | Delft Hydraulics | Z4210 | Fig. S5.3b

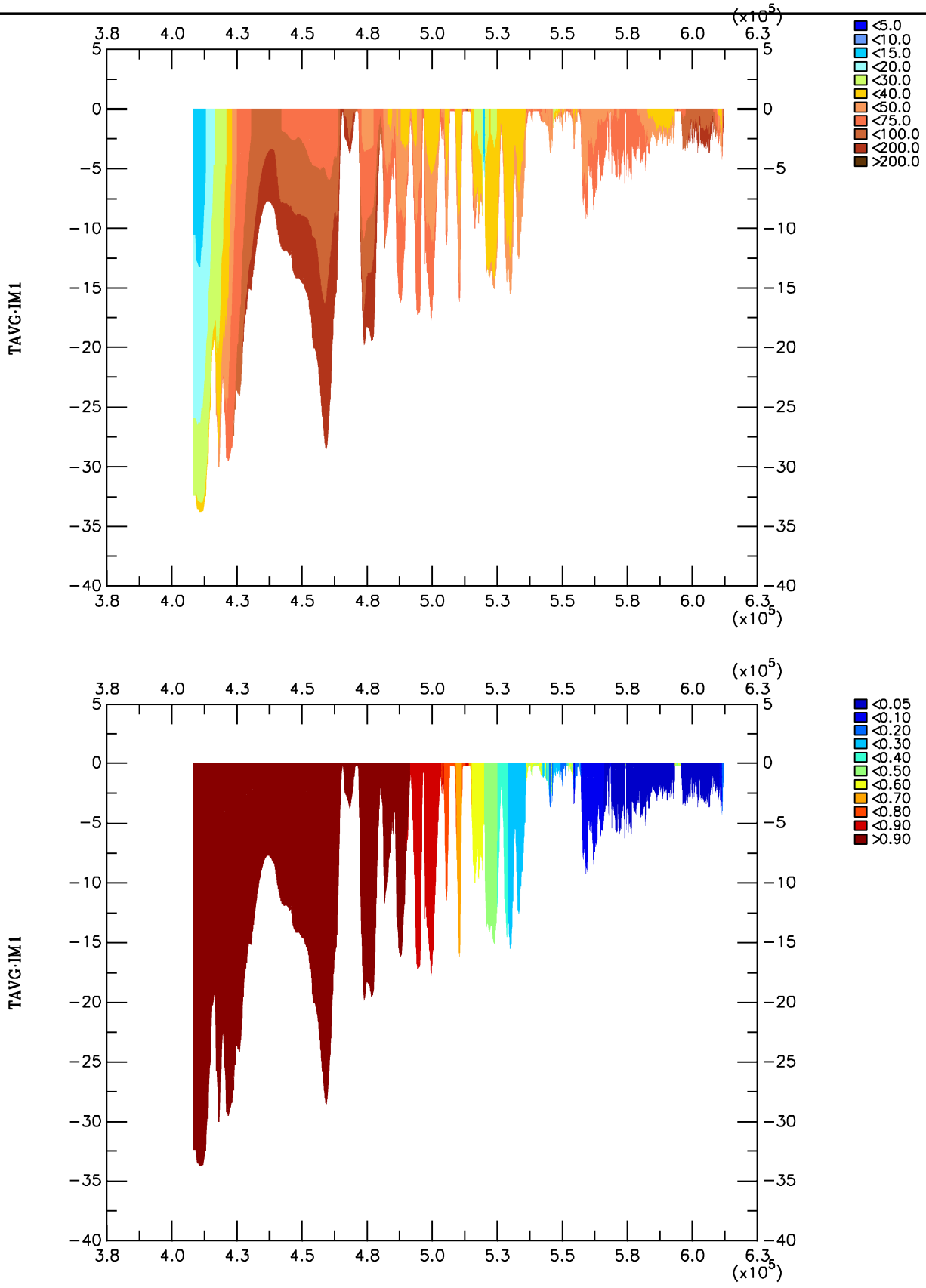

SPM concentration (mg/l) along Scheldt estuary winter upper panel: fluvial + marine fraction (mg/l) lower panel: marine fraction only (ratio)	hydro 14dw	ws16r
WL | Delft Hydraulics		Fig. S5.4a

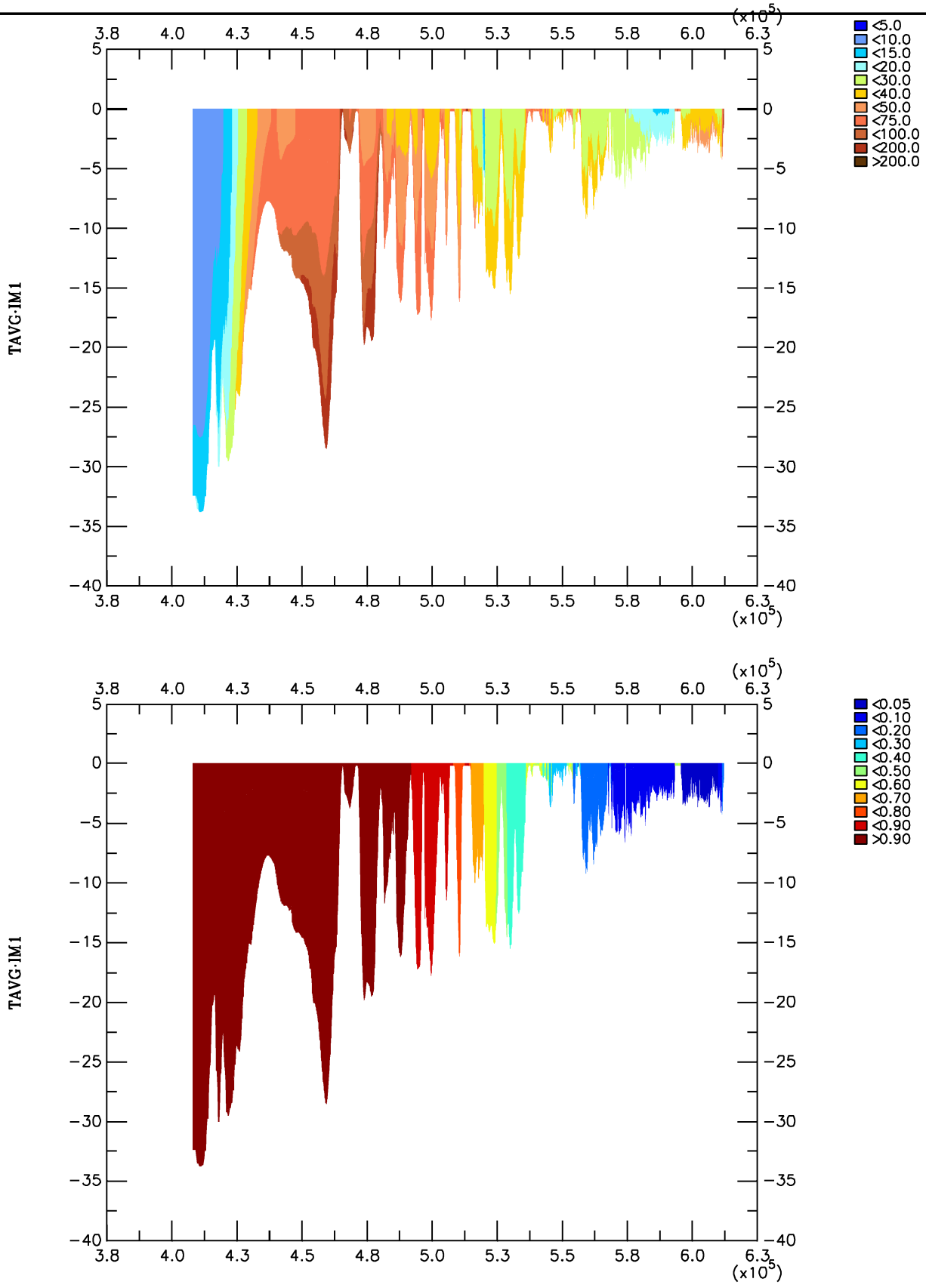

SPM concentration (mg/l) along Scheldt estuary summer upper panel: fluvial + marine fraction (mg/l) lower panel: marine fraction only (ratio)	hydro 14dw	ws16r
WL | Delft Hydraulics		Fig. S5.4b

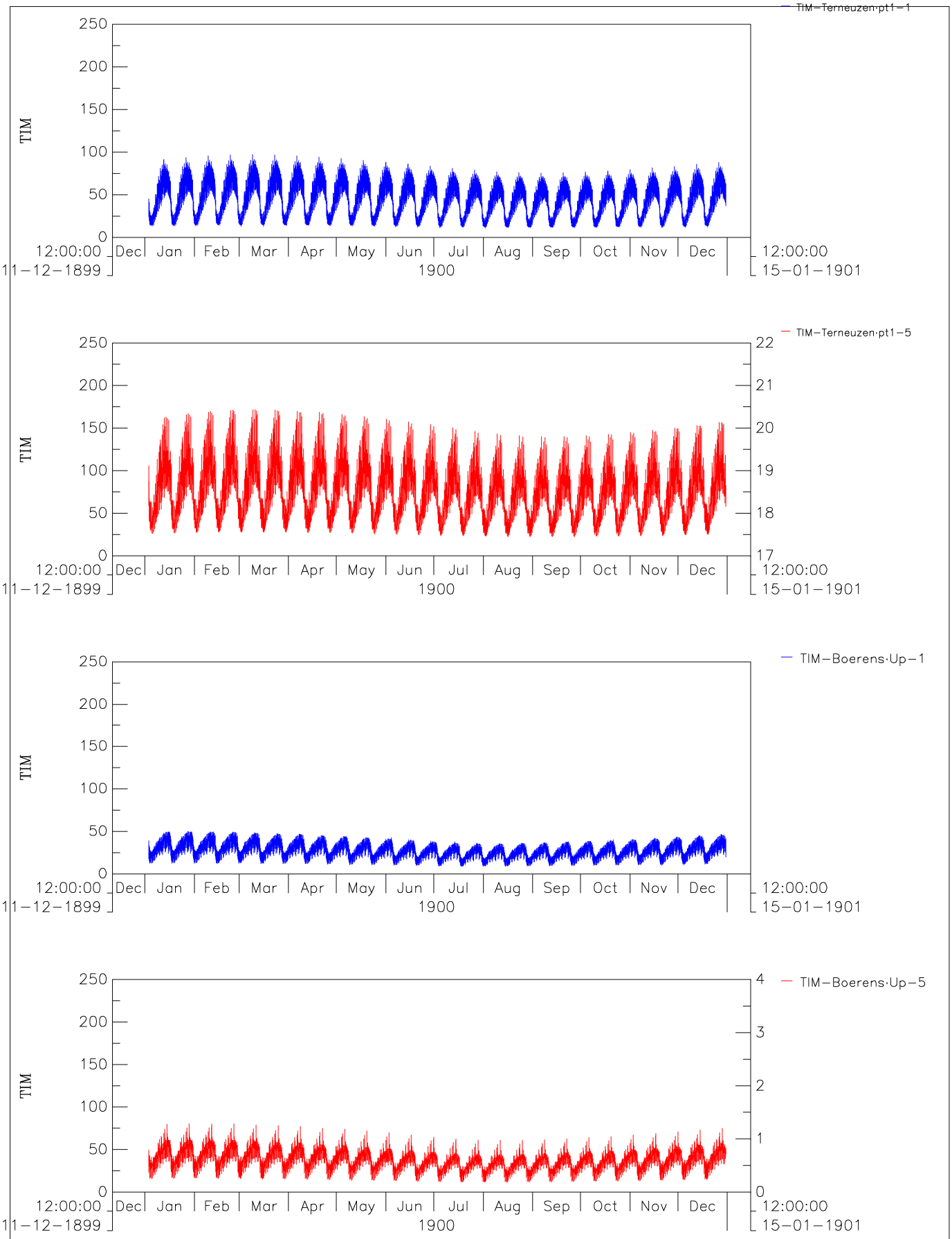

Time series SPM concentration (mg/l) top panels: Terneuzen DOW jetty year surface/bottom bottom panels: Boerenschans year surface/bottom	hydro 14dw	ws16r
WL | Delft Hydraulics		Fig. S5.5

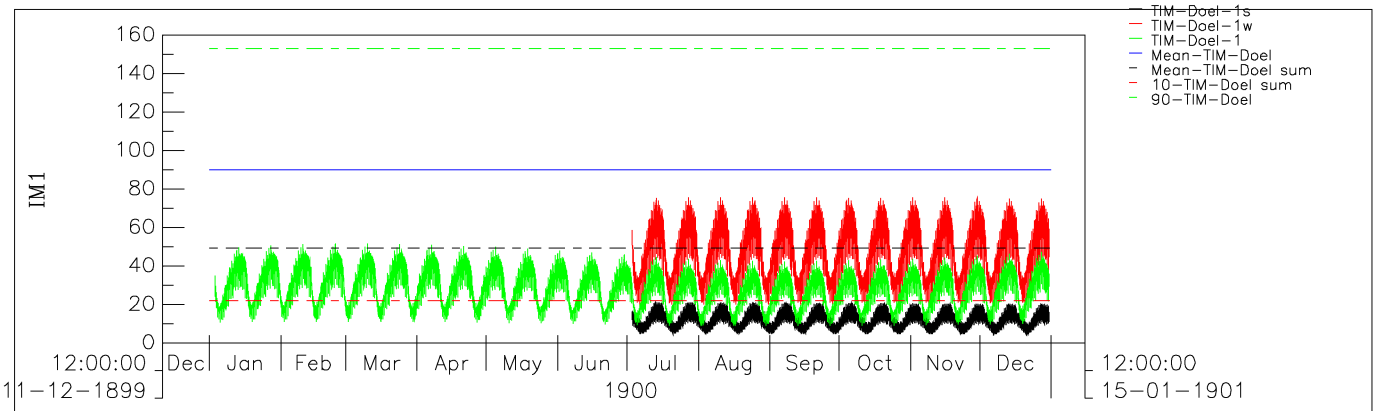

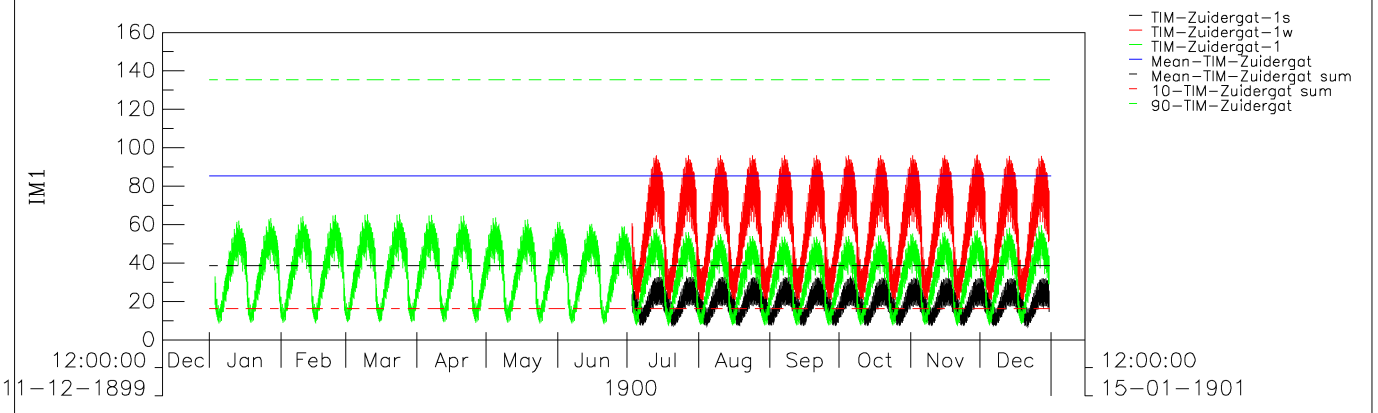

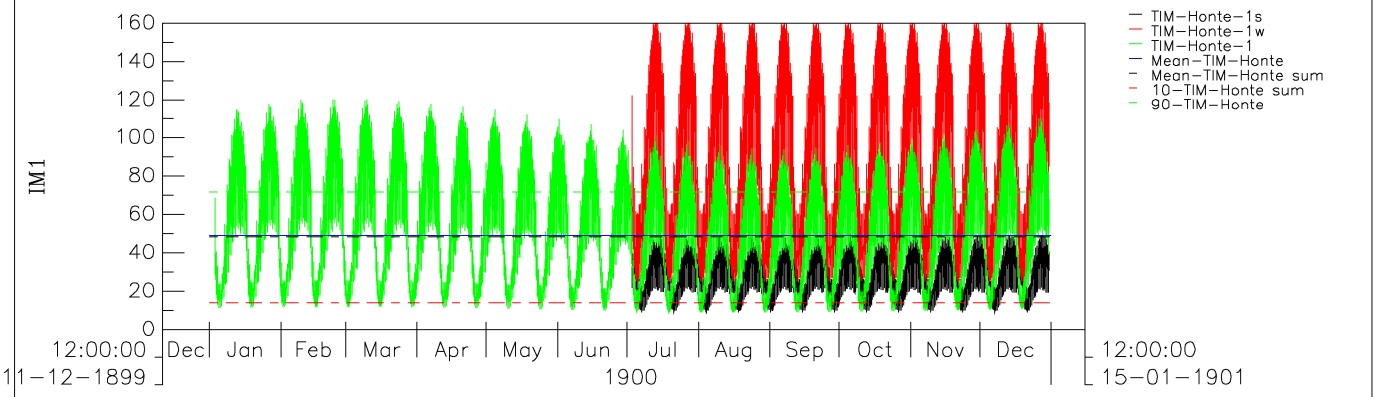

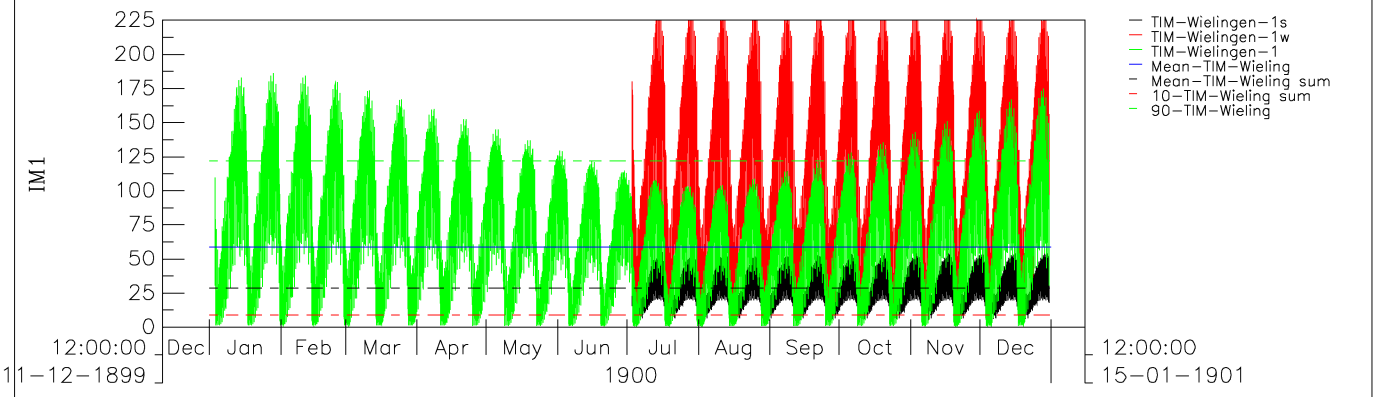

Time series SPM concentration (mg/l)
top panels: Schaar van Doel (top) and Zuidergat neap-spring
bottom panels: Honte and Wielingen (bottom) neap-spring

hydro 14dw | ws16r

WL | Delft Hydraulics

Fig. S5.6b

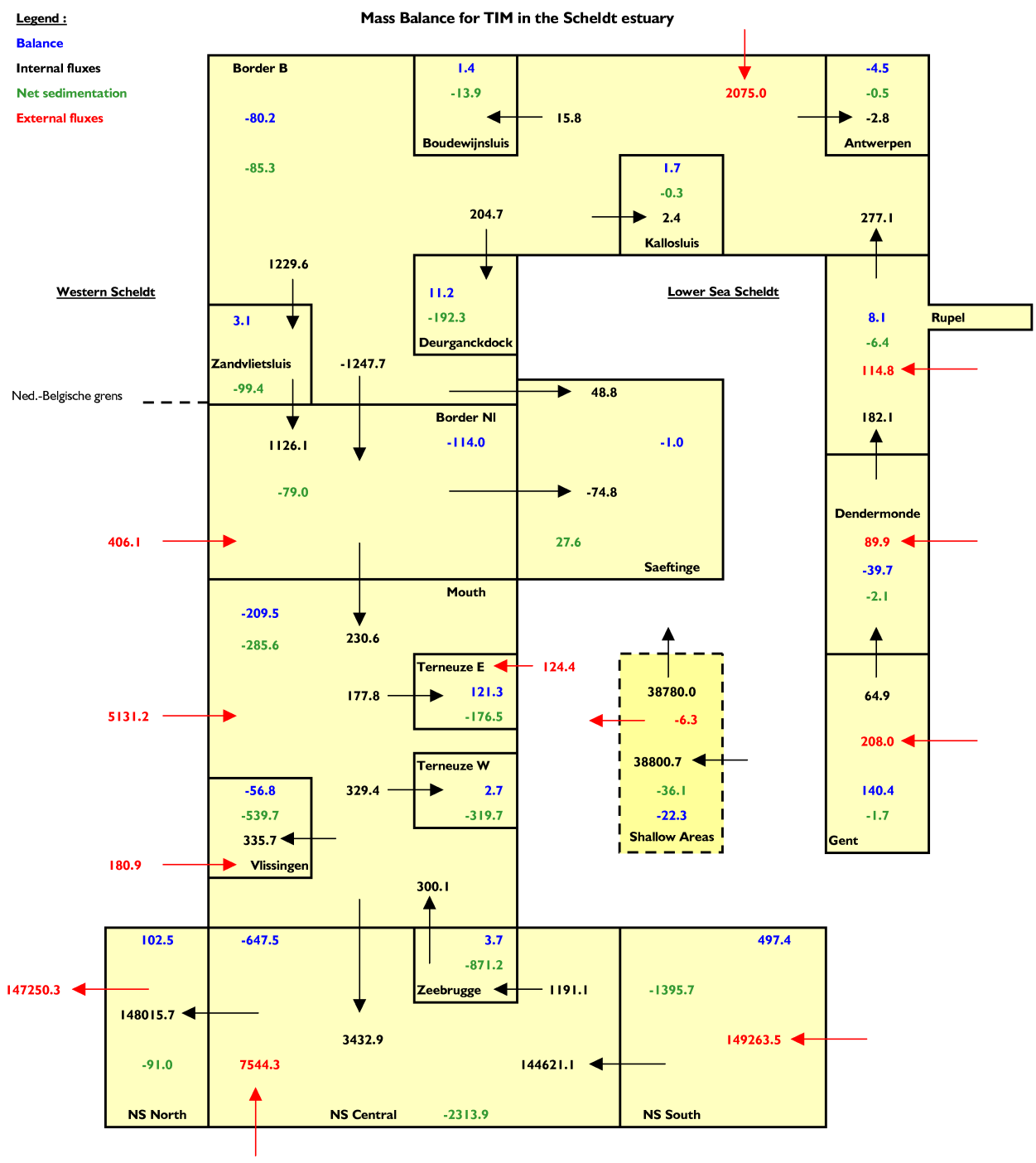

DELWAQ results
Net mud transport, 4th quarter [kT/year]

Z4210

WS16Q4

WL | DELFT HYDRAULICS

Fig. S5.7a

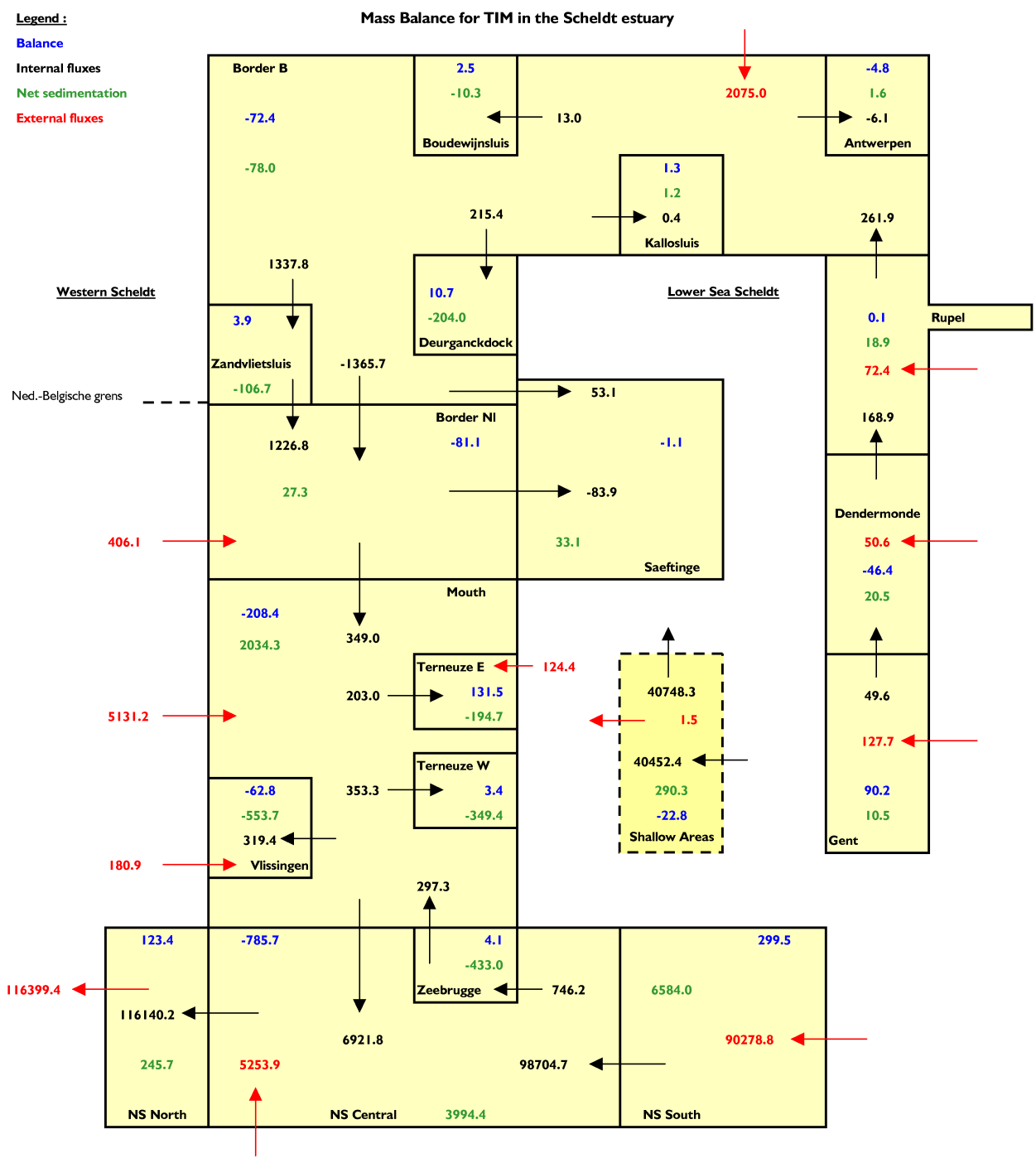

DELWAQ results
Net mud transport, 2nd quarter [kT/year]

Z4210

WS16Q2

WL | DELFT HYDRAULICS

Fig. S5.7b

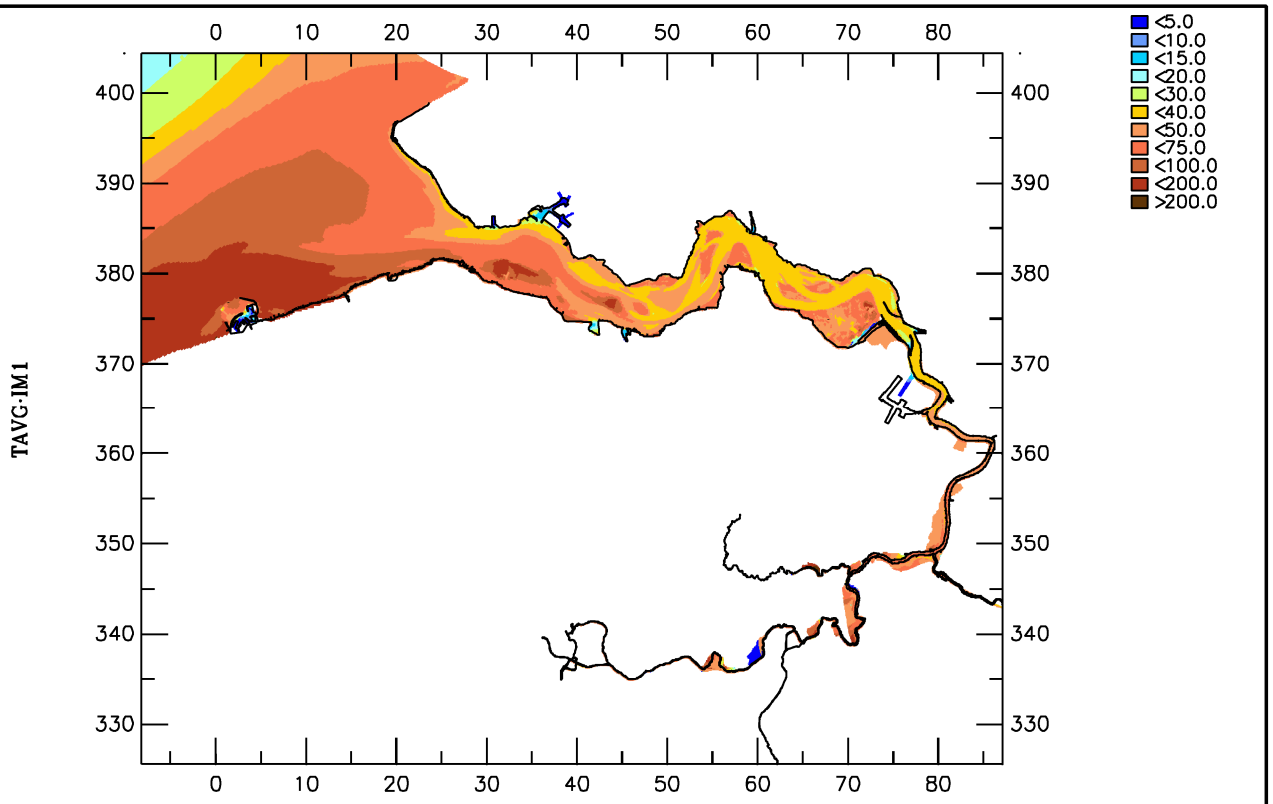

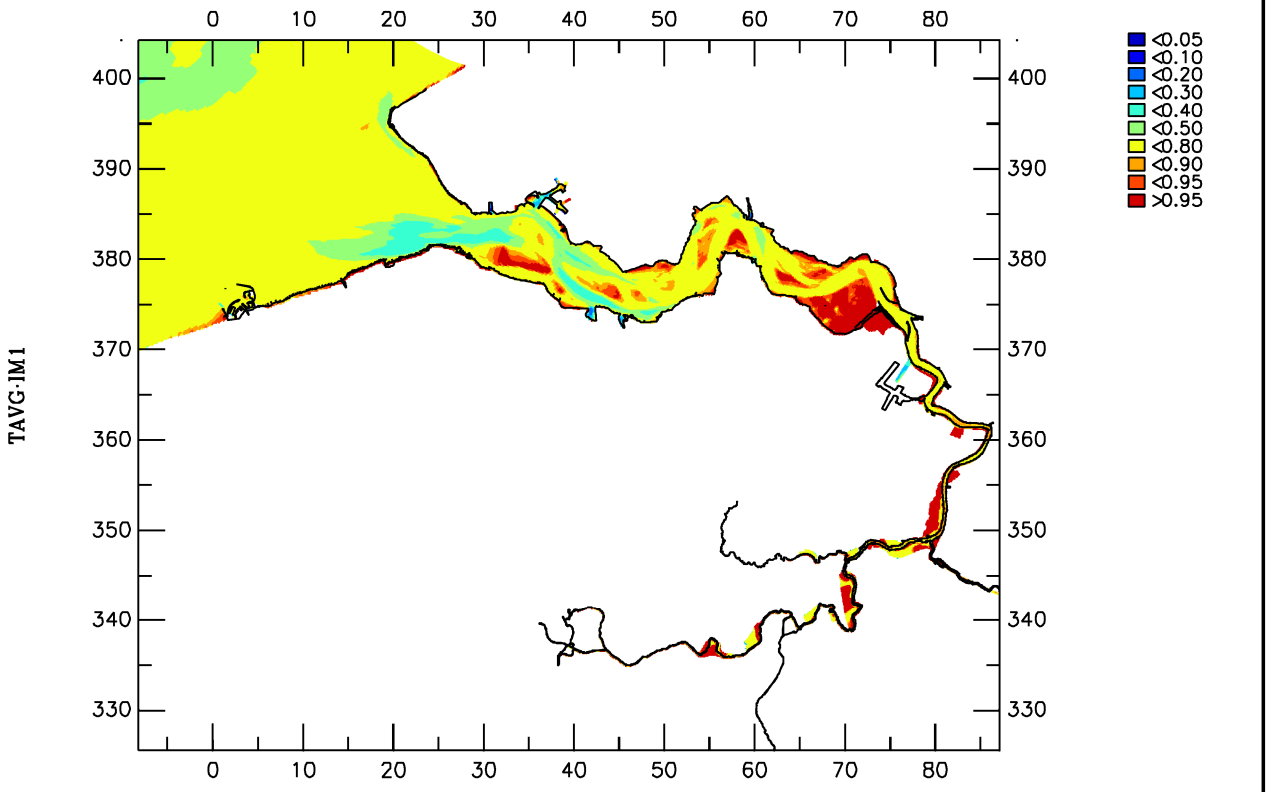

top: SPM concentration in surface layer (mg/l) bottom: concentration ratio surface/bottom (–) winter conditions	hydro 14dw	ws18r
WL | Delft Hydraulics	Z4210	Fig. S6.1a

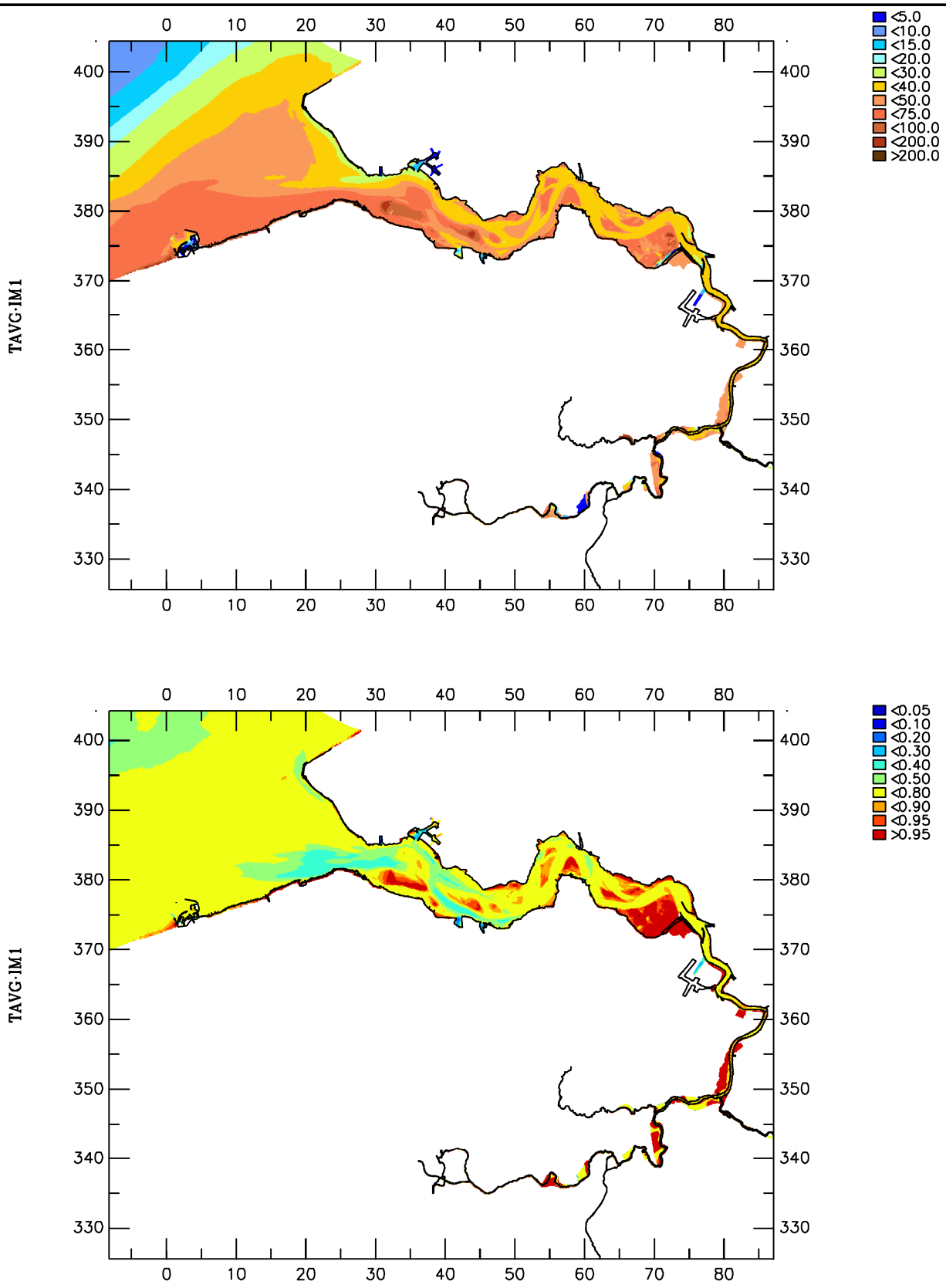

top: SPM concentration in surface layer (mg/l) bottom: concentration ratio surface/bottom (–) summer conditions	hydro 14dw	ws18r
WL | Delft Hydraulics	Z4210	Fig. S6.1b

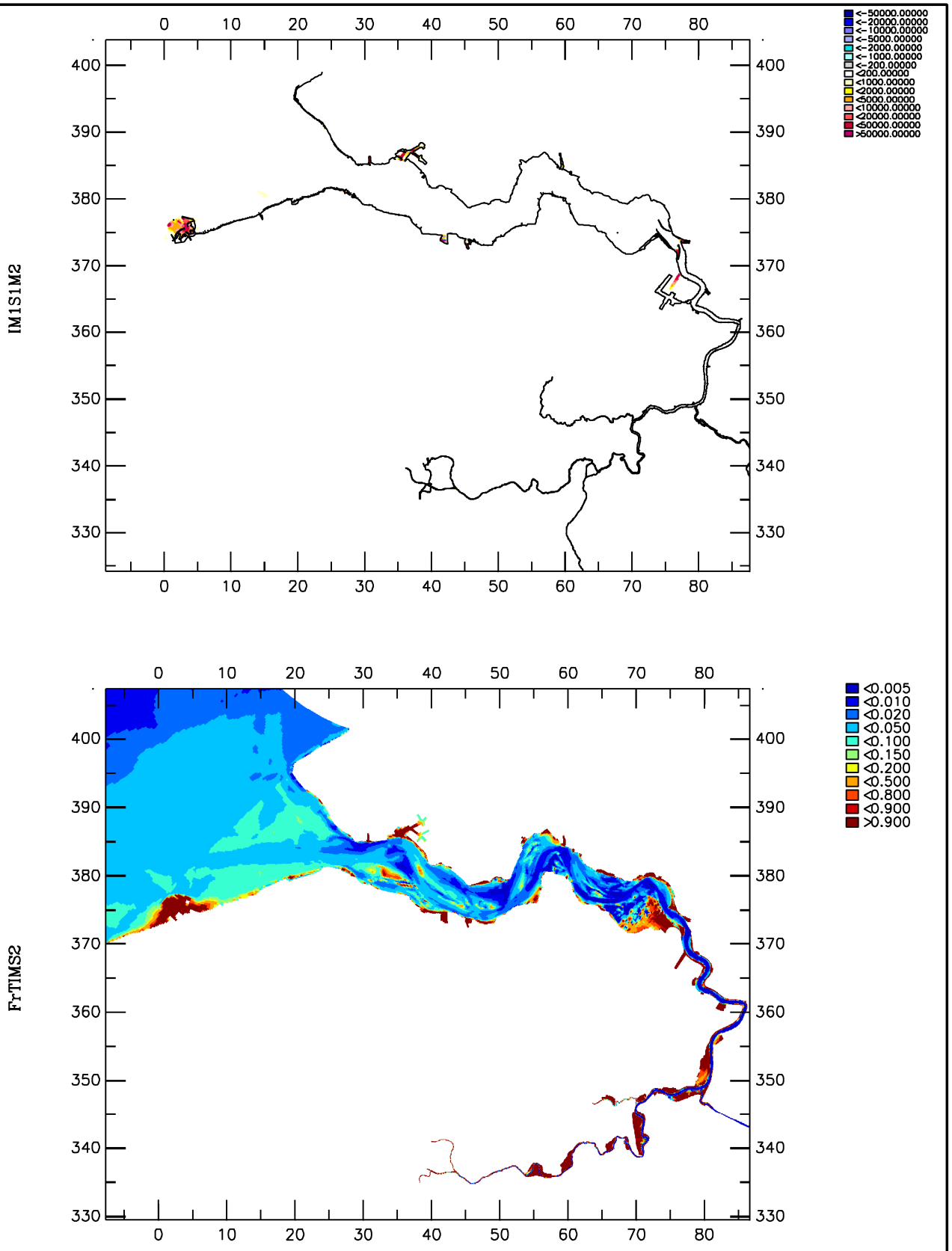

top panel: net siltation over 1 month (g/m2)
bottom panel: mud fraction in bottom
winter conditions

hydro 14dw	ws18r
WL | Delft Hydraulics	Fig. S6.2a

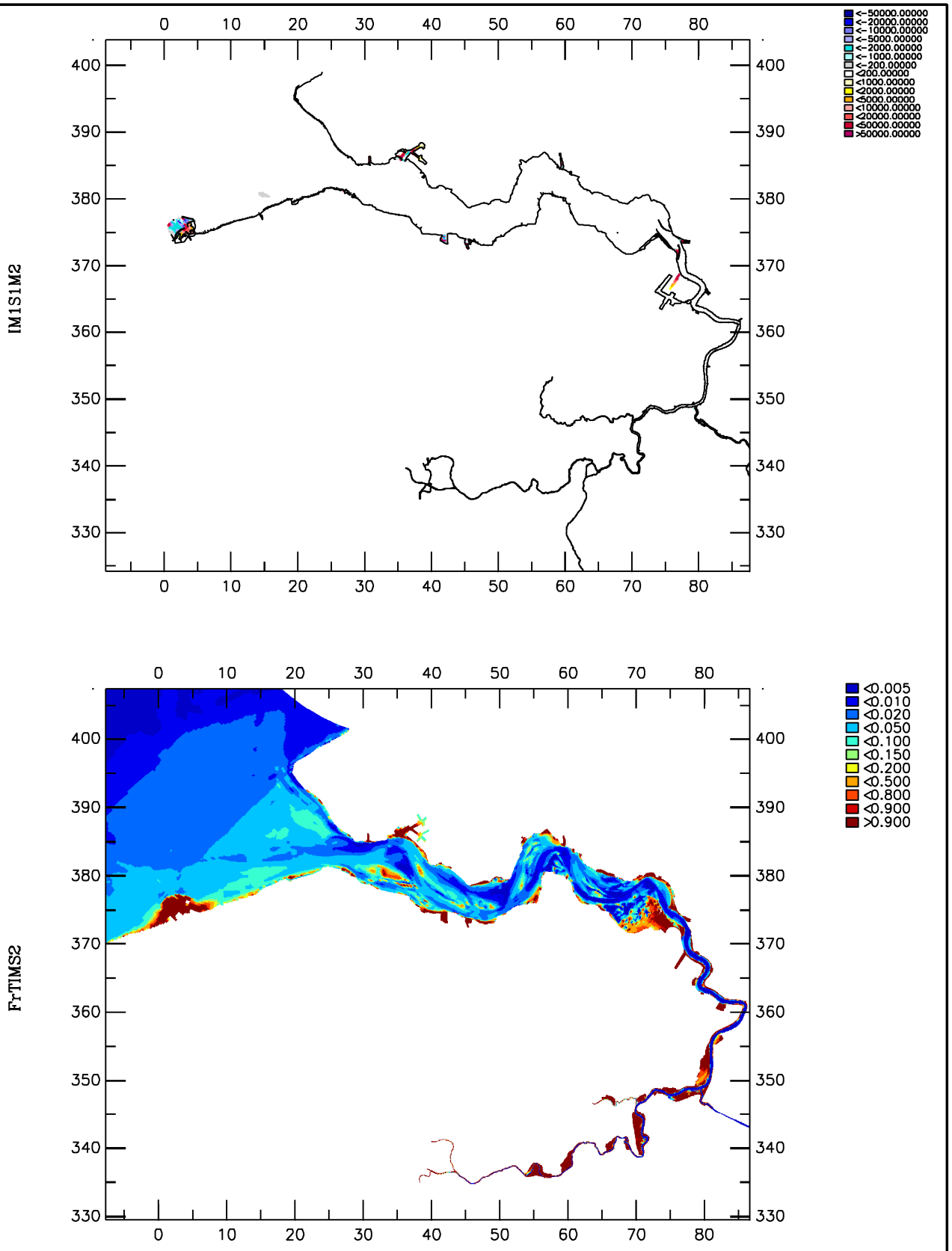

top panel: net siltation over 1 month (g/m2)
bottom panel: mud fraction in bottom
summer conditions

hydro 14dw | ws18r

WL | Delft Hydraulics

Fig. S6.2b

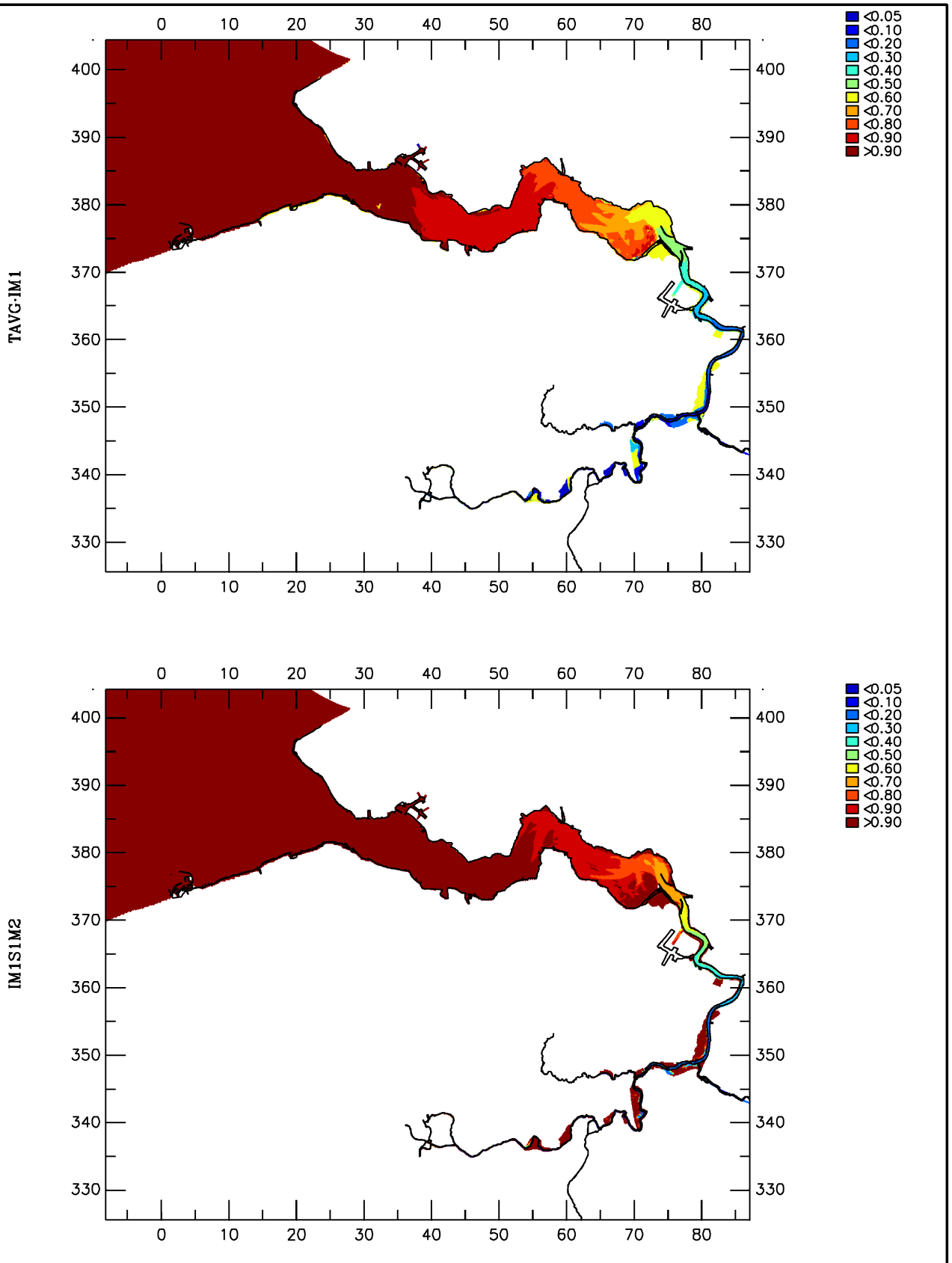

fraction marine mud (–) winter conditions upper panel: in the water column lower panel: in the bottom	hydro 14dw	ws18r
WL | Delft Hydraulics	Z4210	Fig. S6.3a

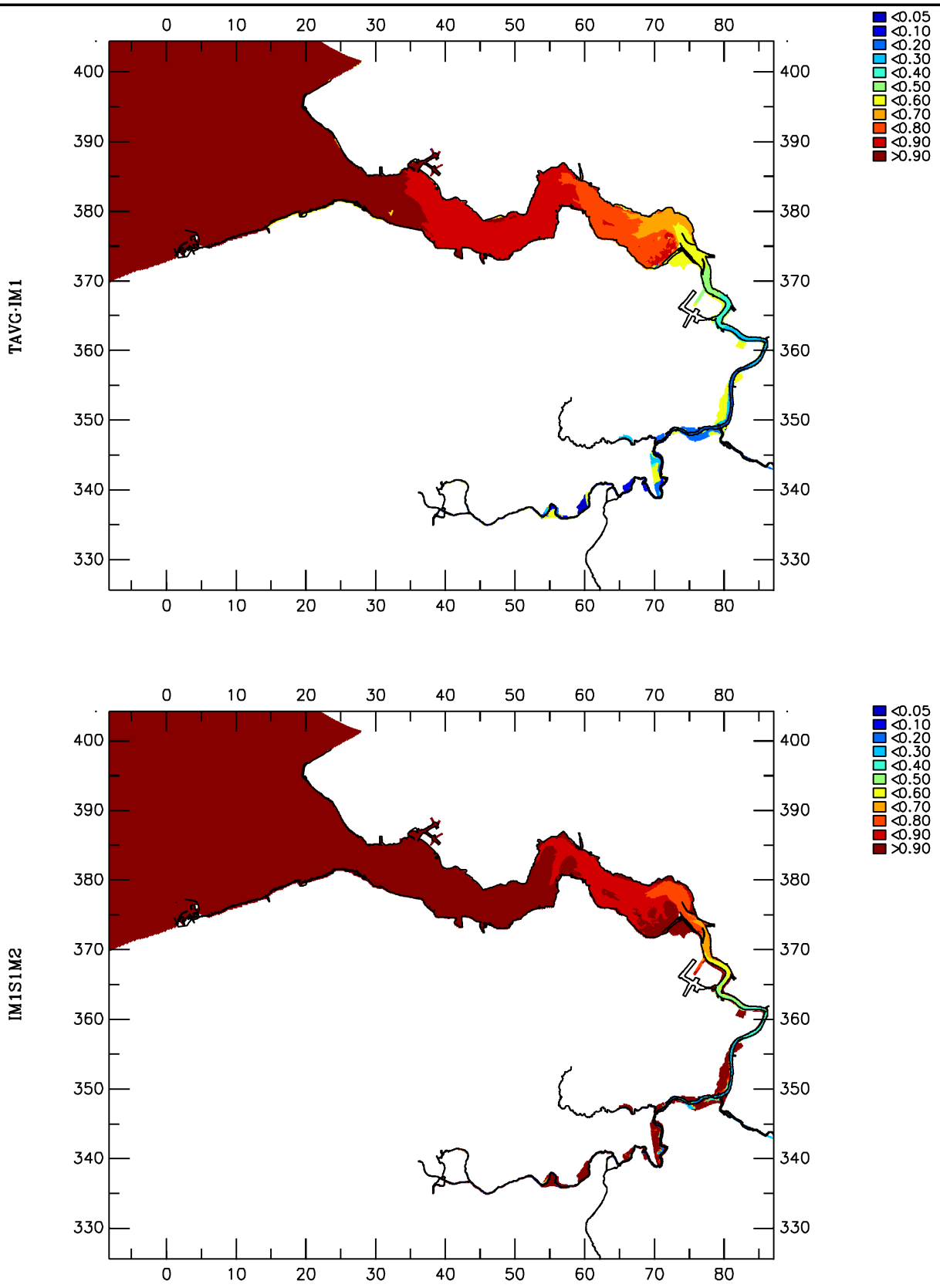

fraction marine mud (–) summer conditions upper panel: in the water column lower panel: in the bottom	hydro 14dw	ws18r
WL | Delft Hydraulics	Z4210	Fig. S6.3b

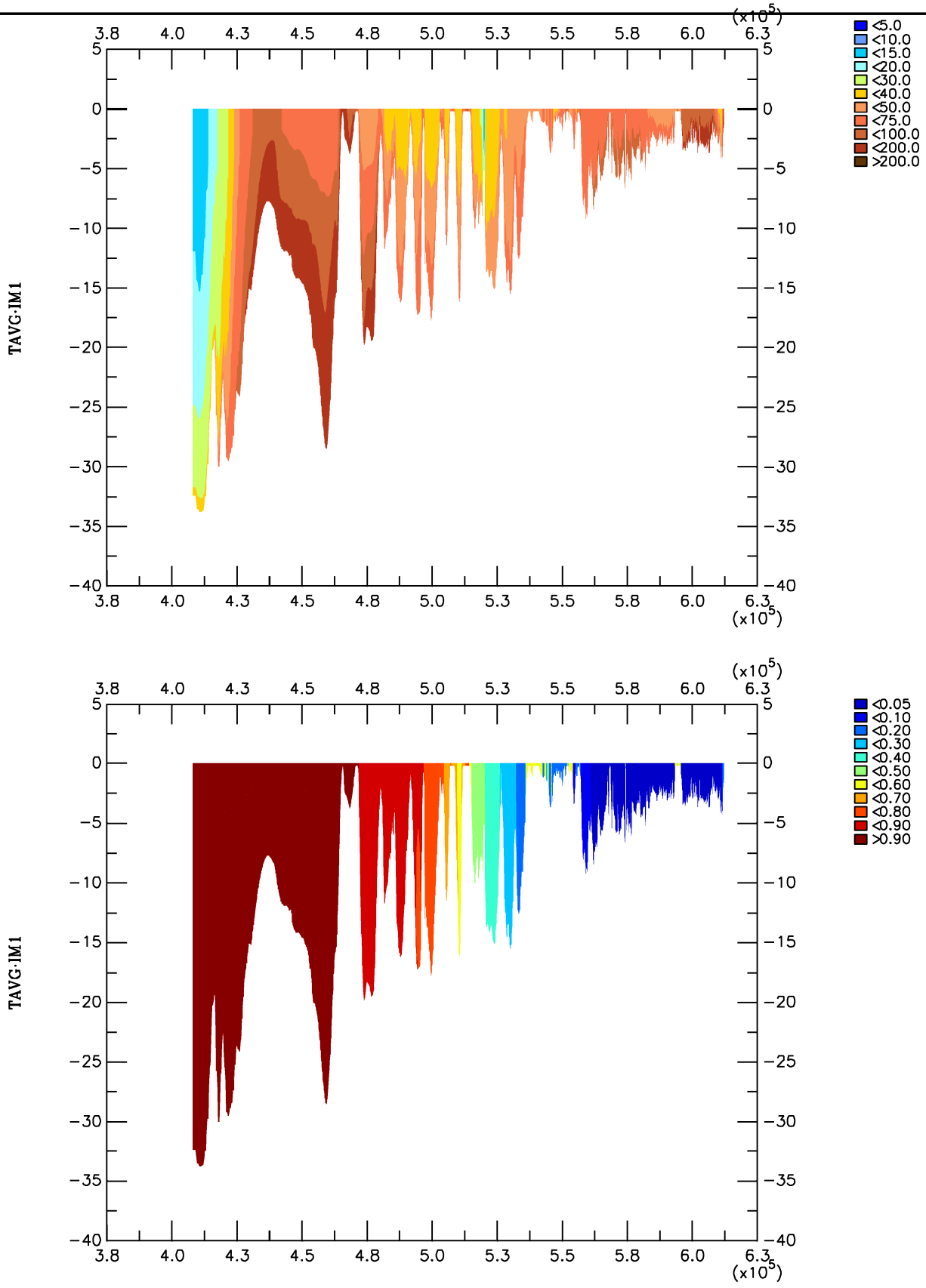

SPM concentration (mg/l) along Scheldt estuary winter upper panel: fluvial + marine fraction (mg/l) lower panel: marine fraction only (ratio)	hydro 14dw	ws18r
WL | Delft Hydraulics		Fig. S6.4a

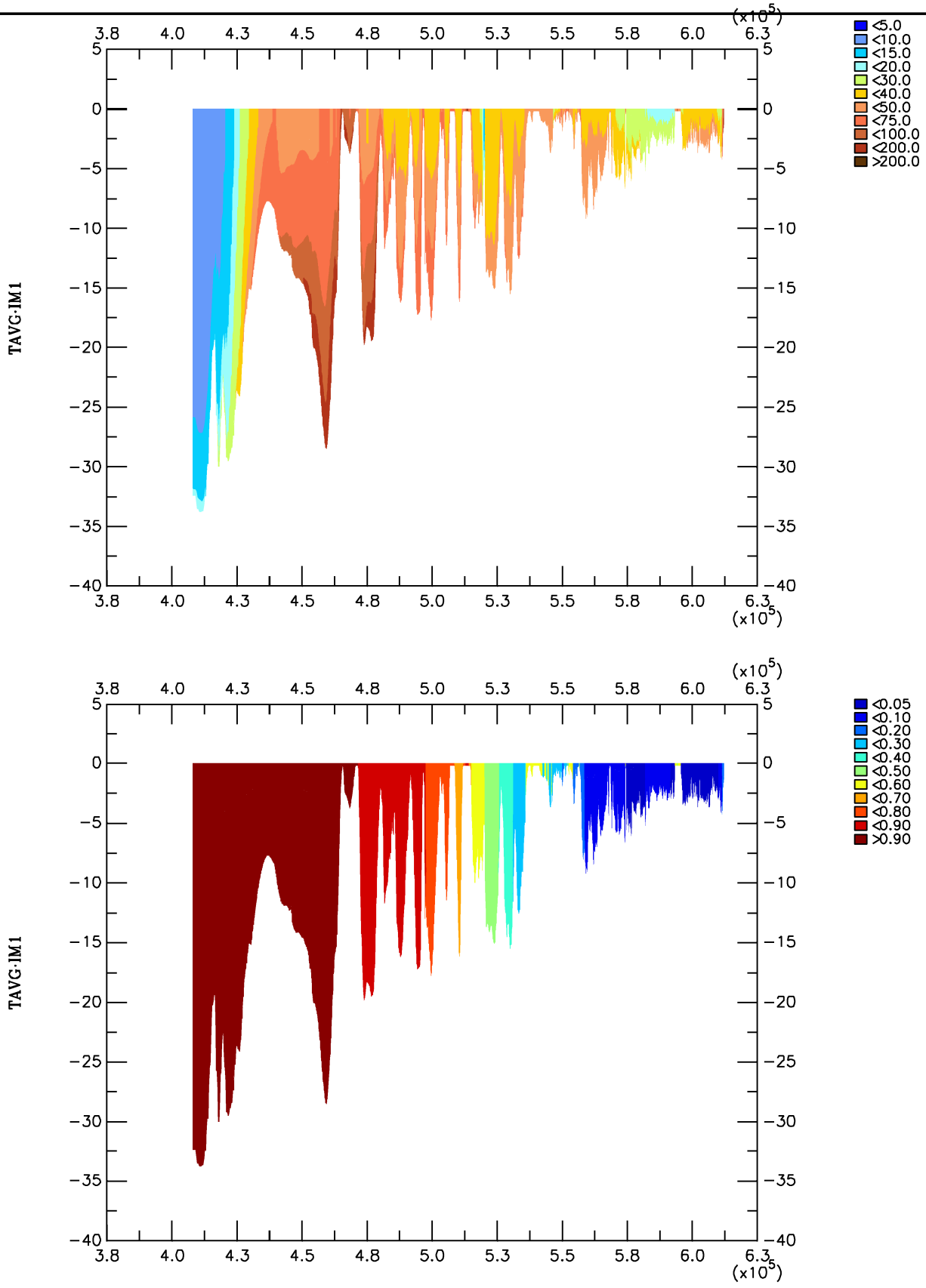

SPM concentration (mg/l) along Scheldt estuary summer upper panel: fluvial + marine fraction (mg/l) lower panel: marine fraction only (ratio)	hydro 14dw	ws18r
WL | Delft Hydraulics		Fig. S6.4b

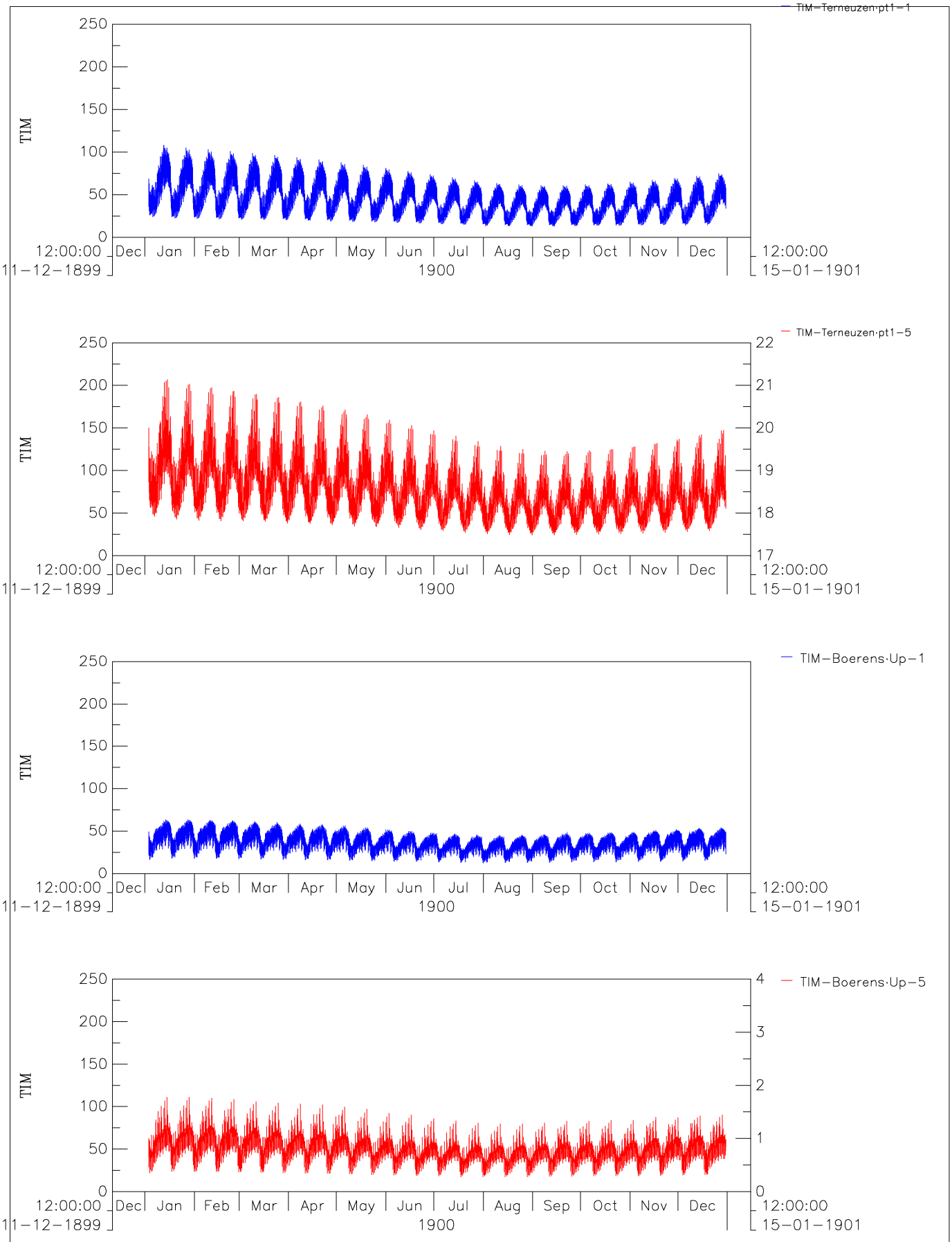

Time series SPM concentration (mg/l) top panels: Terneuzen DOW jetty year surface/bottom bottom panels: Boerenschans year surface/bottom	hydro 14dw	ws18r
WL | Delft Hydraulics		Fig. S6.5

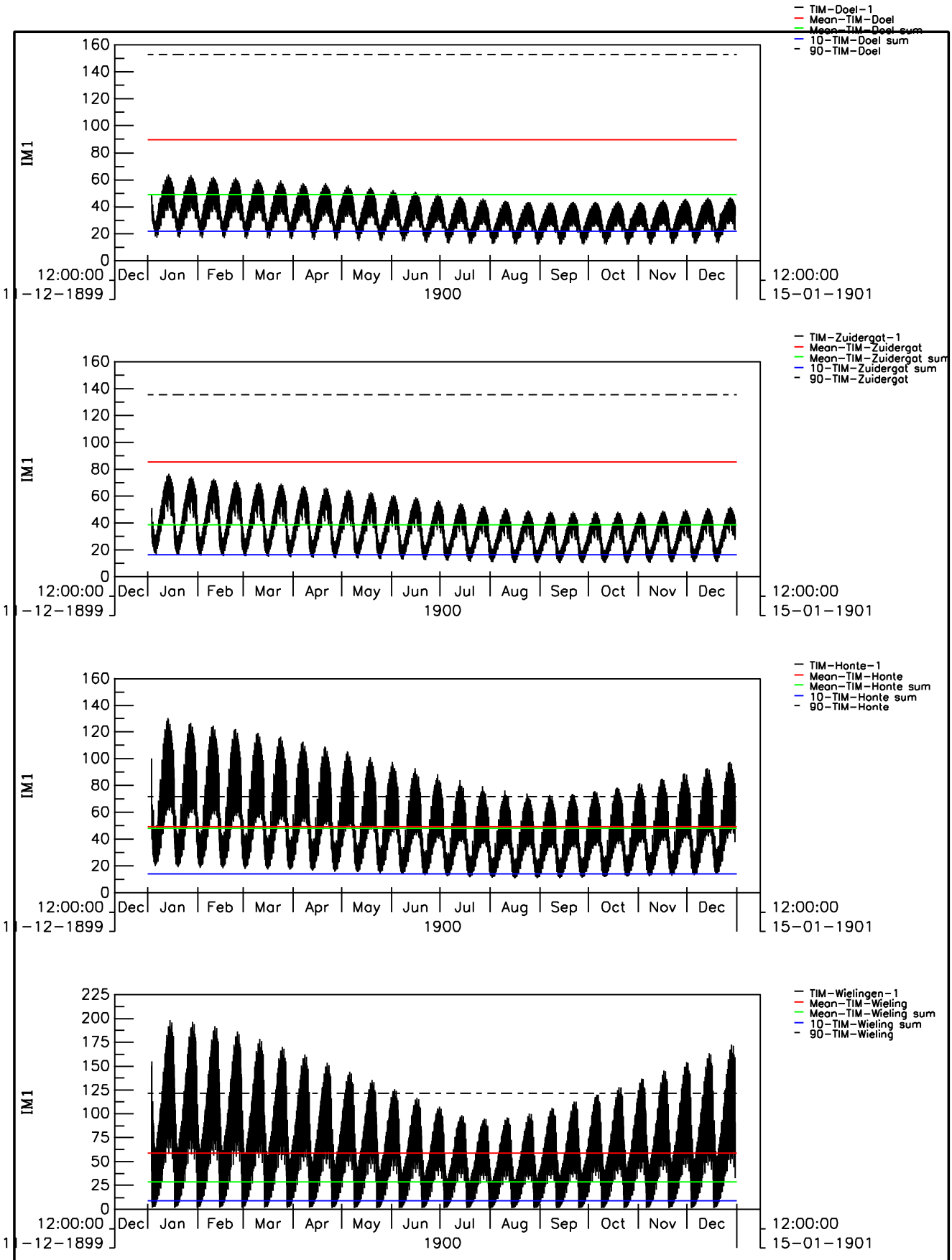

Time series SPM concentration (mg/l)
top panels: Schaar van Doel (top) and Zuidergat neap-spring
bottom panels: Honte and Wielingen (bottom) neap-spring

hydro 14dw | ws18r

WL | Delft Hydraulics

Fig. S6.6

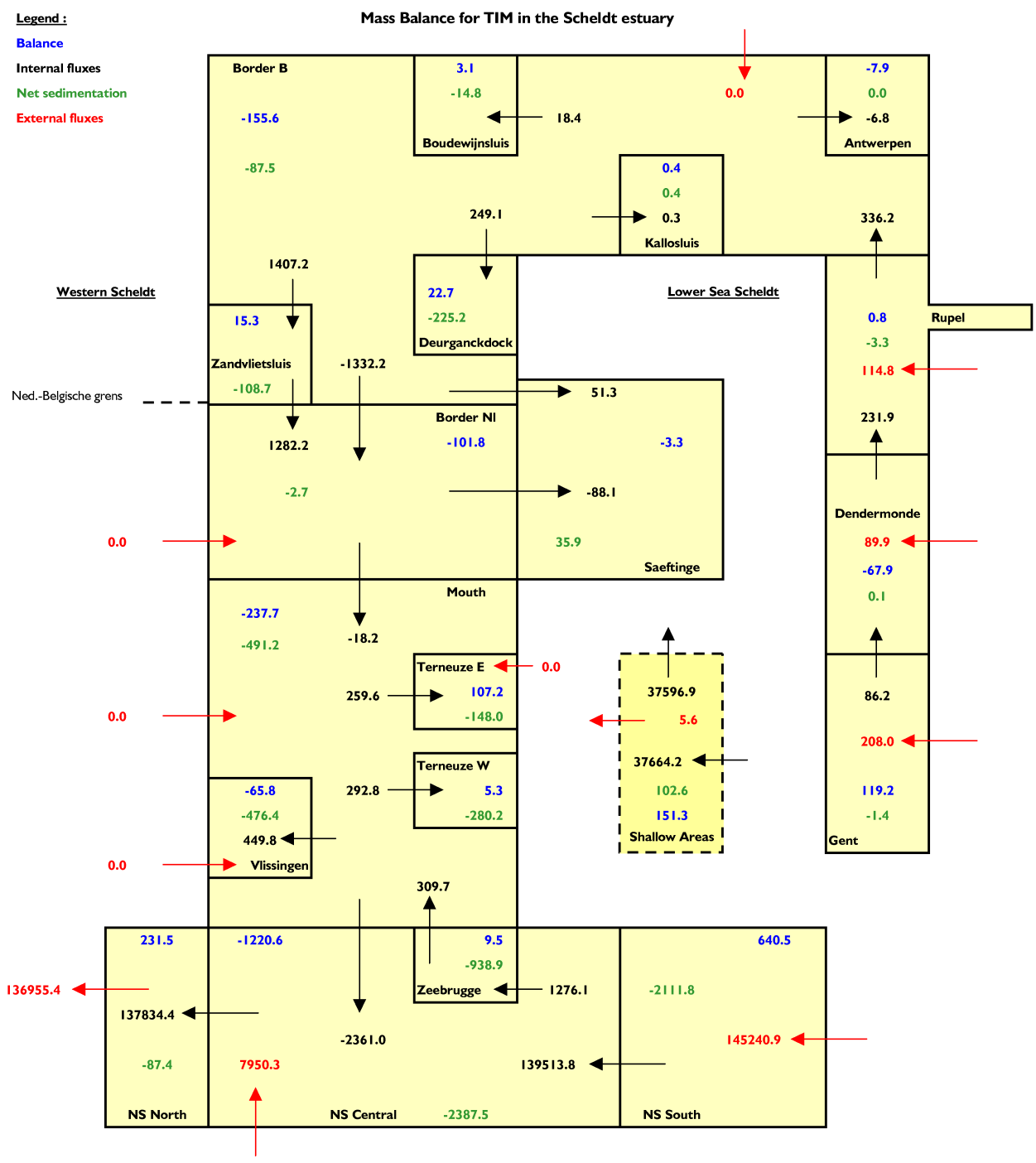

DELWAQ results
Net mud transport, 4th quarter [kT/year]

Z4210

WS18Q4

WL | DELFT HYDRAULICS

Fig. S6.7a

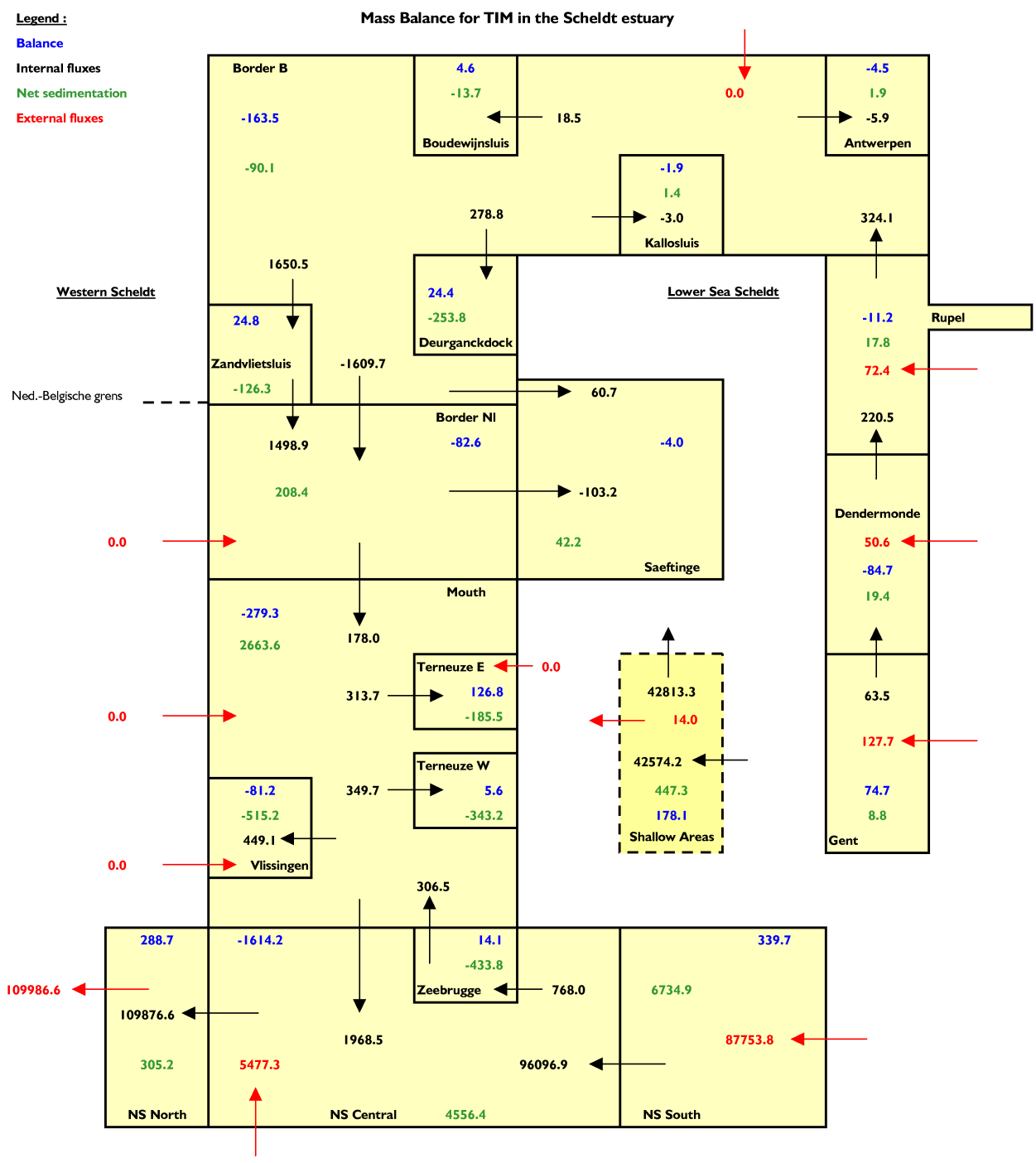

DELWAQ results
Net mud transport, 2nd quarter [kT/year]

Z4210

WS18Q2

WL | DELFT HYDRAULICS

Fig. S6.7b

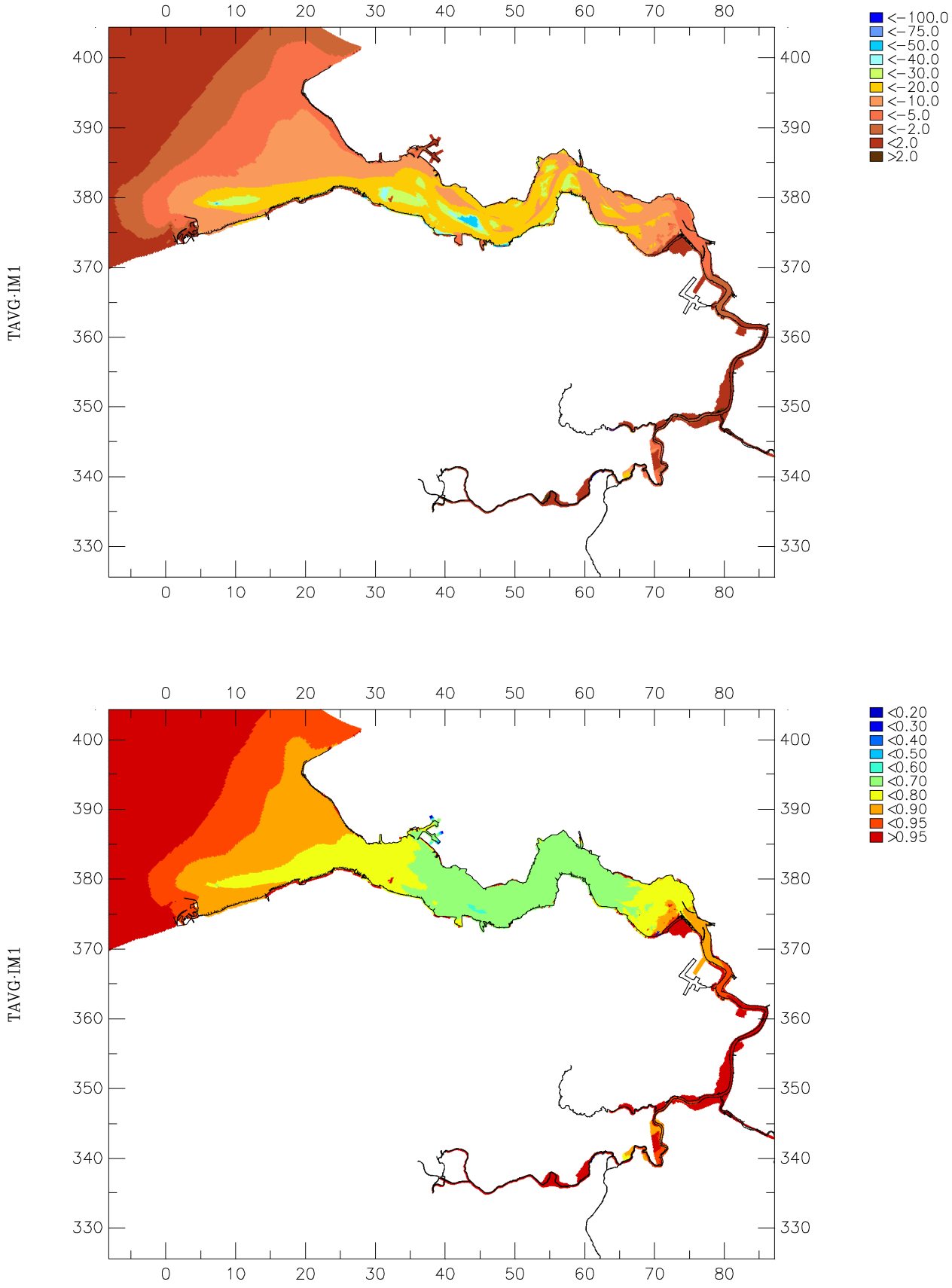

top: SPM concentration reduction in surface layer (mg/l)
bottom: SPM concentration reduction in surface layer (−)
after 1 year without mud dumping

hydro 14dw	ws18r
WL | Delft Hydraulics	Z4210
	Fig. S6.8

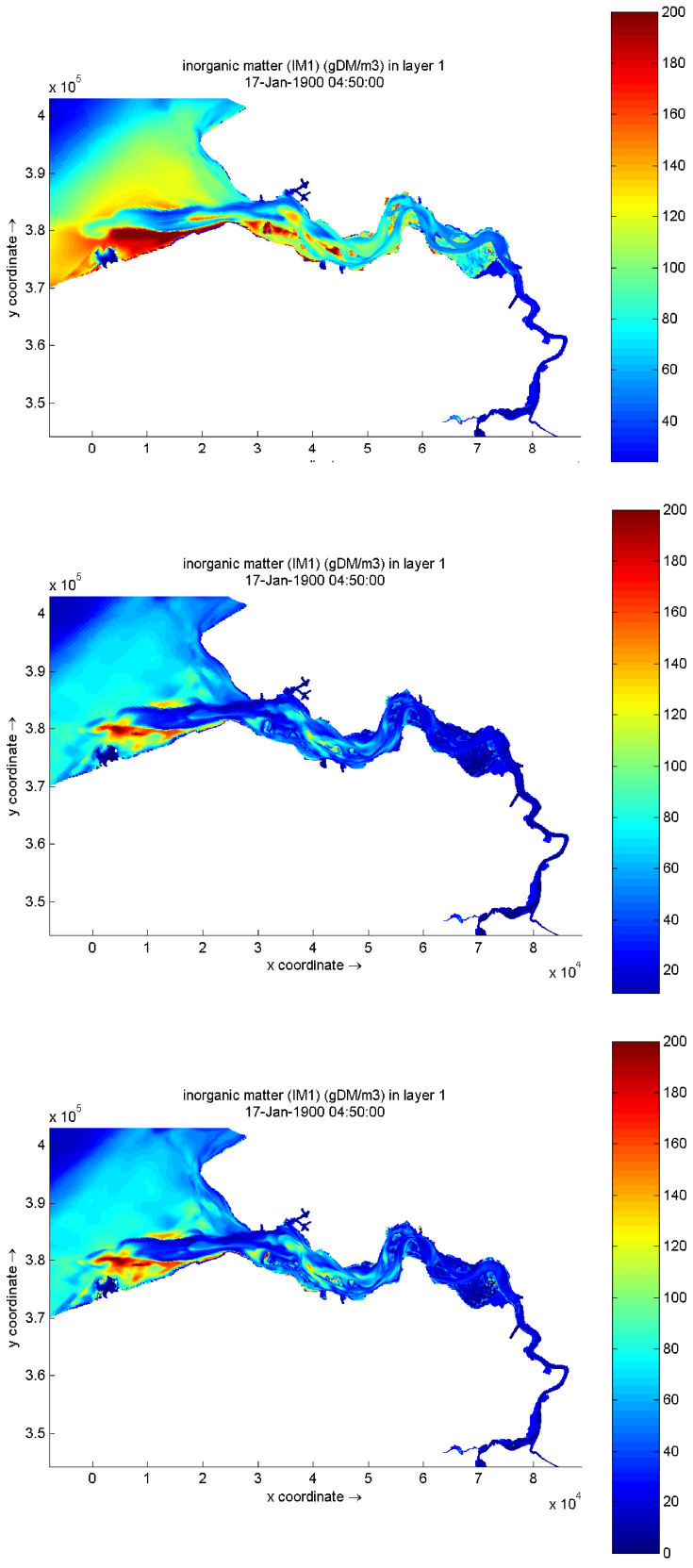

Comparison of surface concentration with scheme 16 (top), scheme 12 (middle) and scheme 12 1x1 (bottom)

Z4210

WL | DELFT HYDRAULICS

Fig. S7.1

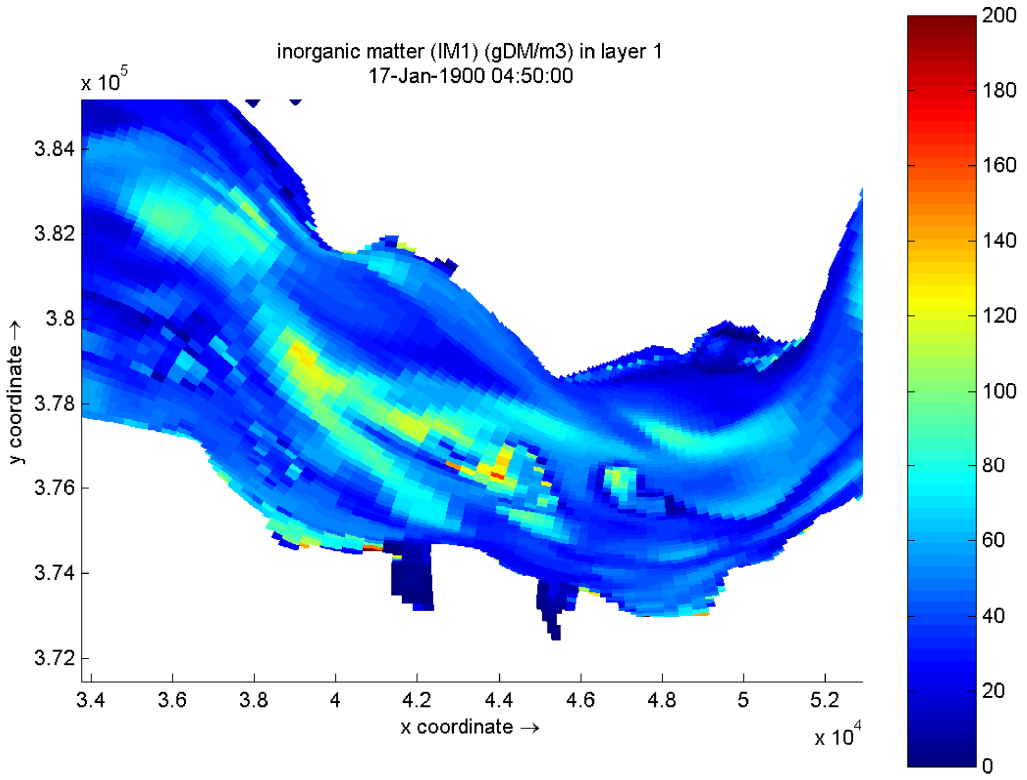

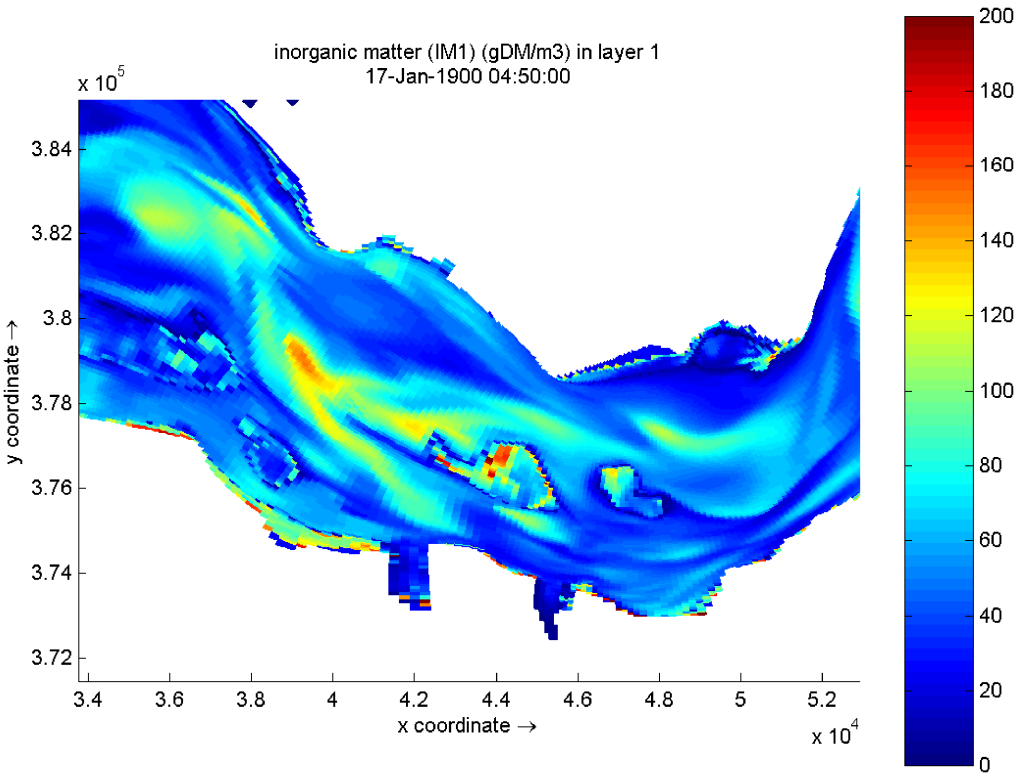

Comparison of surface concentration with scheme12 2x2 (top), scheme 12 and scheme 12 1x1 (bottom)

Z4210

WL | DELFT HYDRAULICS

Fig. S7.2